Physiological and chemical negotiations of the squid-vibrio symbiosis

By

Julia A. Schwartzman

A dissertation submitted in partial fulfillment of

the requirements for the degree of

Doctor of Philosophy

(Microbiology)

at the

UNIVERSITY OF WISCONSIN-MADISON

2015

Date of final oral examination: 05/11/15

The dissertation is approved by the following members of the Final Oral Committee:

Edward G. Ruby, Professor, Medical Microbiology and Immunology
Margaret J. McFall-Ngai, Professor, Medical Microbiology and Immunology
Rodney A. Welch, Professor, Medical Microbiology and Immunology
Helen Blackwell, Professor, Chemistry
Jennifer Reed, Associate Professor, Chemical Engineering
Kalin Vetsigian, Associate Professor, Bacteriology

Dedication

If I have seen further, it is by standing
on the shoulders of giants.
-Sir Isaac Newton, 1676

To my giants: GO, RDM, TFM, CW, RC, SS, GR, LK, HB, RW, MI, MMN, NR, CAB, AH, MB, JPG, ADC, KM, NAS and most of all, JDS.

PHYSIOLOGICAL AND CHEMICAL NEGOTIATIONS OF THE SQUID-VIBRIO SYMBIOSIS

Julia A. Schwartzman

Under the supervision of Professor Edward G. Ruby

The exchange of metabolites- whether signals or nutrients, forms the fulcrum point around which the forces that structure host-microbe interaction are balanced. In turn, the chemistry of the tissue environment structures this metabolic exchange by limiting the physiological permutations by which signaling and metabolism can take place. In this context, it is important to characterize the conserved chemical dialogue that distinguishes mutualism from pathogenesis. The microbiota of metazoans is often highly diverse, and in addition to exogenous environmental factors such as diet, this can create an astonishingly complex web of interaction, from which it is often difficult to discover the molecular basis of host-microbe interaction. Among the metazoans, invertebrates are a taxonomic branch characterized by less complex microbial consortia. Thus, invertebrates present a wealth of model systems in which to interrogate the mechanisms of metabolic exchange between host and microbiota. The symbiosis of the marine bioluminescent bacterium *Vibrio fischeri* with the squid host *Euprymna scolopes* stands out even among the invertebrates for the simplified structure of its microbiota: the squid forms a spatially isolated and monospecific partnership with *V. fischeri* in a behavioral organ adapted to manipulate bacterial bioluminescence. An extracellular population of *V. fischeri* grows within the epithelium-lined crypts of this organ throughout the life of the host. The amazing specificity of the initial symbiont selection, and the subsequent

maintenance of the symbiont, has motivated 25 years worth of research on the squid-vibrio model. In this dissertation, the squid-vibrio symbiosis is developed as a model to study metabolic exchange between host and microbe during the initiation, development, and maintenance of mutualism.

Host mucus is the first site of symbiont contact. In the mucus matrix, signals such as chitin oligosaccharides and nitric oxide prime *V. fischeri* for colonization of the light organ. The mucus is an important site of 'winnowing' or the selection of *V. fischeri* from non-symbiotic bacterioplankton. Recent work has demonstrated that the mucus is also mildly acidic, and that this acidic pH of may modulate the activities of host enzymes secreted into the mucus matrix. Acid pH cues the induction of stress responses in diverse host-associated microbes, including medically relevant pathogens *Escherichia coli*, *Salmonella typhimurium*, and *Vibrio cholerae*, which coordinate the expression of virulence and colonization factors. In this dissertation, we characterize the acid-induced resistance of *V. fischeri* to cationic antimicrobial peptide stress. Further characterization of the physiological functions coordinated by this host-derived environmental cue, as well as the transcriptional regulation underlying perception of acid by *V. fischeri*, will help to inform future studies of specificity in the context of symbiotic initiation, as well as provide a non-pathogenic perspective the coordination of microbial physiology by host pH.

Once the symbiosis has been initiated, *V. fischeri* grows to high cell density in the crypts. This diffusion-limited environment leads to accumulation of quorum signaling pheromones, and the activation of group behaviors such as bioluminescence. The expression of luciferase, a mixed-function oxidase that produces bioluminescence, is required for the

maintenance of the symbiont by the host: even in a mixed population of luciferase-positive and –negative *V. fischeri*, the non-bioluminescent cells are eliminated by the host. In this dissertation we demonstrate that a minimum threshold of quorum signaling-induced bioluminescence is required for the symbiont to maintain a colonization of the crypts.

We also investigate the mechanism by which the symbiont accesses sufficient oxygen to support bioluminescence during the development of the symbiotic organ. We identify chitin oligosaccharides (COS) as a host-derived glycan that, when catabolized by *V. fischeri*, acidifies the symbiotic tissues. Tissue acidification creates an environment that favors delivery of oxygen to the symbiont, due to the Bohr effect of the squid's extracellular oxygen-carrying protein hemocyanin. Additionally, the catabolism of chitin sugars by the bacterial PTS system favors aerobic fermentation by excluding non-fermentable carbohydrates. The resultant decrease in respiration consumption is proposed to support production of bioluminescence by the symbiont. Finally, the squid's immune cells, called hemocytes, carry granules of chitin, and we present evidence that hemocytes are a prominent source of COS in the context of the crypts.

In summary, the chemical and themes explored in this dissertation: pH, oxygen, and chitin are all linked, like words in the symbiotic conversation. The context of this conversation is the negotiation for symbiont bioluminescence, which is produced at night, creating a diel bioluminescent rhythm. We demonstrate that hemocyte behaviors, symbiont chitin sugar catabolism, and tissue acidification all coincide with the bioluminescent rhythm, and propose that this complex biological rhythm supports the stability and specificity of the symbiosis throughout the lifetime of the association.

Acknowledgments

I thank my thesis committee members: Helen Blackwell, Kalin Vetsigian, Jennifer Reed, Rod Welch, Margaret McFall-Ngai, and my doctoral adviser Ned Ruby for supporting and overseeing the research reported in this thesis, as well as training grant faculty advisers Heidi Goodrich-Blair, Bruce Klein, and Laura Kiessling, who have been involved in my professional and scientific development. I thank my co-authors: Natacha Kremer, Elizabeth Heath-Heckman, and Eric Koch for their work to foster successful collaborations, as well as lab members past and present, for training and troublehooting, and Thursdays. I especially thank Min Pan and Lawrence Zhou for teaching me an enormous amount about how to be a mentor. My doctoral training would not have been possible without the support of Cathy Davis-Gray, Nell Bekiares, Eva Ziegelhoffer, Tracy Wiklund, Alicia Hamilton, and Kris Turkow, and the financial support of the Microbiology Doctoral Training Program, the National Science Foundation Graduate Research Fellowship, the Chemical Biology Training Grant (National Institutes of Health NIH-NIGMS T32 GM008505, and Microbes and Health and Disease Training Grant (National Institutes of Health, National Research Service Award AI55397), NIH research grant RR12294/OD11024 to EGR and MM-N, and NIH research grant AI050661 to MM-N.

Table of Contents

List of Figures

Chapter 1

Chapter 2

Chapter 3

Chapter 4

Chapter 5

Appendix B

Appendix C

List of Tables

Chapter 2

Chapter 3

Chapter 4

Chapter 5

Appendix C

Chapter 1

General Introduction and Thesis Outline

PREFACE:

A portion of this chapter is in preparation for submission to *Microbes and Infection* as:

JA Schwartzman and EG Ruby. “The conserved chemical dialogue of mutualism: lessons from squid and vibrio”

JAS wrote the chapter and designed the figures.

ABSTRACT

Microbes shape, and are shaped by their environment. This environment is defined by host tissue chemistry, which reflects local and global physiology and inflammatory status. In this chapter, a review of how host and symbiont shape tissue chemistry in the squid-vibrio mutualism is presented, to illuminate common themes governing tissue homeostasis in animal-microbe associations.

INTRODUCTION

Animals exist in, and have evolved with, a sea of microbes (1). Some of these microbes form beneficial alliances with host tissues, that contribute to nutrient acquisition or defense (2, 3). The composition of the microbiota is structured by the host tissue environment (4), and host tissue chemistry reflects both underlying physiological function and inflammatory status (5). In turn, microbe-associated molecular patterns (MAMPs), are signals perceived by innate immune system that define the balance of inflammation in the tissue environment, and mediate the activation of adaptive immunity (6). The threshold of MAMP signaling that induces inflammation varies, even within tissues of the same organ system. For example, the intestinal epithelium is much more tolerant of inflammation-inducing microbial products in the colon: a major site of immune maturation, than in the ileum: the primary site of nutrient absorption (7). Thus, host tissue chemistry defines, and is defined by, interactions with the microbiota.

Invertebrate model systems have provided a window into the mechanisms by which microbial products contribute to tissue homeostasis: for example, toll-like receptors were first discovered in drosophila (8). Moreover, invertebrate immune systems lack a defined adaptive branch (9), thus, they present an evolutionary record of nature's experiments in achieving balance between host and microbe using only tissue-level responses and innate-immune functions such as pattern recognition. Microbial communities associated with invertebrates are also typically less complex than that of vertebrates, perhaps reflecting the absence of a malleable adaptive immune response (10). In essence, the lack of adaptive immunity reduces both the complexity of immune cell types, and the possible permutations by which host and

microbiota might interact to achieve homeostasis. Thus, there is great value in looking beyond drosophila and the arthropods to other invertebrate lineages such as annelids, nematodes, and molluscs, because it is through comparative studies that the conserved 'chemical dialogue' of symbiosis might be revealed (9, 11-13). In this introduction, I focus on the molluscan branch of the metazoan tree, and what the specific symbiosis of the squid *Euprymna scolopes* with the microbe *Vibrio fischeri* has revealed about the chemical cues that orchestrate the initiation, development, and maintenance of mutualism.

The squid-vibrio model *E. scolopes* forms a specific association with the bioluminescent marine gammaproteobacterium *V. fischeri*. The mutualism takes place in the epithelium-lined crypts of a specialized anatomical structure of the squid called the light organ (14) (**Fig. 1-1*A***). The basis of the mutualism is the bioluminescence provided by *V. fischeri*, which is used for host behaviors (15). The light organ shares much of the anatomical and physiological features of an eye: a lens and reflector manipulate the intensity and appearance of bioluminescence, and the light-organ tissues express both photoreceptors (16), as well as genes involved in eye development (17) (**Fig. 1-1*B***). Unlike the eye, which collects and perceives light from a dense (10^8 CFU/mature light organ) population of *V. fischeri* (18). Only *V. fischeri* can colonize this tissue habitat, and a persistent, monospecific population of the symbiont is maintained in the light organ throughout the squid's ~9-month life. The squid's immune response is orchestrated by circulating macrophage-like immune cells, called hemocytes, and tissue-specific responses to MAMPs (19, 20). In the following sections, I review the chemical selection for *V. fischeri* during the initiation, development and maintenance of mutualism.

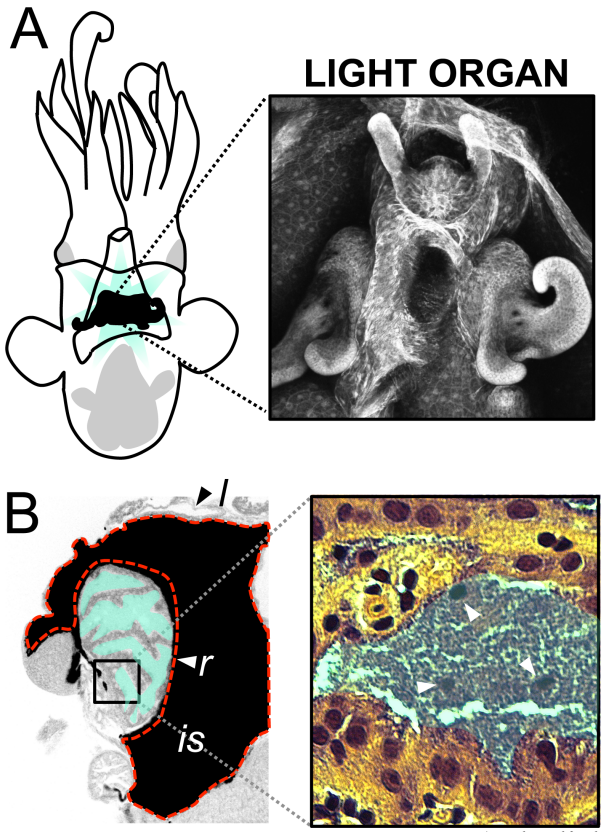

Figure 1-1. The anatomy of the squid-vibrio mutualism. *A)* The light organ is the anatomical structure of the squid that maintains the bioluminescent symbiont *V. fischeri*. The organ is located underneath the mantle of the squid, just atop the funnel: a structure used to ventilate the mantle. The immature light organ (pictured at right) is characterized by bilateral ciliated fields, as well as anterior and posterior appendages. At the base of the appendages are pores, leading into the crypts of the light organ. *B*) A cross-section of the light organ shows that the symbiont (teal) is maintained in extracellular crypts lined with a polarized epithelium. Structures surrounding the crypts, such as the reflector (*r,* indicated in red dashed lines), ink sac (*is*), and lens (*l*), are photoreceptive, and manipulate the light produced by the symbiont for host behaviors. *V. fischeri* contacts two host cell types: epithelial cells that line the crypts, and immune cells present in the crypt lumen (host cells indicated by white arrows).

INITIATION: THE WINNOWING PROCESS

Symbiosis is initiated in a multi-step process, beginning with the harvesting of *V. fischeri* from the bacterioplankton by newly hatched squid. Ecological studies have demonstrated that *V. fischeri* is enriched in the squid's habitat, but still represents a minor constituent of the total population (21). Therefore, the challenge is two-fold: the host must first sample sufficient seawater to isolate *V. fischeri*, and then select a symbiont from the microbes that have also been collected, in a process named 'winnowing' (22). Winnowing take places outside of the light organ, in bilateral ciliated fields that are unique to the uncolonized, or aposymbiotic, state. This complex, multi-step process occurs over about a hundred microns, highlighting the importance of understanding the structure of host tissue microenvironments. In this section, I review the chemical exchange that takes place during winnowing.

First contact and mucus shedding Upon hatching, ventilation of the mantle cavity brings bacterioplankton-rich seawater in contact with the light organ surfaces. Peptidoglycan (PGN) fragments released from these bacteria induce a non-specific shedding of sialylated host mucus (23) (**Fig. 1-2*A***). The acidic glycosylation of the mucins creates a pH 6.3 matrix (24), which traps the bacterioplankton. Host antimicrobial peptides such as galaxin and peptidoglycan recognition protein 2 (PGRP2), establish an early selective barrier in the mucus that likely excludes gram-positive microbes (25, 26). Combined with other antimicrobial constituents of the mucus, such as the phenoloxidase hemocyanin (27), the chemistry that defines this first site of host contact is sufficient to exclude all gram-positive microbes, and the majority of other seawater bacteria. In **Chapter 2** of this dissertation, I propose

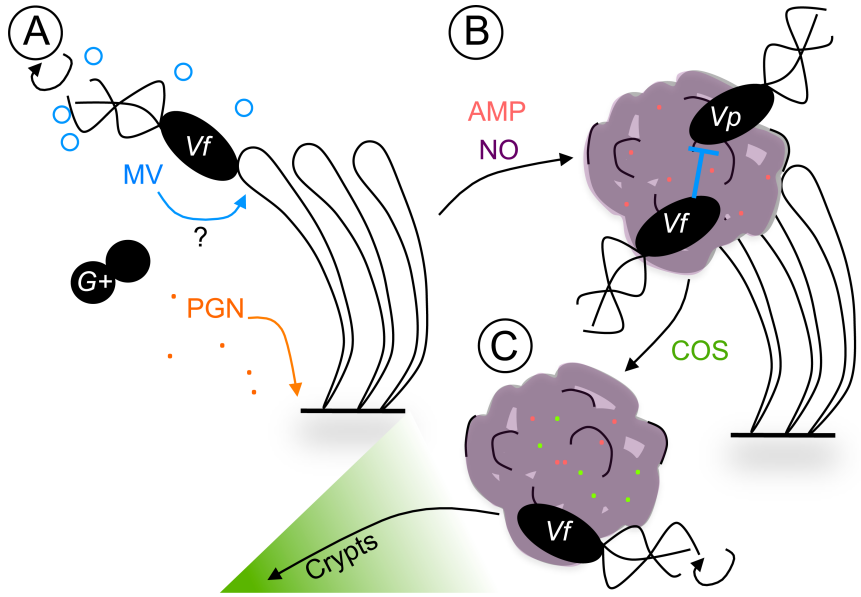

Figure 1-2. The winnowing of the symbiont. *A*) The first contact between *V. fischeri* and *E. scolopes* is binding to cilia on the outside of the light organ. The binding event may also promote presentation of microvesicles (MV) to host tissues, which are shed by *V. fischeri* during rotation of its sheathed flagella. Peptidoglycan (PGN), from seawater bacteria, also induces mucus shedding. *B*) The mucus is a site of selection. In addition to sialylated mucins (pH 6.3), antimicrobial peptides (AMP), and nitric oxide (NO) shape the chemistry of the mucus matrix. The mucus is an environment that excludes Gram-positive microbes (G+), and also allows *V. fischeri* to out-compete any co-aggregating gram-negative microbes such as *Vibrio parahaemolyticus. C*) Contact with *V. fischeri* induces the expression of host enzymes that cause chitin oligosaccharides (COS) to accumulate in the mucus matrix. The exposure to COS, as well as to NO, primes *V. fischeri* for migration into the light organ. The transition out of the mucus takes place after *V. fischeri* has been primed by exposure to COS to chemotax towards a gradient of the sugar that emanates from the entrance to the crypts.

that the acidic pH of the mucus acts as a cue to induce physiological states of microbes in the aggregate that enhance or diminish survival in the context of host antimicrobial defenses.

Establishing dominance in the mucus In conjunction with PGN-induced mucus shedding, any *V. fischeri* that are sampled from the environment by ventilation become trapped by adhering directly to the cilia (28) (**Fig. 1-2*A***). Adhesion, and perhaps the release of microvesicles from the symbiont's sheathed flagellum (29), induce a transcriptional response in light-organ tissues. This initial response to the symbiont includes transcripts encoding antimicrobial factors such as lysozyme, chitinase, and ferritin (24), a subset of which accumulate in the mucus, and may represent an additional, symbiont-induced stage of winnowing (**Fig. 1-2*B***). The metachronal beat of the cilia eventually traps *V. fischeri* in the acidic mucus with non-symbiotic gram-negative bacteria, such as *Vibrio parahaemolyticus.* To survive in the mucus, *V. fischeri* must carry the gene *rscS*, a regulator of pellicle formation that is conserved only in squid-specific strains (30, 31). RscS is necessary, but not sufficient to coordinate the colonization program of *V. fischeri*. A complex regulatory network, reviewed elsewhere (32), underlies the process of colonization. The mucus may also be a site of competition between the small number of microbial species that can survive the mucus chemistry: *V. parahaemolyticus* survives contact with host mucus, but only in the absence of *V. fischeri* (33). In **Chapter 2** of this dissertation, I demonstrate that exposure to acid pH in a seawater-like environment containing mucin induces the resistance of *V. fischeri* to the cationic antimicrobial peptide polymyxin B. This acid-induced physiological response is not shared by *V. parahaemolyticus,* or other members of the seawater microbiota. Future characterization of the mucus chemistry, and the signaling between the host and the specific

symbiont, will reveal whether such acid-induced stress responses contribute to the dominance of *V. fischeri* in the mucus environment.

Preparing for colonization Once dominant in the aggregate, exposure to nitric oxide (NO), and chitin oligosaccharides (COS) prepare, or 'prime', *V. fischeri* for the next steps of colonization (24, 34) (**Fig. 1-2*C***). NO is present in the mucus at levels that are below the lethal threshold for *V. fischeri* (35), but that are sufficient to induce resistance to killing by NO and iron-linked oxidative stress (34, 36-38). In addition, the symbiont is exposed to COS in the mucus. The hydrolysis of chitin, a polymer of beta-1,4-linked *N*-acetylglucosamine (GlcNAc) residues, by host enzymes creates a chemotactic gradient of COS that emanates from pores leading into the light organ. It is towards this sugar gradient that *V. fischeri* migrates to traverse from the ciliated fields into the light organ (24, 39). Chemotaxis towards COS requires priming of *V. fischeri* in the mucus (24). Thus, the mucus is both a site of selection and a platform that coordinates the transition of symbiosis-competent *V. fischeri* from the seawater and into the host.

How does the squid-vibrio association contribute to our understanding of the initial selection for cooperation? The complexity of light-organ colonization highlights a theme among co-evolved animal-microbe associations: the host tailors the tissue chemistry to select for the microbiota (40). Other examples of this strategy include the secretion of antimicrobial peptides on the epithelial surface of hydra, which structure colonization by a specific, and robust microbial community from the surrounding seawater using antimicrobial peptides (41), and pregnancy-driven changes in the tissue chemistry of the mammalian gut and vaginal canal, which shift the composition of the maternal microbiota at sites from which neonatal

colonization is initiated (4). Moreover, the squid-vibrio model demonstrates that MAMPs are involved in establishing sites of symbiont selection, such as mucus. The key to specific signaling of host and symbiont lies not in the chemical properties of the MAMPs, which are broadly conserved among bacteria, but in the ability of the symbiont to withstand the chemical and physiological barriers of the host, and reach the relevant site of signaling.

DEVELOPMENT: TRANSITIONING THE ENVIRONMENT

The colonization of the crypts sets in motion an irreversible program of host development and morphogenesis. The signal for this transition is presented at dawn following light-organ colonization (42, 43), and is characterized by bioluminescence-dependent and independent transcriptional responses (44). Accompanying this transcriptional response, MAMPs presented by the symbiont in the crypts induce the irreversible morphogenesis of the light organ (42). The initiation of this irreversible program marks the transition from the initiation of the symbiosis to the accommodation of *V. fischeri* as a persistent colonizer of the crypt epithelium. Morphogenesis and the accommodation of the symbiont are correlated with bioluminescence (45-47). In this section, I review the chemistry and physiology that characterizes symbiont-induced morphogenesis of host tissue and the selection for bioluminescence.

Creating barriers: irreversible morphogenesis The priming of the symbiont that takes place in the aggregate enables the survival of *V. fischeri* during the encounter with nitric oxide (NO) in structures leading into the light-organ crypts: a stringent barrier that the symbiont must survive to orchestrate the next steps of colonization (**Fig. 1-3*A***). Symbionts that survive

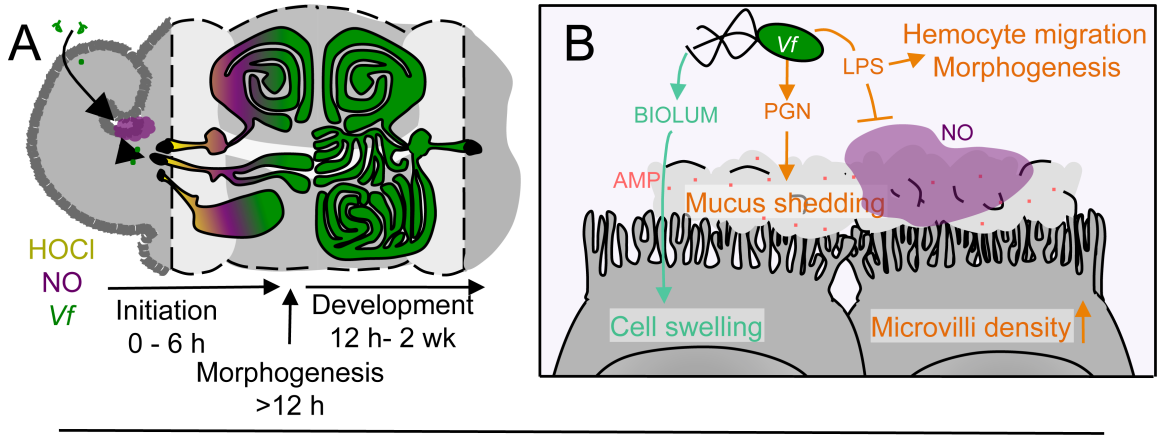

Figure 1-3. Accommodations of host and symbiont in the light-organ crypts. *A*) *V. fischeri* (*Vf,* green), attenuates host production of hypochlorous acid (HOCl, yellow), and nitric oxide (NO, purple), upon transit into the crypts. The process of initial colonization occurs in the first 6 h after contact of host and symbiont. At dawn, at least 12 h post-colonization, the presentation of MAMPs by the symbiont delivers an irreversible morphogenic stimulus to light organ tissues. During subsequent development, the ciliated fields of the light organ regress, and the crypts become more complex. The ducts leading to the crypts condense from 3 passages to one. By 2 weeks, continued colonization of the symbiont induces physiological state in the host tissues that prevents secondary colonization. *B*) Symbiont-derived chemical cues orchestrate physiological and morphological changes in the light organ. Bioluminescence (biolum, teal) induces swelling of the crypt epithelium. Peptidoglycan (PGN) induces shedding of mucus, and the secretion of antimicrobial factors (AMP, pink) into the crypts. Lipopolysaccharide (LPS), attenuates the local production of NO in the crypts, and induces the migration of hemocytes to the ciliated appendages, followed by apoptosis and regression of these structures.

the migration into the light organ and present PGN in this context attenuate the production of NO in the crypts, and induce mucus shedding (23, 35) (**Fig. 1-3*A***). The attenuation of NO by PGN and LPS signaling induces the trafficking of hemocytes into the ciliated fields (48) (**Fig. 1-3*B***). MAMP signaling from the crypts orchestrates the apoptosis and regression of these structures (42, 43, 45, 49-52) (**Fig. 1-3*B***). Although the crypts remain open to the environment *via* pores, the loss of the ciliated fields create a significant physical bottleneck to subsequent colonization (14) (**Fig. 1-3*A***). Moreover, the symbiont induces global changes in the protein composition of host symbiotic tissues (53), and cues the secretion of the enzymes galaxin (25), PGRP2 (26), and alkaline phosphatase (54), into the crypts (**Fig. 1-3*B***). Thus, MAMP signaling by *V. fischeri* re-shapes light organ anatomy to 'shut the door' behind those few symbiont cells winnowed from the environment, and shifts the chemical composition of the crypts. It remains to be seen if this symbiont-induced chemical shift contributes to the specific and stable colonization of *V. fischeri.*

The first exchange: bioluminescence allows persistence in the crypts. Once *V. fischeri* reaches the crypt, it must begin to grow and produce bioluminescence. The few progenitor cells that survive winnowing undergo approximately 10 doublings within the first 12 h of initial colonization to populate the crypts (or ~1 generation per hour (18)). Growth in the crypts is supported by amino acids (55), but is potentiated by the constant production of bioluminescence (47): an enzymatic process that consumes molecular oxygen and chemical energy (56). The metabolic demands of bioluminescence must be balanced with those of growth to maintain both a robust colonization and a minimum threshold of light throughout the first days of symbiosis (56). In **Chapter 3** of this dissertation, chemical agonists and

antagonists of pheromone signaling are used to demonstrate that there is a threshold of pheromone-induced bioluminescence, below which the symbiont cannot maintain a stable colonization of the light organ (47). The regulatory network surrounding bioluminescence is highly complex (57), but from a broad perspective, the expression of the bioluminescence-producing enzyme luciferase is transcriptionally regulated by the cell-density dependent accumulation of quorum-signaling pheromones in *V. fischeri* (58), and is tied to the metabolic state of the symbiont (56). Thus, the balance between growth and bioluminescence in the crypt is necessary for *V. fischeri* to maintain a robust colonization of the light organ.

Symbionts tailor the physiology of the tissue environment. The bioluminescence and growth of the symbiont population also induces reversible physiological changes in the crypt epithelium, such as cell swelling (46), and an increase in the density of microvilli at epithelial surfaces in contact with symbionts (59). The function of these physiological changes is not fully understood, but may be evidence of the host's provision of nutrients to the symbiont. The crypt matrix contains millimolar levels of several amino acids, which are used by the symbiont to support growth (55). Some amino acids, such as lysine, are not provided to the symbiont, and because of this, a subset of *V. fischeri* amino acid auxotrophs fail to reach a full colonization of the crypts (55). The contribution of the crypt amino-acid composition to the persistence of the symbiont is not known, but may structure metabolism to promote certain physiological functions, such as bioluminescence. Additionally, symbionts incorporate host lipids into their membranes (60), leading to an enrichment of long-chain unsaturated fatty acids. The incorporation of eukaryotic lipids into *Vibrio cholerae* (61, 62), and *Enterococcus faecalis* (63) confers resistance to host-associated stressors, suggesting that this modification

might confer stress resistance to symbiotic *V. fischeri*.

Chapter 4 of this dissertation demonstrates that as the light organ matures, COS become available (64). Host-derived COS have profound consequences on the metabolism and physiology of the crypt. Prior to the provision of COS to the symbiont, the stability of colonization is positively correlated with the strength of the DNA-binding repressor NagC, which is inactivated by symbiont COS catabolism (65). Thus, the host selects for symbionts that do not respond to COS during the initial phase of symbiosis, and then requires COS catabolism in the mature state. In **Chapter 5** of this dissertation, a strategy is proposed by which the catabolism of host-derived COS, monomeric, and dimeric chitin sugars regulate *V. fischeri* metabolism and physiology, thereby contributing to the stability of light-organ colonization.

An indelible first impression: the development of a host refractory state A key transition is reached in light-organ development after 2 weeks symbiosis: if a non-bioluminescent strain of *V. fischeri* has colonized the crypts, it is not maintained past this point (66). The 'imprint' of a bioluminescent symbiont is lasting: experimental curing of the light organ following colonization reveals that bioluminescent *V. fischeri* induce a physiological state in the light organ that is refractory to re-colonization (66). In addition, the continual exposure to *V. fischeri* 'educates' the circulating population of immune cells called hemocytes. The symbiotic state changes the proteome of hemocytes (67), perhaps reflecting that the protracted interaction of hemocytes with the *V. fischeri* major outer membrane porin OmpU decreases in the binding and phagocytosis of the symbiont (68). *V. cholerae ompU* (59% identical to *V. fischeri* OmpU), is transcribed in response to environmental cues in host

tissues, such as bile (69), suggesting that the epitopes central to hemocyte education may reflect the surface proteins expressed by *V. fischeri* during stable colonization. Thus, further study of the environmental regulation of *V. fischeri* epitopes that contribute to hemocyte education may help to reveal the physiological parameters that define homeostasis of light organ tissues in the symbiotic state.

How do squid and vibrio contribute to our understanding of the development of mutualism? The squid was one of the first examples of MAMP-directed tissue morphogenesis (42), and subsequent studies in this system have reinforced the theme that microbial metabolites direct normal host tissue maturation. Mammalian systems provide multiple examples of how initial, even transient, dysbiosis of the microbiota during development can have lasting detrimental consequences on host health, due to disregulation of pattern recognition and microbe-dependent tissue development. For example, antibiotic exposure at birth affects ileal immunity in mice, leading to inflammation, metabolic imbalances an increased adiposity (70). In this context, the resilience of the symbiont to the constraints of the host environment is a key determinant of stability. The squid-vibrio system has revealed that the metabolic and physiological accommodations of *V. fischeri* make it resilient to the host environment, and perhaps tailor the squid's immune defenses. This is echoed by the resistance of the intestinal symbiont *Bacteroides thetaiotaomicron* to host antimicrobial peptides, which contributes to the resilience of this abundant member of the gut microbiota in the intestinal lumen (71). Squid derived nutrition also structures the development of symbiont metabolism, much as a changing profile of mammalian mucin glycans selects for microbes that are able to metabolize plant starches, long before these

starches enter the infant diet (4). The resilience of *V. fischeri* is linked to its metabolic repertoire: the host's selection favors symbionts that repress COS-responsive genes during the initial stages of symbiosis, then hinges on the ability of the symbiont to express these genes in the mature association. Perhaps genetic manipulation of primary colonizers of the gut will reveal that an expanded metabolic repertoire promotes the resilience of a symbiont over the trajectory of host development.

PERSISTANCE: DAILY AND CIRCADIAN RHYTHMS

Once established in a morphologically mature light organ, the symbiont is maintained in a dynamic, daily cycle for the life of the host (72). This period of 'persistence' constitutes 90% of the lifetime of the squid (66). Remarkably, the host maintains a monospecific colonization of *V. fischeri* throughout its life, and does so while preventing the loss of bioluminescence over approximately 3000 microbial generations (73). The light organ is subject to a daily biological rhythm, in which photoreceptive tissues perceive the dawn light cue, and cause expulsion of the crypt contents, including the majority of the symbiont population (72) (Fig. 4). The remaining symbionts repopulate the crypts, and are expelled anew the following morning (18). If a bioluminescent population has been established, it will be maintained throughout host development: a process that occurs over several weeks, during which time the anatomical features of the light organ develop and the crypts increase in morphological complexity (14, 74, 75).

The establishment and maintenance of the mature symbiotic state is driven by the host's daily response to environmental cues, as well as by circadian rhythms (**Fig. 1-4**). In

animals, including the squid, the circadian rhythm is orchestrated by the central nervous system, which coordinates the peripheral oscillatory circuits, or clocks, of individual organ systems (76). The circadian clock is entrained by both transcriptional and redox-responsive post-translational regulation (77, 78). In this section, I review the development of daily and entrained rhythms in the squid-vibrio symbiosis, and the consequences of these rhythms on tissue chemistry.

Initial rhythms From the onset of the squid-vibrio symbiosis, the daily expulsion and subsequent re-growth of the symbiont population establish a biological rhythm (72). Expulsion occurs even in the absence of the symbiont, but is only triggered by a light stimulus to the squid's eyes (79). These factors indicate that expulsion is a rhythmic, but not circadian, function (**Fig. 1-4**). In contrast to expulsion, other symbiosis-dependent rhythms in the initial light-organ tissues show signs of circadian underpinnings. For example, the microvilli at the apical surfaces of the crypt epithelium are shed just preceding dawn (60) (**Fig. 1-4**). Cytoskeletal remodeling genes are also subject to a daily transcriptional rhythm, perhaps reflecting the daily effacement and renewal the microvilli (60). It is these initial light-dependent rhythms that define the physiology upon which the symbiosis is established, and thus the baseline from which the symbiont can shift tissue homeostasis.

The symbiont adds to the existing rhythms of the light organ tissue by bioluminescence-dependent and -independent processes. Symbiont bioluminescence entrains the tissue-specific circadian oscillation of the clock gene *escry1* (80). The regulatory targets of the bioluminescence-entrained light-organ clock have yet to be identified, but perhaps include genes transcribed in response to bacterial bioluminescence, such as eye specification

genes (17), a predicted vasoconstrictor octopressin, a matrix metalloprotease, and hemocyanin (44). Bioluminescence-independent, but symbiont-dependent rhythms include the LPS and PGN regulated transcription of alkaline phosphatase (54), and the daily rhythm of immune cell migration characterized in **Chapter 4** and **Appendix B** (64). Further study of the light organ's symbiont-dependent rhythmic biology will delineate the separate contributions of microbial products to the diel and circadian biology of the light organ.

The mature daily rhythm. The initial biological rhythms of the light organ take on additional metabolic and physiological complexity during post-embryonic development (64, 72). In conjunction with the development of the symbiotic rhythm, the host's behavior shifts: the squid begins to bury in the day, and emerge at night to hunt in the open water (81). It is not known to what extent this behavioral transition influences the physiology of the light organ, or the animal as a whole, although it is likely that the daytime burying behavior is accompanied by a period of metabolic quiescence, as the animal has reduced ventilation while buried. In conjunction with the establishment of the behavioral rhythm, light-organ structures such as the lens, ink sac, reflector and crypt epithelium undergo a period of morphogenesis (74). Behavioral and morphological development is complete by 4 weeks of colonization, marking the onset of the mature symbiotic state (66, 82).

Coincident with light-organ maturation, the symbiont's metabolism of carbon develops a daily rhythm. Reflecting this rhythm, transcripts associated with host chitin synthesis and breakdown, as well with symbiont COS catabolism, increase in abundance in

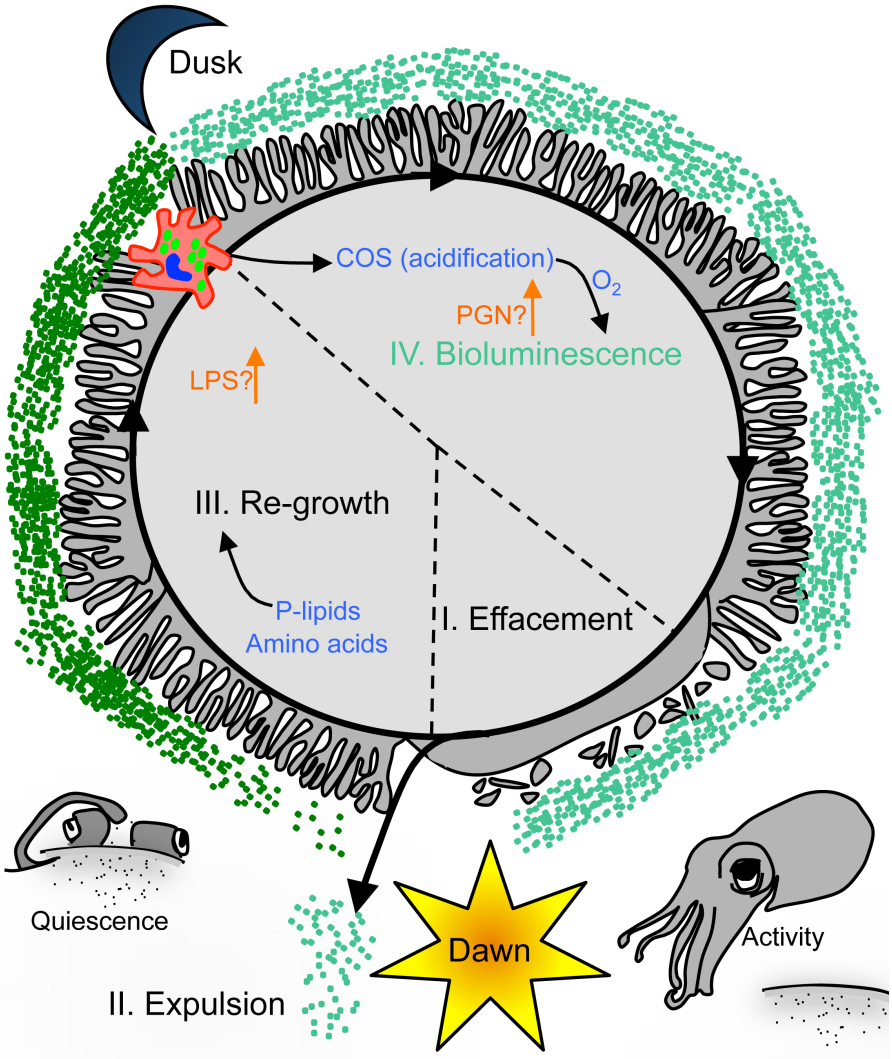
Dusk
COS (acidification)
O_2
PGN?
IV. Bioluminescence
LPS?
III. Re-growth
P-lipids
Amino acids
I. Effacement
Quiescence
Dawn
Activity
II. Expulsion

Figure 1-4. Biological rhythms of host and symbiont. The daily cycle of symbiosis is characterized by 4 stages. The physiological and behavioral attributes of this rhythm are a combination of symbiont-independent (grey/black), and symbiont-dependent (colored) events. I. Just before dawn, the microvilli at the apical surfaces of the epithelial cells efface. II. The contents of the light-organ crypts are expelled by the host. If colonized by a symbiont, the expulsion event clears the crypts of 95% of the symbiont population. III. The host microvilli, and symbiont population re-grow during the day: a period of behavioral quiescence for the squid. Host-derived nutrients, including amino acids and phospholipids (P-lipids) support this proliferative period. Just before dusk, several events take place: lipopolysaccharide (LPS) levels in the crypt are predicted to increase due to a decrease in host alkaline phosphatase production, and chitin oligosaccharide (COS)-bearing hemocytes migrate into symbiont-colonized light organ tissues. IV. At dusk, the symbiont population ferments COS, producing acid, and releasing oxygen from the host carrier protein hemocyanin. The oxygen released from hemocyanin fuels bioluminescence, while the acidification of the crypts may lead to an increase in peptidoglycan levels due to a decrease in peptidoglycan recognition protein 2 activity. The host is active in the water column during this phase, and uses symbiont bioluminescence in its behaviors.

light-organ tissues (60). In **Chapter 4** of this dissertation, I dissect the biology of this rhythm, revealing that COS are provided to the symbiont by the daily migration of hemocytes (64), which carry granules of chitin, a polymeric 'storage' form of COS, and enzymes required to hydrolyze the chitin into smaller fragments (83) (**Fig. 1-4**). The provision of COS is positively correlated with the nocturnal migration of hemocytes. The migratory behavior that begins in the first days of symbiosis (64). However, the maturation of the crypt, or perhaps education of the hemocytes, is required for the nocturnal delivery of COS to the symbiont, as the symbiont does not sense or catabolize COS in the immature crypts.

Chemical cycling in the mature symbiosis The consequence of the symbiont's metabolic rhythm is a nocturnal acidification of the crypts (**Chapter 4**). The fermentation of COS at night is sufficient to acidify the crypt (nocturnal pH ~5.7) (27, 64). Moreover, *in vitro* studies have demonstrated that the acidification of the crypt is sufficient to decrease the activities the secreted immune proteins alkaline phosphatase and PGRP2 (26, 54). Alkaline phosphatase dephosphorylates LPS, while PGRP2 degrades PGN, suggesting that acidification may lead to an increase in MAMP signaling in the crypt. In support of this hypothesis, proteomic studies of the crypt contents also reveal an abundance of oxidative stress-associated host and symbiont enzymes (84), indicative of tissue inflammation. It is yet not known whether the redox status of light-organ crypt tissues is part of the rhythmic biology of the light organ, however, such a rhythm might contribute to the symbiont-dependent peripheral circadian oscillation of the light-organ tissues.

The signs of oxidative stress in the crypt may also reflect the partitioning of oxygen between symbiont luciferase and ROS-producing host enzymes (27, 85). Supporting the latter

hypothesis, the affinity of the host oxygen carrier protein hemocyanin for oxygen decreases at acidic pH (27), potentiating the delivery of oxygen to the symbiont (**Fig. 1-4**). If the consumption of oxygen by the symbiont is not efficient (*i.e.,* if bioluminescence is not produced), then the nocturnal window of acidification may enhance the strength of oxygen-consuming antimicrobial defenses, such as phenoloxidase and/or halide peroxidase. Further characterization of the source of reactive oxygen species in the crypts promises to reveal additional rhythmic attributes of host tissue chemistry, and to inform our understanding of mechanism by which the host selects for bioluminescence.

What does the squid-vibrio symbiosis reveal about biological rhythms and mutualism? Biological rhythms are a ubiquitous characteristic of animals. Underlying these rhythms are the light-entrained oscillation of circadian clocks, as well as light-cued behaviors. The squid-vibrio symbiosis was among the first biological systems in which a microbe-dependent circadian oscillation was characterized (80). Increasingly, light-independent physiological inputs, such as the cellular redox state (78), and microbiota-dependent immune rhythms (86), have been tied to the regulation of the circadian clock. It remains to be seen how many of the mechanisms emerging to describe the microbe-dependent maintenance of tissue homeostasis, such as the modulation of gut-associated macrophage function by *n*-butyrate (87), or of dendritic cell antigen presentation by the skin microbiota (88), are coordinated by diel or circadian biological rhythms. Because the functional basis of the squid-vibrio mutualism, bioluminescence, is tied to both the stability of the symbiosis, and the entrainment of the light-organ specific circadian oscillation, this system is poised to reveal how circadian biology contributes to homeostasis between host and microbe.

CONCLUDING REMARKS

When interpreted as a negotiation between host and symbiont, the squid-vibrio mutualism reveals a chemical language that is selective, dynamic, and rhythmic. From the host perspective, the squid has demonstrated chemical strategies to select for the acquisition and maintenance of a beneficial microbe that are conserved throughout the metazoans, such as the immune-dependent structuring of the environment by antimicrobial peptides, NO, and host-associated glycans. Future studies of the immune signaling in the squid could reveal novel strategies evolved by mollusks to maintain tissue homeostasis and prevent inflammation via induction of these conserved chemical responses. From the perspective of the microbe, *V. fischeri* provides an example of how regulation of metabolic functions, in addition to MAMP signaling, tailor the tissue chemistry and immune function to support stable colonization. For example, the regulation of COS catabolism and bioluminescence are central to the acquisition, development and maintenance of *V. fischeri* in the squid light organ. As studies of the commensal microbiota shift from the descriptive to the mechanistic, a broad perspective, encompassing studies of invertebrate model systems such as the squid, will help decipher the reciprocal, and interconnected nature of symbiont stability and host tissue homeostasis.

THESIS STRUCTURE

In my dissertation, I sought to characterize the chemistry of the host tissue environment, and the metabolic accommodations of the symbiont to this environment. My dissertation research has revealed both developmental, and diel shifts in the physiology of both symbiotic partners. The thesis chapters describing this work are structured roughly in the order in which the symbiosis is initiated, and develops.

How does the acidic pH of host mucus shape the physiology of V. fischeri*?*

In **Chapter 2**, the transcriptional response of *V. fischeri* to an *in vitro* acidic mucus-rich environment is globally profiled. A comparative analysis of the pH-induced stress responses of *V. fischeri* and other seawater microbes is presented, and acid-induced resistance to the cationic antimicrobial peptide polymyxin B is highlighted as a physiological response characteristic of *V. fischeri*. The environmental and genetic basis of pH-induced polymyxin B resistance is interrogated.

At what stage of symbiotic initiation is bioluminescence required to maintain colonization?

In **Chapter 3**, chemical agonists and antagonists of *Vibrio fischeri* are characterized as specific modulators of LuxIR quorum signaling, and subsequently used to investigate the requirement for LuxIR-induced bioluminescence in the squid. The induction of LuxIR is found to be required throughout the first days of symbiosis, and this

requirement is correlated to the ability of the symbiont to produce a minimum threshold of bioluminescence

What are the metabolic requirements of V. fischeri *in the mature light organ?*

In **Chapter 4**, I characterize symbiont catabolism of the host-associated glycan chitin, in the context of symbiosis. I propose a mechanism of host-provision of chitin oligosaccharides (COS) involving the rhythmic behaviors of hemocytes. Symbiont COS catabolism is found to be sufficient to drive a nocturnal cycle of acidification, and the induction of the *V. fischeri* acid tolerance response. This acidification is proposed to support the nocturnal delivery of oxygen to the symbiont, which supports the production of oxygen-consuming symbiont bioluminescence.

How does host chitin sugars contribute to the colonization of the symbiont?

In **Chapter 5**, I interrogate the metabolic and physiological consequences of symbiont catabolism of chitin sugars. I show that these host-derived sugars are transported by the phosphoenolpyruvate-pyruvate phosphotransferase system (PTS). This transport represses three nodes of *V. fischeri* metabolism: i) non-PTS-dependent carbohydrate transport, ii) the quorum-signaling induced uptake of acetate, and iii) the respiratory consumption of oxygen. The introduction of chitin sugars into the immature light-organ crypts (a developmental state during which these sugars are not provided by the host), is shown to shift the dynamics of colonization in a manner that is consistent with the metabolic regulation described in culture.

REFERENCES

1. McFall-Ngai M*, et al.* (2013) Animals in a bacterial world, a new imperative for the life sciences. *Proc Natl Acad Sci U S A* 110(9):3229-3236.

2. Belkaid Y & Segre JA (2014) Dialogue between skin microbiota and immunity. *Science* 346(6212):954-959.

3. Nicholson JK*, et al.* (2012) Host-gut microbiota metabolic interactions. *Science* 336(6086):1262-1267.

4. Gilbert SF (2014) A holobiont birth narrative: the epigenetic transmission of the human microbiome. *Front Genet* 5.

5. Chovatiya R & Medzhitov R (2014) Stress, inflammation, and defense of homeostasis. *Mol Cell* 54(2):281-288.

6. Janeway CA (1989) Approaching the asymptote? Evolution and revolution in immunology. *Cold Spring Harbor symposia on quantitative biology*, (Cold Spring Harbor Laboratory Press), pp 1-13.

7. Mowat AM & Agace WW (2014) Regional specialization within the intestinal immune system. *Nat Rev Immunol*.

8. Hashimoto C, Hudson KL, & Anderson KV (1988) The Toll gene of Drosophila, required for dorsal-ventral embryonic polarity, appears to encode a transmembrane protein. *Cell* 52(2):269-279.

9. Nyholm SV & Graf J (2012) Knowing your friends: invertebrate innate immunity fosters beneficial bacterial symbioses. *Nat Rev Microbiol* 10(12):815-827.

10. McFall-Ngai M (2007) Adaptive immunity: care for the community. *Nature* 445(7124):153.

11. Mandel MJ (2010) Models and approaches to dissect host-symbiont specificity. *Trends Microbiol* 18(11):504-511.

12. Erkosar B, Storelli G, Defaye A, & Leulier F (2013) Host-intestinal microbiota mutualism: 'learning on the fly'. *Cell Host Microbe* 13(1):8-14.

13. Chaston J & Goodrich-Blair H (2010) Common trends in mutualism revealed by model associations between invertebrates and bacteria. *FEMS Microbiol Rev* 34(1):41-58.

14. Sycuro LK, Ruby EG, & McFall-Ngai M (2006) Confocal microscopy of the light organ crypts in juvenile Euprymna scolopes reveals their morphological complexity and dynamic function in symbiosis. *J Morphol* 267(5):555-568.

15. Stabb EV & Millikan DS (2009) Is the *Vibrio fischeri-Euprymna scolopes* symbiosis a defensive mutualism (Boca Raton, FL: Taylor and Francis).

16. McFall-Ngai M, Heath-Heckman EA, Gillette AA, Peyer SM, & Harvie EA (2012) The secret languages of coevolved symbioses: Insights from the *Euprymna scolopes-Vibrio fischeri* symbiosis. *Semin Immunol* 24:3-8.

17. Peyer SM, Pankey MS, Oakley TH, & McFall-Ngai MJ (2014) Eye-specification genes in the bacterial light organ of the bobtail squid *Euprymna scolopes*, and their expression in response to symbiont cues. *Mech develop* 131:111-126.

18. Ruby EG & Asato LM (1993) Growth and flagellation of *Vibrio fischeri* during initiation of the sepiolid squid light-organ symbiosis. *Arch Microbiol* 159(2):160-167.

19. McFall-Ngai M, Nyholm SV, & Castillo MG (2010) The role of the immune system in the initiation and persistence of the *Euprymna scolopes–Vibrio fischeri* symbiosis. *Semin Immunol*, (Elsevier), pp 48-53.

20. Rader BA & Nyholm SV (2012) Host/microbe interactions revealed through "omics" in the symbiosis between the Hawaiian bobtail squid *Euprymna scolopes* and the bioluminescent bacterium *Vibrio fischeri*. *Biol Bull* 223(1):103-111.

21. Lee KH & Ruby EG (1994) Effect of the squid host on the abundance and distribution of symbiotic *Vibrio fischeri* in nature. *Appl Environ Microbiol* 60(5):1565-1571.

22. Nyholm SV & McFall-Ngai MJ (2004) The winnowing: establishing the squid-vibrio symbiosis. *Nat Rev Microbiol* 2(8):632-642.

23. Nyholm SV, Deplancke B, Gaskins HR, Apicella MA, & McFall-Ngai MJ (2002) Roles of *Vibrio fischeri* and nonsymbiotic bacteria in the dynamics of mucus secretion during symbiont colonization of the *Euprymna scolopes* light organ. *Appl Environ Microbiol* 68(10):5113-5122.

24. Kremer N*, et al.* (2013) Initial symbiont contact orchestrates host-organ-wide transcriptional changes that prime tissue colonization. *Cell Host Microbe* 14(2):183-194.

25. Heath-Heckman EA*, et al.* (2014) Shaping the microenvironment: evidence for the influence of a host galaxin on symbiont acquisition and maintenance in the squid-vibrio symbiosis. *Environ Microbiol*. 16(12): 3669-82.

26. Troll JV*, et al.* (2010) Taming the symbiont for coexistence: a host PGRP neutralizes a bacterial symbiont toxin. *Environ microbiol* 12(8):2190-2203.

27. Kremer N*, et al.* (2014) The dual nature of haemocyanin in the establishment and persistence of the squid–Vibrio symbiosis. *Proc. R. Soc. B* 281(1785).

28. Altura MA*, et al.* (2013) The first engagement of partners in the *Euprymna scolopes*–*Vibrio fischeri* symbiosis is a two-step process initiated by a few environmental symbiont cells. *Environ Microbiol* 15(11):2937-2950.

29. Brennan CA*, et al.* (2014) A model symbiosis reveals a role for sheathed-flagellum rotation in the release of immunogenic lipopolysaccharide. *Elife* 3:e01579.

30. Yip ES, Geszvain K, DeLoney-Marino CR, & Visick KL (2006) The symbiosis regulator *rscS* controls the syp gene locus, biofilm formation and symbiotic aggregation by *Vibrio fischeri*. *Mol Microbiol* 62(6):1586-1600.

31. Mandel MJ, Wollenberg MS, Stabb EV, Visick KL, & Ruby EG (2009) A single regulatory gene is sufficient to alter bacterial host range. *Nature* 458(7235):215-218.

32. Visick KL (2009) An intricate network of regulators controls biofilm formation and colonization by *Vibrio fischeri*. *Mol Microbiol* 74(4):782-789.

33. Nyholm SV & McFall-Ngai MJ (2003) Dominance of *Vibrio fischeri* in secreted mucus outside the light organ of *Euprymna scolopes*: the first site of symbiont specificity. *Appl Environ Microbiol* 69(7):3932-3937.

34. Wang Y*, et al.* (2010) H-NOX–mediated nitric oxide sensing modulates symbiotic colonization by *Vibrio fischeri*. *Proc Natl Acad Sci U S A* 107(18):8375-8380.

35. Davidson SK, Koropatnick TA, Kossmehl R, Sycuro L, & McFall-Ngai MJ (2004) NO means 'yes' in the squid-vibrio symbiosis: nitric oxide (NO) during the initial stages of a beneficial association. *Cell Microbiol* 6(12):1139-1151.

36. Wang Y*, et al.* (2010) *Vibrio fischeri* flavohaemoglobin protects against nitric oxide during initiation of the squid–Vibrio symbiosis. *Mol Microbiol* 78(4):903-915.

37. Dunn AK*, et al.* (2010) The alternative oxidase (AOX) gene in *Vibrio fischeri* is controlled by NsrR and upregulated in response to nitric oxide. *Mol Microbiol* 77(1):44-55.

38. Septer AN, Wang Y, Ruby EG, Stabb EV, & Dunn AK (2011) The haem-uptake gene cluster in *Vibrio fischeri* is regulated by Fur and contributes to symbiotic colonization. *Environ Microbiol* 13(11):2855-2864.

39. Mandel MJ*, et al.* (2012) Squid-derived chitin oligosaccharides are a chemotactic signal during colonization by *Vibrio fischeri*. *Appl Environ Microbiol* 78(13):4620-4626.

40. Costello EK, Stagaman K, Dethlefsen L, Bohannan BJ, & Relman DA (2012) The application of ecological theory toward an understanding of the human microbiome. *Science* 336(6086):1255-1262.

41. Fraune S & Bosch TC (2007) Long-term maintenance of species-specific bacterial microbiota in the basal metazoan Hydra. *Proc Natl Acad Sci U S A* 104(32):13146-13151.

42. Koropatnick TA*, et al.* (2004) Microbial factor-mediated development in a host-bacterial mutualism. *Science* 306(5699):1186-1188.

43. Doino JA & McFall-Ngai M (1995) A transient exposure to symbiosis-competent bacteria induces light organ morphogenesis in the host squid. *Biol Bull* (189):347-355.

44. Chun CK*, et al.* (2008) Effects of colonization, luminescence, and autoinducer on host transcription during development of the squid-vibrio association. *Proc Natl Acad Sci U S A* 105(32):11323-11328.

45. Koropatnick TA, Kimbell JR, & McFall-Ngai MJ (2007) Responses of host hemocytes during the initiation of the squid-Vibrio symbiosis. *Biol Bull* 212(1):29-39.

46. Visick KL, Foster J, Doino J, McFall-Ngai M, & Ruby EG (2000) *Vibrio fischeri lux* genes play an important role in colonization and development of the host light organ. *J Bacteriol* 182(16):4578-4586.

47. Studer SV*, et al.* (2013) Non-native acylated homoserine lactones reveal that LuxIR quorum sensing promotes symbiont stability. *Environ Microbiol* (doi:10.1111/1462-2920.12322).

48. Altura MA, Stabb E, Goldman W, Apicella M, & McFall-Ngai MJ (2011) Attenuation of host NO production by MAMPs potentiates development of the host in the squid–vibrio symbiosis. *Cell Microbiol* 13(4):527-537.

49. Koropatnick T, Goodson MS, Heath-Heckman EA, & McFall-Ngai M (2014) Identifying the cellular mechanisms of symbiont-induced epithelial morphogenesis in the squid-vibrio association. *Biol Bull* 226(1):56-68.

50. Troll JV*, et al.* (2009) Peptidoglycan induces loss of a nuclear peptidoglycan recognition protein during host tissue development in a beneficial animal-bacterial symbiosis. *Cell Microbiol* 11(7):1114-1127.

51. Foster JS & McFall-Ngai MJ (1998) Induction of apoptosis by cooperative bacteria in the morphogenesis of host epithelial tissues. *Dev Genes Evol* 208(6):295-303.

52. Foster JS, Apicella MA, & McFall-Ngai MJ (2000) *Vibrio fischeri* lipopolysaccharide induces developmental apoptosis, but not complete morphogenesis, of the *Euprymna scolopes* symbiotic light organ. *Dev Biol* 226(2):242-254.

53. Doino Lemus J & McFall-Ngai MJ (2000) Alterations in the proteome of the *Euprymna scolopes* light organ in response to symbiotic *Vibrio fischeri*. *Appl Environ Microbiol* 66(9):4091-4097.

54. Rader BA, Kremer N, Apicella MA, Goldman WE, & McFall-Ngai MJ (2012) Modulation of symbiont lipid A signaling by host alkaline phosphatases in the squid-vibrio symbiosis. *mBio* 3(3).

55. Graf J & Ruby EG (1998) Host-derived amino acids support the proliferation of symbiotic bacteria. *Proc Natl Acad Sci U S A* 95(4):1818-1822.

56. Dunn AK (2012) *Vibrio fischeri* metabolism: symbiosis and beyond. *Adv Microb Physiol* 61:37.

57. Miyashiro T & Ruby EG (2012) Shedding light on bioluminescence regulation in *Vibrio fischeri*. *Mol microbiol* 84(5):795-806.

58. Boettcher KJ & Ruby EG (1995) Detection and quantification of *Vibrio fischeri* autoinducer from symbiotic squid light organs. *J Bacteriol* 177(4):1053-1058.

59. Lamarcq LH & McFall-Ngai MJ (1998) Induction of a gradual, reversible morphogenesis of its host's epithelial brush border by *Vibrio fischeri*. *Infect Immun* 66(2):777-785.

60. Wier AM*, et al.* (2010) Transcriptional patterns in both host and bacterium underlie a daily rhythm of anatomical and metabolic change in a beneficial symbiosis. *Proc Natl Acad Sci U S A* 107(5):2259-2264.

61. Giles DK, Hankins JV, Guan Z, & Trent MS (2011) Remodelling of the *Vibrio cholerae* membrane by incorporation of exogenous fatty acids from host and aquatic environments. *Mol Microbiol* 79(3):716-728.

62. Pride AC, Herrera CM, Guan Z, Giles DK, & Trent MS (2013) The outer surface lipoprotein VolA mediates utilization of exogenous lipids by *Vibrio cholerae*. *MBio* 4(3):e00305-00313.

63. Saito HE, Harp JR, & Fozo EM (2014) Incorporation of exogenous fatty acids protects *Enterococcus faecalis* from membrane-damaging agents. *Appl Environ Microbiol* 80(20):6527-6538.

64. Schwartzman JA*, et al.* (2015) The chemistry of negotiation: Rhythmic, glycan-driven acidification in a symbiotic conversation. *Proc Natl Acad Sci U S A* 112(2):566-571.

65. Miyashiro T*, et al.* (2011) The *N*-acetyl-d-glucosamine repressor NagC of *Vibrio fischeri* facilitates colonization of *Euprymna scolopes*. *Mol Microbiol* 82(4):894-903.

66. Koch EJ, Miyashiro TI, McFall-Ngai MJ, & Ruby EG (2013) Features governing symbiont persistence in the squid-vibrio association. *Mol Ecol* (doi:10.1111/mec.12474).

67. Schleicher TR, VerBerkmoes NC, Shah M, & Nyholm SV (2014) Colonization state influences the hemocyte proteome in a beneficial squid–vibrio symbiosis. *Mol Cell Proteom* 13(10):2673-2686.

68. Nyholm SV, Stewart JJ, Ruby EG, & McFall-Ngai MJ (2009) Recognition between symbiotic *Vibrio fischeri* and the haemocytes of *Euprymna scolopes*. *Environ Microbiol* 11(2):483-493.

69. Provenzano D, Schuhmacher DA, Barker JL, & Klose KE (2000) The virulence regulatory protein ToxR mediates enhanced bile resistance in *Vibrio cholerae* and other pathogenic*Vibrio* species. *Infect immun* 68(3):1491-1497.

70. Cox LM*, et al.* (2014) Altering the intestinal microbiota during a critical developmental window has lasting metabolic consequences. *Cell* 158(4):705-721.

71. Cullen T*, et al.* (2015) Antimicrobial peptide resistance mediates resilience of prominent gut commensals during inflammation. *Science* 347(6218):170-175.

72. Boettcher K, Ruby E, & McFall-Ngai M (1996) Bioluminescence in the symbiotic squid *Euprymna scolopes* is controlled by a daily biological rhythm. *J Comp Physiol* 179(1):65-73.

73. Wollenberg MS & Ruby EG (2012) Phylogeny and fitness of *Vibrio fischeri* from the light organs of *Euprymna scolopes* in two Oahu, Hawaii populations. *ISME* 6(2):352-362.

74. Montgomery MK & McFall-Ngai MJ (1998) Late postembryonic development of the symbiotic light organ of *Euprymna scolopes* (Cephalopoda: Sepiolidae). *Biol Bull* 195(3):326-336.

75. Montgomery MK & McFall-Ngai M (1994) Bacterial symbionts induce host organ morphogenesis during early postembryonic development of the squid *Euprymna scolopes*. *Development* 120(7):1719-1729.

76. Bass J & Takahashi JS (2010) Circadian integration of metabolism and energetics. *Science* 330(6009):1349-1354.

77. Hoyle NP & O'Neill JS (2014) Oxidation-reduction cycles of peroxiredoxin proteins and non-transcriptional aspects of timekeeping. *Biochemistry*. 54(2):184-93.

78. Edgar RS*, et al.* (2012) Peroxiredoxins are conserved markers of circadian rhythms. *Nature* 485(7399):459-464.

79. Nyholm SV & McFall-Ngai MJ (1998) Sampling the light-organ microenvironment of *Euprymna scolopes*: description of a population of host cells in association with the bacterial symbiont *Vibrio fischeri*. *Biol Bull* 195(2):89-97.

80. Heath-Heckman EA*, et al.* (2013) Bacterial bioluminescence regulates expression of a host cryptochrome gene in the squid-vibrio symbiosis. *mBio* 4(2).

81. Singley C (1983) *Euprymna scolopes*. Cephalopod Life Cycles: Species accounts 1:69.

82. Claes MF & Dunlap PV (2000) Aposymbiotic culture of the sepiolid squid *Euprymna scolopes*: role of the symbiotic bacterium *Vibrio fischeri* in host animal growth, development, and light organ morphogenesis. *J Exp Zool* 286(3):280-296.

83. Heath-Heckman EA & McFall-Ngai MJ (2011) The occurrence of chitin in the hemocytes of invertebrates. *Zoology* 114(4):191-198.

84. Schleicher TR & Nyholm SV (2011) Characterizing the host and symbiont proteomes in the association between the bobtail squid, *Euprymna scolopes*, and the bacterium, *Vibrio fischeri*. *PloS One* 6(10):e25649.

85. Small AL & McFall-Ngai MJ (1999) Halide peroxidase in tissues that interact with bacteria in the host squid Euprymna scolopes. *J Cell Biochem* 72(4):445-457.

86. Mukherji A, Kobiita A, Ye T, & Chambon P (2013) Homeostasis in intestinal epithelium is orchestrated by the circadian clock and microbiota cues transduced by TLRs. *Cell* 153(4):812-827.

87. Chang PV, Hao L, Offermanns S, & Medzhitov R (2014) The microbial metabolite butyrate regulates intestinal macrophage function via histone deacetylase inhibition. *Proc Nat Acad Sciences U S A* 111(6):2247-2252.

88. Naik S*, et al.* (2015) Commensal-dendritic-cell interaction specifies a unique protective skin immune signature. *Nature*.

Chapter 2

Acidic pH cues resistance to polymyxin B stress in the microbial symbiont *Vibrio fischeri*

PREFACE:

JAS planned the experiments, performed the experiments (with help from Lawrence Zhou), analyzed the data, and wrote the chapter.

ABSTRACT

To better understand the contribution of acidic pH to the symbiosis-associated physiology of *V. fischeri*, I performed global transcriptional analysis of cultured *Vibrio fischeri* at different pH values. I demonstrate that, upon contact with acidic mucus, *V. fischeri* induces a physiological response originating from regulation of several encoded resistance genes, including putative phosphoethanoloamine transferase *eptA*. The involvement of *eptA* suggests that the mechanism of *V. fischeri* polymyxin B (PMB) resistance may be similar to that of *S. typhimurium,* which modifies its lipid A with phosphoethanolamine, changing the electrochemical properties of this membrane component. A transposon screen to identify regulatory elements and alternate PMB resistance elements identified putative components of the sigma-E regulated envelope-stress response. In addition, two transcription factors were identified that contribute to PMB resistance, but do not regulate *eptA,* suggesting that polymyxin resistance may be the result of *eptA*-dependent and independent pathways. Characterization of this response has revealed key differences between pH-responsive regulation between *V. fischeri* and other Gram-negative microbes.

INTRODUCTION:

Acidic pH is often a cue associated with the transition of microbes into a host-associated state, and this cue coordinates the induction of stress responses that facilitate colonization (1-3). In the case of gastrointestinal pathogens, such as *Escherichia coli, Salmonella typhimurium*, and *Vibrio cholerae*, exposure to sub-lethal amounts of acid promote survival upon transit through the extremely low pH of the stomach (4). In addition to resistance to acid-linked stress, mildly acidic pH can also cue the induction of virulence factors, as well as other stress responses (a strategy called cross protection). Thus, acidic pH is an important cue that can mediate multiple aspects of microbial physiology in the context of a host environment.

Cationic antimicrobial peptides (CAP) are a prominent constituent of the innate immune defenses of metazoans (5-7). Intracellular pathogens such as *S. typhimurium* must contend with CAP within phagocytic vacuoles (8), however extracellular microbes, such as the constituents of the gut microbiota (5), also encounter CAP. Microbial community structure is shaped by environmental cues, and acidic pH, as well as CAP, are both attributes of the epithelial tissue environment (9, 10). The responses of beneficial microbes to acid are under-studied, and acid-induced physiological responses represent an important window into understanding the conserved mechanisms by which the microbiota maintains homeostasis, or falls into dysbiosis, in response to host ecology (11).

The *Euprymna scolopes*-*Vibrio fischeri* symbiosis presents a model system well suited to study the contribution of acidic pH to microbial homeostasis. The symbiosis takes place in the squid's light organ, and the association is established by horizontal transmission: the specific symbiont is selected from the bacterioplankton by the host (12). The transition from

the bacterioplankton to the host takes place in several stages; however, the first host environment sensed by the symbiont is acidic host mucus outside of the light organ (2)(**Fig. 2-1*A***). I hypothesized that acidic pH is a factor that contributes to the initial and continued selection for the specific symbiont (2). To test the hypothesis that acidic pH induces cross-protection against host-associated stressors, I characterized the *V. fischeri* acid-responsive transcriptome in the context of seawater. I demonstrate that the acid-induced resistance of *V. fischeri* to the cationic antimicrobial peptide polymyxin B (PMB) is a transcriptionally regulated response that involves the *eptA* gene. the results present the framework for characterization of the *V. fischeri* acid-induced stress response, and represent the first step toward situating this response in the context of the host environment.

MATERIALS AND METHODS:

Bacterial strains and growth conditions Bacterial strains and plasmids used in this work are listed in **Table 2-1**. *Escherichia coli* was cultured at 37 °C with shaking at 250 rpm in Luria-Bertani medium (LB) (13), with 150 μg mL^{-1} erythromycin, 25 μg/mL chloramphenicol or 50 μg mL^{-1} kanamycin. Unless otherwise noted, *V. fischeri* was grown in Luria-Bertani salt medium (LBS) at 28 °C. Unless otherwise noted, cultures were aerated by shaking at 225 rpm in an incubated chamber (New Brunswick), with 5 μg mL^{-1} erythromycin, 5 μg/mL chloramphenicol or 100 μg mL^{-1} kanamycin where indicated. All *Vibrio fischeri* mutant strains were derived from isolate ES114 (14, 15).

Table 2-1. Strains and plasmids used in this study

Strain or plasmid	Description	Reference
V. fischeri		
ES114	Wild-type *E. scolopes* light-organ isolate	(14)
MJ11	Wild-type isolate from *Monocentris japonica* light organ	(16, 17)
JG01	Δ*ompU* (VF_0475) in ES114	Joe Graber
KV2507	*ompR::erm* (VF_0114) insertional mutant	(18)
JAS340	Δ*eptA* (VF_A0210) in ES114	This work
MB06256	VF_A0176 Tn::*erm*	This work
MB13215	VF_2503 Tn::*erm*	This work
MB13278	VF_2503 Tn::*erm*	This work
MB13555	VF_2503 Tn::*erm*	This work
Seawater isolates		
KNH1	*Vibrio parahaemolyticus*	(19)
NK_St13	*Vibrio azureus*-like	(20)
Lna	*Photobacterium leiognathi*	(21)
CNJ771	*Exiguobacterium aestuartii*-like	(22)
E. coli		
DH5a-λpir	F^- φ80*lacZ*Δ*M15* Δ(*lacZYFargF*)U169 *supE44 deoR hsdR17 recA1 endA1 gyrA96 thi-1 relA1*, lysogenized with λ*pir*	(23)
β-3914	F^- RP4-2-Tc::Mu Δ*dapA*::(*erm-pir*)	(24)
Plasmids		
pVSV105	Cm^r, *lacZ*α-(SphI, SalI/HincII, XbaI, SmaI/XmaI, KpnI, SacI)	(25)
pEVS104	R6Kori RP4 *oriT trb tra* Kn^r	(26)
pKV363	Mobilizable suicide vector; Cm^r; pSW7848 + multiple cloning site	(27)
pTM267	Two-color fluorescent reporter, *mCherry* expressed by the *tetA* promoter, *GFP* downstream of a multiple cloning site, Cm^r	(28)
pJAS340	Δ*eptA*::pKV363	This work
pJAS341	*eptA::*pVSV105	This work
pJAS342	*eptA'::GFP tetA'::mCherry* in pTM267	This work
pJAS343	*ompU'::GFP tetA'::mCherry* in pTM267	This work

Sample collection, RNA extraction and transcriptional analysis.

Growth of the cells To assess the transcription of *V. fischeri* in an environment approximating the squid's mucus, strain ES114 was cultured in an artificial seawater medium (ASW: 0.3 M NaCl, 0.05 M $MgSO_4$-$7H_2O$, 0.01 M $CaCl_2$-$2H_2O$, 0.01 M KCl) containing 50 mM PIPES buffer and 0.1% hog gastric mucin (HGM, w/v, 1% bound sialic acid, Sigma #M2378). The

medium was buffered at pH 6.5 or pH 8.0, to characterize transcription in response to acidic pH. Triplicate overnight cultures of ES114 in LBS were diluted 1:100 into 25 mL high osmolarity seawater tryptone medium (SWTO, (29)) in 125 mL flasks, and grown with shaking at 225 rpm at 28 °C. When the cultures reached 0.60 +/- 0.05 optical density (600 nm, 1 cm-path length), they were centrifuged for 8 min at 6000 rcf and at 4 °C to pellet the cells. The supernatants were aspirated, and the pellets were resuspended in 25 mL of pH 8.0 50 mM PIPES ASW, again in a 125 mL flask. Cultures were incubated for 1 h at 28 °C with shaking at 225 rpm. The cultures were spun again to pellet cells (as before), and this time, the pellet was resuspended in 1 mL of pH 8.0 50 mM PIPES ASW. 500 µL of this resuspension was used to inoculate 15 mL of 0.1% HGM 50 mM PIPES ASW, buffered at pH 6.5 or at pH 8.0. Cultures were incubated for 2 h in 125 mL flasks at 28 °C with shaking at 225 rpm. The cultures were centrifuged once more, and the pellet was resuspended in 4 mL RNAlater (Life Technologies). Cultures contained 2.5 x 10^8 CFU/mL +/- 5%.

Isolation of RNA Cells suspended in RNA later were pelleted by centrifugation at 5000 rcf and 4 °C for 5 minutes. A RNeasy mini kit (Qiagen) was used to extract RNA, according to the manufacturer's instructions. Samples were eluted in RNase-free water, and treated with RQ-DNase (Promega), according to the manufacturer's instructions. An on-column sample cleanup was performed, following the protocol outlined in the RNeasy mini kit. Samples were at least 1 µg/µL, with absorbance ratios at 260:280 and 260:230 nm >2.1. Samples were submitted to the University of Wisconsin-Madison Gene Expression Center for further quality assessment using an Agilent RNA NanoChip. 10 µg of total RNA was used for cDNA

synthesis, following protocols defined by NimbleGen array analysis (Roche NimbleGen). cDNA was submitted to NimbleGen for prokaryotic gene expression microarray analysis. The expression values were processed to yield the fold change in expression between experimental conditions using ArrayStar software (DNAStar, Madison, WI). Differential regulation was defined as >2-fold difference in gene expression between the two conditions with at least 95% confidence. The linear correlation in signal intensities between the two conditions was 0.97. BLAST2GO software (BioBam Bioinformatics Solutions) was used to perform functional enrichment analysis of the dataset based on gene ontology classification.

Quantitative RT-PCR procedures were conducted in accordance with the MIQE guidelines (30). Primers were designed by OligoAnalyzer software (Integrated DNA Technologies) with a 60 °C annealing temperature. Primer pair efficiencies were between 95 and 105%. Candidate gene expression was normalized using the geometric mean of *polA*, a previously defined endogenous control gene (31), whose expression was confirmed to be invariant between the conditions compared in this experiment. The distribution of the data was measured by Shapiro's test (all data fit a normal distribution), and a two-way ANOVA with post-hoc Bonferroni comparison was used to compare gene expression among time points, and between colonization states.

Minimum Inhibitory Concentration (MIC) assay. MIC assays were performed in *V. fischeri* based on previously described protocols (20, 32). To assay for pH-dependent resistance to various stressors, MIC assays were set up in pH 6.5 or 8.0 PIPES MIC buffer (50 mM $MgSO_4$, 10 mM $CaCl_2$, 300 mM NaCl, 10 mM KCl, 10 mM PIPES)(20). Two-fold serial

dilutions of stressors of interest (starting concentrations: 0.26 mg/mL PMB, 0.003% H_2O_2, 1% NaOCl solution (Sigma 425044), or 1% sodium dodecyl sulfate were set up in 96-well plates containing 90 µL total volume. The bacterial cultures (**Table 2-1**) were started in SWT medium (14), at 28°C, and grown to an OD600 of 0.10 +/- 0.02. Cultures were diluted 1:100 into 3 mL PIPES buffer at pH 8.0, and incubated for 3 h 28°C with 225 rpm shaking. Another 1:100 dilution into SWT was performed upon completion of the 3 h incubation and 10 µL of the bacterial culture was added to the 90 µL of pH 6.5 or 8.0 PIPES MIC buffer plus stressor. The plates were incubated under static conditions at 28°C and checked at 24 h for colony formation at the bottom of the plate, and any turbidity in the wells. Inoculation levels that fell between 10 and 100 colony-forming units per well were found to produce consistent MIC values. All MIC assays reported in this chapter fell within this acceptable starting inoculum range.

Molecular techniques.

Construction of a clean deletion of Δ*eptA.* An in-frame deletion of *V. fischeri eptA* was constructed using a previously described strategy (24, 26, 27), by CcdB-toxin mediated double homologous recombination, using a *V. fischeri*-specific suicide vector pKV363 (**Table 2-1**). Briefly, segments above and below the coding region were amplified, and ligated together using a unique restriction enzyme site. The resulting chimeric DNA was ligated directionally into the pKV363 backbone at EcoRI and SpeI restriction sites. Conjugative transfer was used to introduce the plasmid into *V. fischeri* ES114, and the double crossover of the resultant chloramphenicol-resistant integrant (*i.e.,* the deletion of the gene), was selected

for by arabinose induction of the CcdB toxin encoded on the pKV363 plasmid backbone. The in-frame deletion left a lesion consisting of 9 nucleotides of 5' coding region, and 6 nucleotides of 3' coding region, joined by a 6-nucleotide restriction enzyme recognition site. The deletion was confirmed by sequencing around the *eptA* locus.

*Construction of complementation vector*s To test whether the addition of the native promoter and coding region of a mutated gene could restore a phenotype of interest, the intact locus was amplified from wild-type *V. fischeri*, and cloned into the plasmid pVSV105: a shuttle vector carrying an origin of replication derived from a *V. fischeri*-specific plasmid pES213 (25). Cloning was carried out in the *E. coli* strain DH5α-λ pir. The resultant vector was introduced into *V. fischeri* by pEVS104-assisted conjugation (26).

Construction of two-color fluorescent reporters The region 400 bp upstream and 200 bp downstream of the predicted translational start sites of the *eptA* gene was amplified, and cloned into XmaI and XbaI sites of the of plasmid pTM267 (**Table 2-1**). The plasmid encodes a constitutively activated copy of red fluorescent protein mCherry, as well as gene encoding GFP, downstream of multiple cloning site (MCS) (28). The insertion of the putative promoter region into the MCS of pTM267 results in the promoter-dependent transcription of *GFP*. The reporter plasmid is maintained at ~10 copies per cell, and encodes *mCherry* transcribed from a constitutively active *tetA* promoter. The expression of GFP is linked to a promoter of interest.

Screening of an arrayed transposon mutant library for genetic components of PMB resistance. I screened 13,686 mutants of an existing 23,904 strain library (33), for a loss of resistance to PMB (Sigma 81334). Briefly, a pin replicator was used to inoculate 96-well

plates containing 100 µL of LBS-erm from frozen glycerol stocks of the 'A' plates created in the original screen. After overnight growth, the pin replicator was used to inoculate fresh 96-well plates containing 100 µL pH 6.5 SWTO with the LBS-erm overnight cultures. The plates were placed on a shaker, for 3 h at 28 °C prior to being used to inoculate 100 µL pH 6.5 PIPES MIC buffer containing 10 % SWT medium, with and without 8 µg/mL PMB, in a round-bottomed 96-well plate. Plates were incubated under static conditions overnight at 28 °C, prior to assessment of growth in the presence and absence of PMB. Five microliters of culture material from strains of interest were combined with 95 µL of elution buffer (Qiagen), and frozen at -20 °C to create template mixes for arbitrarily primed PCR. Arbitrarily primed PCR was performed as described previously (33), with the addition of ExoSAP-IT treatments (Affymetrix), following the manufacturer's instructions between successive rounds of PCR to remove excess single-strand oligonucleotide primers. Amplified reactions were sent for Sanger sequencing at the University of Wisconsin-Madison Gene Expression Center.

Two-color fluorescent reporters. To monitor promoter activity in response to pH, and other environmental cues, strains carrying reporter plasmids were grown to an OD of 0.60 +/- 0.05 in LBS with appropriate selection. 1 mL of this culture was centrifuged for 1 min at 10,000 rcf to pellet the cells, and the cell pellet was resuspended in 0.5 mL of PIPES MIC buffer, modified by adjusting pH, cation concentrations, or adding stressors, as indicated in the text. Duplicate 200 µL aliquots of cell suspension were added to a 96-well plate, and the plate was incubated with shaking for 3 h at 28 °C.A Tecan Genios Pro plate reader (Tecan Group, Mannedorf Switzerland), was used to monitor the accumulation of GFP (485 nm and 535 nm

excitation/emission filter sets) and mCherry (535 nm and 612 nm ex/em), in the pTM267-based transcriptional reporter constructs. Non-fluorescent ES114 was used as a control for autofluorescence, and emission values obtained from this sample were subtracted from experimental measurements.

RESULTS

pH-induced transcription in *V. fischeri*. To simulate the transcriptional response that is induced by planktonic *V. fischeri* upon transition from pH 8.0 seawater to pH 6.5 mucus, I performed a global gene expression analysis. Seventy-seven genes were differentially regulated more than 2-fold with 95% confidence (**Fig. 2-1*B*, Table 2-2**). I validated the differential expression of a subset of these genes using qRT-PCR (**Fig. 2-1*C***). An assessment of gene ontology classifications revealed a significant functional enrichment in membrane-associated transcripts (**Table 2-3**). These open-reading frames represented 18 of 35 GO annotations in the microarray, but only 670 annotations of 2646 GO terms represented in the ES114 genome (GO-ID:0016020; Fisher's Exact test: P=0.004, FDR=0.88). Thus, upon exposure to an acidic mucus environment, such as the first contact with the host, *V. fischeri* modulates transcription of genes associated with membrane function.

Contribution of pH to induction of acid-independent stress responses. I hypothesized that the transcriptional regulation of membrane-associated genes in response to acidic pH might reflect the induction of responses protective against host-associated stressors. I tested

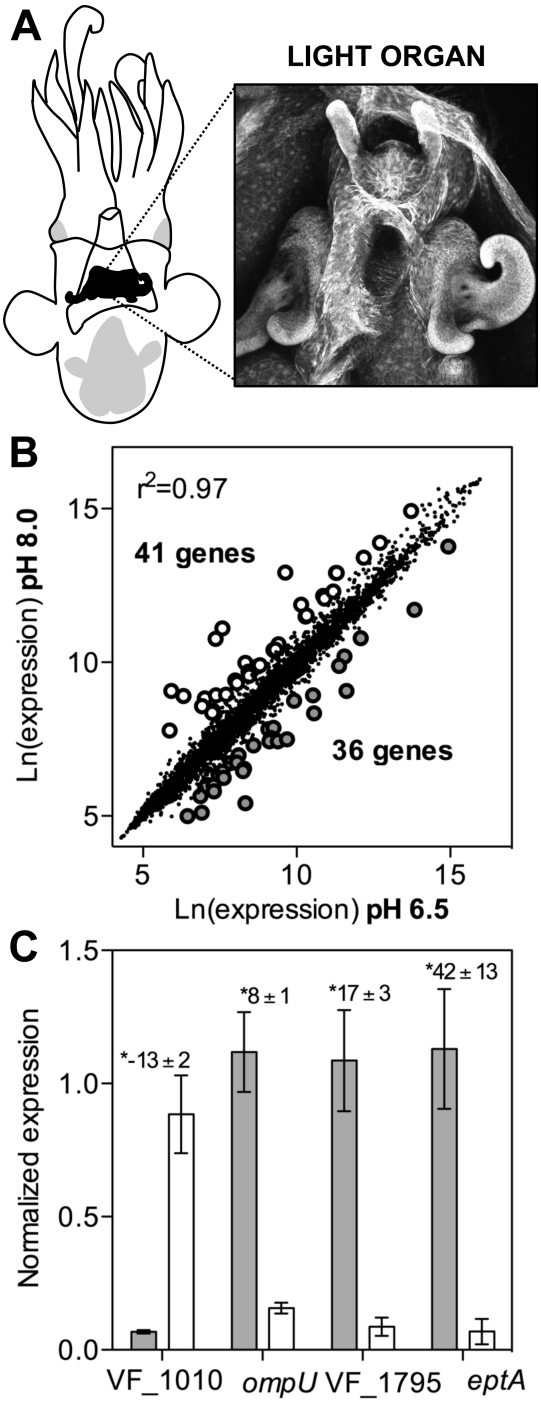
A
LIGHT ORGAN
B
r2=0.97
41 genes
36 genes
Ln(expression) pH 8.0
Ln(expression) pH 6.5
5
10
15
C
Normalized expression
0.0
0.5
1.0
1.5
*-13 ± 2
*8 ± 1
*17 ± 3
*42 ± 13
VF_1010
ompU
VF_1795
eptA

Figure 2-1. Sites at which *V. fischeri* encounters acidic pH, and genes induced in response to acidic pH. ***A***) The light organ of *V. fischeri* (Left: indicated in black under the squid's mantle), is an organ with bilateral symmetry. In newly hatched squid, ciliated fields are present on either side of the light organ. The ciliated these fields promote the harvesting of *V. fischeri* from the bacterioplankton during ventilation of the mantle. Upon exposure to peptidoglycan, the surfaces of the ciliated fields secrete mucus, which is acidic (~pH 6.5). ***B***) A comparison of *V. fischeri* transcripts expressed in pH 8.0 or 6.5 seawater containing mucins (a mimic of the environment encountered upon first contact with the host), reveals a linear correlation between populations of RNA (r^2=0.97), as well as a subset of genes differentially expressed greater than 2-fold (open circles). The expression of 41 genes is greater at pH 8.0 than pH 6.5, while the expression of 36 genes is greater at pH 6.5 than pH 8.0. Data represent an analysis of 3 independent pools of RNA. ***C***) qRT-PCR was used to validate the pH-dependent transcription of a subset of genes identified in the microarray, using the same growth conditions (grey bars, pH 6.5; open bars, pH 8.0; error represents SD; n=6 biological replicates; numbers above bars indicate the fold change in expression between pH 6.5 and pH 8.0 +- standard deviation, *polB* (VF_0074), was used as an endogenous control gene).

Table 2-2. Genes differentially regulated by exposure to acidic pH in seawater

VF_ID	Gene	Predicted Function	Fold Δ 6.5/8.0
VF_0041	*mdtL*	Multidrug efflux system protein	-2.14
VF_0150	-	Hypothetical protein	2.14
VF_0406	*pyrB*	Aspartate carbamoyltransferase	-2.28
VF_0461	-	Sodium-dependent phosphate transporter	2.06
VF_0472	*carA*	Carbamoyl phosphate synthase small subunit	-2.17
VF_0475	*ompU*	OmpU, outer membrane protein	4.36
VF_0804	*asnB*	Asparagine synthetase B	-2.03
VF_0828	*znuB*	Zinc ABC transporter membrane protein	2.13
VF_0829	*znuC*	Zinc ABC transporter ATP-binding protein	2.39
VF_0830	*znuA*	Zinc ABC transporter periplasmic substrate-binding protein	2.48
VF_0831	*yebA*	Peptidase	2.02
VF_0833	*feoA*	Ferrous iron transport protein A	3.89
VF_0834	*feoB*	bifunctional ferrous iron transporter, protein B/ GTP-binding protein/membrane protein	2.58
VF_1010	-	Putative porin	-11.51
VF_1011	-	Putative porin	-2.29
VF_1067	*yqjF*	Quinol oxidase subunit	-10.51
VF_1068	-	Pirin	-9.80
VF_1069	-	Hypothetical protein	-8.87
VF_1076	-	Sulfite-dehydrogenase	-2.38
VF_1077	*nirV*	Formylglycine-generating sulfatase NirV	-3.52
VF_1147	*cstA*	Peptide transporter induced by carbon starvation	-6.00
VF_1160	*sscR*	6-pyruvoyl tetrahydrobiopterin synthase	2.84
VF_1373	-	Putative Fe2+/Mn2+ transporter	2.24
VF_1374	*ybgK*	Allophanate hydrolase subunit 2	2.61
VF_1375	*ybgJ*	Allophanate hydrolase subunit 1	4.56
VF_1376	*ybgL*	LamB/YcsF family protein	4.64
VF_1377	-	Hypothetical protein	5.88
VF_1410	*abgT*	Aminobenzoyl-glutamate transporter	-2.19
VF_1513	*ydjN*	Sodium:dicarboxylate symporter family protein YdjN	-2.15
VF_1522	*zntA*	Zinc/cadmium/mercury/lead-transporting ATPase	-3.09
VF_1597	*oppA*	Oligopeptide-binding protein OppA	-2.17
VF_1795	*ompC*	Outer membrane protein OmpC	16.58
VF_2042	-	Methyl-accepting chemotaxis protein	-2.14
VF_2150	*sfuB*	Iron(III)-transport system permease SfuB	2.11
VF_2151	-	Iron(III) ABC transporter periplasmic binding protein	2.46
VF_2157	-	Glycerate kinase	-2.03
VF_2220	-	Ubiquinol-cytochrome c reductase iron-sulfur subunit	-2.45

VF_ID	Gene	Predicted Function	Fold Δ 6.5/8.0
VF_2265	*leuO*	Leucine transcriptional activator	3.03
VF_2394	*purH*	Bifunctional phosphoribosylaminoimidazolecarboxamide formyltransferase/IMP cyclohydrolase	-2.05
VF_2446	*fliL2*	Flagellar basal body protein FliL	2.20
VF_2458	-	Hypothetical protein	2.04
VF_2492	*scsC*	Copper sensitivity protein ScsC	2.19
VF_2520	-	Cytochrome c5	-2.40
VF_2527	*ilvC*	Ketol-acid reductoisomerase	2.50
VF_2528	*ilvC*	Ketol-acid reductoisomerase	2.01
VF_A0070	-	Lipoprotein	2.06
VF_A0124	*tppB*	Di-/tripeptide transporter permease	28.40
VF_A0210	*eptA*	Metal-dependent hydrolase	67.03
VF_A0371	-	Hypothetical protein	2.12
VF_A0447	-	Methyl-accepting chemotaxis protein	2.21
VF_A0610	-	Hypothetical protein	7.51
VF_A0738	-	Hypothetical protein	2.60
VF_A0748	*bioA*	Adenosylmethionine-8-amino-7-oxononanoate aminotransferase	-2.93
VF_A0852	*ydcR*	Fused DNA-binding transcriptional regulator/ amino transcriptional regulatory protein	-3.76
VF_A0863	*hcp*	Hydroxylamine reductase	3.47
VF_A0995	-	High-affinity iron permease	2.75
VF_A1112	*lysE*	Amino acid transporter LysE	-3.14
VF_B23	-	Hypothetical protein	-2.15
VF_B24	-	Putative conjugative region transfer protein	-2.13
VF_B27	-	Hypothetical protein	-2.11
VF_B28	-	Hypothetical protein	-2.06
VF_B30	-	Putative type II secretion component PulF	-2.01
VF_B37	-	Hypothetical protein	-2.40
VF_B38	-	Attachment mediating protein VirB2-like protein	-2.30
VF_B46	-	DNA topoisomerase III	-2.10
VF_B47	-	OmpA-like outer membrane protein	-2.13
VF_B48	-	Hypothetical protein	-2.21

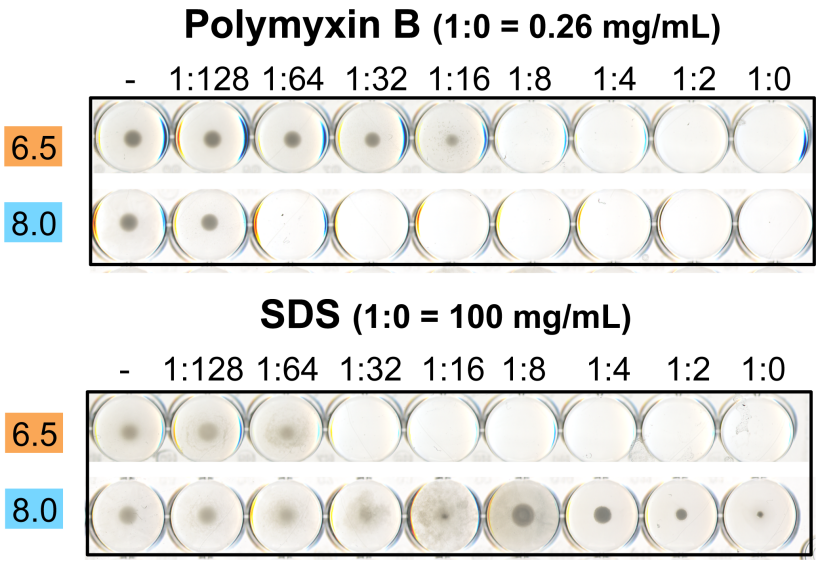

Figure 2-2. pH-dependent responses of *V. fischeri* to membrane-associated stress. MIC assays of *V. fischeri* ES114 are shown for PMB and sodium dodecyl sulfate (SDS). The assays were performed in pH 6.5 or 8.0 MIC assay buffer. Prior to assay, cells were incubated for 3 h in pH 8.0 PIPES MIC buffer. Data are representative of at least four biological replicates.

this prediction by determining whether exposure to acidic pH enhanced the minimum inhibitory concentration (MIC) of hydrogen peroxide, sodium hypochlorite, nitric oxide, and PMB (a cationic antimicrobial peptide) for *V. fischeri* (**Table 2-4**). The pH range of the assay (pH 8.0-6.5) is not sufficient to change the charge of any of the stressors. Moreover, the addition of the stressors did not change the pH of the experimental medium. Thus, any difference in growth was assumed to reflect a pH-dependent change in *V. fischeri* physiology. MIC assays revealed that, relative to pH 8.0, a mildly acidic pH (6.5) enhanced the survival of *V. fischeri* in the presence of PMB (**Table 2-4, Fig. 2-2**). Acidic pH also made a modest, although not statistically significant, contribution to hydrogen peroxide sensitivity and hypochlorous acid resistance (**Table 2-4**), but did not change the toxicity of nitric oxide. I also tested the pH-dependence of *V. fischeri* ES114 in response to another source of membrane stress: the anionic detergent sodium dodecyl sulfate (SDS, **Fig. 2-2**). The strain was significantly more sensitive to SDS killing at pH 6.5, relative to pH 8.0. Collectively, these results indicate that acidic pH does not modulate resistance to known stressors present in the mucus, such as reactive oxygen species, but does change the resilience of *V. fischeri* to charged membrane stressors, such as PMB and SDS. I hypothesize that the opposite effects of acidic pH on PMB and SDS resistance reflects a link between environmental pH and a modification of the electrostatic properties of the membrane.

To determine whether pH-dependent stress resistance is a common attribute of other constituents of the marine bacterioplankton, I performed MIC assays on a taxonomically diverse assortment of seawater microbes, including strains of *V. fischeri* isolated from squid,

and fish (*V. fischeri* strains ES114 and MJ11, respectively), other *Vibrio* spp. (*Vibrio azureus*

Table 2-3. Differentially expressed genes associated with membrane function

VF_ID	Gene	Function	Fold Δ (8.0/6.5)	qRT-PCR
VF_0041	***mdtL***	**Multidrug efflux protein**	2.1	
VF_0150	**-**	**Hypothetical**	-2.1	
VF_0461	**-**	**Sodium-dependent phosphate transporter**	**-2.1**	
VF_0475	*ompU*	Outer membrane protein	-4.4	-7.5
VF_0828	***znuB***	**Zinc ABC transporter membrane protein**	-2.1	
VF_0829	***znuC***	**Zinc ABC transporter ATP-binding protein**	**-2.1**	
VF_0833	*feoA*	Ferrous iron tranport protein	-3.9	
VF_0834	***feoB***	**Ferrous iron transporter, protein B (GTP-binding)**	**-2.6**	
VF_1010	-	Putative porin	11.5	11.8
VF_1067	*yqjF*	Quinol oxidase subunit	10.5	
VF_1147	***cstA***	**Peptide transporter**	**6.0**	
VF_1373	-	Putative Fe2+/Mn2+ transporter	-2.2	
VF_1373	**-**	**Putative Fe(II)/Mn(II) transporter**	**-2.2**	
VF_1410	*abgT*	Aminobenzoyl-glutamate transporter	2.2	
VF_1513	***ydjN***	**Sodium:dicarboxylate symporter**	**2.2**	
VF_1522	***zntA***	**Zinc/cadmium/mercury/lead-transporting ATPase**	**3.1**	
VF_1795	***ompC***	**Outer-membrane protein**	**-16.6**	**-16.5**
VF_2024	-	Methyl-accepting chemotaxis protein	2.1	
VF_2150	***sfuB***	**Iron(III)-transport system permease**	**-2.1**	
VF_2220	**-**	**Ubiquinol-cytochrome c reductase iron-sulfur subunit**	**2.5**	
VF_2492	*scsC*	Copper sensitivity protein	-2.2	
VF_2520	-	Cytocrhome c5	2.4	
VF_A0124	***tppB***	**Di/tripeptide permease**	**-28.4**	
VF_A0210	***eptA***	**Metal dependent hydrolase**	**-67.0**	**-42.6**
VF_A0447	**-**	**Methyl-accepting chemotaxis protein**	**-2.2**	
VF_A0995	**-**	**High-affinity iron permease**	**-2.8**	
VF_A1112	***lysE***	**Amino acid transporter**	**3.1**	
VF_B30	-	Putative type II secretion component PulF	2.0	
VF_B38	-	Putative attachment-mediating protein VirB2	2.3	
VF_B47	-	OmpA outer membrane protein	2.1	

Entries in bold correspond to genes used in enrichment analysis.
Fold change in gene expression calculated from n=3 samples (Array), or n=5 samples (qRT).

and *Vibrio parahaemolyticus*), a non-Vibrio Gram-negative microbe (*Photobacterium leiognathi,* and a gram-positive marine microbe (*Exiguobacterium aestuarii*) (**Table 2-4**). Like *V. fischeri* strain ES114, resistance to PMB was acid-induced in *V. fischeri* MJ11, a strain isolated from the fish *Monocentris japonica,* which shares 90% orthologous open-reading frames with *V. fischeri* (17), (**Table 2-4**). No other strain tested revealed this correlation, and I observed no correlation between acidic pH and HOCl resistance among any of the strains tested. Basic pH induced resistance to SDS in all strains tested (data not shown). Notably, the Gram-positive microbe *E. aestuarii was* more sensitive to hydrogen peroxide at

acidic pH. Collectively, this comparative analysis suggests that, among the marine microbes assayed, some pH-induced responses, such as pH 8.0-dependent resistance to SDS, are broadly conserved, while acidic-pH induced responses are is more narrowly represented. Specifically, the acid-induced resistance to the cationic antimicrobial peptide PMB appears to be a species-specific taxonomic characteristic of *Vibrio fischeri*.

Genetic components of *V. fischeri* acidic pH-induced polymyxin stress resistance. I was intrigued by the observation that PMB resistance appears to be a phenotype induced by acidic pH that differentiates *V. fischeri* from other members of the seawater bacterioplankton. Thus, I conducted forward genetic screen to define loci associated with PMB resistance in *V. fischeri*. To differentiate between genes associated with membrane stress, and PMB-specific responses, I screened 13,686 individual mutations in an existing transposon mutagenesis

Table 2-4. pH-induced stress responses of *V. fischeri* and marine microbes

	H_2O_2	HOCl	Polymyxin
Gram-Negative			
Vibrio fischeri			
ES114	-2.3	2.4	**5.3**
MJ1	1.0	-2.0	**8.0**
Vibrio parahaemolyticus			
KNH1	1.3	1.3	1.6
Vibrio azureus			
F77118	-1.2	1.0	-1.3
Photobacterium leiognathi			
Lna	1.0	-2.0	1.0
Gram-Positive			
Exiguobacterium aestuarii			
CNJ771	**-16.0**	-2.0	-1.0

Number reported is the average fold change in MIC (pH 6.5/8.0), n=3 biological replicates.

library (33), and identified a total 142 mutants, representing 124 unique genetic loci that contribute to resistance to both membrane stressors (**Table 2-5**). Fourteen loci only contributed to PMB resistance, and 45 loci only contributed to SDS resistance. Thirteen loci were shared between the microarray and transposon mutagenesis screen (**Table 2-5**).

Of these loci, I singled out *eptA* (VF_A0210), because it was the only locus identified that was specific to PMB resistance, and transcribed in response to pH. This locus carried a cluster of independent transposon insertions (**Fig. 2-3*A***). Homologs of *V. fischeri eptA* participate in the transfer of positively charged phosphoethanolamine (PEA) to lipid A in diverse microbes, contributing to PMB resistance (34) *V. fischeri* lipid A can be decorated with two PEA moieties (35), suggesting that the mechanism of PMB resistance may be conserved in *V. fischeri*. Therefore, I constructed a clean deletion of the *eptA* locus, and assessed the acid-induced resistance the resultant strain to PMB. The loss of *eptA* led to a 14-fold reduction in the minimum inhibitory concentration (MIC) for PMB (**Fig. 2-3*B***). An effort to complement the mutation at a neutral location on the *V. fischeri* chromosome (the Tn7 site), was unsuccessful, however, complementation of the mutation *in cis* by the expression of the gene from a multicopy plasmid using the native promoter (**Fig. 2-3*B***), restored pH-inducible PMB resistance to Δ*eptA V. fischeri*. Moreover, the complementation plasmid conferred approximately 2-fold greater PMB resistance than wild-type *eptA*, suggesting that increased copies of *eptA* may contribute to an increased PMB resistance.

Transcriptional regulation of *eptA* To better understand the transcriptional regulation of *eptA*, I characterized the activity of the promoter in response to changes in the chemical

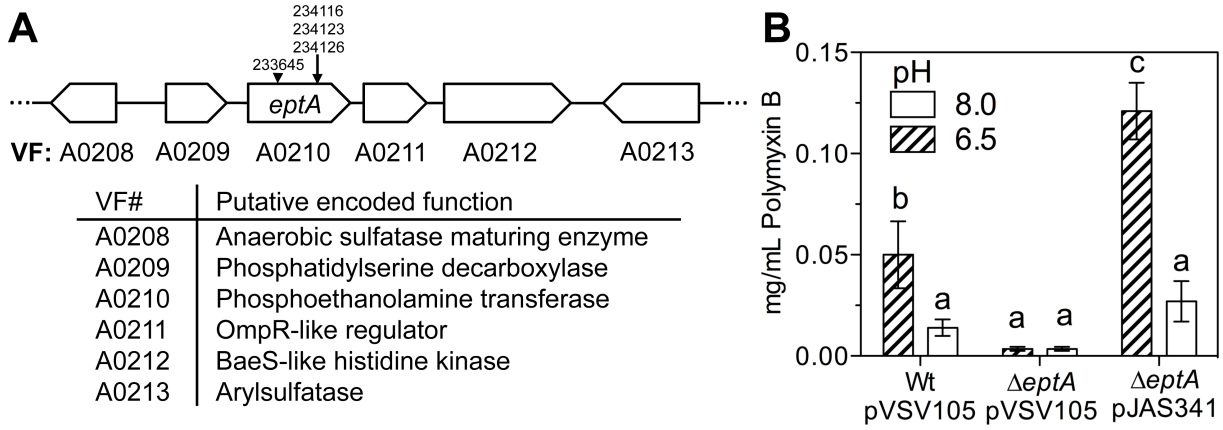

VF#	Putative encoded function
A0208	Anaerobic sulfatase maturing enzyme
A0209	Phosphatidylserine decarboxylase
A0210	Phosphoethanolamine transferase
A0211	OmpR-like regulator
A0212	BaeS-like histidine kinase
A0213	Arylsulfatase

Figure 2-3. The *V. fischeri eptA* gene encodes a putative phosphoethanolamine transferase that is required for acid-induced resistance to PMB. ***A***) Insertions of the transposon mutagenesis plasmid pMJM10 at the *eptA* locus. The sites of insertion on the chromosome are noted above the gene. The open reading frames surrounding *eptA* on Chromosome II of *V. fischeri* are noted below the gene map. ***B***) Minimum inhibitory concentration (MIC) of PMB for *V. fischeri* strains in pH 8.0 and pH 6.5 PIPES MIC buffer. Error bars indicate standard deviation, n=4 biological replicates; pVSV105, blank complementation vector; pJAS340, complementation vector carrying the *eptA* locus and native promoter; 'a', and 'b' indicate groups of statistically similar means, determined by Two-Way ANOVA and post-hoc Bonferroni tests.

Table 2-5. PMB and SDS sensitive mutations

VF_ID	Gene	P[a]	S[b]	pH[c]	Predicted Function
VF_0075	*engB*		N		Ribosome biogenesis GTP-binding protein YsxC
VF_0112	*pyrE*	N			Orotate phosphoribosyltransferase
VF_0149	*mltC*	N	N		Membrane-bound lytic murein transglycosylase C
VF_0151	*waaL*	N	I	/	O-antigen ligase
VF_0152	*rfaD*	N	I		ADP-L-glycero-D-manno-heptose-6-epimerase
VF_0153	*rjg*		N		Right junction gene, LPS locus
VF_0170	*rfbX*	N	I		Polisoprenol-linked O-antigen transporter
VF_0173		N	N		Hypothetical
VF_0181	*ddhD*	I	I		CDP-6-deoxy-delta-3,4-glucoseen reductase
VF_0182	*ddhA*	N	I		Glucose-1-phosphate cytidylyltransferase
VF_0183	*ddhB*		N		CDP-glucose 4,6-dehydratase
VF_0185		N	I		Acetolactate synthase, large subunit
VF_0186	*wcaG*	N	I		dTDP-glucose 4,6-dehydratase
VF_0187		N	I		Glycosyltransferase
VF_0188		N	I		Glycosyltransferase
VF_0189		N			Hypothetical
VF_0190		N	I		Hypothetical- unique to VF
VF_0191	*fnlA*	N			UDP-N-acetylglucosamine 4,6-dehydratase
VF_0193	*rffE*	N	I		UDP-N-acetyl glucosamine-2-epimerase
VF_0194	*wbjE*	N	I		Putative N-acetyl-L-fucosamine (L-FucNAc) transferase.
VF_0196		N	I		Undecaprenyl-phosphate beta-N-acetyl-D-fucosaminephosphotransferase
VF_0197		N	I		UDP-D-quinovosamine 4-dehydrogenase
VF_0223	*slyD*	N	N		FKBP-type peptidylprolyl isomerase
VF_0309		I	N		Hypothetical protein
VF_0310	*cysJ*		N		Sulfite reductase subunit alpha
VF_0311	*cysI*	N	N		Sulfite reductase subunit beta
VF_0312	*cysH*		N		Phosphoadenosine phosphosulfate reductase
VF_0322	*yfbS*	I	I		Divalent anion:sodium symporter family protein
VF_0323	*cysC*	N	N		Adenylylsulfate kinase
VF_0356	*mshI*	I	I		MSHA biogenesis protein MshI
VF_0361	*mshN*		N		MSHA biogenesis protein MshN
VF_0362	*mshE/pulE*	N	N		MSHA biogenesis protein MshE
VF_0387	*rpoN*	N			RNA polymerase factor sigma-54
VF_0473	*carB*	N	N	/	Carbamoyl phosphate synthase large subunit
VF_0509	*serB*	N	I		Phosphoserine phosphatase
VF_0513	-		N		General secretion pathway protein D
VF_0534	*mutS*	N	I		DNA mismatch repair protein MutS
VF_0593	*ygdE*		N		RNA 2'-O-ribose methyltransferase
VF_0637	*guaB*		N		Inosine 5'-monophosphate dehydrogenase
VF_0638	*guaA*	I	I		GMP synthase
VF_0648		N	I		Glutathione-dependent formaldehyde dehydrogenase
VF_0652	*purL*	N	I	/	Phosphoribosylformylglycinamidine synthase
VF_0687	*gmhB*		N		D,D-heptose 1,7-bisphosphate phosphatase
VF_0697			I		Lipoprotein
VF_0793	*adk*	N	I		Adenylate kinase

VF_ID	Gene	P[a]	S[b]	pH[c]	Predicted Function
VF_0804	*asnB*	N	I	/	Asparagine synthetase B
VF_0807	*nagA*	N			*N*-acetylglucosamine-6-phosphate deacetylase
VF_0957	*ybgC*		N		Acyl-CoA thioesterase
VF_0975	*mdlB*	I	N		Multidrug ABC transporter ATP-binding protein
VF_0983		N	I		Lipoprotein
VF_0989	*mifA*		I		Diguanylate cyclase (GGDEF), inhibitor of flagellar motility
VF_0999		I	N		ATP-dependent protease subunit
VF_1009	*dinG*		N		ATP-dependent DNA helicase DinG
VF_1044	*rrt*		N		Reverse transcriptase
VF_1046		N	N		Hypothetical
VF_1075		N			Amino acid transporter LysE
VF_1154		I	I		Hypothetical
VF_1159	*asnC*	I	I		Asparaginyl-tRNA synthetase
VF_1168	*sbcC*	I	N	/	Exonuclease, dsDNA, ATP-dependent
VF_1184			N		Acriflavin resistance plasma membrane protein
VF_1204	*gyrA*		N		DNA gyrase subunit A
VF_1209		N	N		Membrane metalloprotease
VF_1257			I		Hypothetical
VF_1293		I	I		ATP-dependent protease (Lon-like)
VF_1356		I	N		Hypothetical
VF_1477		N	N		Hypothetical
VF_1513	*ydjN*		N	/	transporter
VF_1531		N			Ferrochelatase
VF_1550	*nrfE*	N	I		Heme lyase (NrfEFG) for insertion of heme into c552, subunit NrfE
VF_1565	*cbiO*	N	I		Cobalt transport ATP-binding protein CbiO
VF_1630			N		Sodium:proton antiporter
VF_1652			N		Methyl-accepting chemotaxis protein
VF_1679			N		Hypothetical
VF_1691	*purF*	N	N		Amidophosphoribosyltransferase
VF_1755	*pyrF*	N			Orotidine 5'-phosphate decarboxylase
VF_1809	*ptrA*		N		Protease III
VF_1823	*ccmB*	N	I		Heme exporter subunit B
VF_1834	*fliA*	N	N		Flagellar biosynthesis sigma factor
VF_1851	*fliG*	N	I		Flagellar motor switch protein G
VF_1870	*flgI*	I	N		Flagellar basal body P-ring biosynthesis protein FlgA
VF_1871	*flgH*	N			Flagellar basal body L-ring protein
VF_1955	*resP*	N	I		Membrane-associated zinc protease
VF_2015			N		Capsid portal protein
VF_2054			N		Hypothetical
VF_2150	*sfuB*		N	/	Iron(III)-transport system permease SfuB
VF_2152	*amtB*		N		Ammonium transporter
VF_2226	*degS*	N	I		Serine endoprotease DegS, periplasmic
VF_2389	*dusB*	N	I		tRNA-dihydrouridine synthase B
VF_2394	*purH*	I	I	/	Bifunctional phosphoribosylaminoimidazolecarboxamide formyltransferase/IMP cyclohydrolase
VF_2446	*fliL2*	N	N	/	Flagellar basal body protein FliL
VF_2503		N	N		Transcriptional regulator

VF_ID	Gene	P[a]	S[b]	pH[c]	Predicted Function
VF_2538	*purK*		N	/	Phosphoribosylaminoimidazole carboxylase ATPase subunit
VF_2547	*trkH2*	N	I		Trk system potassium uptake protein TrkH
VF_2581		I	I		Hypothetical
VF_A0075	*mshQ2*		N		MshQ protein
VF_A0083	*dmsD*	I	I		Twin-argninine leader-binding protein for DmsA and TorA
VF_A0176		I	N		ArsR family transcriptional regulator
VF_A0210	*eptA*	N		/	Metal dependent hydrolase
VF_A0212		N	I		Two component sensor histidine kinase
VF_A0220			N		General secretion pathway protein D
VF_A0226	*tadD2*		N		Similar to TadD
VF_A0233			N		Hypothetical
VF_A0235	*glpF*		N		Glycerol uptake facilitator protein GlpF
VF_A0239	*glpD*	N	I		Glycerol-3-phosphate dehydrogenase
VF_A0249	*glpB*	N	N		Anaerobic glycerol-3-phosphate dehydrogenase subunit B
VF_A0260	*kefC*	N	I		Glutathione-regulated potassium-efflux system protein KefC
VF_A0281	*nrd*		N		Anaerobic ribonucleoside triphosphate reductase
VF_A0299	*torA*		N		Trimethylamine N-oxide (TMAO) reductase I, catalytic subunit
VF_A0338		N			Glucosyl hydrolase precursor
VF_A0428	*ycbC*	N			Hypothetical protein
VF_A0512			N		Phage integrase family protein
VF_A0519		N	N		Hypothetical
VF_A0527		N			Methyl-accepting chemotaxis protein
VF_A0580	*rstB2*		N		RstB2 protein
VF_A0785			N		AraC family transcriptional regulator
VF_A0857	*smtB*	N			Transcriptional repressor SmtB (poss. Metal-ion dependent)
VF_A0880			N		AraC family transcriptional regulator
VF_A1019			N		Cytoplasmic protein
VF_A1071			N		Methyl-accepting chemotaxis protein, aerotaxis receptor
VF_A1112			N	/	Amino acid transporter LysE
VF_A1139			N		Hypothetical protein
VF_B0039			N	/	VirB4 ATPase

[a] P, polymyxin B
[b] S, sodium dodecyl sulfate
[c] pH indicates a gene that is responsive to pH 6.5 vs. 8.0 seawater.

environment. The activity of the *eptA* promoter was positively correlated with acidic pH: activity increased linearly from pH 6.5 to pH 5.5 (**Fig. 2-4*A***). The pH scale is logarithmic, indicating that increasing concentrations of protons exponentially activate the *eptA* promoter (**Fig. 2-4*A***). I next asked whether additional environmental cues might alter the transcriptional response of *eptA* to acidic pH. Below pH 6.5 I observed that PMB was an agonist of acid-

induced *eptA* promoter activity, while HOCl was an antagonist of this activity, relative to a vehicle control (**Fig. 2-4*A***). Moreover, the anionic detergents SDS and bile inhibited the acid-induced activity of the *eptA* promoter, relative to pH 8.0 (**Figs. 2-4*A*,*B***). Promoter activity was insensitive to H_2O_2, as well as to low calcium and magnesium: the major cationic constituents of seawater (**Fig. 24*A*,*C***). Thus, transcription of *V. fischeri eptA* responds to pH, PMB, HOCl and anionic detergents in the context of seawater, but not to oxidative stressors or to a decrease in calcium or magnesium.

Identification of other pathways leading to pH-dependent PMB resistance

I hypothesized that the transcription factor(s) responsible for coordinating the expression of *eptA* in response to acidic pH and other environmental cues would be present in the list of PMB-sensitive transposon mutants. Two transcription factors (VF_2503, and VF_A0176) were identified among the list of PMB-sensitive transposon insertions (**Table 2-5**). I assessed the transcription of *eptA* in these two mutant backgrounds, and found that neither regulator contributed to the induction of the *eptA* promoter at pH 6.5 (data not shown). I also assessed the activity of the promoter in two previously constructed strains of *V. fischeri* carrying disruptions in two putative *phoP* homologs (VF_0526 and VF_1396) (18), and detected no pH-dependent regulation resulting from either promoter (data not shown). This insensitivity is perhaps not surprising, given that acid-dependent activation of *eptA* by PhoP in *Salmonella typhimurium* occurs in low magnesium environments (36), and requires the PmrD protein, and that *V. fischeri* exists in a high magnesium environment, and does not encode an identifiable *pmrD* homolog. Thus, it is likely that i) the regulation of *V. fischeri eptA* differs from the

well-characterized example of *Salmonella typhimurium*, and ii) additional VF_2503 and VF_A0176-regulated pathways that exist in *V. fischeri* to confer resistance to PMB in acidic environments.

Notably, a transcription factor responsible for pH-dependent regulation of *eptA* was not identified in the transposon mutagenesis screen. It is possible that the transposon screen simply was not deep enough do identify the transcription factor, or the mutant may have only reduced sensitivity to PMB. Alternately, mutation of this factor may confer a growth defect in the strain, which would have excluded it from screening. Supporting these possibilities, I did not identify transposon insertions in the *ompU* gene (VF_0475), which has been associated with susceptibility of *V. fischeri* to the antimicrobial peptide protamine (37). I confirmed that *V. fischeri ompU* contributes to pH-induced PMB resistance (MIC Δ*ompU*=0.01 mg/mL). A homolog of *V. fischeri* OmpU confers resistance to PMB in *V. cholerae* in a ToxR-dependent manner (38). Previous studies in *V. fischeri* have revealed that a *V. fischeri* ToxR homolog (VF_0791) does not regulate *ompU* (37). Instead, *V. fischeri ompR* (VF_0114) was required to fully induce the *ompU* promoter in response to acid (**Fig. 2-5*A***). The *ompU* promoter was also induced by low magnesium, bile and SDS in a pH-independent manner (**Fig. 2-5*B-D***). Thus, acidic pH is the only environmental cue that activates both *eptA* and *ompU* promoters. Anionic detergents such as SDS and bile have opposite effects on the two promoters, and low magnesium is a specific cue for *ompU* transcription.

I was intrigued by reports that the mechanism by which *V. cholerae* OmpU confers resistance to PMB involves post-translational regulation of the periplasmic protease DegS, and the alternative sigma factor RpoE (39). Moreover, the *degS* gene (VF_2226) was

identified in the screen of PMB sensitive mutants (**Table 2-5**). Thus, I currently hypothesize that *V. cholerae*-like post-translational regulation of RpoE by OmpU might be conserved in *V. fischeri*, and propose that this pathway is the most likely candidate responsible for the pH-dependent regulation of PMB resistance at the level of transcription (**Fig. 2-6**). In support of this hypothesis, I also identified the *V. fischeri rseP* homolog (VF_1955) in the screen for PMB sensitive transposon mutants (**Table 2-5**). To activate the envelope-stress response in *Salmonella* and *Escherichia*, DegS and RseP proteases sequentially cleave anti-sigma factor RseA, freeing RpoE (40), thus, disruption of the *rseP* gene might be expected to disrupt RpoE-dependent regulation in *V. fischeri* (**Fig. 2-6**). Effort*s* are currently underway to determine whether the OmpU-DegS-RseP-RpoE pathway is intact in *V. fischeri*, and whether this pathway responds to acidic pH, although research in this direction has been complicated by the fact that the *V. fischeri* genome encodes five *rpoE* homologs (15).

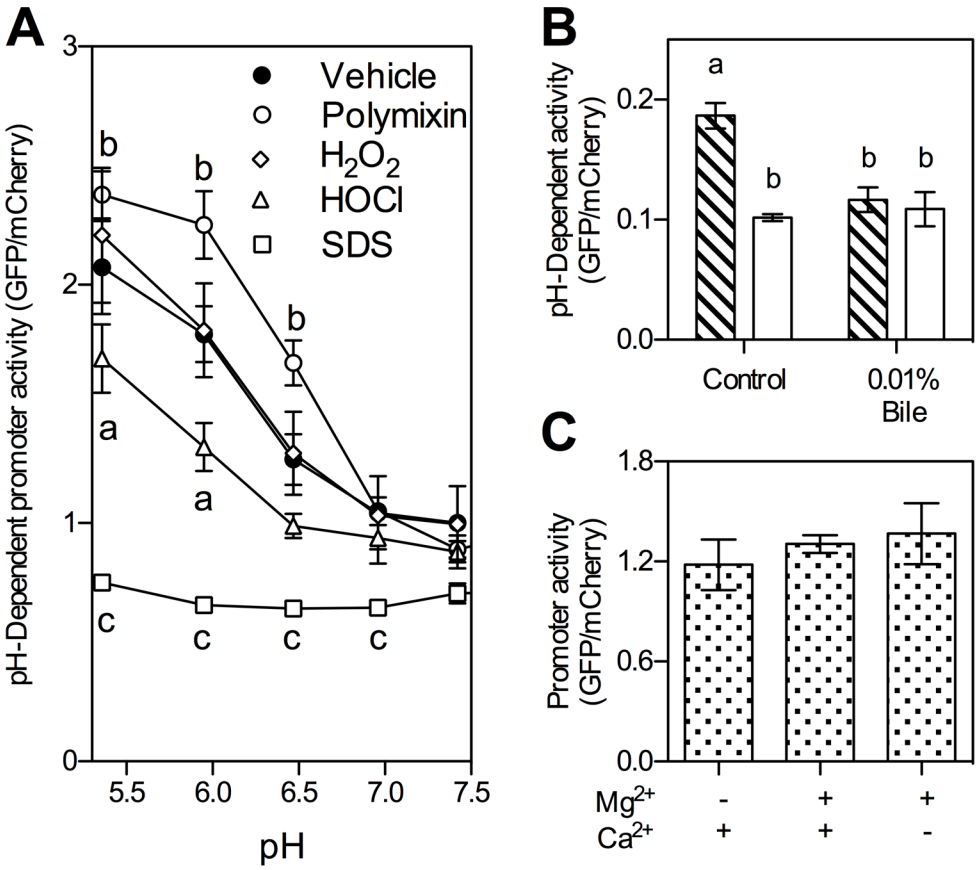
A
pH-Dependent promoter activity (GFP/mCherry)
pH
Vehicle
Polymixin
H2O2
HOCl
SDS
B
pH-Dependent activity (GFP/mCherry)
Control
0.01% Bile
C
Promoter activity (GFP/mCherry)
Mg2+
Ca2+

Figure 2-4. Transcriptional regulation of *V. fischeri eptA* (VF_A0210) in response to acid and other environmental stimuli. The pJAS342 reporter construct was used to measure transcriptional activity. Throughout, standard error is shown. Statistical relationships among mean GFP/RFP ratios were determined by Two-Way ANOVA with Post-hoc Bonferroni multiple comparisons. ***A***) pH-dependent activity of the *eptA* promoter, in the presence of 0.001% PMB, 0.001% hydrogen peroxide (H_2O_2), 0.001% hypochlorous acid (HOCl), and 0.01% SDS stock solutions. These concentrations of added stressors are at least 4-fold lower than the reported MIC. 'a', 'b' and 'c' indicate groups in which the mean GFP/mCherry ratio is statistically different from that of the vehicle control at the same pH. The signal was normalized to the ratio of the vehicle conrol at pH 8.0. Two biological replicates are shown. Data are representative of two separate experiments. ***B***) Contribution of 0.01% bile to pH-dependent *eptA* promoter activity. 'a' and 'b' indiate groups of similar mean GFP/RFP ratios, n=3 biological replicates. ***C***) Contribution of magnesium and calcium to *eptA* promoter activity. pH 6.5 PIPES MIC buffer was made without magnesium, or without calcium by substituting in sodium chloride to achieve an equivalent final osmolarity. Three biological replicates were assessed.

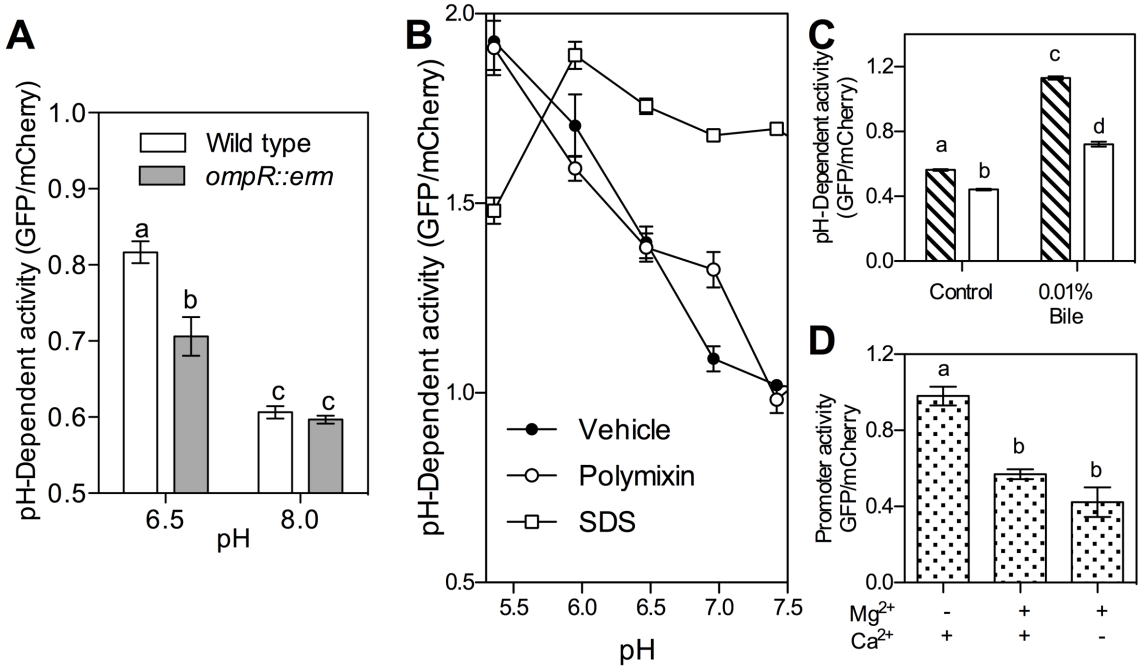
A
pH-Dependent activity (GFP/mCherry)
1.0
0.9
0.8
0.7
0.6
0.5
Wild type
ompR::erm
a
b
c
c
6.5
8.0
pH
B
pH-Dependent activity (GFP/mCherry)
2.0
1.5
1.0
0.5
Vehicle
Polymixin
SDS
5.5
6.0
6.5
7.0
7.5
pH
C
pH-Dependent activity (GFP/mCherry)
1.2
0.8
0.4
0.0
a
b
c
d
Control
0.01% Bile
D
Promoter activity GFP/mCherry
1.2
0.8
0.4
0.0
a
b
b
Mg2+ - + +
Ca2+ + + -

Figure 2-5. Contribution of *ompR* (VF_0114), pH, and additional environmental stimuli to *ompU* promoter activity. The pJAS343 GFP/mCherry reporter construct was used to measure promoter activity. Statistics were performed as in **Fig. 2-4**. Standard error is shown throughout. ***A***) Activity of the *ompU* promoter in wild type and the *ompU::erm* strain KV2507. 'a', 'b' and 'c' represent groups of statistically similar mean GFP/mCherry ratios, n=3 biological replicates. ***B***) pH-dependent transcription of *ompU* in the presence of of 0.001% PMB and 0.01% SDS stock solutions. GFP/mCherry signals were normalized to the ratio of the vehicle control at pH 8.0. Two biological replicates for each condition are shown. Data representative of two independent experiments. C) Contribution of 0.01% bile to *ompU* promoter activity in pH 6.5 (hatched bars) or pH 8.0 (open bars) PIPES MIC buffer. 'a' and 'b' 'c' and 'd' indicate groups of statistically equivalent means, n=3. ***D***) Contribution of magnesium and calcium to transcription of *ompU*. Experimental conditions same as **Fig. 2-3*C***. 'a' and 'b' are groups of equivalent means, n=3.

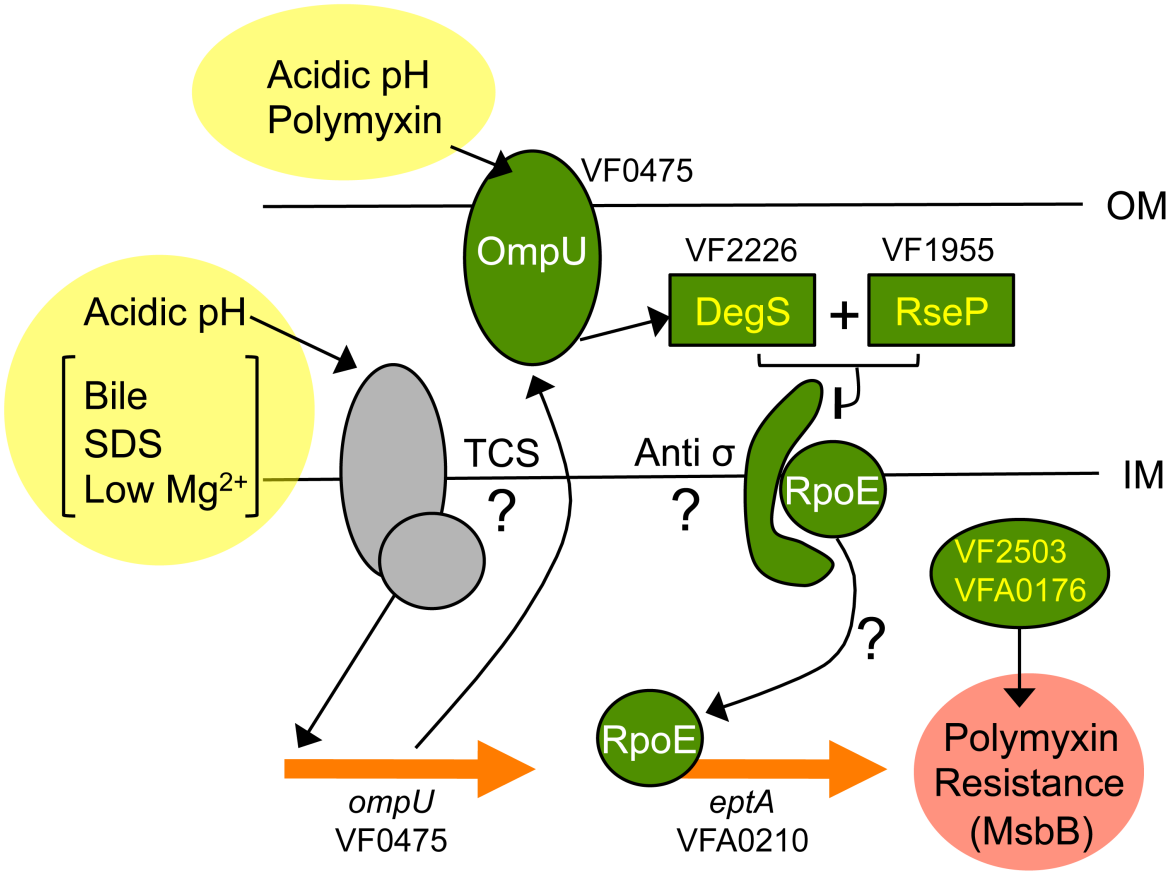
Acidic pH
Polymyxin
VF0475
OM
OmpU
VF2226
VF1955
DegS
+
RseP
Acidic pH
Bile
SDS
Low Mg2+
TCS
?
Anti σ
?
RpoE
IM
VF2503
VFA0176
?
RpoE
Polymyxin
Resistance
(MsbB)
ompU
VF0475
eptA
VFA0210

Figure 2-6. Proposed regulation of acid-induced PMB stress resistance in *V. fischeri*. Acidic pH induces transcription of both *ompU* and *eptA*. The pH-dependent transcription of *ompU* is not dependent on the ToxRS two component system in *V. fischeri* (37), but the regulator(s) involved (indicated by a question mark) activate *ompU* promoter activity in response to acidic pH, bile, SDS and low magnesium. *eptA* is requred for PMB resistance induced by acidic pH. The activity of the *eptA* promoter is repressed by anionic detergents, but is activated by polymxin and acidic pH. Regulatory elements predicted to coordinate PMB resistance are indicated green. Four paralogs of the RpoE sigma factor are encoded by *V. fischeri*, thus the identitiy of the anti-sigma factor that sequesters RpoE cannot be postulated. Components identified in the transposon mutagenesis screen for polymyxin-sensitivity are indicated by yellow lettering. Two additional transcription factors (VF2503 and VFA0176) induce polymyxin resistance, although *eptA* is not regulated by these elements, and the genes targeted by this regulation are not known. MsbB has been previously identified as a gene that confers polymyxin resistance in *V. fischeri* (41). OM, outer membrane; IM, inner membrane.

DISCUSSION

In this chapter, I present evidence that acidic pH induces a transcriptional response that is enriched in genes associated with membrane functions (**Fig. 2-1, Table 2-3**). I find that resistance to the cationic antimicrobial peptide PMB is induced by acidic pH (**Fig. 2-2**). This regulation is not conserved in the *V. cholerae* El Tor biotype, which is characterized by its resistance to PMB (42). Comparisons of the genetic constituents of *V. fischeri* with *V. cholerae* El Tor and other Gram-negative organisms in which PMB resistance have been characterized indicate several interesting differences.

First, the regulation of *V. fischeri* PMB is unlike that of *V. cholerae* and *S. typhimurium*. PMB activates the RpoE-dependent envelope stress response of *V. cholerae El Tor* in a manner that involves the OmpU outer membrane porin and the DegS protease (39).ToxR is also sensitive to DegS and RpoE-dependent proteolysis at alkaline pH in seawater (43). However, ToxR-dependent regulation of *ompU* is not conserved in *V. fischeri* (37). Other regulators of PMB resistance include the CarRS two component system of *V. cholerae* (44), but this response regulator induces PMB resistance under low calcium, which is inconsistent with the transcriptional regulation of the *V. fischeri* PMB resistance gene *eptA* (**Fig. 2-4**). PMB resistance in *Salmonella typhimurium* is induced under acidic conditions (45), however, the PmrA-B-D signaling pathway that coordinates this response cannot be identified by sequence homology in *V. fischeri.* Notably, the *V. fischeri degS, ompU*, and *rpoE4* (VF_0766) were identified as essential for the colonization of squid in recent InSeq study (46). The *degS* and *ompU* mutations have been confirmed to confer a defect in light-organ colonization (46) (37), however, *eptA* was neither detected in the InSeq screen, nor

identified as a gene that enhances infectivity of *V. fischeri* (data not shown). Thus, further characterization of the RpoE pathway in *V. fischeri*, might help to reveal regulatory targets that are involved in colonization of the squid, which perhaps include *eptA*, and other PMB resistance genes.

Second, the demonstration of *eptA*-dependent polymyxin resistance in *V. fischeri* is, to the knowledge, the first example of this mechanism of polymyxin resistance in the genus *Vibrio*. EptA, also called PmrC, transfers phosphoethanolamine to lipid A in *S. typhimurium* and *Acinetobacter baumannii* (47, 48). There are two potential sites of phosphoethanolamine (PEA) modification on *V. fischeri* lipid A (49), suggesting that *eptA* may be involved in at least one of these PEA decorations. Notably, *V. cholerae* El Tor LPS is also modified by PEA, and this species encodes a putative EptA homolog, although a link between *eptA* and PMB resistance has yet to be demonstrated in this pathogen. Instead, polymyxin resistance is in *V. cholerae* El Tor is attributed to an unusual modification of lipopolysaccharide lipid A with glycine at the 3 position of the acyl chain (50). Neither the modification, nor the associated genes (*almEFG*), have been identified in *V. fischeri*, although the squid symbiont modifies its lipid A by the addition of an unusual phosphoglycerol, lysophosphatidic acid or phosphatidic acid at the same position (51). PMB resistance in *V. cholera* El Tor is also attributed to the MsbB acyltransferase (52), and *msbB*-dependent PMB resistance is conserved in *V. fischeri* (41), indicating possible redundancy of this physiological function. In *Vibrio vulnificus*, PMB resistance is linked to the *trkA* gene (53), which was identified in the polymyxin sensitivity screen, but is not transcriptionally regulated by *V. fischeri* in response to acidic pH. Multiple mechanisms of lipid A modification may confer PMB resistance to *V.*

fischeri, although it is already apparent that the regulation of PMB resistance is not widely conserved among *Vibrio spp*. Thus, further study of lipid A modification in *V. fischeri* will inform general understanding of the diversity of polymyxin resistance mechanisms in the genus *Vibrio*, and perhaps reveal strategies by which these modifications promote the selection and maintenance of *V. fischeri* by its symbiotic host.

A source of PMB-like stress is not currently known in the light-organ environment. However, *E. scolopes* expresses bactericidal permeability increasing (BPI) proteins, which can act like PMB. Two of the three BPI-like protein identified are predicted to be secreted: LBP2 (pI 9.6), and LBP3 (pI 9.4) (54). In the context of *V. cholerae* pathogenesis, the OmpU protein confers resistance to mammalian BPI (38). In the context of the squid-vibrio symbiosis, it is interesting that PMB resistance is induced under acidic conditions (**Fig. 2-2**). BPI proteins are positively charged in acidic environments, increasing their affinity for negatively charged bacterial membranes (54). Thus, future studies of acid-linked PMB resistance in *V. fischeri* should test whether *eptA* is required for resistance to squid BPI proteins. Known acidic environments in the squid include mucus secreted outside of the light organ during the initiation of symbiosis (2), as well as the lumen of the light-organ crypts during the nocturnal period of the mature symbiosis (**Chapter 4** (55)). It remains to be seen whether BPI is present in either of these environments. Notably, transcription and secretion of one BPI homolog is induced after symbiosis has been initiated (56). Thus, the characterization of the environmental pH of the crypts at 18 h may also help to reveal the context in which *V. fischeri* acid-induced stress responses contribute to symbiotic fitness. Such a link would be

the first example of a role for BPI proteins acting on a beneficial microbial symbiont to structure host-microbe association.

ACKNOWLEDGEMENTS

I thank Joe Graber for the Δ*ompU* mutant, as well as for previous characterization of this mutant in the context of the acid tolerance response. I also thank Karen Visick for generously sharing her strains and advice. Work presented in the chapter was funded by NIH grants. This work was funded by NIH grants RR12294/OD11024 to EGR and M. McFall-Ngai, and AI050661 to M. McFall-Ngai and EGR. JAS was funded by a NSF Graduate Research Fellowship, the Chemical Biology Training Program (UW-Madison, NIH-NIGMS T32 GM008505), and the Microbes in Health and Disease Training Program (UW-Madison NIH-NIAID T32 AI055397).

REFERENCES

1. Merrell DS & Camilli A (2002) Acid tolerance of gastrointestinal pathogens. *Curr Opin Microbiol* 5(1):51-55.

2. Kremer N*, et al.* (2013) Initial symbiont contact orchestrates host-organ-wide transcriptional changes that prime tissue colonization. *Cell Host Microbe* 14(2):183-194.

3. Foster JW (1999) When protons attack: microbial strategies of acid adaptation. *Curr Opin Microbiol* 2(2):170-174.

4. Krulwich TA, Sachs G, & Padan E (2011) Molecular aspects of bacterial pH sensing and homeostasis. *Nat Rev Microbiol* 9(5):330-343.

5. Mukherjee S & Hooper LV (2015) Antimicrobial defense of the intestine. *Immunity*. 42(1):28-39.

6. Fraune S & Bosch TC (2007) Long-term maintenance of species-specific bacterial microbiota in the basal metazoan Hydra. *Proc Natl Acad Sci U S A* 104(32):13146-13151.

7. McFall-Ngai M*, et al.* (2013) Animals in a bacterial world, a new imperative for the life sciences. *Proc Natl Acad Sci U S A* 110(9):3229-3236.

8. Matamouros S & Miller SI (2015) *S. Typhimurium* strategies to resist killing by cationic antimicrobial peptides. *Biochim Biophy Acta*. S0005-2736(15): 00023-1.

9. Belkaid Y & Segre JA (2014) Dialogue between skin microbiota and immunity. *Science* 346(6212):954-959.

10. Mowat AM & Agace WW (2014) Regional specialization within the intestinal immune system. *Nat Rev Immunol*. 14(10):667-85.

11. Lozupone CA, Stombaugh JI, Gordon JI, Jansson JK, & Knight R (2012) Diversity, stability and resilience of the human gut microbiota. *Nature* 489(7415):220-230.

12. Nyholm SV & McFall-Ngai MJ (2004) The winnowing: establishing the squid-vibrio symbiosis. *Nat Rev Microbiol* 2(8):632-642.

13. Sambrook J, Fritsch EF, & Maniatis T (1989) *Molecular Cloning* (Cold Spring Harbor Laboratory Press New York).

14. Boettcher KJ & Ruby EG (1990) Depressed light emission by symbiotic *Vibrio fischeri* of the sepiolid squid *Euprymna scolopes*. *J Bacteriol* 172(7):3701-3706.

15. Mandel MJ, Stabb EV, & Ruby EG (2008) Comparative genomics-based investigation of resequencing targets in *Vibrio fischeri*: focus on point miscalls and artefactual expansions. *BMC Genomics* 9:138.

16. Ruby EG & Nealson KH (1976) Symbiotic association of *Photobacterium fischeri* with the marine luminous fish *Monocentris japonica*; a model of symbiosis based on bacterial studies. *Biol Bull* 151(3):574-586.

17. Mandel MJ, Wollenberg MS, Stabb EV, Visick KL, & Ruby EG (2009) A single regulatory gene is sufficient to alter bacterial host range. *Nature* 458(7235):215-218.

18. Hussa EA, O'Shea TM, Darnell CL, Ruby EG, & Visick KL (2007) Two-component response regulators of *Vibrio fischeri*: identification, mutagenesis, and characterization. *J Bacteriol* 189(16):5825-5838.

19. Nyholm SV, Stabb EV, Ruby EG, & McFall-Ngai MJ (2000) Establishment of an animal–bacterial association: recruiting symbiotic vibrios from the environment. *Proc Natl Acad Sci U S A* 97(18):10231-10235.

20. Kremer N*, et al.* (2014) The dual nature of haemocyanin in the establishment and persistence of the squid–vibrio symbiosis. *Proc R Soc B* 281(1785).

21. Dunlap PV (1985) Osmotic control of luminescence and growth in *Photobacterium leiognathi* from ponyfish light organs. *Arch Microbiol* 141(1):44-50.

22. Gontang EA, Fenical W, & Jensen PR (2007) Phylogenetic diversity of gram-positive bacteria cultured from marine sediments. *Appl Environ Microbiol* 73(10):3272-3282.

23. Hanahan D (1983) Studies on transformation of *E. coli* with plasmids. *J Mol Biol* 166(4):557-580.

24. Le Roux F, Binesse J, Saulnier D, & Mazel D (2007) Construction of a *Vibrio splendidus* mutant lacking the metalloprotease gene *vsm* by use of a novel counterselectable suicide vector. *Appl Environ Microbiol* 73(3):777-784.

25. Dunn AK, Millikan DS, Adin DM, Bose JL, & Stabb EV (2006) New rfp- and pES213-derived tools for analyzing symbiotic *Vibrio fischeri* reveal patterns of infection and lux expression in situ. *Appl Environ Microbiol* 72(1):802-810.

26. Stabb EV & Ruby EG (2002) RP4-based plasmids for conjugation between *Escherichia coli* and members of the vibrionaceae. *Methods Enzymol* 358:413-426.

27. Shibata S & Visick KL (2012) Sensor kinase RscS induces the production of antigenically distinct outer membrane vesicles that depend on the symbiosis polysaccharide locus in *Vibrio fischeri*. *J Bacteriol* 194(1):185-194.

28. Miyashiro T, Wollenberg MS, Cao X, Oehlert D, & Ruby EG (2010) A single *qrr* gene is necessary and sufficient for LuxO-mediated regulation in *Vibrio fischeri*. *Mol Microbiol* 77(6):1556-1567.

29. Stabb EV, Butler MS, & Adin DM (2004) Correlation between osmolarity and luminescence of symbiotic *Vibrio fischeri* strain ES114. *J Bacteriol* 186(9):2906-2908.

30. Bustin SA*, et al.* (2009) The MIQE guidelines: minimum information for publication of quantitative real-time PCR experiments. *Clin Chem* 55(4):611-622.

31. Wang Y*, et al.* (2010) H-NOX–mediated nitric oxide sensing modulates symbiotic colonization by *Vibrio fischeri*. *Proc Natl Acad Sci U S A* 107(18):8375-8380.

32. DeLoney CR, Bartley TM, & Visick KL (2002) Role for phosphoglucomutase in *Vibrio fischeri-Euprymna scolopes* symbiosis. *J Bacteriol* 184(18):5121-5129.

33. Brennan CA, Mandel MJ, Gyllborg MC, Thomasgard KA, & Ruby EG (2013) Genetic determinants of swimming motility in the squid light-organ symbiont *Vibrio fischeri*. *MicrobiologyOpen* 2(4):576-594.

34. Raetz CR, Reynolds CM, Trent MS, & Bishop RE (2007) Lipid A modification systems in gram-negative bacteria. *Annu Rev Biochem* 76:295.

35. Post DM*, et al.* (2012) O-antigen and core carbohydrate of *Vibrio fischeri* lipopolysaccharide composition and analysis of their role in *Euprymna scolopes* light organ colonization. *J Biol Chem* 287(11):8515-8530.

36. Chen HD & Groisman EA (2013) The biology of the PmrA/PmrB two-component system: the major regulator of lipopolysaccharide modifications. *Annu Rev Microbiol* 67:83-112.

37. Aeckersberg F, Lupp C, Feliciano B, & Ruby EG (2001) *Vibrio fischeri* outer membrane protein OmpU plays a role in normal symbiotic colonization. *J Bacteriol* 183(22):6590-6597.

38. Mathur J & Waldor MK (2004) The *Vibrio cholerae* ToxR-regulated porin OmpU confers resistance to antimicrobial peptides. *Infect Immun* 72(6):3577-3583.

39. Mathur J, Davis BM, & Waldor MK (2007) Antimicrobial peptides activate the *Vibrio cholerae* σE regulon through an OmpU-dependent signalling pathway. *Mol Microbiol* 63(3):848-858.

40. Requena JM (2012) *Stress Response in Microbiology* (Horizon Scientific Press).

41. Adin DM*, et al.* (2008) Characterization of *htrB* and *msbB* mutants of the light-organ symbiont *Vibrio fischeri*. *Appl Environ Microbiol* 74(3):633-644.

42. Gangarosa EJ, Bennett JV, & Boring 3rd J (1967) Differentiation between *Vibrio cholerae* and *Vibrio cholerae* biotype El Tor by the polymyxin B disc test: comparative results with TCBS, Monsur's, Mueller-Hinton and nutrient agar media. *Bulletin of the World Health Organization* 36(6):987.

43. Almagro-Moreno S, Kim TK, Skorupski K, & Taylor RK (2015) Proteolysis of virulence regulator ToxR is associated with entry of *Vibrio cholerae* into a dormant state. 11(4):e1005145.

44. Bilecen K*, et al.* (2015) Polymyxin B Resistance and biofilm formation in *Vibrio cholerae* is controlled by the response regulator CarR. *Infect Immun*:IAI. 02700-02714.

45. Chen HD & Groisman EA (2013) The biology of the PmrA/PmrB two-component system: the major regulator of lipopolysaccharide modifications. *Annu Rev Microbiol* 67:83-112.

46. Brooks JF*, et al.* (2014) Global discovery of colonization determinants in the squid symbiont *Vibrio fischeri*. *Proc Natl Acad Sci U S A* 111(48):17284-17289.

47. Arroyo LA*, et al.* (2011) The *pmrCAB* operon mediates polymyxin resistance in *Acinetobacter baumannii* ATCC 17978 and clinical isolates through phosphoethanolamine modification of Lipid A. *Antimicrob Agen Chemother*:AAC. 00256-00211.

48. Lee H, Hsu F-F, Turk J, & Groisman EA (2004) The PmrA-regulated *pmrC* gene mediates phosphoethanolamine modification of lipid A and polymyxin resistance in *Salmonella enterica*. *J Bacteriol* 186(13):4124-4133.

49. Post DM*, et al.* (2012) O-antigen and core carbohydrate of *Vibrio fischeri* lipopolysaccharide composition and analysis of their role in *Euprymna scolopes* light-organ colonization. *J Biol Chem* 287(11):8515-8530.

50. Hankins JV, Madsen JA, Giles DK, Brodbelt JS, & Trent MS (2012) Amino acid addition to *Vibrio cholerae* LPS establishes a link between surface remodeling in Gram-positive and Gram-negative bacteria. *Proc Natl Acad Sci U S A* 109(22):8722-8727.

51. Phillips NJ*, et al.* (2011) The Lipid A from *Vibrio fischeri* Lipopolysaccharide: a unique structure bearning a phosphoglycerol moiety. *J Biol Chem* 286(24):21203-21219.

52. Matson JS, Yoo HJ, Hakansson K, & DiRita VJ (2010) Polymyxin B resistance in El Tor *Vibrio cholerae* requires lipid acylation catalyzed by MsbB. *J Bacteriol* 192(8):2044-2052.

53. Chen Y-C, Chuang Y-C, Chang C-C, Jeang C-L, & Chang M-C (2004) A K+ uptake protein, TrkA, is required for serum, protamine, and polymyxin B resistance in *Vibrio vulnificus*. *Infect Immun* 72(2):629-636.

54. Krasity BC, Troll JV, Weiss JP, & McFall-Ngai MJ (2011) LBP/BPI proteins and their relatives: conservation over evolution and roles in mutualism. *Biochem Soc Trans* 39(4):1039.

55. Schwartzman JA*, et al.* (2015) The chemistry of negotiation: rhythmic, glycan-driven acidification in a symbiotic conversation. *Proc Natl Acad Sci U S A* 112(2):566-571.

56. Chun CK*, et al.* (2008) Effects of colonization, luminescence, and autoinducer on host transcription during development of the squid-vibrio association. *Proc Natl Acad Sci U S A* 105(32):11323-11328.

Chapter 3

Non-native acylated homoserine lactones reveal that LuxIR quorum sensing promotes symbiont stability

PREFACE:

Published in *Environmental Microbiology* in 2014 as:

Studer SV*, Schwartzman JA*, Ho JS, Geske GD, Blackwell HE, and Ruby EG. "Non-native acylated homoserine lactones reveal that LuxIR quorum sensing promotes symbiont stability."

*These authors contributed equally.

JAS, SVS, HEB and EGR formulated ideas and planned experiments. JAS and SVS performed experiments. JAS analyzed the data. JSH and GDG performed preliminary experiments. JAS and EGR wrote and edited the chapter, and SVS contributed to the writing of the experimental methods.

ABSTRACT:

Quorum sensing, a group behavior coordinated by a diffusible pheromone signal and a cognate receptor, is a typical characteristic of bacteria that form symbioses with plant and animal hosts. LuxIR-type acyl homoserine-lactone (AHL) quorum sensing is common in Gram-negative proteobacteria, and many members of this group have additional quorum-sensing networks. The bioluminescent symbiont *Vibrio fischeri* encodes two AHL signal synthases: AinS and LuxI. AinS-dependent quorum sensing converges with LuxI-dependent quorum sensing at the LuxR regulatory element. Both AinS- and LuxI-mediated signaling are required for efficient and persistent colonization of the squid host, *Euprymna scolopes*. The basis of the mutualism is symbiont bioluminescence, which is regulated by both LuxI- and AinS-dependent quorum sensing, and is essential for maintaining a colonization of the host. In the present study, chemical and genetic approaches were used to probe the dynamics of LuxI- and AinS-mediated regulation of bioluminescence during symbiosis. I demonstrate that both native AHLs and non-native AHL analogs can be used to non-invasively and specifically modulate induction of symbiotic bioluminescence *via* LuxI-dependent quorum sensing. The data suggest that the first day of colonization, during which symbiont bioluminescence is induced by LuxIR, is a critical period that determines the stability of the *V. fischeri* population once symbiosis is established.

INTRODUCTION:

A common thread among microbes that initiate symbioses with plant and animal hosts is the quorum sensing-dependent regulation of colonization factors (1, 2). Quorum sensing relies on perception of an endogenously synthesized secreted pheromone signal molecule, called an autoinducer, by a cognate receptor in a concentration-dependent manner. LuxIR quorum-sensing systems are widespread among Gram-negative bacteria, which use a LuxR-type quorum-sensing receptor to perceive an *N*-acyl L-homoserine lactone (AHL) chemical signal(s) (3). The importance of AHL-based quorum sensing in pathogens such as *Pseudomonas aeruginosa,* or mutualists such as *Sinorhizobium meliloti* (4, 5), has led to significant interest in developing methods to manipulate this regulatory circuit *via* interception of the native AHL signal molecule (6-9).

Despite this interest, only a few studies (10-12) have chemically modulated bacterial AHL quorum-sensing in a host model to ask whether signaling affects colonization robustness in the host environment, and all of these studies have focused on pathogenic associations (13). Pathogens represent only a small fraction of the microbes that both encode LuxIR-type systems and colonize animal or plant hosts; thus, I chose to apply a chemical approach, in combination with existing strains of *V. fischeri* carrying mutations in AinS-LitR and LuxIR branches of quorum sensing, to study the role of the LuxIR signal circuit in the maintenance of stable, beneficial host-microbe associations.

The symbiosis between the marine bacterium *Vibrio fischeri* and the squid *Euprymna scolopes* is a model system to study the initiation and maintenance of a natural, two-partner mutualism (14). A monospecific, and extracellular population of *V. fischeri* is maintained in a

specialized host structure called the light organ, where, as the name would suggest, symbionts produce light in exchange for the habitat provided by the host. Bioluminescence, and other behaviors that promote the stable association of a microbe and its host, are regulated by quorum sensing in *V. fischeri* (15).

The principal quorum-sensing circuit in *V. fischeri* is composed of the AHL signal molecule *N*-(3-oxo-hexanoyl)-L-homoserine lactone (3-oxo C6 HL), the signal synthase LuxI, and the AHL-binding transcriptional regulatory element LuxR. The LuxIR circuit is auto-regulated; LuxR bound to an AHL signal activates transcription of *luxI*, and promotes accumulation of the LuxI-synthesized 3-oxo-C6 HL (**Fig. 3-1*A***). In addition to LuxIR, *V. fischeri* encodes a second AHL-based quorum-sensing system, which is mediated by the *N*-octanoyl L-homoserine lactone (C8 HL) signal synthesized by AinS (**Fig. 3-1*A***). The C8 HL signals through the histidine kinase AinR in a concentration-dependent manner (16-18). A third, non-AHL, quorum signal is expressed in *V. fischeri*: a furanosyl borate diester (AI-2) that is synthesized by LuxS, and likely signals through LuxP and LuxQ, similar to the homologous set of genes in *Vibrio harveyi* (19, 20).

All quorum-sensing pathways in *V. fischeri* intersect at LuxR (**Fig. 3-1*A***). I have previously shown that in culture, both C8 HL and AI-2 accumulation contribute to activation of *luxR* transcriptional activator LitR (**Fig. 3-1*A***) (16, 19). C8 HL may also weakly bind to the non-cognate receptor LuxR, and contribute to an additional overlap between signaling systems (**Fig. 3-1*A***) (16, 21). In addition to the downstream targets of LuxR regulation (22, 23), C8 HL controls an extensive set of genes, independent of LuxR (22, 23).

a

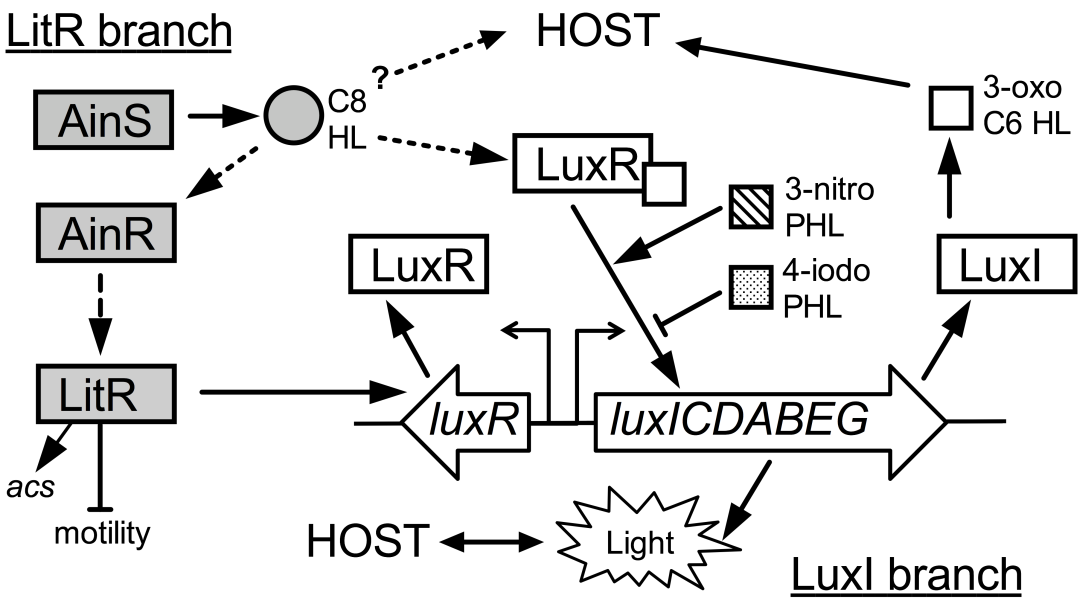
LitR branch
HOST
AinS
C8
HL
?
3-oxo
C6 HL
LuxR
AinR
3-nitro
PHL
LuxR
4-iodo
PHL
LuxI
LitR
luxR
luxICDABEG
acs
motility
HOST
Light
LuxI branch

b

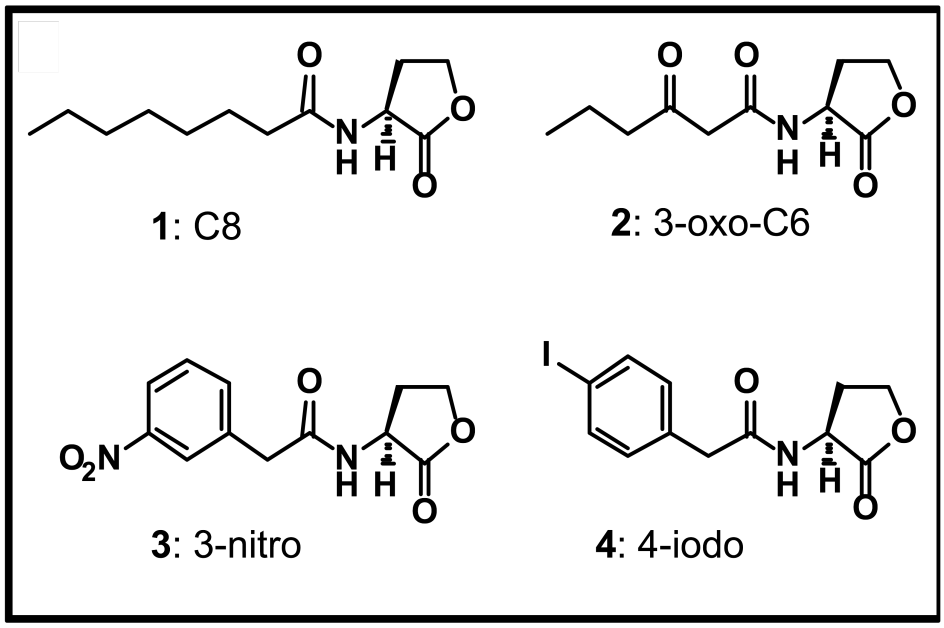
1: C8
2: 3-oxo-C6
3: 3-nitro
4: 4-iodo

Figure 3-1. The core AHL-dependent pathways of quorum signaling in *V. fischeri. A*) AinS synthesizes C8 HL, which is released into the environment and, when at a sufficiently high concentration, diffuses back into the cell. Subsequent interaction of C8 HL with LuxR may potentiate a weak, but potentially priming, induction of the *lux* operon (*luxICDABEG*). When a threshold concentration of C8 HL is reached, C8 HL is thought to bind its cognate receptor AinR, initiating a multi-step signaling cascade leading to an increase in LitR translation (18). LitR further activates transcription of *luxR*, increases the amount of LuxR. When it binds 3-oxo C6, LuxR strongly activates transcription of the *luxICDABEG* operon. Activation of *luxI* transcription increases the synthesis of 3-oxo C6, and amplifies induction of the *lux* operon, leading to an exponential increase (autoinduction) in the synthesis of the luciferase complex and light production. 3-nitro PHL and 4-iodo PHL are structural analogs of the HL family of quorum-sensing signals, and specifically enhance or depress LuxR function, respectively. The presence of native AHL molecules, C8 HL and 3-oxo C6 HL have been shown to also alter host gene expression. ***B***) Structures of the natural autoinducers (1 & 2) and non-native autoinducer analogs (3 & 4) used in this study: (1) octanoyl homoserine lactone; (2) 3-oxo-hexanoyl homoserine lactone; (3) 3-nitrophenyl homoserine lactone; and, (4) 4-iodophenyl homoserine lactone.

These convergent signal cascades culminate with the transcriptional regulation of the *luxICDABEG* operon, which encodes the light-producing luciferase enzyme complex, as well as LuxI itself. Previous studies suggest that regulation by AHL quorum sensing, mediated by AinS and LuxI, is necessary for colonization and bioluminescence of *V. fischeri* in the squid host, while the contribution of LuxS signaling is not essential for either process (19). The bioluminescence of *V. fischeri* is required to maintain a stable, and long-term partnership between host and symbiont, and possibly to signal the host (24, 25). A recently recognized role for quorum signals is as effectors of cross-kingdom communication (26); notably, the *E. scolopes* transcriptome responds to the presence of LuxI signal 3-oxo-C6 HL (27).

Despite the centrality of quorum sensing in the 'conversation' between squid and vibrio, much work remains to decipher to contribution of this regulatory network and its signals to the establishment and maintenance of a stable and robust symbiosis. To bring a new perspective to studies of quorum regulation and signaling in the squid-vibrio association, I took a combined chemical and genetic approach to disentangle the signaling cascade upstream and downstream of the regulatory element LitR, and to assess the relative contributions of each branch of the cascade to colonization of *E. scolopes*. I have identified a series of synthetic, non-native AHLs that are capable of strongly modulating luminescence (presumably *via* interaction with LuxR) in laboratory cultures of *V. fischeri* ES114, a squid light-organ isolate (28-30). Amongst these compounds, the phenylacetanoyl homoserine lactone (PHL) derivatives were found to be the most potent as both agonists and antagonists of luminescence. Two PHLs of particular interest were 3-nitro PHL, an agonist that, at a comparable molarity, induced higher levels of luminescence than the native LuxR ligand 3-

oxo-C6 HL, and 4-iodo PHL, an antagonist that strongly inhibited luminescence induction by 3-oxo-C6 HL (structures shown in **Fig. 3-1*B***).

In the current study, I show that in *V. fischeri* (i) the effects of these two PHL derivatives are specific to targets of the signal synthesized by LuxI, and do not perturb known LuxI-independent quorum signaling, and (ii) these compounds can be used, at concentrations comparable to those observed in culture studies (28), to manipulate bacterial activities within the squid host. The chemical studies highlight an intriguing and novel role for LuxIR quorum sensing during the initial stages of the symbiotic 'conversation'. Specifically, I demonstrate that the first day of colonization is a critical period in which regulation by LuxIR quorum sensing predicates the long-term stability of the symbiotic partners. These studies underscore the value of chemical methods to probe mechanisms of quorum sensing and, to the knowledge, do so for the first time in the context of a beneficial eukaryotic-prokaryotic symbiosis.

MATERIALS AND METHODS:

Bacterial strains and growth conditions. Strains and plasmids used in this work are listed in **Table 3-1**. *V. fischeri* strains are derivatives of ES114 (31), and were grown at 28° C in either a seawater-tryptone medium (SWT) (31) or Luria-Bertani salt medium (LBS) (32). *Escherichia coli* strains were grown in Luria-Bertani (LB) medium (33). Media were solidified with 1.5% agar as needed. When appropriate, antibiotics were added to LB and LBS media at the following concentrations: chloramphenicol, 5 μg/ml for *V. fischeri,* and 25 μg/ml

for *E. coli*; erythromycin, 5 µg/ml for *V. fischeri*; kanamycin 100 µg/ml for *V. fischeri*. Medium reagents were purchased from ThermoFisher Scientific.

β-galactosidase assay. The β-galactosidase activity assays were preformed as described previously (34). Briefly, strains were cultured in SWT, the optical density (OD) at 600 nm was measured, and β-galactosidase activity was determined after 4 h, using a microtiter-dish method modified from Slauch and Silhavy (35). Cell-pellets were frozen at -20° C before resuspension, and the SDS/chloroform step was omitted. The A_{420} values of the microtiter wells were read every 30 s for 1 h using a GENiosPro 96-well plate reader (TECAN, Research Triangle Park, NC). Three replicates of two dilutions were tested for each cell pellet. The relative units of β-galactosidase activity were calculated using the formula: rate [V_{max}] / ([OD] x volume [mL]).

Motility assay. The swimming behavior of *V. fischeri* was determined by growing strains to approximately 1.0 OD in SWT with 0.25% dimethysulfoxide (DMSO) containing the appropriate signal-molecule additions. The cells were collected by centrifugation of 1 ml of the culture, the cell pellet washed with SWT, and resuspended to 0.6 OD units in SWT containing the additions. Three microliters of a suspension of each strain was spotted onto the surface of a 0.25% agar plate containing defined seawater minimal medium (MM) base (23) supplemented with 0.3% casamino acids and 0.25% DMSO containing the appropriate signal molecules. The ring diameter was determined at 16 h as a measure of the relative rate of bacterial migration.

Chemical synthesis. Procedures for synthesizing 3-oxo-C6 HL, C8 HL, 3-nitro PHL and 4-iodo PHL have been previously described (29). All compounds were suspended as stock solutions in DMSO, and stored sealed in the freezer when not in use. In biological experiments, DMSO was added to a final concentration of 0.25% in all conditions, including those with no added compound.

Squid colonization assays. For animal colonization experiments, newly hatched squid were placed in filter-sterilized seawater (FSW) (Instant Ocean, Aquarium Systems) containing the appropriate *V. fischeri* strain at approximately 3000 CFU/ml; a control group of animals was placed in uninoculated FSW, supplemented with 0.25% DMSO containing either the natural AHL or non-native analog, or no added compound, as indicated. All animals were transferred to fresh, uninoculated FSW at 3 h, and again at approximately 16 h, after inoculation. There was no evidence that additions of up to 100 μM of the AHLs or analogs had any adverse effects on the animals. At 48 or 72 h post-inoculation, individual animal bioluminescence was determined using a TD 20/20 (Turner Designs) luminometer, and the animals were sacrificed to determine the CFU/squid. To monitor animal bioluminescence over time, measurements were acquired with Light a Packard Tri-Carb 2100TR scintillation counter (Packard Instruments, Meriden, CT) modified to operate as an automated photometer. In all experiments, uninoculated animals had no detectible bioluminescence or CFUs.

Statistics. Statistical analysis was performed using the GraphPad Prism software package (Version 5.0, 2010). The experimental data sets were assessed for normal distribution using

the D'Agostino and Pearson omnibus test (36). Data that fit a normal distribution were tested for significant variation among experimental groups by one- or two-factor analysis of variance (ANOVA), with post-hoc Bonferroni T-testing. Data that failed to fit a normal distribution were assessed by the Kruskal-Wallis test with Post-Hoc Dunn's multiple comparisons to identify groups of statistically equivalent means.

Table 3-1. Strains and plasmids used in this study

Strain or Plasmid	**Description**	**Reference or source**
V. fischeri		
ES114	Wild-type *E. scolopes* light-organ isolate	(31)
CL21	*ainS*::*cam*	(16)
CL53	*luxR*::*erm*	(19)
PMF8	*litR*::*kan*	(37)
VCW2G7	*luxI* (frameshift)	(16)
EVS102	Δ*luxCDABEG*	(38)
E. coli		
DH5a-λpir	Reporter vector	(39)
Plasmids		
pSVS101	*acs'-lacZ*$^{+}$ reporter, Kan^{R}	(34)

RESULTS:

Non-native analogs of 3-oxo-C6 HL do not affect AinS phenotypes. Certain native AHL autoinducers or non-native antagonists are able to signal through two AHL receptors (12, 40-42). To determine whether the PHL analogs interact only with the LuxI-dependent quorum-sensing pathway, or if the molecules also modulate quorum signaling upstream of LuxI, I examined the effects of added native autoinducer and non-native PHLs on two phenotypes that are regulated by LitR and AinS, but that are independent of the LuxI branch of quorum

sensing in *V. fischeri* (**Fig. 3-1*A***). Using concentrations of native and non-native AHLs sufficient to modulate LuxI signaling in previous studies (28), I examined motility on soft agar (repressed by LitR and AinS), and the metabolic shift known as the acetate switch (activated by LitR and AinS) (**Figs. 2-1*A*, 2-2**).

I first performed motility assays to determine the effects of the native AHLs and the PHL analogs on AinS and LitR-dependent signaling. As previously reported (23), cells of an *ainS* mutant spotted onto soft-agar medium swam faster, and produced significantly larger outer rings of migration, than those of their wild-type parent, consistent with AinS- and LitR-dependent repression of motility (**Fig. 3-2*A***). Previous work has demonstrated that none the molecules used in the present study alter growth of *V. fischeri* (28). As anticipated, *ainS*$^-$ cells spotted onto agar containing C8 HL migrated the same distance as their similarly treated parent (**Fig. 3-1*A***), although neither 3-oxo-C6 nor the PHL analogs influenced migration. The addition of 3-nitro PHL slightly increased the motility of the *litR* mutant but not the *ainS* mutant relative to wild type, while 4-iodo-PHL had no effect on the migration of either mutant. The effect of 3-nitro PHL on motility was slight compared to that of C8 HL, however it is possible that this analog may also contribute to LitR-dependent signaling. Notably, the effect of 3-nitro PHL was only apparent in the absence of C8 HL, suggesting that the signaling interaction would not be biologically relevant in an environment where C8 HL accumulates, such as the squid light organ. This hypothesis is consistent with the finding that 3-oxo-C6 HL may also have the capacity to signal via the LitR-dependent pathway, although with much less sensitivity than 3-oxo-C6 HL-LuxR signaling (18).

The transcription of the acetyl-CoA synthetase gene, *acs*, is a measure of the alteration of the AinS-dependent induction of the acetate switch (**Fig. 3-1*A***). Wild-type and *ainS*-mutant strains, each carrying an *acs'-lacZ*$^{+}$ promoter-reporter plasmid, were grown in liquid medium supplemented with the native autoinducer or non-native analog, and assayed for *acs* expression (**Fig. 3-2*B***). Consistent with previous results (34), without any additions, *ainS*$^{-}$ *V. fischeri* had a 41% lower level of *acs* expression relative to wild-type cells. Neither the native autoinducer nor the PHL analogs significantly altered the expression of *acs* in the wild-type cultures. In contrast, the addition of C8 HL to the medium raised *acs* expression in the *ainS* mutant to 110% of wild-type levels, as expected (34). Further, 3-oxo-C6 HL, 3-nitro PHL and 4-iodo PHL did not significantly alter the expression by *ainS*$^{-}$ *V. fischeri*, indicating that 3-nitro PHL is unable to induce the AinSR system in the absence of C8 HL, and that 4-iodo PHL does not suppress this system in wild-type cells. Together with the motility data, these results indicate that, although 3-nitro PHL and 4-iodo PHL interact with the 3-oxo-C6 HL-regulated LuxIR system, they do not alter C8 HL-regulated phenotypes through LitR, and therefore do not target this branch of quorum sensing in *V. fischeri* in an environment with active C8 HL signaling.

Native and non-native LuxR-binding molecules can signal during symbiosis. To determine whether experimentally added autoinducer signals affect *V. fischeri* during colonization of its natural host, I first examined whether the presence of 4-iodo PHL, an antagonist of 3-oxo-C6 HL in culture (28), was also effective in *V. fischeri* within the host. Specifically, I asked whether 4-iodo PHL could antagonize LuxIR quorum sensing in the host,

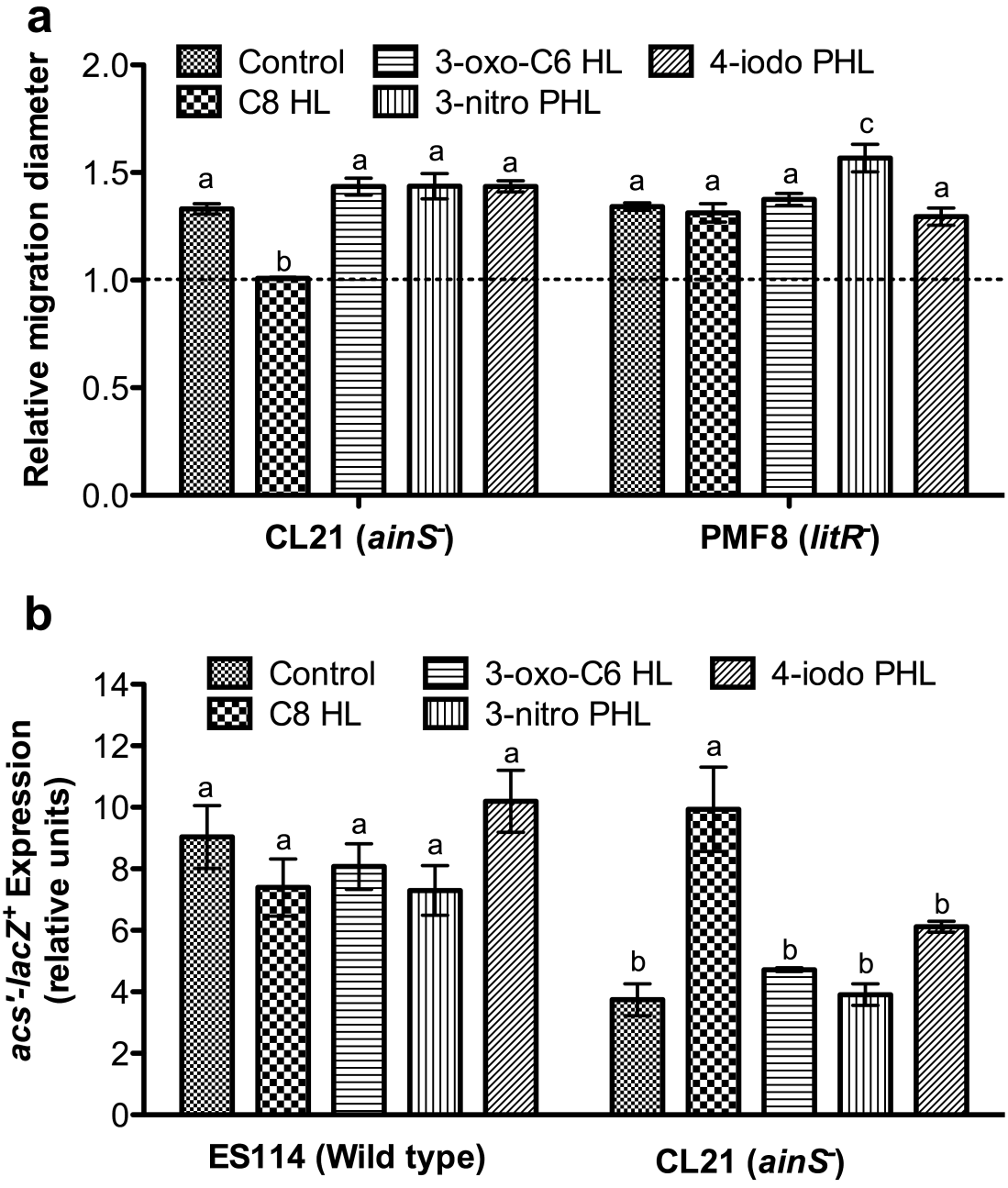
a
Relative migration diameter
2.0
1.5
1.0
0.5
0.0
Control
C8 HL
3-oxo-C6 HL
3-nitro PHL
4-iodo PHL
a
b
a
a
a
a
a
a
c
a
CL21 (ainS-)
PMF8 (litR-)
b
acs'-lacZ+ Expression (relative units)
14
12
10
8
6
4
2
0
Control
C8 HL
3-oxo-C6 HL
3-nitro PHL
4-iodo PHL
a
a
a
a
a
b
a
b
b
b
ES114 (Wild type)
CL21 (ainS-)

Figure 3-2. AinS-dependent transcriptional and phenotypic regulation is unaffected by non-native PHL derivatives. ***A***) The migration of the indicated mutant strains of *ainS*$^-$ and *litR*$^-$ *V. fischeri* was measured, relative to migration of a wild-type control, after 16 h on motility agar supplemented with either a solvent control (DMSO), or 120 nM of the indicated HL or PHL analog. Error bars represent S.E.M. of nine replicate plates. 'a', 'b' and 'c' indicate distinct treatment groups with statistically equivalent means; Two-way ANOVA (interaction $F(4,80) = 10.1$, $P < 0.001$; HL addition $F(4,80) = 20.8$, $P < 0.0001$; strain $F(1,80) = 4.0$, $P = 0.049$), with Post-hoc Bonferroni T-tests. ***B***) The level of *acs* expression in wild-type and *ainS*$^-$ strains of *V. fischeri* containing the *acs'-lacZ*$^+$ reporter plasmid were determined after 4 h of growth in SWT supplemented with 40 nM of the indicated AHL or PHL analog. Error bars represent S.E.M. of 4 biological replicates. Significance was determined by Two-way ANOVA (interaction $F(4,20) = 7.2$, $P = 0.0009$; strain $F(1,20) = 28.7$, $P < 0.0001$; addition $F(4,20) = 5.3$, $P = 0.0045$), with Post-hoc Bonferroni comparison testing: 'a' and 'b' indicate distinct treatment groups with statistically equivalent means.

and reduce the level of wild-type bioluminescence to that of mutants deficient in LuxIR signaling. Wild-type colonized animals maintained in seawater containing 50 or 100 μM 4-iodo PHL had 20- to 40-fold lower levels of luminescence at 48 h of colonization than in seawater without added antagonist (**Fig. 3-3*A***). As little as 5 μM 4-iodo PHL was sufficient to reduce the bioluminescence of *V. fischeri* cells to the level of the *luxI* mutant, which attains approximately 5% of the bioluminescence of wild-type cells in symbiosis, while a concentration of 0.5 μM had no significant effect on symbiotic bioluminescence (**Fig. 3-3*A***). Notably, the amount of 4-iodo PHL observed to reduce bioluminescence is within the range of the concentration for 50% inhibition (IC_{50}) for this molecule obtained in culture studies (IC_{50} = 0.9 mM) (28), and suggests that the delivery of the analogs to the symbiont population is not greatly hindered by host tissues.

I next measured the contribution of native and non-native LuxR agonists to the induction of bioluminescence. As expected (43), in the absence of added signal, the bioluminescence of animals colonized by the *luxI* mutant was lower than that of wild-type colonized animals (**Fig. 3-3*B,C***). In contrast, addition of as little as 0.5 mM of either 3-oxo-C6 HL (**Fig. 3-3*B***) or 3-nitro PHL (**Fig. 3-3*C***) to animals colonized by *luxI⁻ V. fischeri* restored induction of bioluminescence. Higher concentrations of the experimentally added signals did not further increase the bioluminescence of either wild-type *V. fischeri*, or the *luxI* mutant, and I noted no significant difference in the maximum level of bioluminescence achieved by the superactivator 3-nitro PHL when compared to the native LuxR agonist, 3-oxo-C6 (concentration for 50% activation, EC_{50} values = 0.3 and 3.0 mM, respectively, in *V. fischeri* culture; (28)). It is still possible that the concentration of exogenously added signal

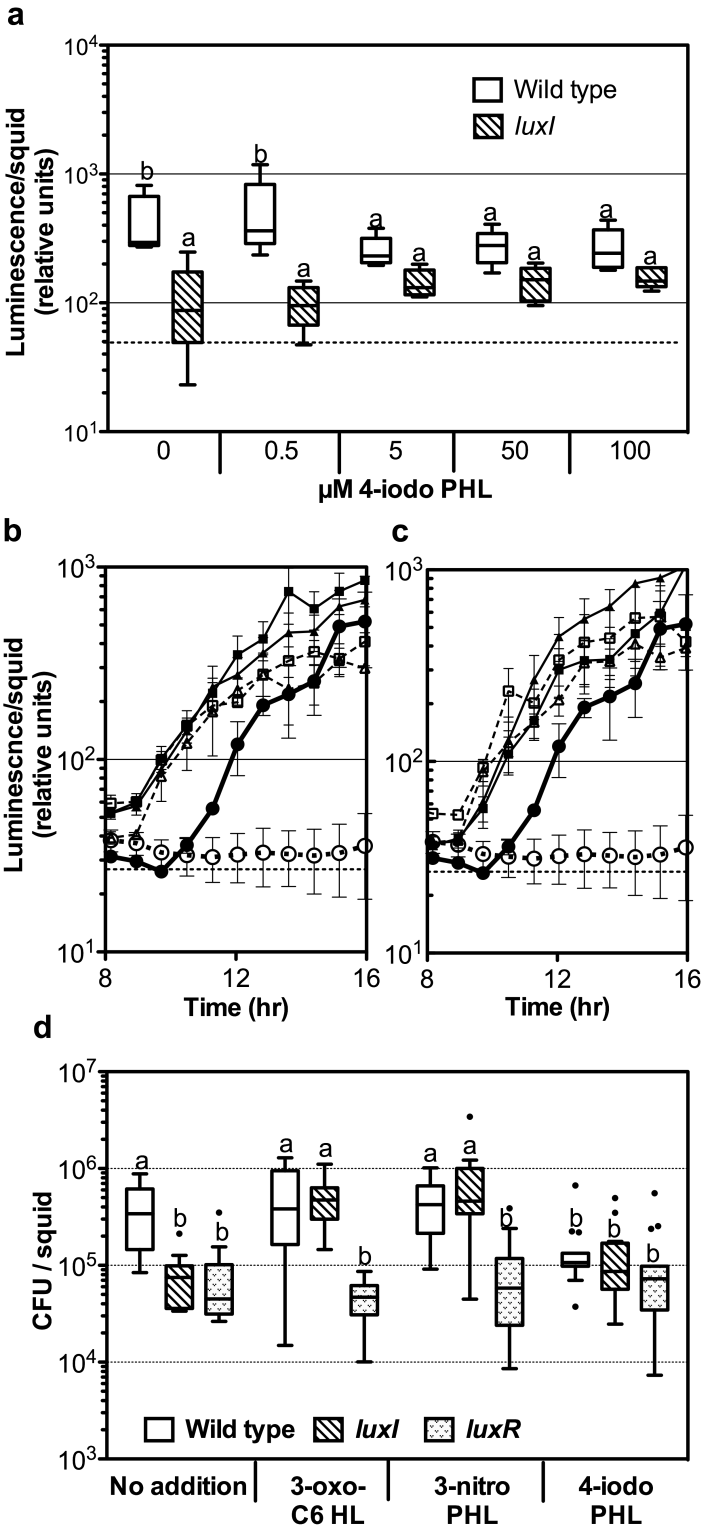
a
Luminescence/squid (relative units)
Wild type
luxI
μM 4-iodo PHL
b
c
Luminescnce/squid (relative units)
Time (hr)
d
CFU / squid
Wild type
luxI
luxR
No addition
3-oxo-C6 HL
3-nitro PHL
4-iodo PHL

Figure 3-3. Contribution of native and non-native HL analogs to symbiotic colonization and bioluminescence at 48 h post-inoculation. ***A***) Bioluminescence of wild-type (open boxes) was compared to *luxI*$^-$ *V. fischeri* (diagonal boxes) in the presence of different concentrations of 4-iodo PHL. Significant differences in mean bioluminescence were determined by the Kruskal-Wallis test (H = 36.2, 10 d.f., P<0.0001), with Post-Hoc Dunn's multiple comparisons ('a' and 'b' indicate distinct groups with equivalent means; P<0.05). Inner fences determined by Tukey's method, dashed line indicates background level of luminescence. Induction of bioluminescence of wild type (closed symbols), or *luxI* (open symbols) was monitored in the presence of ***B***) no added HL (circles), 0.5 μM C6 HL (triangles), or 5 μM C6 HL (squares), or ***C***) no added HL (circles), 0.5 μM 3-nitro PHL (triangles), or 5 μM 3-nitro PHL (squares). Bars represent S.E.M. of n=5; dashed line indicates level of detectable luminescence. ***D***) Animal colonization at 48 h was compared between inoculations with wild-type (open boxes), *luxI*$^-$ (diagonal boxes), or *luxR*$^-$ (dotted boxes) *V. fischeri* in the presence of 5 μM added HL, as indicated. Significant differences in mean colony-forming units (CFU) per animal were determined by the Kruskal-Wallis test (H = 172.4, 15 d.f., P<0.0001), with Post-Hoc Dunn's multiple comparisons ('a' and 'b' indicate distinct groups with equivalent means; P<0.05). Inner fences determined by Tukey's method; dots represent outliers.

experienced by the symbionts inside the squid's light organ is lower than that present in the surrounding seawater due to diffusion limitation; however, addition of either 3-oxo-C6 HL (**Fig. 3-3*B***) or 3-nitro PHL (**Fig. 3-3*C***) resulted in induction of luminescence in wild-type colonized animals 1 h earlier than it occurred without the added compounds, suggesting that both compounds swiftly and effectively diffuse into the light organ, reaching concentrations that result in induction of LuxIR activity.

LuxIR signaling is required for *V. fischeri* to maintain a colonization of the light organ; thus, I also examined the effect of exogenously added autoinducers on colonization levels (*i.e.*, CFUs/squid) of LuxIR pathway mutants. Addition of 5 μM of the LuxR antagonist 4-iodo PHL to wild type *V. fischeri* diminished the host's maintenance of a light-organ colonization to a level typical of *luxI*⁻ *V. fischeri* (**Fig. 3-3*D***). However, 4-iodo PHL had no effect on the colonization of the *luxI* mutant, supporting the conclusion that the molecule suppresses colonization by wild-type cells solely through its inhibition of the LuxIR pathway. Colonization levels of the *luxI* mutant in the squid light organ were fully restored to those of wild-type *V. fischeri* when either 3-oxo-C6 HL or 3-nitro PHL were added (**Fig. 3-3*D*)**. Additions of 5 μM 3-oxo-C6, 3-nitro PHL, or 4-iodo PHL (**Fig. 3-3*D***) had no impact on the colonization defect of the *luxR* mutant, indicating that the distinct effects of both these autoinducer analogs are dependent on a functioning LuxIR signal pathway. Taken together, these results show that exogenously added autoinducers, both the native signal and the non-native agonist, induce expected LuxIR-system responses, even when the bacteria are within host tissues.

LuxR ligands do not perturb AinS-dependent symbiosis factors. To assess the effect of exogenous autoinducers on AinS-dependent quorum sensing during squid colonization by *V. fischeri*, animals colonized by wild-type, *ainS*$^-$ or *litR*$^-$ strains were exposed to either the native autoinducers or the non-native analogs. In the absence of added compounds, animals colonized by the *ainS* mutant had both a lower level of luminescence (**Fig. 3-4*A***) and a lower number of CFU/squid (**Fig. 3-4*B***) when compared to wild-type colonized animals. Luminescence, and colonization by *litR*$^-$ *V. fischeri* was indistinguishable from wild-type *V. fischeri* in the absence of added compounds (**Fig. 3-4*A,B***). The addition of C8 HL, but not 3-oxo-C6 HL, restored the luminescence and CFU/squid of animals colonized by the *ainS* mutant to wild-type levels, demonstrating that the mutant's defect in symbiosis is not caused solely by a repression of signal synthesis by LuxI. The addition of the antagonist, 4-iodo PHL, decreased the luminescence and colonization levels of all strains, further indicating that the LuxIR system is active, and subject to inhibition, during colonization of squid by *ainS*-deficient symbionts. Because there are regulatory targets of LuxIR quorum sensing other than the bioluminescence gene cluster *luxCDABEG* (22), I reasoned that if a target of LuxIR quorum sensing apart from bioluminescence contributed to host colonization, the symbiotic population would be sensitive to the addition of LuxR antagonist 4-iodo PHL, even in the absence of the *luxCDABEG* genes. Accordingly, I observed that the level of the symbiotic population of a Δ*luxCDABEG* mutant (38), which lacks the genes that encode the luciferase complex, was significantly lower than that of wild-type *V. fischeri* at 48 hours post-colonization (**Fig. 3-5**). While the population level of Δ*luxCDABEG* cells was not altered by 5 μM 4-iodo PHL, the addition of 4-iodo PHL to a wild-type colonization did not completely

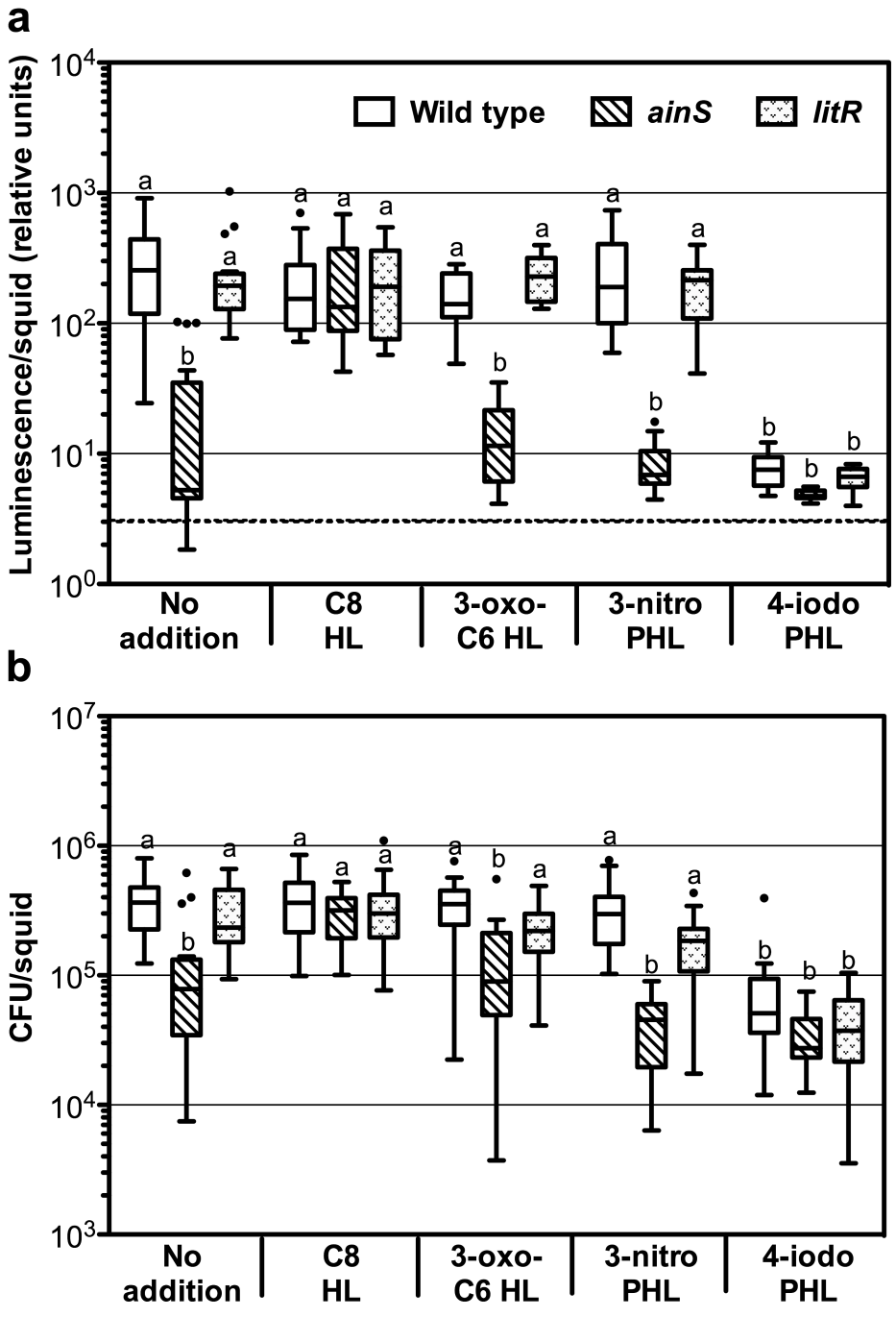
a
Luminescence/squid (relative units)
10^4
10^3
10^2
10^1
10^0
Wild type
ainS
litR
No addition
C8 HL
3-oxo-C6 HL
3-nitro PHL
4-iodo PHL
b
CFU/squid
10^7
10^6
10^5
10^4
10^3
No addition
C8 HL
3-oxo-C6 HL
3-nitro PHL
4-iodo PHL

Figure 3-4. AinS- and LitR- dependent colonization dynamics are not perturbed by analogs of 3-oxo C6 homoserine lactone. Squid colonized by wild-type (white), *ainS*$^-$ (diagonal) or *litR*$^-$ (dotted) *V. fischeri* was treated with either a DMSO solvent control (No addition), or 5 μM additions of C8 HL, 3-oxo-C6 HL, 3-nitro PHL or 4-iodo PHL as indicated. ***A***) Differences in bioluminescence among treatments and strains at 48 h were assessed by the Kruskal-Wallis test ($H = 78.8$, 15 d.f., $P<0.0001$), with Post-Hoc Dunn's multiple comparisons ('a' and 'b' indicate distinct groups with equivalent means, $P<0.05$); dashed line indicates background level of luminescence. ***B***) Differences in colonization levels at 48 h were assessed by the Kruskal-Wallis test ($H = 149.7$, 15 d.f., $P<0.0001$) with Post-Hoc Dunn's multiple comparisons ('a' and 'b' indicate distinct groups with equivalent means, $P<0.05$). Inner fences determined by the Tukey method; black dots indicate outliers; CFU, colony-forming units.

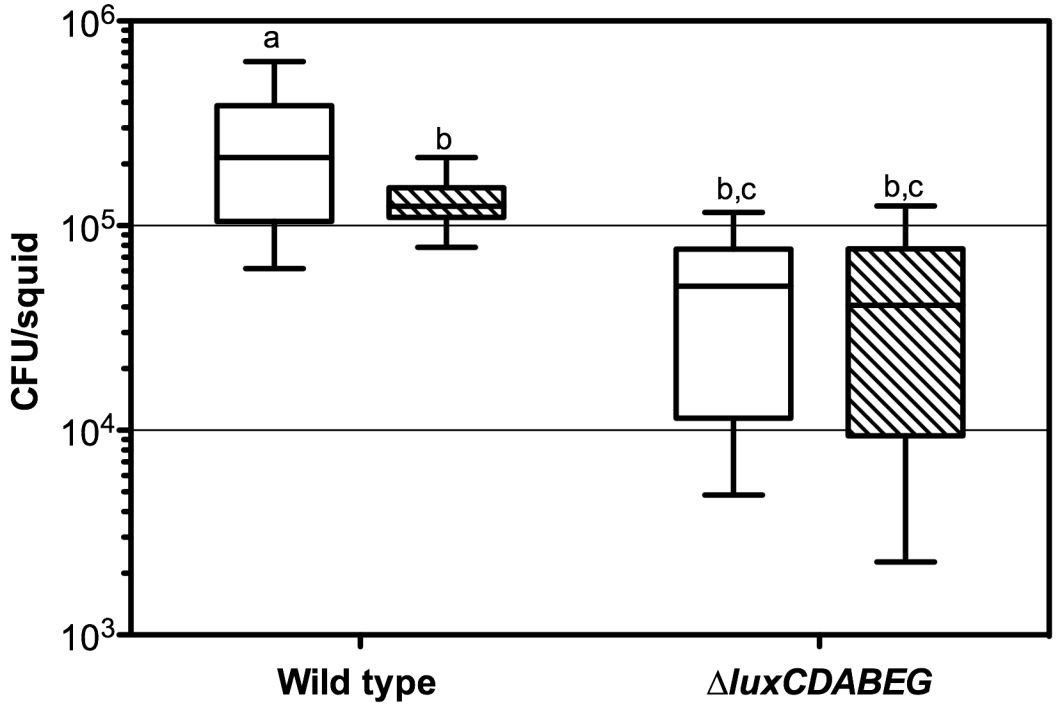

Figure 3-5. LuxIR-dependent changes in symbiont population density require the bioluminescence gene cluster. Animals were colonized with wild-type or Δ*luxCDABEG V. fischeri* in the presence of a DMSO-only solvent control (open boxes), or exogenous HL 4-iodo PHL (diagonal boxes). Bars represent Tukey's inner fences, n=24 squid. Significance determined by the Kruskal-Wallis test (H= 67.5, 4 d.f., P<0.0001) with Post-hoc Dunn's multiple comparisons ('a', 'b', and 'c' indicate distinct groups of equivalent means, P<0.05). CFU: colony-forming units.

decrease the level of symbiotic bioluminescence to that of Δ*luxCDABEG* (data not shown), and this small amount of residual bioluminescence correlated with a slightly larger population (**Fig. 3-5**). Together, these data suggest that bioluminescence is the key LuxIR-regulated factor that contributes to initial light-organ colonization, and that even a low level of light production during symbiosis can contribute to the maintenance of a normal symbiont population level.

An initial, yet transitory, appearance of bioluminescence is sufficient to result in robust and persistent colonization. LuxIR induction of bioluminescence is required for *V. fischeri* to maintain colonization of the light organ, but the population levels of Δ*luxCDABEG, luxI* and *luxR* mutants only begin to decrease after the first 24 h of symbiosis (38, 43). Surprisingly, I found that chemically inhibiting LuxIR activation of bioluminescence by the addition of 5 μM 4-iodo-PHL after 24 h of light-organ colonization did not significantly alter colonization of *V. fischeri* at 48 h (**Fig. 3-6**), even though addition of the antagonist was sufficient to lower symbiotic bioluminescence to levels comparable to the colonization-deficient *luxI*⁻ strain. More unexpected was the observation that, after 24 hours or colonization, even doubling the length of the symbiont's exposure to 4-iodo PHL had no significant impact on colonization of the light organ (**Fig. 3-6**). Collectively, these results suggest that induction of bioluminescence by LuxIR within the first 24 h of symbiosis is sufficient to maintain robust symbiont colonization more than a day later.

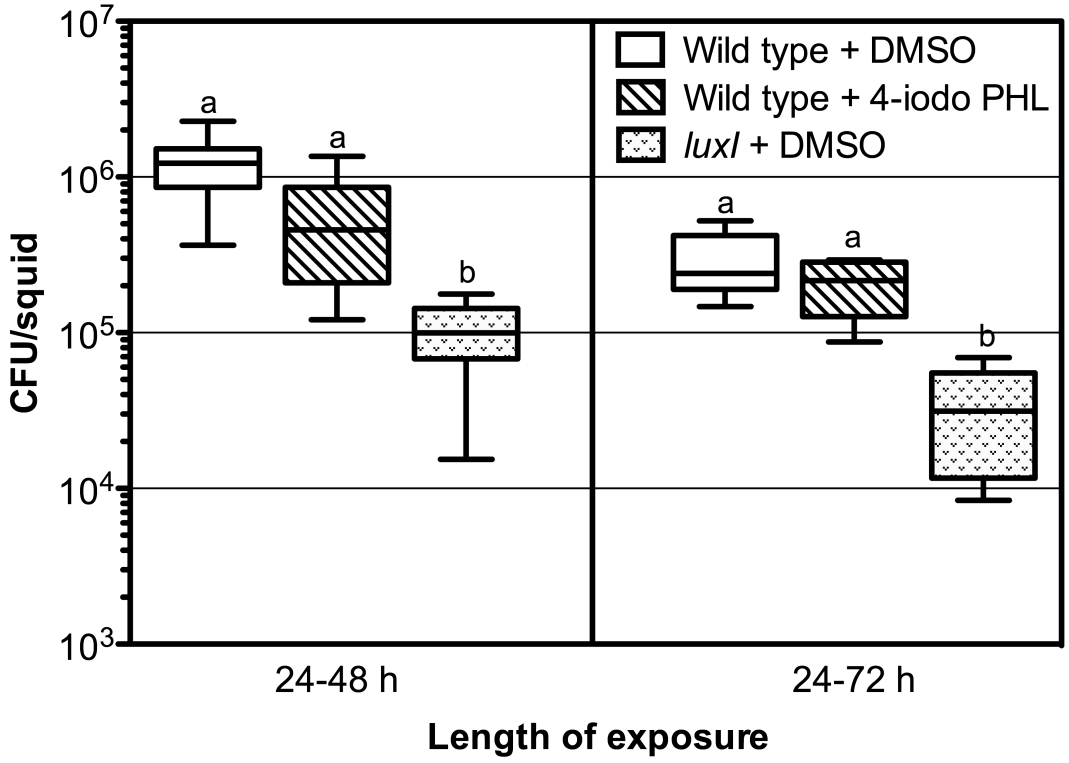

Figure 3-6. Squid colonized with wild-type *V. fischeri* for 24 were either left untreated (open boxes), or treated with 4-iodo PHL (diagonal boxes) for an additional 24 h (end-point = 48 h), or 48 h (end-point = 72 h) prior to enumeration of colony-forming units (CFU). Populations of squid were also colonized by *luxI*⁻ in the presence of a DMSO solvent control (dotted boxes) as a comparison for 4-iodo-PHL inhibitory activity. The mean CFU value was compared to that of the control wild-type populations by Kruskal-Wallis test ($H=47.9$, 6 d.f., $P<0.0001$), with Post-hoc Dunn's multiple comparisons ('a' and 'b' indicate distinct groups with equivalent means, $P<0.05$).

To better define the window in which LuxIR-regulated bioluminescence is critical for persistent colonization of the host, I perturbed the LuxIR circuit by addition of PHL analogs in the symbiosis after 18 h of infection. I reasoned that by this point in the symbiosis: (i) the symbiont has reached its peak population in the light organ (44), and (ii) the host has initiated irreversible, symbiont-dependent, morphogenic programs (45). I first modulated the loss or gain of bioluminescence at 18 h either by adding 4-iodo PHL to squid colonized by wild-type *V. fischeri*, or by adding 3-nitro PHL to squid colonized by *luxI⁻ V. fischeri* from 18-48 h post-colonization. The rapid loss of animal bioluminescence upon addition of 4-iodo-PHL at 18 h (**Fig. 3-7*A***), which occurred within a few hours of exposure to the antagonist (**Fig. 3-8**), was sufficient to decrease the population of wild-type *V. fischeri* to levels comparable to *luxI* by 48 h of colonization (**Fig. 3-7*B***). Additionally, the rapid gain of bioluminescence achieved by exposing squid colonized by the *luxI* mutant to 3-nitro PHL after 18 h of infection (**Fig. 3-7*A***) did not lead to a significant increase in the colonization level of *luxI⁻ V. fischeri* at 48 h (**Fig. 3-7*B***). Taken together, these data suggest that continual activation of bioluminescence by LuxR, throughout the first day of colonization, rather than the induction of bioluminescence at a specific stage during the initiation of symbiosis (45), is required to maintain a robust population over subsequent days.

If the level of bioluminescence, rather than simply its presence, is the critical determinant of colonization stability, then I reasoned that a gradual decrease in LuxR activation of bioluminescence after 18 h should not impair colonization as severely as the complete loss of bioluminescence at that juncture. To test this hypothesis, I exposed squid colonized by wild-type *V. fischeri* to 4-iodo PHL (to diminish luminescence), or *luxI⁻ V.*

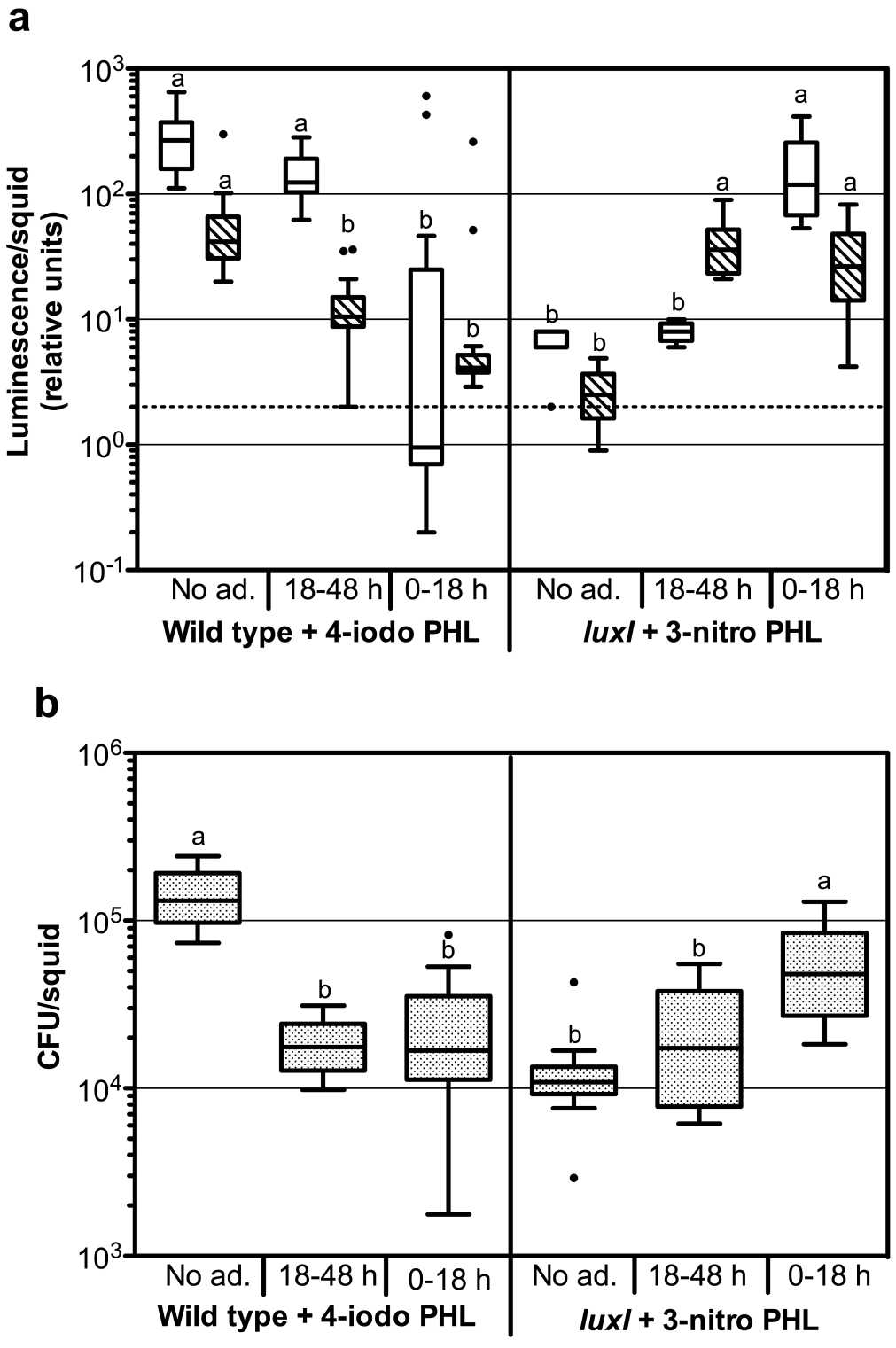
a
Luminescence/squid (relative units)
10^3
10^2
10^1
10^0
10^{-1}
No ad.
18-48 h
0-18 h
Wild type + 4-iodo PHL
luxI + 3-nitro PHL
b
CFU/squid
10^6
10^5
10^4
10^3

Figure 3-7. Induction of bioluminescence by LuxIR quorum sensing is required for establishment of a robust symbiont population. The bioluminescence of an established symbiont population was either inhibited or induced by exogenous exposure to 5 μM of a HL-analog for a period of time (exposure indicated as a range of hours post-colonization: 0-18 h or 18-48 h; No ad. = no analog addition). ***A***) Animal bioluminescence was measured at 18 h (open boxes), and 36 h (diagonal boxes) post-inoculation for each treatment group. Differences in mean luminescence (compared to wild type without additions) were determined by the Kruskal-Wallis test ($H = 147.3$, 12 d.f., $P<0.0001$) with Post-Hoc Dunn's multiple comparisons ('a' and 'b' indicate distinct groups with equivalent means), dashed line indicates threshold of bioluminescence detection. ***B***) Mean CFU at 48 h post-inoculation was compared to the wild type without additions by the Kruskal-Wallis test ($H = 41.3$, 6 d.f., $P<0.0001$), with Post-Hoc Dunn's multiple comparisons ('a', 'b' and 'c' indicate distinct groups with equivalent means, $P<0.05$). Inner fences determined by the Tukey method; black dots indicate outliers; CFU, colony-forming units.

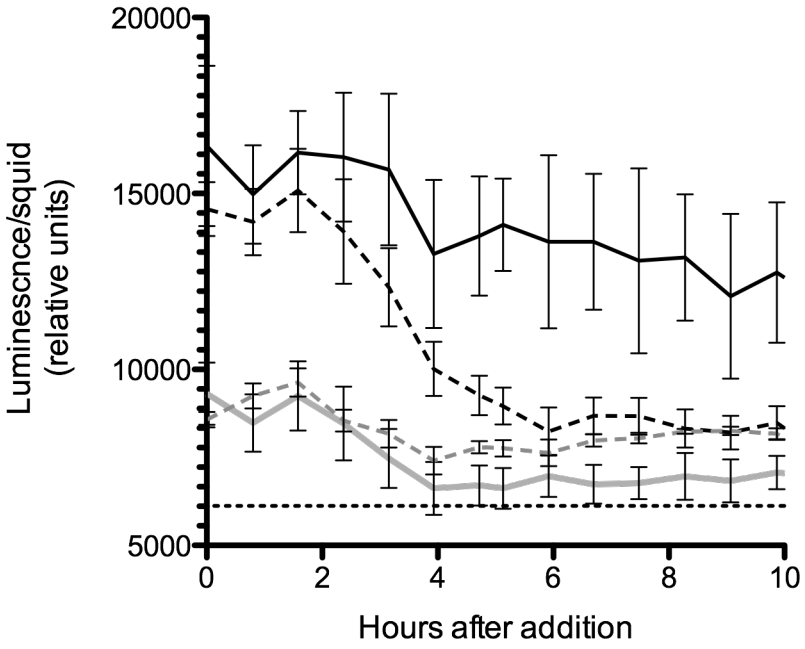

Figure 3-8. Addition of 4-iodo PHL to squid colonized by wild-type *V. fischeri* rapidly decreases symbiotic bioluminescence. Animals were colonized by wild type (black lines), or the *luxI* mutant (grey lines), for 24 h, prior to addition of 50 μM 4-iodo PHL (dashed lines), or a DMSO-only solvent control (solid lines). Bars represent standard error of the mean, n=5.

fischeri to 3-nitro PHL (to enhance luminescence) from 0-18 h of colonization. The small change in the mean luminescence levels of the animals is consistent with the retention of some of the molecule by the animals (**Fig. 3-7*A***). The slight increase of wild-type bioluminescence observed after removal of 4-iodo-PHL at 18 h was not sufficient to support symbiotic colonization at 48 h, consistent with the defect in colonization observed in squid colonized by non-bioluminescent symbionts from 0-18 h (**Fig. 3-7*B***). In contrast, the gradual decrease in bioluminescence of the *luxI* mutant following 18 h exposure to 3-nitro PHL only slightly impaired symbiont colonization at 48 h, compared to the colonization level of wild-type *V. fischeri* in which bioluminescence had been severely impaired by addition of 4-iodo PHL from 18-48 h (**Fig. 3-7*B***). These results suggest that the continued maintenance of a stable symbiont population requires that the symbionts achieve a threshold level of bioluminescence during the first day of colonization.

DISCUSSION:

Synthetic small-molecule probes can help illuminate biological phenomena by providing both temporal and spatial levels of control to experimental manipulations and, thereby, complement traditional biochemical and genetic approaches (46). These tools are particularly powerful for the study of both intercellular signaling and developmental processes, where the timing and sequence of extracellular trigger molecules play crucial roles. As highlighted above, the design and application of such chemical probes to interrogate bacterial quorum sensing has recently become a target of intense study (6-9). Much of the practical interest in quorum-signal manipulation comes from its potential to create a new class

of anti-pathogenic agents designed, for example, to inhibit bacterial virulence (47, 48). However, the use of such therapies to modulate bacterial pathogens within animal tissues requires a much clearer understanding of the response of the co-occurring normal microbiota to any unintended collateral effects of the treatment on their quorum-sensing processes.

The remarkable specificity that the light-organ environment shows for *V. fischeri* makes the squid-vibrio symbiosis ideal for the study of the chemical dialog that promotes a long-term and stable association. In the current study, I report for the first time the use of non-native, synthetic AHLs (3-nitro and 4-iodo PHLs) to probe this symbiosis. As in the squid-vibrio system (22, 23), the legume-rhizobium mutualism also promotes the establishment of a stable colonization by activating genes required for the earliest stages of nodulation in the host (49). In contrast, quorum sensing by the pathogens *Vibrio cholerae* (50) and *Pectobacterium carotovara* (12) represses production of the bacterium's virulence factors, presumably to evade host defenses and/or delay their deployment until the population is dense enough to sustain or transmit an infection (51). Thus, in both mutualism and pathogenesis the timing of signaling during host colonization is key, and addition of chemical signal analogs can help probe this temporal pattern. In addition, it is tempting to speculate that differences in the 'wiring' of quorum-sensing systems among pathogens and mutualists of the same genus, such as *V. cholerae* and *V. fischeri*, contribute in some way to the dichotomy of host responses.

Specific and sensitive chemical modulation of LuxIR quorum sensing

To interpret experiments designed to chemically manipulate quorum sensing, it is necessary for any small-molecule analogs to be specific. *V. fischeri*, like many Gram-negative microbes that encode LuxIR quorum-signaling circuits, encodes an additional AHL quorum signal, synthesized by AinS (17, 52). Although the putative receptor, AinR, is not structurally related to LuxR, both may bind acyl-homoserine lactone signals, including 3-oxo-C6 HL, and C8 HL (18, 53). Furthermore, LuxR has previously been shown to react to the AinS signal, C8 HL, and AinR to the LuxR signal 3-oxo-C6 HL, although neither receptor is as sensitive to the non-cognate signal (Fig. 3-1a) (16, 18). Despite this indication of cross-talk between the natural AHLs of *V. fischeri*, the phenotypic, transcriptional, and symbiotic measurements reported herein indicate that, in the context of functional C8 signaling, the two non-native PHLs do not influence any ainS-dependent phenotypes. In the context of the symbiosis, C8 HL signaling does not function solely as a mechanism by which to induce bioluminescence at low cell density; in fact, I noted that activation of LuxIR by the exogenous addition of a LuxR agonist was not sufficient to restore normal colonization of the host by an *ainS* mutant. This finding supports the hypothesis that LuxIR-independent targets of AinSR regulation, such as motility and acetyl-CoA synthase (23, 34), are required for persistent colonization of the light organ. Perhaps the key to quorum signaling in the context of symbiosis lies in the relative abundance of each AHL signal, and the regulation surrounding these levels.

I also considered the characteristics of LuxIR-mediated quorum sensing by the PHL analogs during light-organ colonization. Both PHL molecules were able to modulate LuxIR signaling at concentrations as low as those previously reported in laboratory-culture

experiments (28). In addition to LuxR activation being highly sensitive to the PHLs, the transient addition of the analogs had a long-lived effect; that is, the symbionts of animals that had been removed from seawater containing PHL continued to respond for up to one day as though the analog were present. This observation is consistent with the light-organ crypts being a diffusion-limited environment, and suggests that the ability to experimentally reverse the action of these small chemical probes will be limited in the context of this, and perhaps other, animal models.

Interestingly, while the analogs retained their efficacy in the symbiotic environment, in the squid I did not observe that the 3-nitro PHL agonist had a higher specific activity of bioluminescence induction than the natural agonist, as had been found in culture (29). Because the host's control of bioluminescence in the light organ is likely to rely on several physiological tissue conditions, such as oxygen availability (53), it is possible that these environmental factors, rather than LuxIR signaling, determine the maximum level of bioluminescence produced by *V. fischeri* cells in the light organ.

Bioluminescence leaves a persistent 'first impression'

The chemical manipulation of LuxIR quorum sensing described here offers new insight into the process by which a robust and stable mutualism is established between *V. fischeri* and *E. scolopes*. I show that LuxIR quorum signaling enhances the transition of symbiotic *V. fischeri* from an initial colonization of the host to a robust, and long-term association, and that the presence of animal bioluminescence during the first 24 h of colonization is predictive of symbiont population dynamics over subsequent days of the

symbiosis. The results define a preliminary framework on which to map existing and future studies of microbial colonization factors and, thereby, suggest principles of host selection and maintenance of a bioluminescent symbiont during initiation of the squid-vibrio mutualism.

The contribution of AHL molecules to the chemical dialogue between host and symbiont cannot be ignored (27) (**Fig. 3-1*A***); however, the data suggest that direct chemical signaling does not itself contribute to the host's control of the number of symbionts in the light organ. Rather, I propose that the host's perception of bioluminescence, or of a product of the bioluminescence reaction itself, is the signal or cue that governs maintenance of symbiont population levels. The centrality of light as a cue for maintenance of a stable symbiosis is consistent with the structural and physiological attributes of the light organ: symbiont bioluminescence is perceived by the tissues of this specialized structure (54), and these tissues also have the capacity to entrain physiological rhythms based on this stimulus (25).

Our data suggest that, below a minimum threshold of bioluminescence, the benefit of bioluminescence to the symbiont is proportional to the amount of light produced. For example, I show that, even in the absence of LuxIR signaling, there is a small amount of light produced by the basal level of luciferase, and this activity may enhance the fitness of *luxI* and *luxR* mutants, relative to a completely 'dark' strain missing the genes encoding luciferase itself. Further, the temporal manipulation of light production during the first 24 h after symbiotic infection indicates the critical contribution of light to the persistent colonization of the light organ. However, the data also demonstrate that even a slowly diminishing bioluminescence output, if it does not fall below a minimum threshold, is sufficient for maintenance of the symbiont population by the host. Finally, I show for the first time that

bioluminescence produced by *V. fischeri* within the first day of colonization appears to be a critical determinant of symbiotic population dynamics over the longer term. It will be interesting to elucidate the mechanism(s) by which this initial bioluminescent 'conversation' between host and symbiont is predictive of the long-term stability of the partnership.

CONCLUSIONS

Regulation of microbial colonization factors by quorum signaling is rarely studied within the host itself. Nevertheless, it is perhaps from this vantage that the contribution of quorum sensing to bacterial population dynamics may be best understood. In this study, I demonstrate that native and non-native HL analogs can be used to modulate LuxIR quorum sensing without perturbing either (i) the AinS-LitR quorum-signaling circuitry of *V. fischeri*, or (ii) non-LuxIR dependent factors required for symbiosis with *E. scolopes*. In addition to these observations, the chemical approach for perturbing quorum-sensing circuitry suggests a novel role for LuxIR regulation of bioluminescence not revealed by previous genetic approaches. That is, I show that the LuxIR quorum-sensing circuit, from the first hours through the first day of colonization, is required to establish the stability of the mutualism, and that the success of this initial signaling has long-term consequences for the maintenance of the symbiont population by the host. Using longitudinal studies that are becoming feasible in the squid-vibrio model (24), future work will determine how long the impact of the first LuxIR-mediated bioluminescent 'conversation' is reflected in the dynamics of the symbiont population.

ACKNOWLEDGMENTS:

The authors thank E. Stabb, C. Brennan, J. Campbell, J.P. Gerdt, and E. Heath-Heckman for contributive discussions, and M. E. Mattmann and P. M. Shipway for compound synthesis. This work was supported by NSF (IOS 9817232) and NIH (RR12294/OD11024) to M. McFall-Ngai and EGR, and NIH (AI063326) to MM-N, as well as grants from the Greater Milwaukee Foundation, Burroughs Welcome Foundation, and Johnson & Johnson to HEB. JAS was supported by an NSF Graduate Research Fellowship, and the Chemical Biology Training Program (UW-Madison, funded by NIH grant NIGMS T32 GM008505), and SVS was supported by fellowships from the Wisconsin Alumni Research Foundation, the Molecular Biology Training Grant (UW-Madison, funded by NIH grant T32 GM07215), and the UW-Madison Graduate School. GDG was supported by a fellowship from the American Chemical Society Division of Medicinal Chemistry. JSH was supported by the Agency for Science, Technology and Research (A*STAR), Singapore.

REFERENCES:

1. Parsek MR & Greenberg EP (2000) Acyl-homoserine lactone quorum sensing in gram-negative bacteria: a signaling mechanism involved in associations with higher organisms. *Proceedings of the National Academy of Sciences* 97(16):8789-8793.

2. González JF & Venturi V (2012) A novel widespread interkingdom signaling circuit. *Trends in plant science*.

3. Churchill ME & Chen L (2010) Structural basis of acyl-homoserine lactone-dependent signaling. *Chem Rev* 111(1):68-85.

4. Teplitski M, Mathesius U, & Rumbaugh KP (2011) Perception and Degradation of N-Acyl Homoserine Lactone Quorum Sensing Signals by Mammalian and Plant Cells. *Chem. Rev.* 111(1):100-116.

5. Galloway WR, Hodgkinson JT, Bowden S, Welch M, & Spring DR (2012) Applications of small molecule activators and inhibitors of quorum sensing in Gram-negative bacteria. *Trends in microbiology*.

6. Galloway WRJD, Hodgkinson JT, Bowden SD, Welch M, & Spring DR (2011) Quorum Sensing in Gram-Negative Bacteria: Small-Molecule Modulation of AHL and Al-2 Quorum Sensing Pathways. *Chem. Rev.* 111(1):28-67.

7. Praneenararat T, Palmer AG, & Blackwell HE (2012) Chemical methods to interrogate bacterial quorum sensing pathways. *Org Biomol Chem* 10(41):8189-8199.

8. Amara N, Krom BP, Kaufmann GF, & Meijler MM (2011) Macromolecular Inhibition of Quorum Sensing: Enzymes, Antibodies, and Beyond. *Chem. Rev.* 111(1):195-208.

9. Rasmussen TB & Givskov M (2006) Quorum sensing inhibitors: a bargain of effects. *Microbiology* 152(Part 4):895-904.

10. Hentzer M*, et al.* (2003) Attenuation of *Pseudomonas aeruginosa* virulence by quorum sensing inhibitors. *Embo J* 22(15):3803-3815.

11. Wu H*, et al.* (2004) Synthetic furanones inhibit quorum-sensing and enhance bacterial clearance in *Pseudomonas aeruginosa* lung infection in mice. *Journal of Antimicrobial Chemotherapy* 53(6):1054-1061.

12. Palmer AG, Streng E, & Blackwell HE (2011) Attenuation of virulence in pathogenic bacteria using synthetic quorum-sensing modulators under native conditions on plant hosts. *ACS Chem. Biol.* 6(12):1348-1356.

13. Bjarnsholt T & Givskov M (2007) Quorum-sensing blockade as a strategy for enhancing host defences against bacterial pathogens. *Phil. Trans. R. Soc. B* 362(1483):1213-1222.

14. Mandel MJ (2010) Models and approaches to dissect host-symbiont specificity. *Trends Microbiol* 18(11):504-511.

15. Stabb EV & Visick KL (2013) *Vibrio fischeri*: A bioluminescent light-organ symbiont of the bobtail squid *Euprymna scolopes*. *The Prokaryotes*, eds Rosenberg E, DeLong EF, Lory S, Stackebrandt E, & Thompson F (Springer-Verlag, Berlin), pp 497-532.

16. Lupp C, Urbanowski M, Greenberg EP, & Ruby EG (2003) The *Vibrio fischeri* quorum-sensing systems *ain* and *lux* sequentially induce luminescence gene expression and are important for persistence in the squid host. *Mol Microbiol* 50(1):319-331.

17. Gilson L, Kuo A, & Dunlap PV (1995) AinS and a new family of autoinducer synthesis proteins. *J Bacteriol* 177(23):6946-6951.

18. Kimbrough JH & Stabb EV (2013) Substrate specificity and function of the pheromone receptor AinR in *Vibrio fischeri* ES114. *J. Bacteriol.* (accepted).

19. Lupp C & Ruby EG (2004) *Vibrio fischeri* LuxS and AinS: comparative study of two signal synthases. *J Bacteriol* 186(12):3873-3881.

20. Neiditch MB*, et al.* (2006) Ligand-induced asymmetry in histidine sensor kinase complex regulates quorum sensing. *Cell* 126(6):1095-1108.

21. Dunlap PV (1999) Quorum regulation of luminescence in *Vibrio fischeri*. *J Mol Microbiol Biotechnol* 1(1):5-12.

22. Antunes LC*, et al.* (2007) Transcriptome analysis of the *Vibrio fischeri* LuxR-LuxI regulon. *J Bacteriol* 189(22):8387-8391.

23. Lupp C & Ruby EG (2005) *Vibrio fischeri* uses two quorum-sensing systems for the regulation of early and late colonization factors. *J Bacteriol* 187(11):3620-3629.

24. Koch EJ, Miyashiro T, McFall-Ngai MJ, & Ruby EG (2013) Features governing symbiont persistence in the squid-vibrio association. *Mol Ecol*.

25. Heath-Heckman EA*, et al.* (2013) Bacterial Bioluminescence Regulates Expression of a Host Cryptochrome Gene in the Squid-Vibrio Symbiosis. *mBio* 4(2).

26. Rumbaugh KP & Kaufmann GF (2012) Exploitation of host signaling pathways by microbial quorum sensing signals. *Current opinion in microbiology* 15(2):162-168.

27. Chun CK, *et al.* (2008) Effects of colonization, luminescence, and autoinducer on host transcription during development of the squid-vibrio association. *Proc Natl Acad Sci U S A* 105(32):11323-11328.

28. Geske GD, O'Neill JC, & Blackwell HE (2007) *N*-phenylacetanoyl-L-homoserine lactones can strongly antagonize or superagonize quorum sensing in *Vibrio fischeri*. *ACS Chem Biol* 2(5):315-319.

29. Geske GD, O'Neill JC, Miller DM, Mattmann ME, & Blackwell HE (2007) Modulation of bacterial quorum sensing with synthetic ligands: systematic evaluation of N-acylated homoserine lactones in multiple species and new insights into their mechanisms of action. *J Am Chem Soc* 129(44):13613-13625.

30. Geske GD, *et al.* (2008) Comparative analyses of N-acylated homoserine lactones reveal unique structural features that dictate their ability to activate or inhibit quorum sensing. *Chembiochem* 9(3):389-400.

31. Boettcher KJ & Ruby EG (1990) Depressed light emission by symbiotic *Vibrio fischeri* of the sepiolid squid *Euprymna scolopes*. *J Bacteriol* 172(7):3701-3706.

32. Graf J, Dunlap PV, & Ruby EG (1994) Effect of transposon-induced motility mutations on colonization of the host light organ by *Vibrio fischeri*. *J Bacteriol* 176(22):6986-6991.

33. Sambrook JF, E.F., and Maniantis, T. (1989) *Molecular Cloning* (Cold Spring Harbor Press, Cold Spring Harbor, New York).

34. Studer SV, Mandel MJ, & Ruby EG (2008) AinS quorum sensing regulates the *Vibrio fischeri* acetate switch. *J Bacteriol* 190(17):5915-5923.

35. Slauch JM, and T. J. Silhavy (1991) *cis*-acting *ompF* mutations that result in OmpR-dependent constitutive expression. *J Bacteriol* 173:4039-4048.

36. D'agostino RB, Belanger A, & D'Agostino Jr RB (1990) A suggestion for using powerful and informative tests of normality. *The American Statistician* 44(4):316-321.

37. Fidopiastis PM, Miyamoto CM, Jobling MG, Meighen EA, & Ruby EG (2002) LitR, a new transcriptional activator in *Vibrio fischeri*, regulates luminescence and symbiotic light organ colonization. *Mol Microbiol* 45(1):131-143.

38. Bose JL, Rosenberg CS, & Stabb EV (2008) Effects of *luxCDABEG* induction in *Vibrio fischeri*: enhancement of symbiotic colonization and conditional attenuation of growth in culture. *Arch Microbiol* 190(2):169-183.

39. Hanahan D (1983) Studies on transformation of *E. coli* with plasmids. *J Mol Biol* 166(4):557-580.

40. Schaefer AL, Hanzelka BL, Eberhard A, & Greenberg EP (1996) Quorum sensing in *Vibrio fischeri*: probing autoinducer-LuxR interactions with autoinducer analogs. *J Bacteriol* 178(10):2897-2901.

41. Swem LR*, et al.* (2009) A quorum-sensing antagonist targets both membrane-bound and cytoplasmic receptors and controls bacterial pathogenicity. *Mol Cell* 35(2):143-153.

42. Palmer AG, Streng E, Jewell KA, & Blackwell HE (2011) Quorum sensing in bacterial species that use degenerate autoinducers can be tuned by using structurally identical non-native ligands. *ChemBioChem* 12(1):138-147.

43. Visick KL, Foster J, Doino J, McFall-Ngai M, & Ruby EG (2000) *Vibrio fischeri lux* genes play an important role in colonization and development of the host light organ. *J Bacteriol* 182(16):4578-4586.

44. Ruby EG (1996) Lessons from a cooperative, bacterial-animal association: the *Vibrio fischeri-Euprymna scolopes* light organ symbiosis. *Annu Rev Microbiol* 50:591-624.

45. Nyholm SV & McFall-Ngai MJ (2004) The winnowing: establishing the squid-vibrio symbiosis. *Nat Rev Microbiol* 2(8):632-642.

46. O' Connor CJ, Laraia L, & Spring DR (2011) Chemical genetics. *Chem. Soc. Rev.* 40(8):4332-4345.

47. Lowery CA, Salzameda NT, Sawada D, Kaufmann GF, & Janda KD (2010) Medicinal Chemistry as a Conduit for the Modulation of Quorum Sensing. *J. Med. Chem.* 53(21):7467-7489.

48. Njoroge J & Sperandio V (2009) Jamming bacterial communication: new approaches for the treatment of infectious diseases. *EMBO Mol Med* 1(4):201-210.

49. González JE & Marketon MM (2003) Quorum sensing in nitrogen-fixing rhizobia. *Microbiology and Molecular Biology Reviews* 67(4):574-592.

50. Liu Z*, et al.* (2008) Mucosal penetration primes *Vibrio cholerae* for host colonization by repressing quorum sensing. *Science Signaling* 105(28):9769.

51. von Bodman SB, Bauer WD, & Coplin DL (2003) Quorum sensing in plant-pathogenic bacteria. *Annual review of phytopathology* 41(1):455-482.

52. Stabb EV, Schaefer A, Bose JL, & Ruby EG (2007) Quorum signaling and symbiosis in the marine luminous bacterium *Vibrio fischeri. Cell-cell signaling in bacteria*, eds Winans S & Bassler B (ASM Press, Washington, DC), pp 233-250.

53. Miyashiro T & Ruby EG (2012) Shedding light on bioluminescence regulation in *Vibrio fischeri*. *Molecular microbiology* 84(5):795-806.

54. Tong D*, et al.* (2009) Evidence for light perception in a bioluminescent organ. *Proc Natl Acad Sci U S A* 106(24):9836-9841.

Chapter 4

The chemistry of negotiation: rhythmic, glycan-driven acidification in a symbiotic conversation

PREFACE:

Published in *Proceedings of the National Academy of Science* in 2014 as:

Schwartzman JA, Koch E, Heath-Heckman EAC, Zhou L, Kremer N, McFall-Ngai MJ, and EG Ruby. "The chemistry of negotiation: rhythmic, glycan-driven acidification in a symbiotic conversation."

JAS, EGR and MMN formulated ideas and planned the experiments within this chapter. JAS performed all experiments and wrote the chapter, with the exception of Figure 4B (EACH), and Figure 4E (LZ). EK helped design experiments and oversaw the squid development model. NK and EACH and provided samples and reagents. JAS analyzed the data. JAS and EGR wrote and edited the chapter.

ABSTRACT:

Glycans have emerged as critical determinants of immune maturation, microbial nutrition and host health in diverse symbioses. In this study, I asked how cyclic delivery of a single host-derived glycan contributes to the dynamic stability of the mutualism between the squid *Euprymna scolopes* and its specific, bioluminescent symbiont, *Vibrio fischeri*. *V. fischeri* colonizes the crypts of a host organ that is used for behavioral light production. *E. scolopes* synthesizes the polymeric glycan chitin in macrophage-like immune cells called hemocytes. I show here that, just before dusk, hemocytes migrate from the vasculature into the symbiotic crypts, where they lyse and release particulate chitin, a behavior that is established only in the mature symbiosis. Diel transcriptional rhythms in both partners further indicate that the chitin is provided and metabolized only at night. A *V. fischeri* mutant defective in chitin catabolism was able to maintain a normal symbiont population level, but only until the symbiotic organ reached maturity (~4 weeks after colonization); this result provided a direct link between chitin utilization and symbiont persistence. Finally, catabolism of chitin by the symbionts was also specifically required for a periodic acidification of the adult crypts each night. This acidification, which increases the level of oxygen available to the symbionts, enhances their capacity to produce bioluminescence at night. I propose that animal hosts may similarly regulate the activities of epithelium-associated microbial communities through the strategic provision of specific nutrients, whose catabolism modulates conditions like pH or anoxia in their symbionts' habitat.

INTRODUCTION:

Animals exist in a microbial world, and are reliant on beneficial associations with certain microbes for nutrition, defense, development or other fitness factors (1). In the case of horizontally acquired symbioses, such as that in the gut, the success of the association hinges on the ability of microbial symbionts to colonize, be nourished by, and deliver a fitness advantage to the host, while maintaining a détente with its immune system (2-4). The negotiations underlying such mutually beneficial relationships must initiate upon first contact, and continue throughout the period of association (5).

Three hallmarks of host-microbe interaction emerge from studies of the complex microbial consortia of animals. First, the provision of nutrients such as host-derived glycans contribute to the microbial community structure and are a source of microbe-derived metabolites such as short-chained fatty acids (SCFA), that promote the maturation of local and systemic immune functions (6-9). Second, the nutritional and environmental changes that mark the developmental trajectory of an organism from its juvenile to adult form are accompanied by distinct shifts in both the composition and functions of the maturing host's microbiota (10, 11). Finally, circadian rhythms coordinate much of the communication between a host and its microbiota, leading to the maintenance of physiological homeostasis (12-14). Taken together, these themes indicate that the terms of the protracted symbiotic negotiation are subject to a dynamic equilibrium that encompasses nutritional, immune, developmental, and circadian inputs.

Given this complexity, the specific costs incurred and benefits derived from a long-term cooperation, as well as their underlying mechanisms, are often difficult to establish,

particularly in symbioses where the microbial member provides nutrients to the host. Natural invertebrate model systems that maintain one or a few symbiotic microbes, such as nematodes, medicinal leeches and squid (15), provide a window through which I can discover themes conserved across the interactions of animals with their coevolved microbiota, whether simple or complex. In particular, the symbiosis of the bobtail squid *Euprymna scolopes* and the luminous bacterium *Vibrio fischeri*, in which the microbial symbiont can be manipulated without compromising the health of the host, presents a rare opportunity to study the chemical and immune dialogues of symbiotic partners at a cellular and molecular level (16).

The squid-vibrio symbiosis takes place in the light-emitting organ of *E. scolopes*, and is based on the bacterium's production of bioluminescence (17), which the host uses in its nocturnal behaviors, such as foraging and camouflage. The symbionts are obtained through horizontal transmission from the ambient seawater by each generation of juvenile squid (18), and are cultured in the epithelium-lined crypts of the light organ (**Fig. 4-1*a***) throughout the animal's ~9-month life. The symbiont induces post-embryonic light-organ development (19), and the organ morphology reaches maturity in 4 weeks (20). Host-derived chitin, a polymeric glycan of *N*-acetylglucosamine, is known to promote the species-specific colonization of the squid by *V. fischeri* (21). Chitin is synthesized by several types of squid tissue, including macrophage-like immune cells called hemocytes (22) (**Fig. 4-1*a***), and has also been implicated, along with amino acids (23), as a nutrient provided to the symbiont population. Specifically, transcription of *V. fischeri* genes associated with the fermentation of chitin oligosaccharides (COS) is elevated during the nocturnal, bioluminescent phase of the

symbiosis (24) (**Fig. 4-1*a***). The importance of chitin in the chemical dialogue between squid and vibrio is reminiscent of the contribution of host glycans and structural polysaccharides to other host-microbe interactions (9). For example, (i) the catabolism of exoskeleton-derived chitin by *Vibrio cholerae* enhances transmission from an invertebrate vector to a susceptible host (25), (ii) pectin catabolism by plant pathogen *Xylella fastidiosa* promotes transmission to leafhopper vectors (26), and (iii) foraging of mammalian mucin-derived glycans, such as fucose and sialic acid, form a nutritional scaffold for the gut microbiota (27-29).

The squid-vibrio association is also characterized by daily rhythms of symbiont growth and bioluminescence (30, 31). Each morning at dawn, the host expels the contents of the light-organ crypts, including 95% of the symbiont population, into the surrounding seawater (**Fig. 4-1*a***). The remaining symbiont cells repopulate the light organ within hours, by growing on substrates including amino acids and glycerophospholipids (23, 24), eventually providing the squid's nocturnal bioluminescence. Light emission, which requires oxygen (32), is highest during the night (33). In the fully developed light organ, where oxygen is limiting to the symbionts (24, 33), the diel bioluminescent rhythm is potentiated by an acidic crypt environment, which creates a Bohr effect that releases oxygen from the carrier protein, hemocyanin (34). Here, I demonstrate that in this mature state of light-organ development, the cyclic provision of COS to symbionts, combined with their fermentation of this glycan, lead to the nightly acidification of the symbiont-containing extracellular crypts. The combined nocturnal activities of host and symbiont thereby promote the diel cycle of bioluminescence: a rhythm critical to the long-term stability of this association.

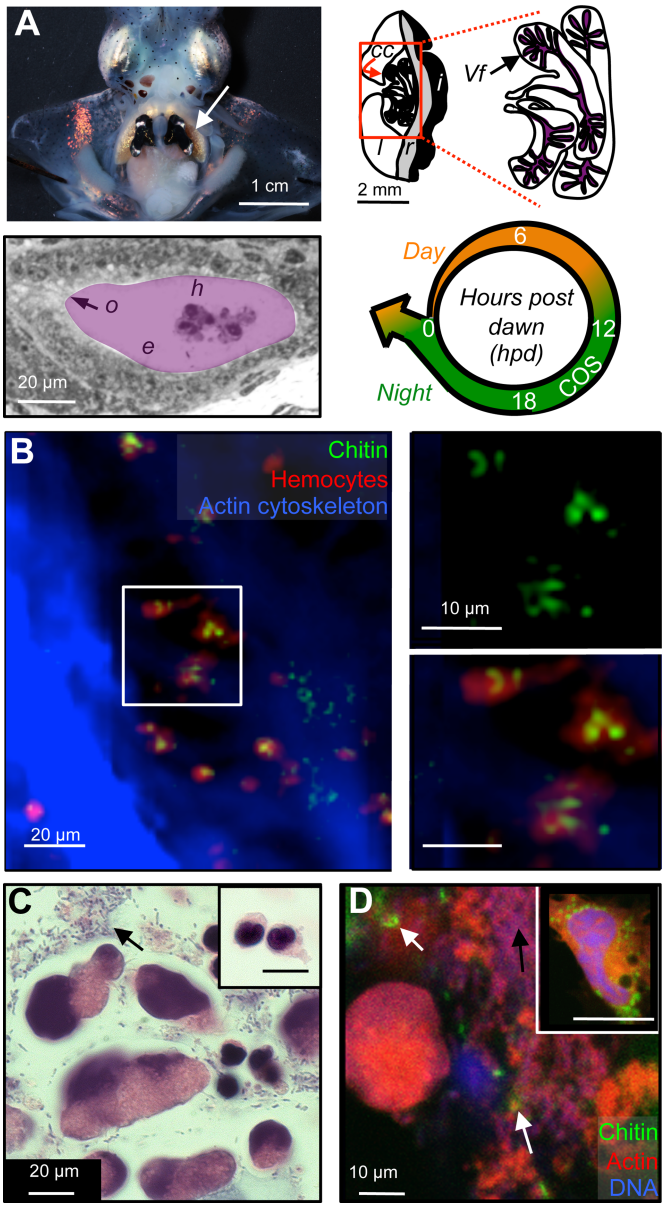

Figure 4-1. Light-organ crypts contain hemocyte-derived chitin. ***A***) Anatomy of the mature light organ. Top right: the mature, bilobed light organ is located ventrally, in the center of the mantle cavity (arrow). Bottom right: schematic of one lobe, indicating the light-organ lens (l), reflector (r), and ink sac (i), and bacteria-containing central-core tissue (cc) in the red box. Polarized epithelial cells form branched crypt spaces, in which the symbionts (*Vf*)

reside. Top left: symbiotic *V. fischeri* occupies extracellular crypts (purple), where it contacts hemocytes (*h*) and the bordering epithelial cells (*e*); the outlet (*o*) to the mantle cavity allows the host to expel most of the crypt contents and symbionts every morning at dawn. Bottom left: The mature diel cycle of the squid-vibrio symbiosis. About 95% of the symbiont population is expelled at dawn (arrow), and the remaining cells repopulate the crypts during the day (orange). At night (green), transcriptional evidence suggests that symbionts metabolize host-derived chitin oligosaccharides (COS) (24). Numbers indicate hours post dawn (hpd). ***B***) Confocal micrograph, showing co-localization of chitin (fluorescent chitin-binding protein; green) and hemocytes (fluorescent DNaseI globular actin-binding protein; red) in central-core tissue (fluorescent phalloidin, a filamentous actin-binding protein; blue). Image is a 3D-reconstruction of 40 confocal sections taken at 1-µm intervals. Tissue was sampled just before nightfall (10 hpd). Upper & lower right: close-up of hemocytes in white box, highlighting particulate-chitin staining. ***C***) Differential interference contrast micrograph of crypt contents, sampled at the end of the night (22 hpd), and stained with hematoxylin (chromatin; dark blue), and eosin (proteins; pink). Two different morphologies of nucleated cells are seen in the crypt contents. Inset (same magnification): the single type of hemocyte morphology present in the hemolymph. Black arrow indicates extracellular material, which includes bacterial cells. ***D***) Detection of free particulate chitin (white arrows), and extracellular material (black arrows) in the contents of the light-organ crypt, sampled 22 hpd. Fluorescent staining as in ***B)***. Inset: image of cytoplasmic particulate chitin within a hemocyte extracted from the hemolymph.

MATERIALS AND METHODS:

General procedures. Bacterial strains and plasmids used in this work are listed in **Table 4-1**. All *Vibrio fischeri* mutant strains are derived from isolate ES114 (35, 36). *V. fischeri* and *Vibrio harveyi* cells were grown at 28 °C, with shaking at 225 rpm unless otherwise noted. In *V. fischeri* culture experiments, 5 μg erythromycin (Em) mL^{-1}, or 100 μg kanamycin (Kn) mL^{-1} were added where indicated. *V. fischeri* cultures were grown in high-osmolarity seawater tryptone medium (SWTO) (37), Luria-Bertani salt medium (LBS) (38), or minimal salts medium (MSM). *Escherichia coli* was cultured at 37°C with shaking at 250 rpm in Luria-Bertani medium (LB) (39), or M9 Minimal Medium (40). Where indicated, 50 mM PIPES buffer (pH 7.5), 150 μg Em mL^{-1}, or 50 μg Km mL^{-1} were added to *E. coli* cultures.

Adult squid, collected at Oahu, Hawaii, U.S.A., were maintained in the laboratory in circulating 35 ppt Instant Ocean (Aquarium Systems), on a 12 h / 12 h light-dark cycle. Squid were colonized and raised as described previously (20, 41), with the following modifications: animals were exposed to ~5,000 colony forming units (CFU)/mL of the indicated *V. fischeri* strains in filter-sterilized Instant Ocean for 16 h, and euthanized by freezing at -80 ºC. Animals were anaesthetized for 5 min in seawater containing 1% ethanol for collection of blood and tissue samples. The mature light organ developmental state was distinguished in living animals by (i) a mantle length of >10 mm, and (ii) a behavioral transition of the animals to a pattern of nocturnal activity. All animal experiments meet the regulatory standards established for invertebrates by the University of Wisconsin-Madison.

TABLE 4-1 Strains and plasmids used in this study

Strain or plasmid	Description-	Reference
V. fischeri		
ES114	Wild-type *E. scolopes* light-organ isolate	(35, 36)
MJ11	Wild-type isolate from fish, *Monocentris japonica*	(42)
TIM313	ES114 Tn*7*::pEVS107 Em^r	(43)
TIM302	ES114 *Tn7::gfp* Em^r	(43)
JAS101	ES114 Δ*nagB Tn7::*pEVS107 Em^r	(44)
JAS102	ES114 Δ*nagB Tn7::*pJAS102 Em^r	This study
V. harveyi		
B392	Wild-type isolate from seawater	(45)
E. coli		
DH5α-λpir	F^- φ80*lacZ*Δ*M15* Δ(*lacZYFargF*)U169 *supE44 deoR hsdR17 recA1 endA1 gyrA96 thi-1 relA1*, lysogenized with λ*pir*	(29)
K-12 (MG1655)	Wild-type *E. coli* F^-λ	ATCC47076
Plasmids		
pEVS104	R6Kori RP4 *oriT trb tra* Kn^r	(46)
pUX-BF13	R6Kori *tns bla*	(47)
pEVS107	R6Kori *oriT mini*-Tn*7 mob* Em^r Kn^r	(48)
pJAS102	*nagB::*Tn*7* pEVS107	This study

Figure S5

>*E. scolopes* putative chitotriosidase EsChit1
MASTFATVFGVLSLCFLGLHLTNGEYKKVCYYTNWSQYRQIPAKFVPENISVSLCTHIIY
TFATLQNNHLKPFEWNDDSTPWMVGMYARVMKLKKKDPNLQVLLGVGGWNMGSYL
FSKMVANIQNRKMFYTNATGFLRKRNFDGLDIDWCYPGSRGSPAVDKKNYVSLLQETS
DYFLNESKISGKKRLLLTASIPVGKKTIIKGYDIPQVEKYLDFMNLMSYDYHGGSFDNVT
GHNSPLYPRKEETGDERTFNVNWSANYWVEHGVPRMKLNIGMPAYGRGFRLANHSCIL
PGCPSIGPNSPGQYTRLAGFLAYYEICDLIKKGAKVFRIADQKVPYLVYNNEWIGYDDV
KSLSIKVDWLKKNQFGGVAIWTLDLDDFFNGCGSGAYILIKTLTQELKLPSVEN

Figure 4-2. Predicted protein sequence of the putative *Es*Chit1 chitotriosidase. Underlined sequence indicates peptide used for antibody production.

***Es*Chit1 antibody design and validation** A polyclonal rabbit antibody against the squid chitotriosidase 1 (*Es*Chit1, Genscript) was generated to the synthetic peptide sequence (CYPGSRGSPAVDKKN) that is predicted to be located at an internal, but surface exposed, portion of the protein (**Fig. 4-2**), and that lacked any significant match to other sequences in the squid databases. To determine the specificity of the anti-*Es*Chit1antibody (α-*Es*Chit1), I performed a Western blot analysis, as previously described (34). The protocol was modified so that proteins were transferred to 0.2 μm nitrocellulose membrane, and blocked overnight in a solution containing 4% milk in 0.1% Tween-20 in Tris-buffered saline (TBS; 20 mM Tris with 0.5 M NaCl; pH 7.4) at 4 °C. After blocking, the membranes were incubated for 3 h at room temperature *in* 4% milk in 0.1% Tween-20, with either a 1:250 dilution of α-*Es*Chit1, or purified rabbit IgG at the same concentration as a negative control. Secondary antibody and detection of antibody hybridization were performed as described elsewhere (34). This antibody was highly specific relative to an immunoglobulin control by Western blot against light-organ central-core tissues, at a concentration of 1:250, and was also used for immunochemistry at this concentration (21, 49).

Immunocytochemistry (ICC), fluorescence microscopy and hemocyte characterization. Fluorochromes were obtained from Life Technologies (Carlsbad, CA, USA), and all other chemicals were purchased from Sigma-Aldrich (St. Louis, MO, USA), except where indicated. ICC and processing of squid tissues were performed as described previously (49), with minor modifications, described below. All samples were mounted in Vectashield (Vector Laboratories) before observation by confocal microscopy. A Zeiss 510 laser-scanning

confocal microscope with AxioImager software (Carl Zeiss Instruments, Oberkochen, Germany). was used to image samples, unless otherwise noted.

Collection of adult central-core tissue, juvenile light organs and hemocytes: Central-core tissue was collected from squid >18 mm in mantle length that were anaesthetized in 2% ethanol in seawater. The light organ was exposed by ventrally dissecting the mantle and removing the funnel. The central cores are located bilaterally on the light organ, in a pocket defined by layers of ink sac and reflector (**Fig. 4-1*A***). The lobes of the organ are surrounded by vitreous lens tissue. To expose the central-core tissue, the lens was dissected just above where the ink sac and reflective tissue fold around the central core- located on the outer edge of the light organ. Weak connective tissue joins the tissue folds between which the central core is located. If this tissue could be removed to fully unfold the reflector and ink sac, then the central core was removed immediately, and incubated in a fixative containing 4% paraformaldehyde (PFA) in mPBS (50 mM sodium phosphate pH 7.4, 0.4 M NaCl) for 16 h at 4 °C to stabilize the tissues. If the central-core tissue could not be removed without compromising its structural integrity, then the whole light organ was removed from the squid's mantle cavity by cutting the connective tissues underneath the organ, as well as the gut and ligaments attaching it from above, and placing the organ in 4% PFA in mPBS for 5 min, prior to removal of central-core tissues. Fixed samples were rinsed 3 times for 10 min in mPBS, and then permeabilized 24 h in 1 % Triton-X100 in mPBS. Immature light organs were collected as described elsewhere, with minor modifications (21). The light-organ ink sac was gently punctured during dissection to permit drainage of ink and better visualization of deep crypt structures. Hemocyte isolation was performed as described previously (22).

Briefly, 15 µL samples of squid hemolymph, extracted from the cephalic vessel, were applied to glass coverslips, and hemocytes were allowed to adhere for 30 min. Following this step, the slides were rinsed 3 times in Squid Ringer's buffer (530 mM NaCl, 10 mM KCl, 25 mM $MgCl_2$, 10 mM $CaCl_2$ and 10 mM HEPES buffer, pH 7.5 (50)) to remove non-adherent cells, and the samples were fixed for 30 min in 4% PFA in mPBS, and permeabilized for 30 min in 1% Triton-X100 in mPBS (mPBST).

Detection of chitin and hemocytes by fluorescent probes. Immature light organs, or central-core tissue were incubated for 7 days in 1:250 dilution of TRITC-conjugated chitin-binding protein (CBP, New England Biolabs) in mPBST (22). To counterstain, tissues were incubated 4 days in a 1:40 dilution of FITC-conjugated DNAse-I to visualize hemocytes by their enrichment in globular actin (51), and 25 µg/mL Alexa-633 phalloidin in for 2 days to visualize the actin cytoskeleton. Hemocytes were incubated at room temperature for 3 h with 1:250 FITC-conjugated CBP in mPBST, rinsed, and counterstained with 1:40 rhodamine phalloidin in mPBST overnight at 4 °C to visualize the actin cytoskeleton. A 1:500 dilution of TOTO-3 iodide was added for 10 min at room temperature to visualize nuclear DNA.

Detection of predicted squid chitinases by immunocytochemistry. Permeabilized central-core tissues were incubated at 4 °C with mPBST block (0.5% goat serum and 1% bovine serum albumin in mPBST) overnight, and then for 7 days with a 1:500 dilution of α-*Es*Chit1 primary antibody, or the same concentration of purified rabbit IgG as a negative control, in mPBST block. To visualize antibody binding, samples were incubated overnight in a 1:40 dilution of TRITC-conjugated goat anti-rabbit/chicken secondary antibody. Tissues were counterstained in mPBST 4 days in a 1:40 dilution of FITC-conjugated DNAse-I, and

overnight with 25 μg Alexa-633 phalloidin per mL. Hemocytes were incubated at room temperature in mPBST block for 1 h, then primary antibody in mPBST block for 3 h and, finally, a 1:40 dilution of FITC-conjugated goat-anti-rabbit in mPBST blocking solution for 45 min. Samples were counterstained overnight at 4 °C with a 1:40 dilution of rhodamine phalloidin in mPBST, and for 10 min at room temperature with a 1:500 dilution of TOTO-3 iodide to visualize nuclear DNA.

Enumeration of hemocytes in immature light organs, and visualization of mature central core tissue. To enumerate hemocytes present in immature light organs, samples stained with FITC-DNAseI and rhodamine phalloidin, as described above, were visualized by confocal microscopy. Hemocytes, defined as DNAse-I positive cells, were enumerated in a region of the light organ extending from the mid-axis line to the ciliated epithelial field. Hemocytes present in the anterior and posterior appendages (structures characteristic of the immature light organ, and not present in the fully-mature structure) were not enumerated in this analysis. To visualize fluorescently labeled structure in central core tissue, I located a field of view where the tissue surface was relatively uniform (*i.e.* the surface tissue had not been disrupted by dissection). Although the boundaries of crypts could not be definitively identified with the fluorescent probes used, I analyzed fields of view where phalloidin, which stains the actin cytoskeleton, formed a honeycomb-like structure, reminiscent of the finger-like projections of the mature light-organ crypt (**Fig. 4-1*A***).

Collection and characterization of expelled crypt contents: To collect crypt contents, anaesthetized squid were exposed to a light cue to induce venting behavior, as described previously (52). Acidic compartments of these cells were labeled by staining for 30 min with

a 1:500 dilution of Lysotracker Red in Squid Ringer's buffer, and visualized by epifluorescence microscopy. To assess nuclear-membrane integrity, cells were stained for 5 min with a 1:10,000 dilution acridine orange, and visualized by confocal microscopy. For analysis of chitin and immunocytochemistry, the expelled crypt contents were collected with a negative-pressure pipette, and placed directly in 4% PFA in mPBS for 4 h. A 20-µL sample of whole hemolymph was also collected as a control to compare cell morphology and staining patterns. Samples were suspended in Histogel matrix (Richard-Allen Scientific, #HG-4000-012), and then embedded in paraffin, and cut into 5 µm sections. The sections were deparaffinized and stained with hematoxylin and eosin to identify hemocytes (53). Embedding, sectioning and staining were performed by the Histology Core Facility in the Surgery Department at the University of Wisconsin-Madison School of Medicine and Public Health. Unstained sections were also processed for fluorescence microscopy and immunocytochemistry using a previously developed protocol (34). The same concentrations of fluorochromes and antibodies were used as described for staining central-core tissue, light organs and hemocytes.

Morphological changes of hemocytes exposed to crypt contents: To characterize acidic compartments in hemolymph-derived hemocytes upon exposure to the light-organ crypt contents, hemocytes were collected, incubated with Lysotracker Red as described above, and then centrifuged at 1300 rpm for 10 min at 4 °C in a tabletop centrifuge to remove excess dye. The cells were resuspended in Squid Ringer's buffer adjusted to either pH 7.5, or pH 5.5 (the nocturnal crypt pH (34)). Fresh crypt contents were collected from the same animal, and placed on ice. When the hemolymph-derived hemocytes had been labeled, 5µL of fresh crypt

contents were added to 20 µL of labeled hemocytes in pH 7.5 or 5.5 buffer. The remaining crypt contents were heated to 95 ºC for 10 minutes, to inactivate heat-labile crypt components. Five microliters of heat-exposed crypt contents was added to 20 µl of Lysotracker-Red labeled cells in pH 7.5 buffer. Samples were incubated for 2 h, and then visualized using a Zeiss Axio Imager M2 epifluorescence microscope. To ensure that morphological irregularities were not a result of experimental manipulations, a control population of hemocytes was collected and processed in the same manner as the experimental samples, except that the hemocytes were not exposed to crypt contents.

RNA extraction, sequence characterization and quantitative RT-PCR. The full-length *eschit1* transcript was obtained by RACE amplification, as described previously (34) (**Fig. 4-2**). The sequence was deposited in GenBank (accession number KM592978). cDNA synthesized from juvenile light organ total RNA was used as the template. The sample collection and transcriptional analysis were performed as described previously (34). Three-day-old and 4-week-old light organs collected at 2 h, 10 h, and 22 h post dawn (hpd) were dissected in RNAlater (either n=4 replicates of 20 juvenile light organs/replicate; or n=4 replicates of 5 adult light organs/replicate). To correct for the presence of bacterial symbiont RNA in the samples, amounts of total RNA added to the cDNA synthesis reactions were scaled, as follows: 2 hpd, 1x; 10 hpd, 1,1x; 22 hpd, 1.2x. Primer-set efficiencies were between 95 and 105% as determined by standard curves using 10-fold dilutions of template. Primers are listed in **Table 4-2**. A 60 °C annealing temperature was used for all primer pairs. Candidate gene expression was normalized using the geometric mean of 40S ribosomal RNA

and serine hydroxymethyltransferase (serine HMT) expression values. The distribution of the data was measured by Shapiro's test (all data fit a normal distribution), and a two-way ANOVA with post-hoc Bonferroni comparison was used to compare gene expression among time points, and between colonization states.

Table 4-2. Primers used in this study.

Gene	**Primer Sequences**	**Amplicon Size (bp)**
Serine hydroxymethyl transferase	SerineHMT-qF: GTCCTGGTGACAAGAGTGCAATGA SerineHMT-qR: TTCCAGCAGAAAGGCACGATAGGT	148 (30)
40S Ribosomal protein S19	40S-qF: AATCTCGGCGTCCTTGAGAA 40S-qR: GCATCAATTGCACGACGAGT	103 (30)
Chitotriosidase 1	*Es*Chit1-qF: CCTGCATATGGACGAGGATTT *Es*Chit1-qR: GTATATTGACCAGGTGAGTTGGG	92
Peptidoglycan recognition protein 5	*Es*PGRP5-qF: TTGGAGCCCACACCAAGTTCTACA *Es*PGRP5-qR: CAAGACAGCAGGCGTTTCAATGCT	N/R (25)

N/R, not reported in original publication; bp, base pairs

Quantitative RT-PCR procedures were conducted in accordance with the MIQE guidelines (54) for sample collection, RNA isolation, cDNA synthesis, quantitative RT-PCR amplification, normalization of experimental gene expression using reference genes, and data analysis. Primers were designed by OligoAnalyzer software (Integrated DNA Technologies).

Molecular genetics. All plasmids were constructed and introduced into *V. fischeri* with standard molecular techniques (55). To construct a vector for *in trans* complementation of the

nagB gene deletion, a segment of DNA corresponding to 500 bp upstream and 100 bp downstream of the annotated *nagB* coding sequence was amplified using primers with unique restriction sites engineered at the 5' end, and cloned into the *V. fischeri* Tn*7*-site integration plasmid, pEVS107 (55) (**Table 4-1**). The plasmid was introduced into the appropriate *V. fischeri* strain by conjugative transfer, and integrated into the Tn7 locus with the help of the pUXBF13 plasmid, as previously described (46, 47, 55) (**Table 4-1**).

Growth-yield measurement. To assess growth on a sole source of carbon, strains were cultivated in MSM (56), modified as described previously (44), for 24 h. The medium was buffered at pH 7.5 with 50 mM PIPES, and contained either 5 mM di-*N*-acetyl chitobiose (Cayman Chemicals), or 10 mM *N*-acetylglucosamine, glucosamine, or glucose. Strains were first grown as LBS cultures, and then sub-cultured 1:100 into 0.2% casamino acids in MSM until they reached an optical density (600 nm, 1 cm path length, OD_{600}), of 0.40 ± 0.05 absorbance units. These cultures were used to inoculate (at a dilution of 1:100) into MSM supplemented with a single carbon source. Optical density was determined after 36 h of growth.

Acid tolerance assays. Induction of acid tolerance in *V. fischeri* was assessed using a modified version of the acid-killing assays developed for *Vibrio cholerae* (57). To measure induction of acid tolerance in cultured cells, 30 mL SWTO cultures of *V. fischeri* were grown in 125 mL flasks with shaking to an OD_{600} of 0.4 +/- 0.05. Cells were harvested by centrifugation for 6 min at 5000 x g. To measure the potential for cells to adapt to a sub-lethal

amount of organic-acid stress, 90% of the cells were resuspended in 0.5 mL SWTO (pH 5.5) containing 50 mM PIPES and 0.075X organic acids (1X organic acids = 74 mM propionic acid, 174 mM acetic acid, and 50 mM butyric acid). The remaining 10% of the cells were re-suspended in 0.5 mL SWTO (pH 7.5) containing 50 mM PIPES without organic acids. Cell suspensions were incubated for 1 h at 28 °C with shaking, prior to centrifugation and resuspension in 0.5 mL SWTO (pH 4.75) containing 0.1 x organic acids and 50 mM PIPES. aliquots of cells (20 µL) were removed at 10-min intervals, serially diluted, and 10 µL of each dilution was spotted onto LBS agar plates for colony enumeration. Percent survival at time T_n was calculated by: $(CFU/mL)T_n$-$(CFU/mL)T_0$*100. To assay for induction of acid tolerance by catabolism of COS, cells were grown in 30 mL of 20 mM COS in SWTO (pH 7.5) with and without an additional 50 mM PIPES buffer, pelleted, and resuspended directly in SWTO (pH 4.75) containing 50 mM PIPES and 0.1X organic acids.

To assay the induction of acid tolerance in symbiotic cells of *V. fischeri*, symbiont-containing tissues (from mature squid with mantle length >15 mm), whole light organs (squid 10-15 mm mantle length), or 50 whole light organs (from juvenile squid <10 mm mantle length) were gently homogenized to release bacterial cells. Symbiont-containing supernatant from the light-organ homogenate was pelleted by centrifugation, and survival was compared between populations resuspended directly in lethal 0.1X SWTO (pH 4.75) containing 50 mM PIPES and 0.1X organic acids, or following a 1-h incubation in the inducing condition SWTO (pH 5.5) containing 50 mM PIPES and 0.075X organic acids.

Acetate and glucose detection Samples of *V. fischeri*, *V. harveyi*, or *E. coli* culture supernatant were assayed for acetate production and glucose consumption: cells were grown in 3 mL LBS (*Vibrio spp.*), or LB (*E. coli*) cultures to OD_{600} 0.5 +/- 0.05, and 0.25 mL of these cultures were pelleted, rinsed, re-suspended in 3 mL of MSM (for *Vibrio spp.,* (56)) or M9 (for *E. coli,* (58)) containing either 5 mM GlcNAc or 5 mM glucose. MSM and M9 are both minimal media, containing similar profiles of minerals, at different compositions. These media have been previously optimized for the growth of marine (MSM), or terrestrial (M9) microbes. Cultures were grown with shaking in 18 mm test tubes at 225 rpm for 2 h. To determine the level of acetate accumulation in the minimal medium supernatant, 100 µL aliquots of bacterial cultures at an OD_{600} of 0.5 +/- 0.05 were centrifuged for 15 min at 13,000 x g and 4° C to remove cells. The cell-free supernatant was stored at -20 °C until assayed. A coupled-enzyme assay (Sigma-Aldrich, #MAK086) was used to detect acetate, following the manufacturer's protocol. Absorbance at 420 nm was monitored to detect the accumulation of the colorimetric substrate with a TECAN plate reader and Magellan automation software (Tecan Group, Ltd.). The concentration of acetate in the culture supernatant was calculated based on a linear regression of measurements for acetate standards of known concentration (R^2= 0.93, over a range of 0-300 µM). Where necessary, samples were diluted to fall within the detection limits of the assay. The amount of acetate per cell was divided by the OD_{600} to normalize between conditions. Glucose was detected by a glucose-oxidase coupled enzyme assay (Sigma-Aldrich, #GAGO20), following the manufacturer's protocol. Absorbance at 600 nm was monitored to detect *o*-dianisidine, the colorimetric product, proportional to the original glucose concentration. The concentration of glucose in the culture supernatant was

calculated by a comparison to a calibration curve generated from standards of known glucose concentration (R^2= 0.99, over a range of 0-500 μM glucose). Samples were diluted as necessary to fall within the linear range of glucose concentration detected by the assay, as defined by the calibration curve.

Hemolymph titration To determine the buffering capacity of hemolymph, 100 μL samples of cell-free hemolymph were first diluted 1:10 in deionized water, and then titrated with 0.1 M HCl. pH measurements were made using an Orion PerpHect LogR meter, and Silver/Silver Chloride reference electrode (Thermo-Fisher Scientific).

RESULTS and DISCUSSION:

Hemocytes deliver chitin to the light organ. The diel transcription of chitin-utilization genes by symbiotic *V. fischeri* (24), together with the presence of chitin within the host's macrophage-like hemocytes (22), suggest that the hemocytes convey this nutrient to the symbionts. To test this hypothesis, I first characterized the distribution of chitin in the light organ's central core. Two major host cell types comprise this tissue: the polarized microvillar epithelium that defines the symbiont-containing crypt spaces, and the hemocytes that migrate into them (**Fig. 4-1*A***). I collected samples of central core tissue at dusk (10 hours post dawn, hpd, **Fig. 4-1*A***), and just before dawn (22 hpd, **Fig. 4-3*A***), and probed for the presence of particulate chitin. Fluorescently labeled chitin-binding protein (CBP) co-localized almost exclusively with the hemocyte-specific, cytoplasmic marker, DNAse-I (**Fig. 4-1*A***). Importantly, while soluble COS molecules (which do not bind CBP) may exist elsewhere, the

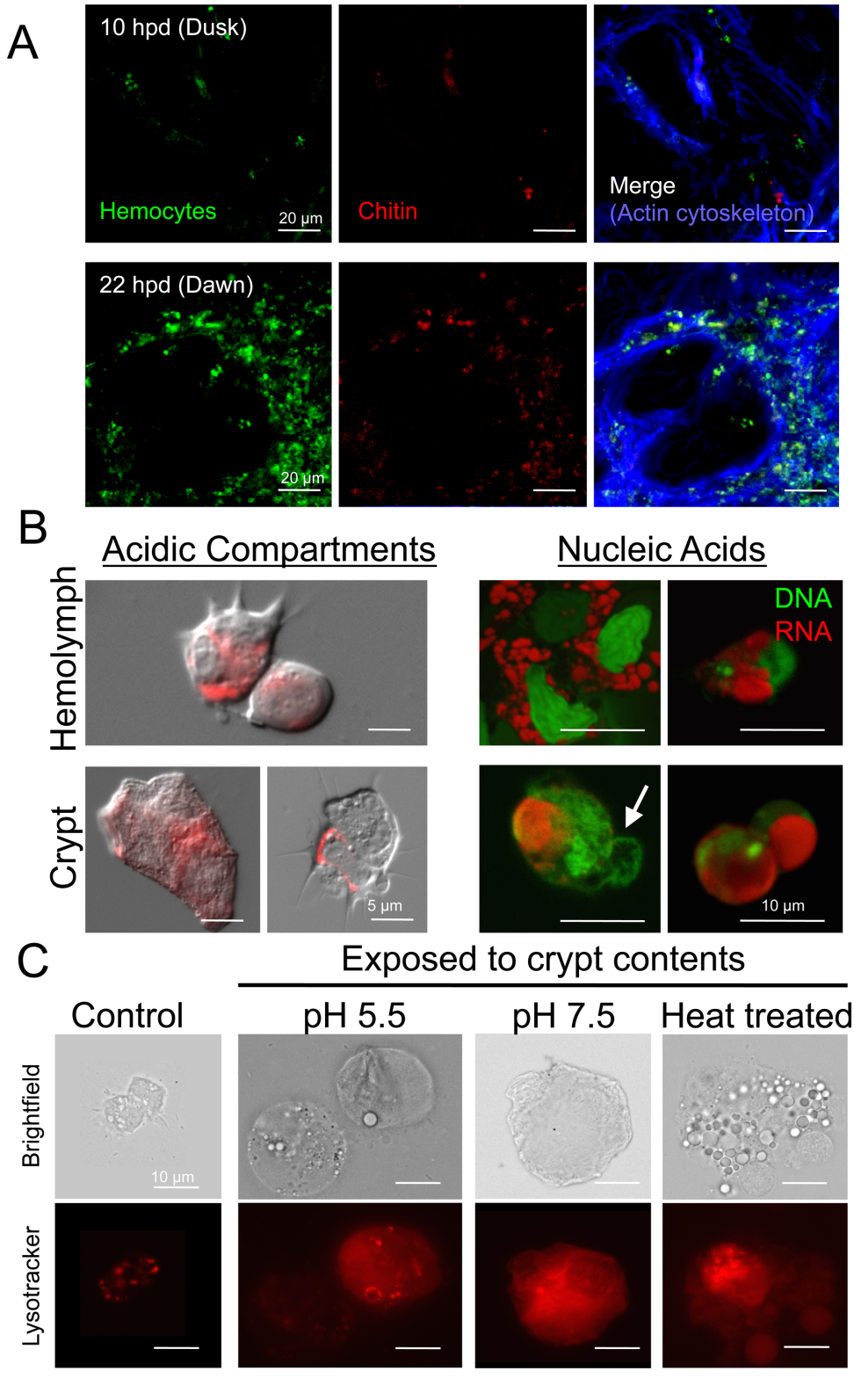
A
10 hpd (Dusk)
Hemocytes
20 µm
Chitin
Merge
(Actin cytoskeleton)
22 hpd (Dawn)
20 µm
B
Acidic Compartments
Nucleic Acids
Hemolymph
Crypt
DNA
RNA
5 µm
10 µm
C
Exposed to crypt contents
Control
pH 5.5
pH 7.5
Heat treated
Brightfield
Lysotracker
10 µm

Figure 4-3. Presence of chitin and hemocytes in light-organ tissue, and morphological changes of hemocytes exposed to the light-organ crypt environment. ***A***) Confocal micrographs, showing co-localization of fluorescently labeled hemocyte-specific marker DNAse-I (green, FITC label, binds globular actin) and chitin-specific chitin binding protein (red, TRITC label, binds particulate chitin). Actin-rich extracellular matrix was detected with Alexa 633 phalloidin (blue). Tissue was sampled at dusk (top panel, 10 hours post dawn, hpd), and before dawn (bottom panel, 22 hpd). ***B***) Left panels: morphology of hemocytes derived from the squid hemolymph (top) and the light-organ crypt (bottom). Images are merged differential interference contrast and fluorescent micrographs. Acidic compartments within cells were labeled with Lysotracker Red. Right panels: DNA (green), and RNA (red) were labeled with acridine orange. Arrow indicates irregular nuclear morphology. ***C***) Morphological changes are induced in hemocytes upon exposure to crypt contents. Hemolymph (containing hemocytes) and crypt contents were collected from a single animal at 22 hpd. Left panel: the acidic vesicles of these hemocytes were labeled with Lysotracker Red. The labeled cells were then exposed to 25% crypt contents in pH 5.5, the nocturnal pH of the crypt (9), in Squid Ringers buffer, and monitored over time. Three right panels: blebbing of the hemocyte cell membrane and loss of vacuolar integrity, indicated by diffuse Lysotracker staining, were observed after 1 h of exposure to crypt contents. Similar results were obtained when the hemocytes were exposed to either 25% heat-treated crypt contents, or 25% crypt contents in pH 7.5 Squid Ringer's buffer.

observations support the idea that hemocytes are the main cell type within the light organ that contain particulate chitin.

Our previous observations of the contents of the light-organ crypts had suggested that both live and dead hemocytes are present among the densely packed symbiotic bacteria (52). Thus, I hypothesized that chitin particles are delivered to the symbiont population by the death and lysis of chitin-containing hemocytes that have migrated into the crypts. A more extensive examination of crypt contents released at night (22 hours post-dawn; hpd) revealed two kinds of host cells: (i) compact 10-µm diameter cells, and (ii) ~20-µm, variable-diameter cells with diffuse DNA staining, ruptured acidic vacuoles and irregular membrane morphology (**Figs. 5-1*C* & 5-3*C***), consistent with living and moribund hemocytes, respectively. The presence of the latter morphology in the nocturnal crypts raised the question of whether exposure to the conditions present in this environment (34) were sufficient to cause hemocyte damage.

When I suspended healthy hemocytes derived from hemolymph (pH ~7) for 1 h in crypt contents buffered at either pH 7.5 or the nocturnal crypt pH of 5.5 (34), the initially intact hemocytes swelled, produced membrane blebs, and showed a loss of integrity of their acidic vacuoles (**Fig. 4-1*C***). If the crypt contents were heat-treated, they elicited the same effect. Thus, a heat-resistant, neutral-pH active, component of the crypt contents can trigger a change in hemocyte appearance that is consistent with hemocyte damage. In addition, when crypt contents were collected 2 h before dawn (22 hpd) and probed with CBP, I observed both healthy-looking cells that contained particles of chitin, free chitin in the extracellular

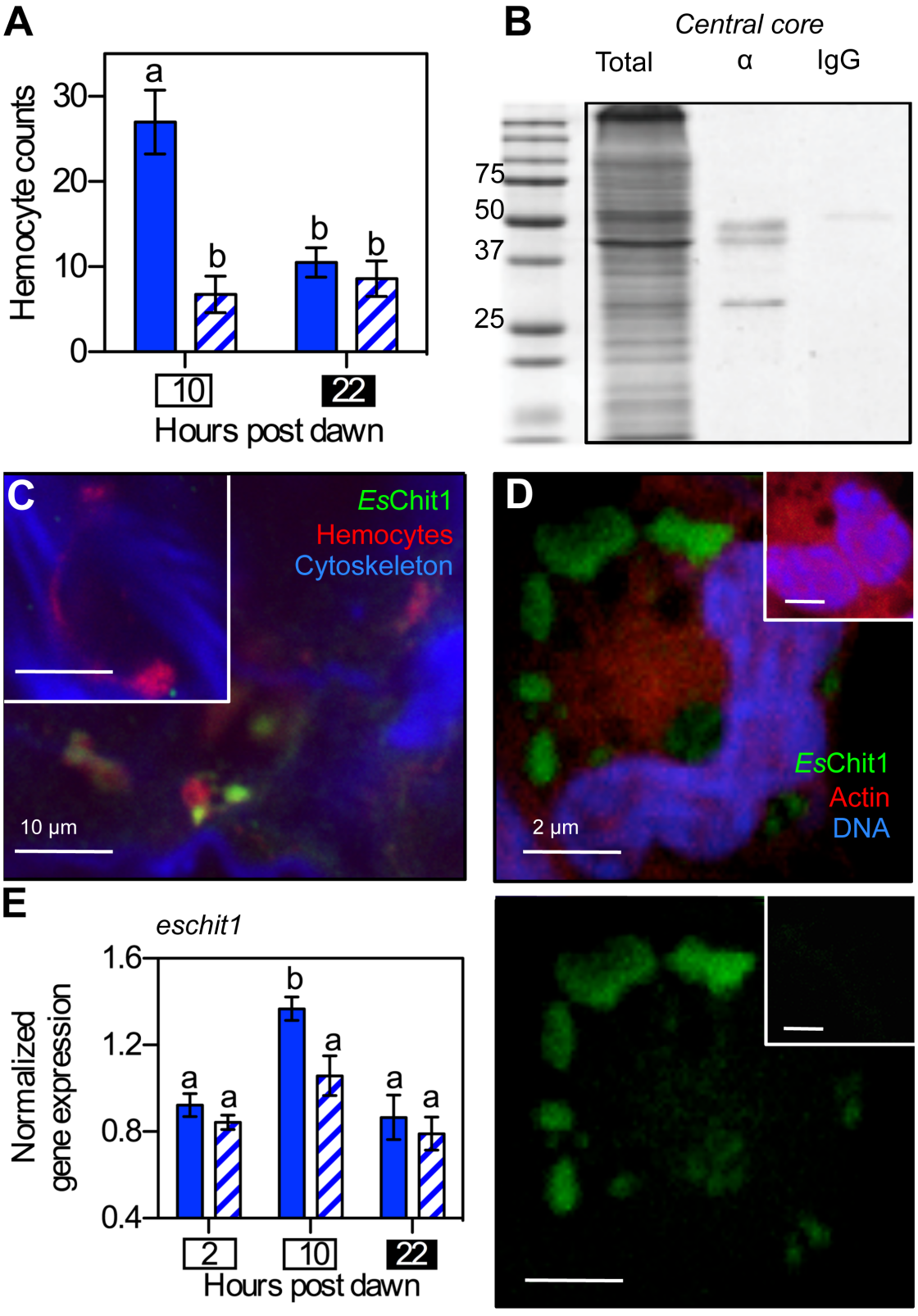
A
Hemocyte counts
30
20
10
0
a
b
b
b
10
22
Hours post dawn
B
Central core
Total
α
IgG
75
50
37
25
C
EsChit1
Hemocytes
Cytoskeleton
10 µm
D
EsChit1
Actin
DNA
2 µm
E
eschit1
Normalized gene expression
1.6
1.2
0.8
0.4
a
a
b
a
a
a
2
10
22
Hours post dawn

Figure 4-4. The diel migration of hemocytes to the light organ is symbiont dependent. (*A*) Enumeration of hemocytes present during the day (10 hpd; white box) and night (22 hpd; black box) in light-organ tissues of 2-day-old, immature symbiotic (solid bars) and aposymbiotic (hatched bars) light organs. n=15 light organs, error bars indicate SEM, data representative of three independent experiments. 'a' and 'b' indicate groups of statistically similar means, determined with Two-Way ANOVA with Post-Hoc Bonferroni T-tests. (*B*) Western blot showing presence of *Es*Chit1 in 25 μg of total soluble protein isolated from central cores. Total soluble protein, Total; anti-*Es*Chit1 antibody, α; immunoglobulin control, IgG. (*C*) Confocal micrograph localizing *Es*Chit1 in whole adult (>4-week old) central cores at dusk (10 hpd). Inset: pre-immune control. (*D*) Localization of *Es*Chit1 in hemocytes extracted from adult symbiotic squid. Top panel, anti-*Es*Chit1 signal alone; bottom panel, anti-*Es*Chit1 signal merged with rhodamine phalloidin (filamentous actin-specific) and TOTO-3 (DNA-specific). Insets: pre-immune control. (*E*) Diel pattern of the transcription of host *eschit1* chitotriosidase in adult symbiotic (solid bars) and aposymbiotic (hatched bars) light organs; error bars indicate SEM, n= 5; statistical tests are as described in (*A*).

crypt matrix, and moribund cells morphologically similar to those observed in the *in vitro* studies described above (**Fig. 4-1*D***). Collectively, the data are consistent with a model wherein chitin particles within host hemocytes are released into the crypts and become accessible to extracellular hydrolysis by both host and symbiont chitinases (21, 24, 44).

Symbiont-dependent hemocyte trafficking into the light organ is on a diel cycle. In order for hemocytes to deliver COS to symbionts during the nocturnal phase of the diel cycle, some aspect of their behavior must be rhythmic. I have previously reported a symbiosis-induced increase in the number of hemocytes associated with the light organ in immature, 2-day-old squid (59). I extended this observation by asking whether the increase in hemocytes was dependent on the time of day, and thus, a symbiosis-dependent diel migratory rhythm. Consistent with previous results (59), approximately four times more hemocytes were found in symbiotic than in aposymbiotic light organs of 2-day-old squid at dusk (10 hpd; **Fig. 4-4*A***). However, I noted that this increase was transient: the number of hemocytes in symbiotic light organs returned to aposymbiotic levels by the end of the night (22 hpd), and no accumulation of hemocytes was noted in the crypts of the immature light organs. This pattern of hemocyte migration recurred the following day (**Fig. 4-5*A***), demonstrating that the migration into symbiotic light organs at dusk is a diel pattern, rather than a single event in the trajectory of an immunological and/or developmentally triggered response to colonization. Thus, a symbiosis-dependent diel rhythm of hemocyte migration is established within the first few days following light-organ colonization.

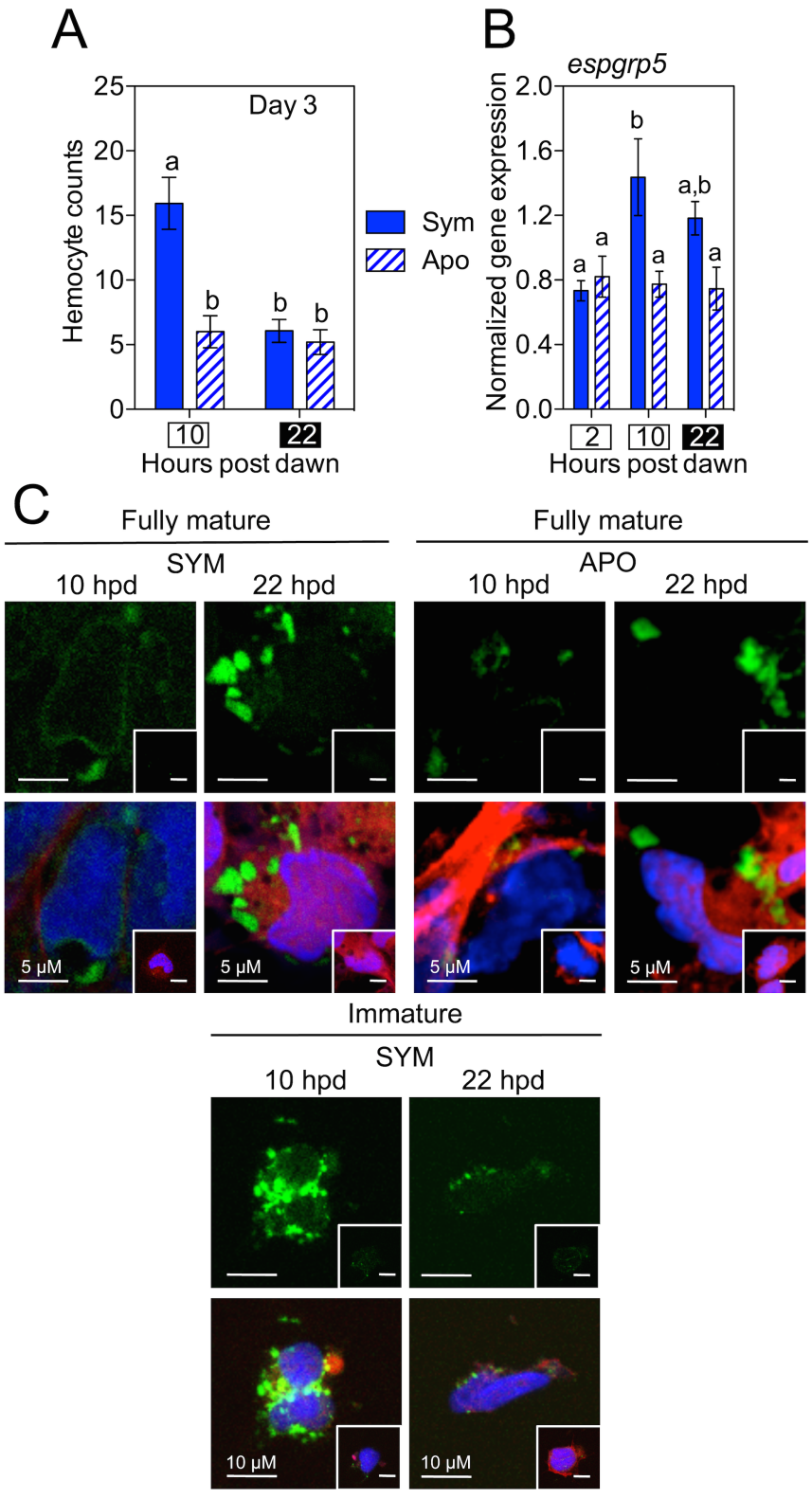
A
Day 3
Hemocyte counts
25
20
15
10
5
0
a
b
b
b
Sym
Apo
10
22
Hours post dawn
B
espgrp5
Normalized gene expression
2.0
1.6
1.2
0.8
0.4
0.0
a
a
b
a
a,b
a
2
10
22
Hours post dawn
C
Fully mature
SYM
10 hpd
22 hpd
Fully mature
APO
10 hpd
22 hpd
5 µM
5 µM
5 µM
5 µM
Immature
SYM
10 hpd
22 hpd
10 µM
10 µM

Figure 4-5. Diel hemocyte-associated phenotypes. ***A-B***) Diel migratory behavior and transcription of a hemocyte-associated gene in symbiotic (Sym) or aposymbiotic (Apo) light organs, assessed during the day (open boxes) and night (black boxes). ***A***) Diel enumeration of hemocytes present in 3-day-old light organs evaluated at 10 and 22 h post dawn. Bars indicate SEM; n=15 light organs per replicate. Data represent two independent experiments. 'a', and 'b' denote groups of statistically similar means, assessed by Two-Way ANOVA with Post-Hoc Bonferrioni T-tests. ***B***) Transcription of the hemocyte-associated gene *espgrp5* (25) in 4-week-old light organs. Bars represent SEM, n= 4. 'a', and 'b' indicate groups of statistically similar means, assessed by Two-Way ANOVA with Post-Hoc Bonferrioni T-tests. ***C***) Detection of *Es*Chit1-positive granules in hemocytes derived from symbiotic (SYM) and aposymbiotic (APO) squid 10 and 22 h post dawn (hpd). Inset shows the corresponding pre-immune control. Top panel: hemocytes were isolated from individual fully mature squid (>4 weeks old). Observations were made from 3 independent samples. Bottom panel: detection of *Es*Chit1in hemocytes isolated from pools of 15 immature squid (2 days post-hatch). Images are represent observations from 2 independent samples.

I next investigated whether a similar rhythm of hemocyte migration occurred in mature light organs. At this stage of development, transcription of the predicted *E. scolopes* chitotriosidase gene *eschit1* exhibits a diel periodicity, with expression highest at night (24). This gene is also transcribed by hemocytes (22). Western-blot analysis demonstrated that the chitotriosidase enzyme itself was present in central core tissue; *i.e.*, the *Es*Chit1 antibody (α-*Es*Chit1) hybridized to a 50 kD band (the molecular weight predicted for *Es*Chit1), as well as two smaller bands in the soluble fraction of central-core proteins (**Fig. 4-4*B***). This multiband pattern is consistent with the post-translational processing that occurs during the activation of invertebrate chitinases (60). In addition, fluorescence immunocytochemistry and confocal microscopy of the central core localized the *Es*Chit1 protein exclusively to the hemocytes found there (**Fig. 4-4*C***). I confirmed these observations by isolating hemocytes and probing them directly for *Es*Chit1: cells from both mature and immature animals exhibited α-*Es*Chit1-positive puncta (**Figs. 5-4*D* & 5-5*C***), irrespective of symbiotic state. Thus, hemocytes express the majority of *Es*Chit1 in light organ tissue, and *eschit1* transcript can be associated with the presence of hemocytes.

To determine whether the diel rhythm of *eschit1* transcription originally observed in mature central-core tissues occurred only in the symbiotic state, I profiled the transcript levels of this gene at three times of day, in both symbiotic and aposymbiotic mature light organs, by quantitative real-time PCR. Consistent with previous results (24), hemocyte-associated *eschit1* transcript levels increased in mature symbiotic light organs just before nightfall (10 hpd; **Fig. 4-4*E***). This increase was not observed in aposymbiotic light organs, although transcript levels were comparable between the two groups, both in the morning and at the end

of the night (2 and 22 hpd, respectively) (**Fig. 4-4*E***). Transcription of another, functionally distinct, hemocyte-associated *E. scolopes* gene, peptidoglycan-recognition protein 5 (*espgrp5*) (61), displayed the same symbiont-dependent peak at dusk as *eschit1* (**Fig. 4-5*C***). This pattern in hemocyte-associated transcripts mirrors the transient, symbiosis-dependent increase in hemocyte numbers observed in immature light organs, and is consistent with the nightly hemocyte migration into the crypts of mature light organs, although it may also indicate a small symbiosis-dependent induction of these two genes as well. While I do not know whether this rhythmic migration has circadian underpinnings, in vertebrates, macrophages migrate into tissues as part of a circadian cycle that is entrained by microbial cues (13).

Delivery of COS to the symbionts begins in the mature light organ. I next asked whether the symbionts metabolize COS and, if so, what consequences it might have for the association. To investigate COS metabolism within the crypts, I constructed a mutant strain of *V. fischeri* that would act as a biosensor. Catabolism of chitin (**Fig. 4-6*A***) is a general characteristic of the *Vibrionaceae*, and this glycan is an important environmental nutrient and cue for both beneficial and pathogenic species in this family (25). To construct the COS biosensor, I deleted the *V. fischeri nagB* gene, which encodes the final enzymatic step by which COS and other amino sugars enter the central carbon metabolism of *V. fischeri* (44). Such a mutant cannot grow on this group of sugars (**Figs. 5-6*A* & 5-7*A***). As with the homologous *Escherichia coli* mutant (62), in a complex growth medium ,*V. fischeri* Δ*nagB* was sensitive to 100 μM of the COS monomer *N*-acetyl glucosamine (GlcNAc), a level even below that required for significant growth (**Fig. 4-*7B***). As expected, genetically complementing the Δ*nagB* strain *in cis* at the Tn*7* site on the *V. fischeri* chromosome, a

neutral site for integration of DNA elements (48), eliminated this sensitivity (**Fig. 4-6*B***). The effect of COS on Δ*nagB* growth was also relieved by the presence of a non-gluconeogenic sugar of the pentose-phosphate pathway (*e.g.*, fructose, glucose, or ribose; **Fig. 4-7*C***), confirming that the arrest phenotype is attributable to substrate inhibition (62).

From these observations, I reasoned that *V. fischeri* Δ*nagB* would have difficulty colonizing the squid light organ under two conditions: (i) where COS is present at a level sufficient to support wild-type growth, or (ii) where there is even a small amount of COS (*e.g.*, ~100 μM), but no ameliorating pentose-phosphate pathway sugars. I compared colonization levels in light organs populated by either wild-type or Δ*nagB* strains of *V. fischeri* during the first 4 weeks post-colonization to determine when symbionts might encounter such environments (**Fig. 4-6*C***). For at least 2 weeks, squid were colonized equally well by wild type or Δ*nagB*; however, by 4 weeks, light organs colonized by the Δ*nagB* strain contained <15% as many symbiont cells as those colonized by either wild type or the *in cis* complement (**Fig. 4-6*C***). The Δ*nagB* strain showed no decrease in fitness during co-colonization with wild type, throughout a 4-week colonization (**Fig. 4-7*D***), probably due to an effective lowering of the ambient COS concentration by wild-type metabolism. Similarly, co-culture of Δ*nagB* and wild-type *V. fischeri* allowed growth of the mutant, even in the presence of up to 2.5 mM GlcNAc (**Fig. 4-7*E***), suggesting that the concentration of COS available to symbionts in the light organ never exceeds a few millimolar. Although I cannot rule out the possibility that COS are present in the immature light-organ crypt at a level below the sensitivity of the biosensor strain (*i.e.*, 10-100 μM), the data do indicate that COS catabolism

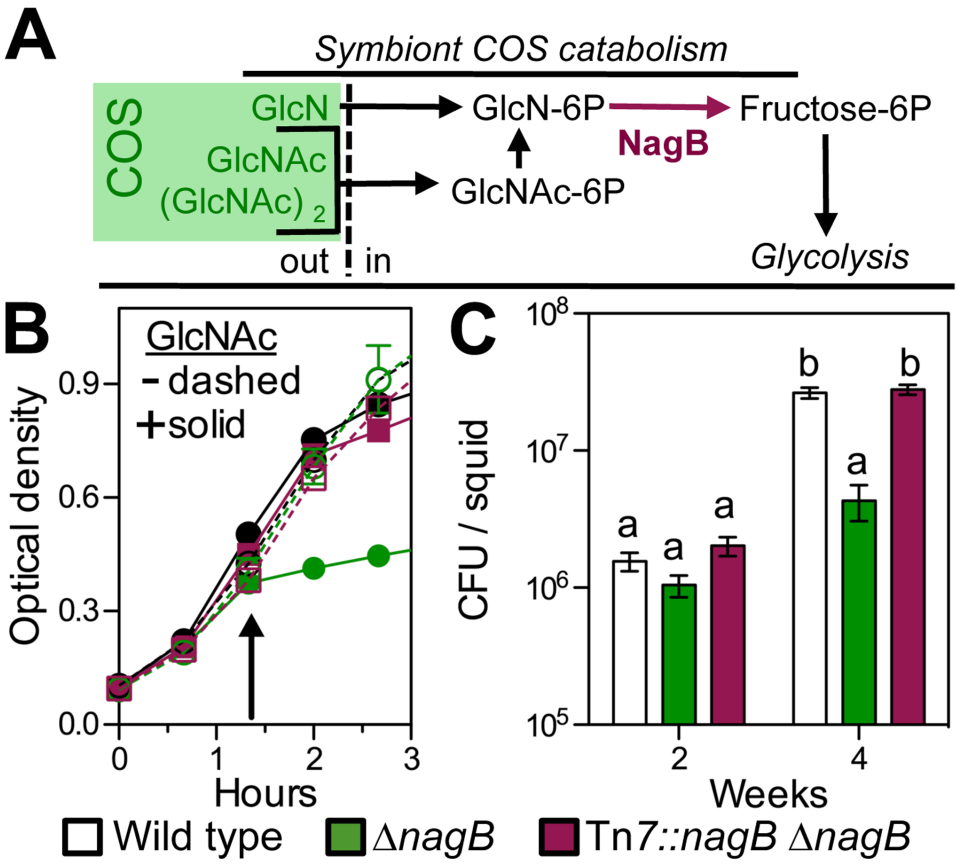
A
Symbiont COS catabolism
COS
GlcN
GlcNAc
(GlcNAc) 2
GlcN-6P
Fructose-6P
NagB
GlcNAc-6P
out
in
Glycolysis
B
GlcNAc
- dashed
+ solid
Optical density
0.0
0.3
0.6
0.9
0
1
2
3
Hours
C
CFU / squid
10^5
10^6
10^7
10^8
a
a
a
b
a
b
2
4
Weeks
Wild type
ΔnagB
Tn7::nagB ΔnagB

Figure 4-6. Symbionts sense COS only in the mature light organ. ***A***) Catabolism of chitin oligosaccharides (COS) in the genus *Vibrio*. COS are derivatives of amino di- and monosaccharides, that represent enzymatic products of chitin hydrolysis (green box). After the COS are transported into the cell as the phosphorylated form, the acetyl and amino groups are removed from the hexose core before it enters glycolysis. The last common step in COS catabolism is the deamination of glucosamine-P by the enzyme NagB. To define amino sugar and COS catabolism in *V. fischeri,* I tested the ability of the Δ*nagB* mutant to grow on sugars as a sole source of carbon (data shown in Figure S3*A*). GlcNAc, *N*-acetyl glucosamine; $(GlcNAc)_2$, *N*-acetylchitobiose; GlcN, Glucosamine; out, extracellular or periplasmic space; in, intracellular space. ***B***) Growth of a Δ*nagB V. fischeri* mutant in high osmolarity seawater-tryptone medium (SWTO), either without or with the addition of 20 mM GlcNAc at the arrow. Error bars indicate SEM, n=4. ***C***) Extent of colonization of the squid light organ at immature and mature stages of host development by wild type, Δ*nagB,* and an *in cis* complement (Δ*nagB* Tn*7::nagB)*. CFU, colony-forming units; error bars indicate SEM, n=12; statistical tests on log-transformed data are as described in Fig. 4-2.

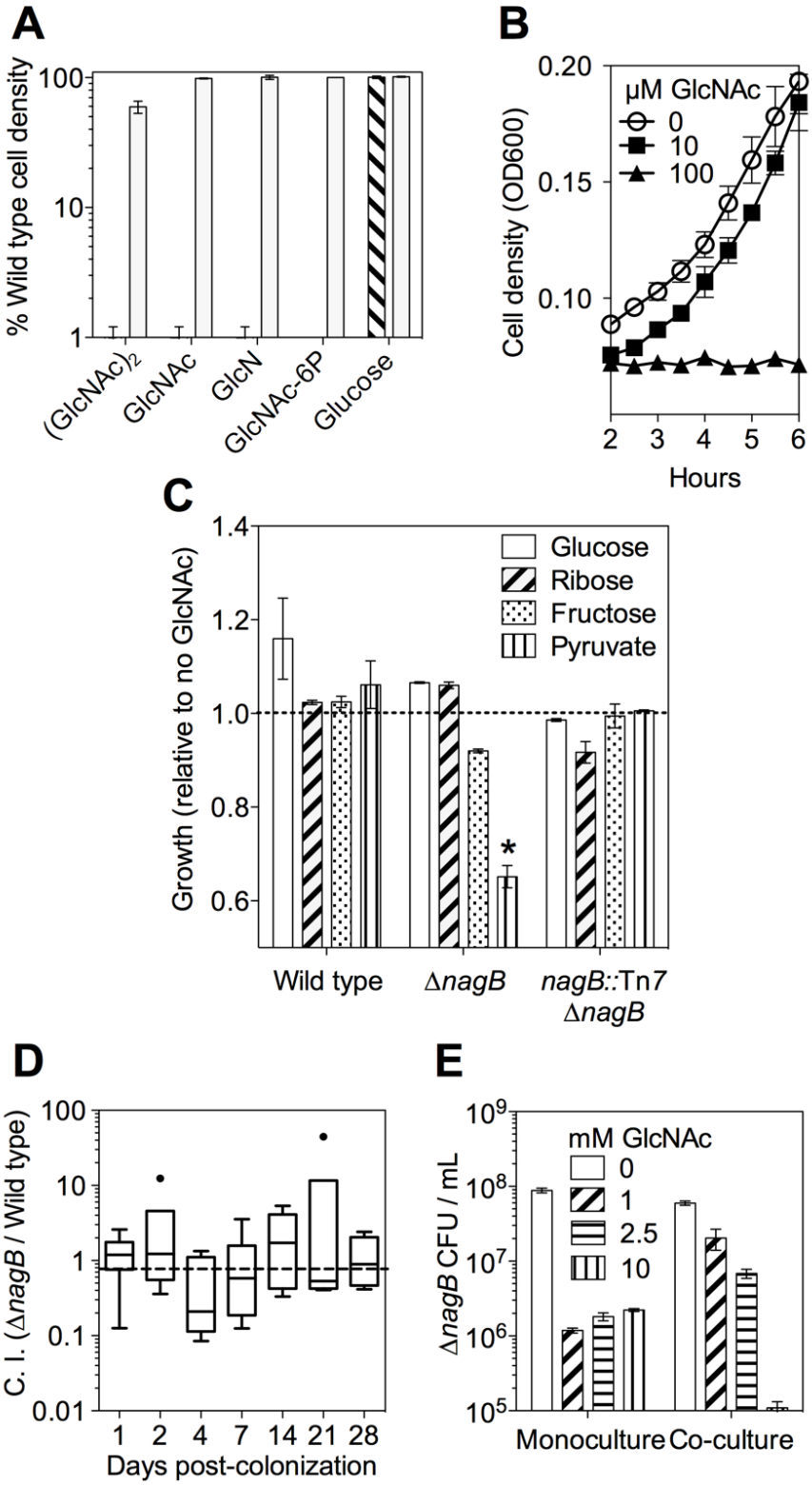
A
% Wild type cell density
100
10
1
(GlcNAc)2
GlcNAc
GlcN
GlcNAc-6P
Glucose
B
Cell density (OD600)
0.20
0.15
0.10
μM GlcNAc
0
10
100
2 3 4 5 6
Hours
C
Growth (relative to no GlcNAc)
1.4
1.2
1.0
0.8
0.6
Glucose
Ribose
Fructose
Pyruvate
*
Wild type
ΔnagB
nagB::Tn7 ΔnagB
D
C. I. (ΔnagB / Wild type)
100
10
1
0.1
0.01
1 2 4 7 14 21 28
Days post-colonization
E
ΔnagB CFU / mL
10^9
10^8
10^7
10^6
10^5
mM GlcNAc
0
1
2.5
10
Monoculture
Co-culture

Figure 4-7. Phenotypes of the COS biosensor strain, Δ*nagB*. ***A***) Growth of Δ*nagB* (hatched bars) and an *in cis* genetic complement, Δ*nagB* Tn7::*nagB* (open bars), relative to wild-type *V. fischeri* on different sugars. $(GlcNAc)_2$, chitobiose; GlcNAc, *N*-acetylglucosamine; GlcN, glucosamine. Bars indicate SEM, n=2. ***B***) Concentration-dependence of COS sensitivity. Cultures were grown in LBS with added GlcNAc, and growth measured by optical density at 600 nm (OD600). Bars indicate SEM, n=3. ***C***) Ability of non-gluconeogenic carbohydrates to reverse Δ*nagB* substrate inhibition. Growth of wild type, Δ*nagB*, and Δ*nagB* Tn7::*nagB* was assessed in the presence of both GlcNAc and the indicated, non-COS, carbohydrate. The capacity of the second carbohydrate to functionally complement substrate inhibition by GlcNAc was assessed by comparison to growth on the carbohydrate in the absence of GlcNAc. Bars indicate SEM; n=3; (*) indicates a mean ratio of growth in the presence versus absence of GlcNAc statistically different from 1.0, assessed by one-sample T-test. ***D***) 4-week co-colonization with both Δ*nagB* and wild-type *V. fischeri*. C.I., competitive index. Center bar indicates median C.I., inner fences determined by Tukey's method, outliers shown as black dots, n=6 squid per time point. ***E***) Growth of Δ*nagB* with COS in complex medium. The Δ*nagB* strain was either cultured alone (monoculture), or co-cultured with wild-type *V. fischeri* at an initial inoculum of 1:1. Bars indicate SEM, n=6.

emerges as a major metabolic strategy for symbiotic *V. fischeri* between 2 and 4 weeks post-hatch. These data also indicate that the presence of COS in the light-organ crypts is not directly linked to the squid's diet: the squid are raised on a chitin-rich diet throughout the rearing process. The developmental, diet-independent regulation of COS availability echoes the life stage-specific presentation of surface sugars to glycan-foraging microbes during mammalian gut development (27).

Catabolism of COS by the symbionts drives a diel cycle of crypt acidification. To determine whether the delivery of *E. scolopes* chitin, like that of mammalian glycans (27), shapes the ecology of the mature state of symbiosis, I asked whether the appearance of COS in the light-organ crypts induced any changes in symbiont physiology and/or the crypt environment. Catabolism of COS produced acid in culture, thus, I performed a comparative study of COS catabolism, and associated acetate production, under aerobic culture conditions in four strains (**Table 4-3**): *V. fischeri* ES114 (the wild-type squid-symbiont used in this study), *V. fischeri* MJ11 (a fish light-organ symbiont), *Vibrio harveyi* (a non-symbiotic seawater isolate) and *Escherichia coli* K-12 (an enteric strain found in the mammalian gut). When grown on either *N*-acetylglucosamine or glucose, the three *Vibrio* strains produced 2-3 times more acetate/unit growth, and more acetate/mole substrate, than did *E. coli*, suggesting that the aerobic catabolism of glycolytic substrates by *Vibrio spp.* relies more on substrate-level phosphorylation for energy generation than *E. coli* does. This excretion of acetate during aerobic growth is consistent with a metabolic imbalance called the Crabtree effect (63). In the context of the light-organ environment, the Crabtree effect would lead to the excretion of

short-chained fatty acids (SCFA) during growth on COS, thereby acidifying the crypt lumen and enhancing the allocation of ambient oxygen toward bioluminescence.

TABLE 4-3. Acetate excretion during aerobic growth on a single sugar

Strain	Sugar	Acetate* per OD unit	Acetate* produced per glucose* used
Vibrio fischeri ES114	GlcNAc	9.8 +/- 0.7	-
	Glucose	7.0 +/- 0.2	0.9 ± 0.1
Vibrio fischeri MJ11	GlcNAc	**11.9 +/- 0.7**	-
	Glucose	**9.1 +/- 0.5**	1.2 ± 0.1
Vibrio harveyi B392	GlcNAc	8.7 +/- 0.2	-
	Glucose	6.7 +/- 0.2	0.9 ± 0.1
Escherichia coli K12 (MG1655)	GlcNAc	**3.6 +/- 0.1**	-
	Glucose	**4.0 +/- 0.5**	**0.5 ± 0.1**

n=3; +/-, SEM; bold indicates a significantly different mean from ES114 on the same sugar. Strains were grown with shaking in minimal medium containing 5 mM of GlcNAc (COS), or glucose; all strains grew to about the same yield (OD=0.6-1.0). pH remained above 6.5 in all strains.* mM

I reasoned that if SCFA accumulate as an excreted product of symbiont COS catabolism, they might cause acidification of the light-organ crypts. In a number of bacteria, including *V. fischeri* (**Fig. 4-8*A***), exposure to low pH induces an acid-tolerance response (ATR) that mitigates a potentially lethal collapse of the cell's proton motive force by protonated weak acids like SCFA (64). As expected (**Table 4-3**), during COS catabolism in an unbuffered media, wild-type *V. fischeri* excreted sufficient acetate to acidify the culture supernatant to pH 5.5, inducing an ATR; however, when the COS medium was strongly

buffered at pH 7.5, there was no ATR (**Fig. 4-9*A***). The Δ*nagB* mutant, which is impaired in COS metabolism, did not acidify even an unbuffered COS medium and, thus, failed to induce an ATR. In contrast, this mutant did reduce the pH, and thus induced a robust ATR, when grown on glucose, a *nagB*-independent, acid-generating carbon source (**Fig. 4-8*B***). Thus, I reasoned that the failure of the Δ*nagB* mutant to induce an ATR on COS was due to its inability to catabolize COS to acetate, rather than to causing a defect in the ATR mechanism.

I next used the ATR as a reporter to indicate whether symbiont catabolism of COS acidifies the light-organ crypts; specifically, I released *V. fischeri* cells from the light organ, and immediately determined whether they had recently induced an ATR. Wild-type symbionts exhibited an ATR when released from the light organs of mature squid at night (18 & 23 hpd; **Figs. 5-8*C* & 5-9*B***), consistent with the acidic pH measured in crypt contents at night (34). In contrast, symbionts released in the morning (3 hpd) showed no evidence of ATR induction, even though they were physiologically capable of inducing this response if they were exposed to acidic conditions before the assay (**Fig. 4-9*B***). In contrast, the Δ*nagB* strain of *V. fischeri* failed to exhibit an ATR when released from the mature light organ at night, indicating it had not experienced a low pH in the crypts (**Fig. 4-8*C* & 5-9*C***). Wild-type symbionts released from immature (2-day old) light organs, even at night, also showed no evidence of an ATR (**Figs. 5-8*D* & 5-9*B***), consistent with the notion that the immature host does not provide its symbionts sufficient COS (or other fermentable carbon sources) to promote acidification.

To estimate the amount of symbiont acid production that would be needed to reduce the pH of the crypts to an ATR-inducing 5.5, I measured the buffering capacity of freshly

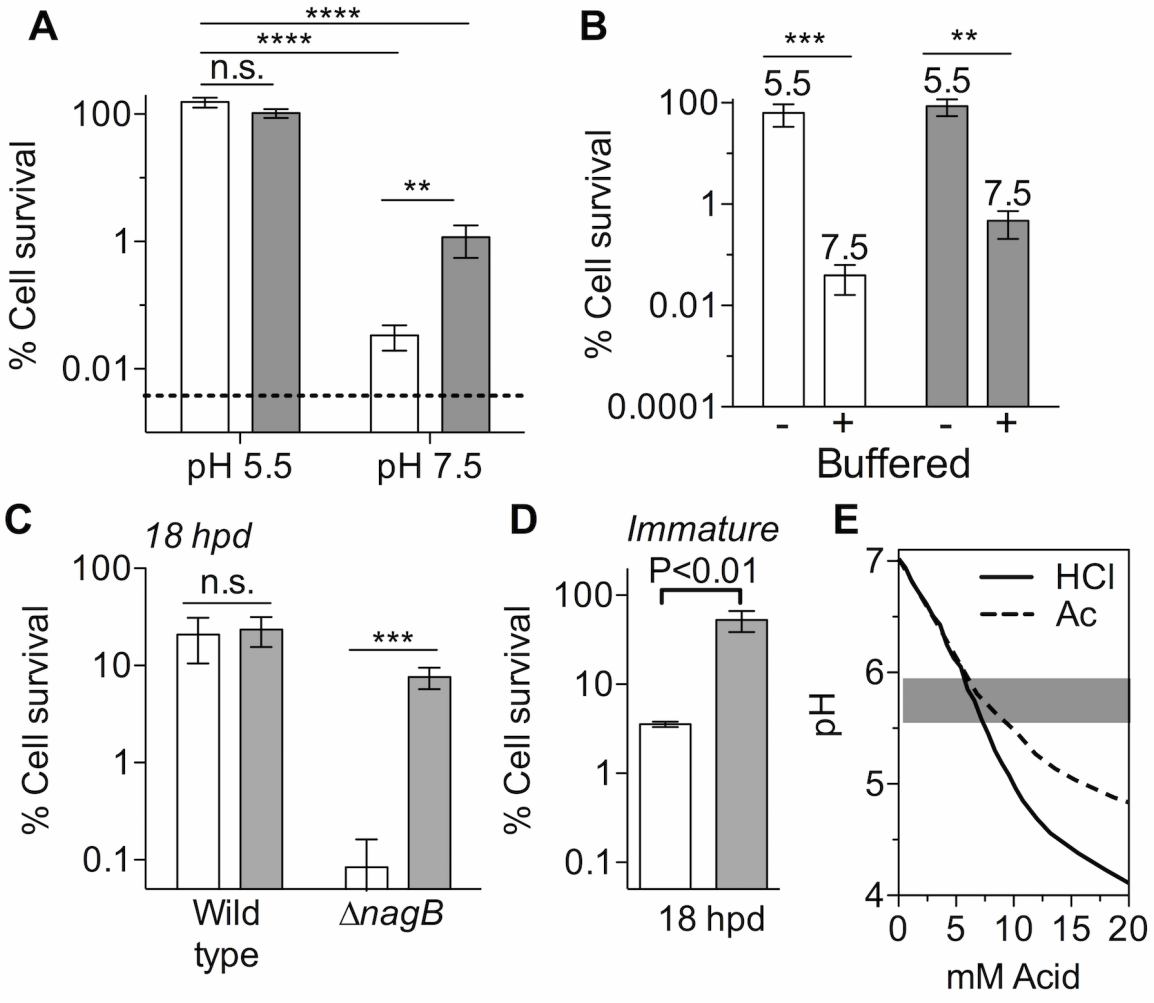
A
****
****
n.s.
**
100
1
0.01
% Cell survival
pH 5.5
pH 7.5
B
***
**
5.5
5.5
7.5
7.5
100
1
0.01
0.0001
% Cell survival
- + - +
Buffered
C
18 hpd
n.s.
***
100
10
1
0.1
% Cell survival
Wild type
ΔnagB
D
Immature
P<0.01
100
10
1
0.1
% Cell survival
18 hpd
E
HCl
Ac
7
6
5
4
pH
0 5 10 15 20
mM Acid

Figure 4-8. Characterization of the conditions sufficient to induce the *V. fischeri* acid tolerance response, and acidify the light-organ crypt. Throughout, bars indicate SEM, groups of statistically different means, determined by Two-Way ANOVA with post-hoc Bonferrioni T-tests. * P<0.05, ** P<0.01, *** P<0.005, **** P<0.001, n.s. no significance. ***A***) *V. fischeri* was grown either in pH 5.5 or pH 7.5 media in the absence (open) or presence (filled) of 30 mM SCFA. **(**n=4). ***B***) Induction of acid tolerance during growth of wild-type (open), or Δ*nagB* (filled) *V. fischeri* on 20 mM glucose in LBS medium. Medium was either buffered at pH 7.5 with 50 mM PIPES, or left unbuffered. Final pH of the culture medium prior to killing challenge is noted above the bars. (n=4). ***C***) Symbiotic wild-type or Δ*nagB V. fischeri* were released from mature light organs at night (18 h post dawn; hpd). Released symbionts were assayed for their survival upon immediate acid exposure (open), or after pre-exposure to 30 mM SCFA medium at pH 5.5 (filled) to compare the potential for induction of acid tolerance. (n=5). ***D***) Induction of acid tolerance of wild-type *V. fischeri* released from a pool of twenty 2-day-old light organs at night (18 hpd), and assayed immediately for survival in 40 mM SCFA medium (pH 4.5), (open). A portion of the released cells was incubated for 1 h in 30 mM SCFA medium (pH 5.5) as a positive control for the capacity to induce acid-tolerance (filled). (n=2). P-value determined by two-tailed T-test. ***E***) Buffering capacity of cell-free squid hemolymph was determined by titration with either hydrochloric acid (HCl), or acetic acid (Ac). The pH range previously measured in light-organ crypts at night is indicated in grey (34).

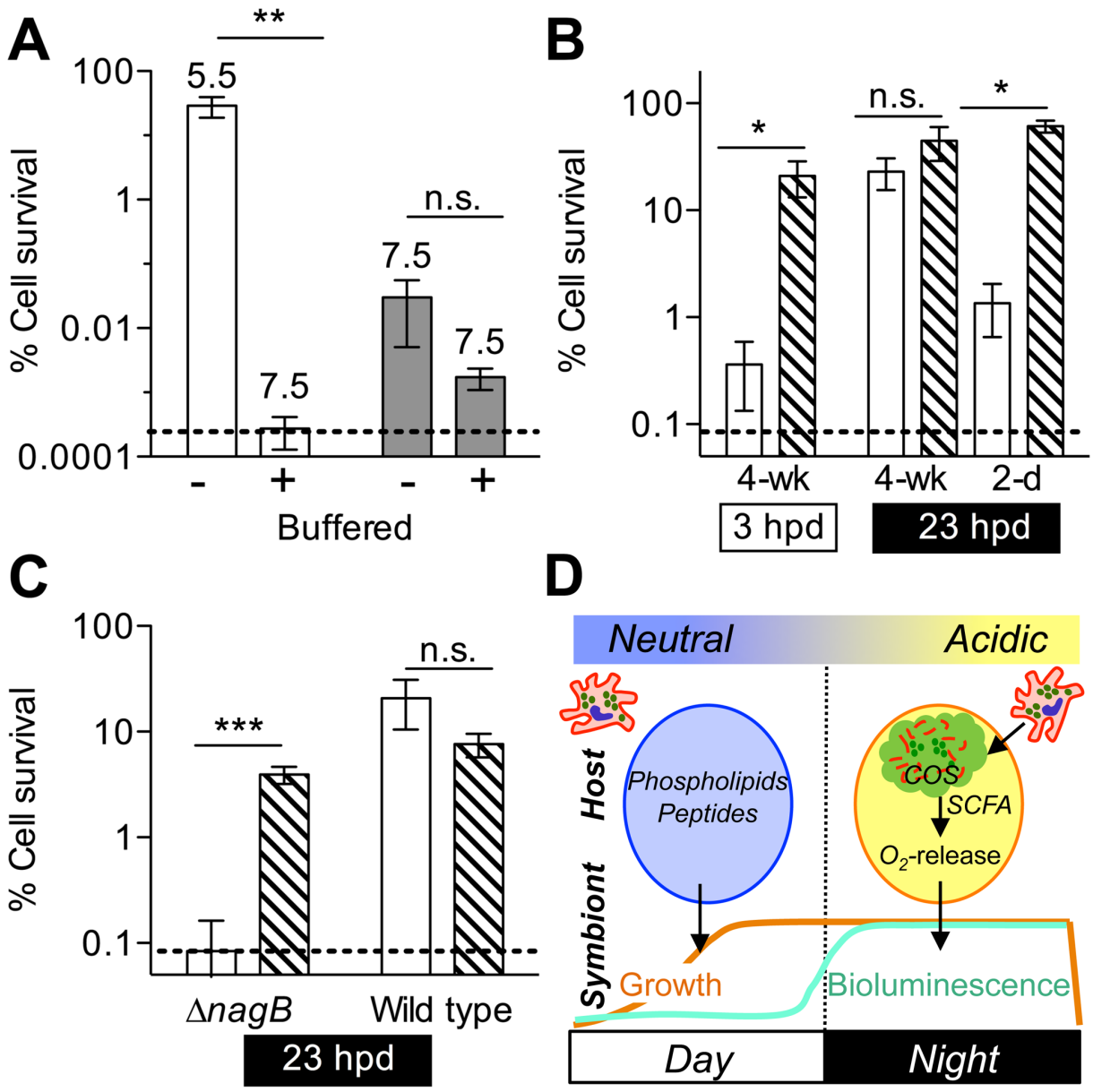
A
**
100
1
0.01
0.0001
% Cell survival
5.5
7.5
n.s.
7.5
7.5
- + - +
Buffered
B
100
10
1
0.1
% Cell survival
*
n.s.
*
4-wk
4-wk
2-d
3 hpd
23 hpd
C
100
10
1
0.1
% Cell survival
***
n.s.
ΔnagB
Wild type
23 hpd
D
Neutral
Acidic
Host
Symbiont
Phospholipids
Peptides
COS
SCFA
O2-release
Growth
Bioluminescence
Day
Night

Figure 4-9. Acidification due to COS catabolism is sufficient to induce the *V. fischeri* acid tolerance response in symbiosis. *V. fischeri* was exposed to different conditions before challenge with 40 mM short-chained fatty acid (SCFA) medium at pH 4.5. Survival (induction of an acid tolerance response, ATR) was evaluated after 20 min. ANOVA with Post-hoc Bonferroni T-tests were performed on log-transformed data; error bars, SEM; dashed line, limit of detection; n.s., no significance, * P<0.05, ** P<0.01, *** P<0.01. ***A***) Wild-type and Δ*nagB V. fischeri* were grown with 40 mM GlcNAc in either unbuffered or buffered medium (final culture pH indicated above bars); (n=6). ***B***) Symbiotic wild-type *V. fischeri* was released either from mature light organs during the day (3 h post dawn; hpd) or night (23 hpd). Alternately, symbionts were released from 6 individual pools of twenty 2-day-old light organs at night (23 hpd). Released symbionts were assayed immediately for ATR (open bars), or after a pre-exposure to 30 mM SCFA medium at pH 5.5 (filled bars) as a positive control; (n=5). ***C***) Δ*nagB* or wild-type *V. fischeri* was released from mature light organs at night (23 hpd). Symbionts were either assayed for ATR either immediately following release (open bars), or after pre-exposure for 1 h as in (*B*), prior to acid killing (filled bars); (n=6). ***D***) Model of diel metabolic cross-talk between the adult host and its symbionts. During the day, growth of symbionts on host-derived nutrients (peptides and phospholipids) in the crypt spaces (circles) is pH-neutral (24). At dusk, hemocytes (red), migrate into the light-organ crypt lumen, lyse and release chitin oligosaccharides (COS, green). The COS is catabolized by symbionts to produce short-chained fatty acids (SCFA), which acidify the crypt lumen, and promote oxygen release (34). Oxygen fuels the enzymatic production of light by symbiont luciferase, the functional basis of the squid-vibrio mutualism.

isolated squid hemolymph. Hemolymph, which is the major constituent of the crypt environment (34), required an addition of approximately 7.5 mM acetic acid to reach a pH of 5.5 (**Fig. 4-8*E***). The incomplete oxidation of a molecule of *N*-acetyl glucosamine produces at least one molecule of acetate (**Table 4-3**), and could stoichiometrically produce 3. Thus, a nightly catabolism by the symbiont population of a few millimolar COS would be sufficient to create the level of acidification measured in the light-organ crypts (**Table 4-4**).

CONCLUSIONS

Collectively, the data presented here support the hypothesis that (i) a nocturnal release of chitin from hemocytes in the light-organ crypts characterizes the mature diel cycle of the squid-vibrio symbiosis, (ii) symbiont catabolism of COS acidifies the crypt environment and induces the *V. fischeri* ATR at night, and (iii) this cycle is not active in the immature association, but only develops as the host matures (**Fig. 4-9*D***). Previous work has shown that an acidic crypt pH potentiates the release of oxygen from hemocyanin (34) at the time when the symbiont's nocturnal light production increases (33). Thus, the host's cyclic provision of chitin, coupled with the symbionts' physiological responses to this rhythm, regulate the output of bioluminescence, the central product of the association (17). To acidify the light-organ crypts to their nighttime pH of ~5.5 (34) would require an amount of acetate released by catabolism of 11 μg of COS; I estimate that to transport this amount of substrate into the crypts would necessitate ~2000 hemocytes, or 5% of the total circulating population (**Table 4-4**) (50, 52). The nightly sacrifice of this number of immune cells may at first seem a costly strategy for the host, and I cannot be certain that other complementary mechanisms of COS

delivery do not exist. However, the data suggest that amount of COS required to acidify the crypts to their observed pH could be delivered by a number of hemocytes well within the number renewed in the circulating population of hemocytes every few days (50), suggesting that the accumulation of a fraction of hemocytes in the crypt may be one strategy by which senescent cells are efficiently re-purposed. Whether or not this strategy of delivering a specific glycan is costly to the host, if immune-cell derived chitin is the key that unlocks a nocturnal cycle of symbiont bioluminescence, then the sacrifice of a fraction of its hemocytes may be a viable strategy for maintaining a stable, cooperative association.

pH homeostasis is emerging as a factor that regulates not only the phylogenetic composition of complex microbial communities, but also immune maturation and host health (65-67). In the squid-vibrio symbiosis, the diel acidification of the host tissue environment by bacterial metabolism is likely to affect activities beyond the bioluminescence phenotype of this association. The squid encodes homologs of zebrafish enzymes that inactivate immunogenic microbe-associated molecular pattern (MAMP) molecules. These enzymes lose activity at a low pH (49, 68-70), suggesting that diel tissue acidification might lead to a local or systemic increase in MAMP levels at night. MAMPs promote the establishment of symbiosis by signaling pattern recognition receptors (PRRs) (8), thus, it is possible that acidification underlies a daily activation of PRR signal cascades. In addition, induction of bacterial acid tolerance has been associated with cross-protection and attenuation of immune-related antimicrobial compounds (71, 72). Consequently, an understanding of the mechanisms of bacterial pH modulation in colonized tissues, whether by mutualists or by pathogens, is of critical importance to deciphering the molecular basis of the interaction.

Table 4-4

Calculations in support of COS delivery by hemocytes
Assumptions and measured quantities:

1. It takes approximately 7.5 mM acetate to acidify hemolymph to pH 5.5 (**Fig. 4-8*e***).
2. The theoretical yield of acetate is 3 molecules of acetate per molecule of GlcNAc.
3. Because COS are made of GlcNAc monomers, these calculations are done assuming GlcNAc is the form of COS.
4. The molecular weight of GlcNAc is 221 g/mol.
5. The crypt contents are approximately 20 µL and contain 10^3-10^4 hemocytes (52).
6. The density of GlcNAc is 1.5 g/cm^3.
7. The hemolymph is approximately pH 7 (34).

I. About how much COS would it take to acidify the light organ?
A. It takes ~7.5 mM acetate to acidify hemolymph from pH 7 to pH 5.5 (**Fig. 4-8*e***).
Assume that the volume acidified is approximately 20 µL hemolymph (vented volume, (52)), and that acetate is the major acidic component.

$7.5\text{x}10^{-3}$ mol acetate/L * $20\text{x}10^{-6}$ L = $1.5\text{x}10^{-7}$ mol acetate
$1.5\text{x}10^{-7}$ mol acetate * 1 mol COS/ 3 mol acetate = ~$5\text{x}10^{-8}$ mol COS/light organ
$5\text{x}10^{-8}$ mol COS/light organ * 221 g/mol = ~**11 µg COS/light organ**

Although the epithelial cells could take up acetate (pKa 4.76), 75% of the acetate will carry a negative charge when the nocturnal crypt pH is 5.5, suggesting that unless acetate uptake is an active process, the amount of protonated acetate lost from the crypt lumen by epithelial absorption will be small.

B. COS cannot be present at concentrations much greater than 2.5 mM at one time, because the co-colonization of Δ*nagB* and wild type is not biased towards wild type (**Figs. 5-7*de***).

2.5 mM COS is equivalent to 11 µg in a 20 µL crypt volume.

II. About how many hemocytes would it take to deliver this amount of COS?

If each hemocyte releases eight 1-µm diameter spherical granules of COS:

The volume of the chitin granule = ~$5\text{x}10^{-10}$ cm^3
1.5 g/cm^3 * $5\text{x}10^{-10}$ cm^3 = $7.5\text{x}10^{-10}$ g/granule * 8 granules/cell = ~$6\text{x}10^{-3}$ µg GlcNAc per cell

This means that the calculated 11 µg COS could be delivered by ~**2000 hemocytes**.

Previous quantification of hemocytes in crypt contents estimated at 10^3-10^4 hemocytes per light-organ crypt (52).

ACKNOWLEDGMENTS:

I thank S. Nyholm, K. Vetsigian, R. Welch, H. Blackwell, and J. Reed for contributive discussions, and Nell Bekiares and the Kewalo Marine Laboratory, University of Hawaii-Manoa for support during animal experiments. This work was funded by NIH grants RR12294/OD11024 to EGR and MM-N, and AI050661 to MM-N. JAS was funded by an NSF Graduate Research Fellowship, and the Chemical Biology Training Program (UW-Madison, NIH-NIGMS T32 GM008505), and the Microbes in Health and Disease Training Program (UW-Madison NIH-NIAID T32 AI055397).

REFERENCES:

1. McFall-Ngai M*, et al.* (2013) Animals in a bacterial world, a new imperative for the life sciences. *Proc Natl Acad Sci U S A* 110(9):3229-3236.

2. Schluter J & Foster KR (2012) The evolution of mutualism in gut microbiota via host epithelial selection. *PLoS Biol* 10(11):e1001424.

3. Hooper LV, Littman DR, & Macpherson AJ (2012) Interactions between the microbiota and the immune system. *Science* 336(6086):1268-1273.

4. Kereszt A, Mergaert P, Maróti G, & Kondorosi É (2011) Innate immunity effectors and virulence factors in symbiosis. *Curr Opin Microbiol* 14(1):76-81.

5. Axelrod R (1984) *The evolution of cooperation* (Basic Books, New York, NY).

6. Lee W-J & Hase K (2014) Gut microbiota-generated metabolites in animal health and disease. *Nat Chem Biol* 10(6):416-424.

7. Maynard CL, Elson CO, Hatton RD, & Weaver CT (2012) Reciprocal interactions of the intestinal microbiota and immune system. *Nature* 489(7415):231-241.

8. Gilbert SF (2014) A holobiont birth narrative: the epigenetic transmission of the human microbiome. *Front Genet* 5.

9. Chaston J & Goodrich-Blair H (2010) Common trends in mutualism revealed by model associations between invertebrates and bacteria. *FEMS Microbiol Rev* 34(1):41-58.

10. Nicholson JK*, et al.* (2012) Host-gut microbiota metabolic interactions. *Science* 336(6086):1262-1267.

11. Tremaroli V & Bäckhed F (2012) Functional interactions between the gut microbiota and host metabolism. *Nature* 489(7415):242-249.

12. Scheiermann C, Kunisaki Y, & Frenette PS (2013) Circadian control of the immune system. *Nat Rev Immunol* 13:190-198.

13. Keller M*, et al.* (2009) A circadian clock in macrophages controls inflammatory immune responses. *Proc Natl Acad Sci U S A* 106(50):21407-21412.

14. Mukherji A, Kobiita A, Ye T, & Chambon P (2013) Homeostasis in intestinal epithelium is orchestrated by the circadian clock and microbiota cues transduced by TLRs. *Cell* 153(4):812-827.

15. Mandel MJ (2010) Models and approaches to dissect host-symbiont specificity. *Trends Microbiol* 18(11):504-511.

16. McFall-Ngai MJ (2014) The Importance of Microbes in Animal Development: Lessons from the Squid-Vibrio Symbiosis. *Annu Rev Microbiol* 68(1).

17. Stabb EV & Visick KL (2013) *Vibrio fisheri*: Squid Symbiosis. *The prokaryotes*, (Springer, Berlin Heidelberg), pp 497-532.

18. McFall-Ngai M, Heath-Heckman EA, Gillette AA, Peyer SM, & Harvie EA (2012) The secret languages of coevolved symbioses: Insights from the *Euprymna scolopes*-*Vibrio fischeri* symbiosis. *Semin Immunol* 24:3-8.

19. Doino JA & McFall-Ngai M (1995) A transient exposure to symbiosis-competent bacteria induces light organ morphogenesis in the host squid. *Biol Bull* (189):347-355.

20. Koch EJ, Miyashiro TI, McFall-Ngai MJ, & Ruby EG (2013) Features governing symbiont persistence in the squid-vibrio association. *Mol Ecol* (doi:10.1111/mec.12474).

21. Kremer N*, et al.* (2013) Initial symbiont contact orchestrates host-organ-wide transcriptional changes that prime tissue colonization. *Cell Host Microbe* 14(2):183-194.

22. Heath-Heckman EA & McFall-Ngai MJ (2011) The occurrence of chitin in the hemocytes of invertebrates. *Zoology* 114(4):191-198.

23. Graf J & Ruby EG (1998) Host-derived amino acids support the proliferation of symbiotic bacteria. *Proc Natl Acad Sci U S A* 95(4):1818-1822.

24. Wier AM*, et al.* (2010) Transcriptional patterns in both host and bacterium underlie a daily rhythm of anatomical and metabolic change in a beneficial symbiosis. *Proc Natl Acad Sci U S A* 107(5):2259-2264.

25. Meibom KL*, et al.* (2004) The *Vibrio cholerae* chitin utilization program. *Proc Natl Acad Sci U S A* 101(8):2524-2529.

26. Killiny N & Almeida RP (2009) Host structural carbohydrate induces vector transmission of a bacterial plant pathogen. *Proc Natl Acad Sci U S A* 106(52):22416-22420.

27. Koropatkin NM, Cameron EA, & Martens EC (2012) How glycan metabolism shapes the human gut microbiota. *Nat Rev Microbiol* 10(5):323-335.

28. Ng KM*, et al.* (2013) Microbiota-liberated host sugars facilitate post-antibiotic expansion of enteric pathogens. *Nature* 502(7469):96-99.

29. Kashyap PC*, et al.* (2013) Genetically dictated change in host mucus carbohydrate landscape exerts a diet-dependent effect on the gut microbiota. *Proc Natl Acad Sci U S A* 110(42):17059-17064.

30. Heath-Heckman EA*, et al.* (2013) Bacterial bioluminescence regulates expression of a host cryptochrome gene in the squid-vibrio symbiosis. *mBio* 4(2).

31. Lee KH & Ruby EG (1994) Effect of the squid host on the abundance and distribution of symbiotic *Vibrio fischeri* in nature. *Appl Environ Microbiol* 60(5):1565-1571.

32. Dunn AK (2012) *Vibrio fischeri* metabolism: symbiosis and beyond. *Adv Microb Physiol* 61:37.

33. Boettcher K, Ruby E, & McFall-Ngai M (1996) Bioluminescence in the symbiotic squid *Euprymna scolopes* is controlled by a daily biological rhythm. *J Comp Physiol* 179(1):65-73.

34. Kremer N*, et al.* (2014) The dual nature of haemocyanin in the establishment and persistence of the squid–Vibrio symbiosis. *Proc. R. Soc. B* 281(1785).

35. Boettcher KJ & Ruby EG (1990) Depressed light emission by symbiotic *Vibrio fischeri* of the sepiolid squid *Euprymna scolopes*. *J Bacteriol* 172(7):3701-3706.

36. Mandel MJ, Stabb EV, & Ruby EG (2008) Comparative genomics-based investigation of resequencing targets in *Vibrio fischeri*: focus on point miscalls and artefactual expansions. *BMC Genomics* 9:138.

37. Stabb EV, Butler MS, & Adin DM (2004) Correlation between osmolarity and luminescence of symbiotic *Vibrio fischeri* strain ES114. *J Bacteriol* 186(9):2906-2908.

38. Graf J, Dunlap PV, & Ruby EG (1994) Effect of transposon-induced motility mutations on colonization of the host light organ by *Vibrio fischeri*. *J Bacteriol* 176(22):6986-6991.

39. Sambrook J, Fritsch EF, & Maniatis T (1989) *Molecular Cloning* (Cold Spring Harbor Laboratory Press New York).

40. Miller JH (1972) *Experiments in molecular genetics* (Cold Spring Harbor Laboratory, Cold Spring Harbor, NY).

41. Lynn M N & Mark J M (2012) Colonization of *Euprymna scolopes* Squid by *Vibrio fischeri*. *J Vis Exp* (61).

42. Ruby EG & Nealson KH (1976) Symbiotic association of *Photobacterium fischeri* with the marine luminous fish *Monocentris japonica*; a model of symbiosis based on bacterial studies. *Biol Bull* 151(3):574-586.

43. Miyashiro T, Wollenberg MS, Cao X, Oehlert D, & Ruby EG (2010) A single *qrr* gene is necessary and sufficient for LuxO-mediated regulation in *Vibrio fischeri*. *Mol Microbiol* 77(6):1556-1567.

44. Miyashiro T*, et al.* (2011) The *N*-acetyl-d-glucosamine repressor NagC of *Vibrio fischeri* facilitates colonization of *Euprymna scolopes*. *Mol Microbiol* 82(4):894-903.

45. Reichelt JL & Baumann P (1973) Taxonomy of the marine, luminous bacteria. *Arch Mikrobiol* 94(4):283-330.

46. Stabb EV & Ruby EG (2002) RP4-based plasmids for conjugation between *Escherichia coli* and members of the vibrionaceae. *Methods Enzymol* 358:413-426.

47. Bao Y, Lies DP, Fu H, & Roberts GP (1991) An improved Tn7-based system for the single-copy insertion of cloned genes into chromosomes of gram-negative bacteria. *Gene* 109(1):167-168.

48. McCann J, Stabb EV, Millikan DS, & Ruby EG (2003) Population dynamics of *Vibrio fischeri* during infection of *Euprymna scolopes*. *Appl Environ Microbiol* 69(10):5928-5934.

49. Troll JV*, et al.* (2009) Peptidoglycan induces loss of a nuclear peptidoglycan recognition protein during host tissue development in a beneficial animal-bacterial symbiosis. *Cell Microbiol* 11(7):1114-1127.

50. Nyholm SV, Stewart JJ, Ruby EG, & McFall-Ngai MJ (2009) Recognition between symbiotic *Vibrio fischeri* and the haemocytes of *Euprymna scolopes*. *Environ Microbiol* 11(2):483-493.

51. Altura MA*, et al.* (2013) The first engagement of partners in the *Euprymna scolopes–Vibrio fischeri* symbiosis is a two-step process initiated by a few environmental symbiont cells. *Environ Microbiol* 15(11):2937-2950.

52. Nyholm SV & McFall-Ngai MJ (1998) Sampling the light-organ microenvironment of *Euprymna scolopes*: description of a population of host cells in association with the bacterial symbiont *Vibrio fischeri*. *Biol Bull* 195(2):89-97.

53. Sheehan DC & Hrapchak BB (1980) *Theory and practice of histotechnology* (Mosby St Louis, MO).

54. Bustin SA*, et al.* (2009) The MIQE guidelines: minimum information for publication of quantitative real-time PCR experiments. *Clin Chem* 55(4):611-622.

55. McCann J, Stabb EV, Millikan DS, & Ruby EG (2003) Population dynamics of *Vibrio fischeri* during infection of *Euprymna scolopes*. *Appl Environ Microbiol* 69(10):5928-5934.

56. Adin DM, Visick KL, & Stabb EV (2008) Identification of a cellobiose utilization gene cluster with cryptic B-galactosidase activity in *Vibrio fischeri*. *Appl Environ Microbiol* 74(13):4059-4069.

57. Merrell SD & Camilli A (1999) The *cadA* gene of *Vibrio cholerae* is induced during infection and plays a role in acid tolerance. *Mol Microbiol* 34(4):836-849.

58. Anonymous (2010) M9 minimal medium (standard). *Cold Spring Harbor Protocols* 2010(8):pdb.rec12295.

59. Koropatnick TA, Kimbell JR, & McFall-Ngai MJ (2007) Responses of host hemocytes during the initiation of the squid-Vibrio symbiosis. *Biol Bull* 212(1):29-39.

60. Renkema GH*, et al.* (1997) Synthesis, sorting, and processing into distinct isoforms of human macrophage chitotriosidase. *European J Biochem* 244(2):279-285.

61. Collins AJ, Schleicher TR, Rader BA, & Nyholm SV (2012) Understanding the role of host hemocytes in a squid/vibrio symbiosis using transcriptomics and proteomics. *Front Immunol* 3.

62. Bernheim NJ & Dobrogosz WJ (1970) Amino sugar sensitivity in *Escherichia coli* mutants unable to grow on *N*-acetylglucosamine. *J Bacteriol* 101(2):384-391.

63. Wolfe AJ (2005) The acetate switch. *Microbiol Mol Biol Rev* 69(1):12-50.

64. Krulwich TA, Sachs G, & Padan E (2011) Molecular aspects of bacterial pH sensing and homeostasis. *Nat Rev Microbiol* 9(5):330-343.

65. Flint HJ, Scott KP, Louis P, & Duncan SH (2012) The role of the gut microbiota in nutrition and health. *Nat Rev Gastroenteroland Hepatol* 9(10):577-589.

66. Guo L, He X, & Shi W (2014) Intercellular communications in multispecies oral microbial communities. *Front Microbiol* 5.

67. Wolf KJ*, et al.* (2014) Consumption of acidic water alters the gut microbiome and decreases the risk of diabetes in NOD mice. *J Histochem Cytochem* 62(4):237-250.

68. Rader BA, Kremer N, Apicella MA, Goldman WE, & McFall-Ngai MJ (2012) Modulation of symbiont lipid A signaling by host alkaline phosphatases in the squid-vibrio symbiosis. *mBio* 3(3).

69. Royet J, Gupta D, & Dziarski R (2011) Peptidoglycan recognition proteins: modulators of the microbiome and inflammation. *Nat Rev Immunol* 11(12):837-851.

70. Bates JM, Akerlund J, Mittge E, & Guillemin K (2007) Intestinal alkaline phosphatase detoxifies lipopolysaccharide and prevents inflammation in zebrafish in response to the gut microbiota. *Cell Host Microbe* 2(6):371-382.

71. Lardner A (2001) The effects of extracellular pH on immune function. *J Leukoc Biol* 69(4):522-530.

72. Foster JW (1999) When protons attack: microbial strategies of acid adaptation. *Curr Opin Microbiol* 2(2):170-174.

Chapter 5

A single host-derived glycan impacts key regulatory nodes of symbiont metabolism in a co-evolved mutualism

PREFACE:

A version of this manuscript is in submission at *MBio* as:

Pan M*, Schwartzman JA*, Dunn AK, Lu Z, and Ruby EG. "A single host-derived glycan impacts key regulatory nodes of symbiont metabolism in a co-evolved mutualism."

*These authors contributed equally.

JAS, MP and EGR formulated ideas and planned the experiments within this chapter. JAS and MP performed the experiments described in the chapter. AKD helped design experiments involving the cytochrome oxidase mutants, and provided related strains. JAS wrote the chapter, with editing from EGR (exclusive of the introduction).

ABSTRACT:

Most animal-microbe mutualisms are characterized by nutrient exchange between the partners. When the host provides the nutrients, it can gain the capacity to shape its microbial community, control the stability of the interaction, and promote its health and fitness. Using the bioluminescent squid-vibrio model I demonstrate how a single host-derived glycan, chitin, regulates the metabolism of *Vibrio fischeri* at key points in the development and maintenance of the symbiosis. I first characterized the pathways for catabolism of chitin-derived sugars by *V. fischeri*, demonstrating that the *crr*-dependent phosphoenolpyruvate-pyruvate phosphotransferase system (PTS) prioritizes transport of these sugars in *V. fischeri* by blocking the uptake of non-PTS carbohydrates, such as glycerol. Next, I found that PTS transport of chitin sugars into the bacterium shifted acetate homeostasis towards a net excretion of acetate, and was sufficient to override an activation of the acetate switch by AinS-dependent quorum sensing. Finally, I showed that catabolism of chitin sugars decreases the rate of cell-specific oxygen consumption. Collectively, these three metabolic functions define a physiological shift that favors fermentative growth on chitin sugars, and may support optimal symbiont bioluminescence, the functional basis of the squid-vibrio mutualism.

INTRODUCTION:

Metabolic coordination between partners is a central factor in the establishment and maintenance of beneficial symbiotic associations (1-3). Well-known examples of metabolic coordination are found in endosymbiotic associations, common among insects, in which the combined metabolic activity of host and microbe compensate for nutritional deficiencies of both partners (4). Host-derived nutrition also structures surface-associated microbial communities. For example, milk oligosaccharides (5), and later, mucin-derived oligosaccharides (6), shape the composition of the mammalian gut microbiota. Vertebrate microbiota are complex, and variable, which complicates the elucidation of the effect of host-derived nutrition on the physiology of any one microbial constituent. Natural, yet less complex, microbial communities are maintained by invertebrate hosts such as the honeybee (7), the medicinal leech (8), or bobtail squid (9). Thus, invertebrates present tractable animal models to elucidate the core principles by which host-derived nutrition impacts symbiont metabolism and physiology.

The squid, *Euprymna scolopes*, maintains a monospecific population of the Gram-negative marine microbe *Vibrio fischeri* (10). *V. fischeri* colonizes epithelium-lined crypt spaces in the squid's light-emitting organ: a structure anatomically designed to use bacteria-produced bioluminescence during the host's nocturnal activities (1). Each newly hatched squid must obtain an inoculum of *V. fischeri* from the ambient seawater; these bacteria quickly proliferate in the crypts, where the symbiont population reaches a high density, and luminescence is induced by quorum signaling (11). Bioluminescence is essential for symbiosis, as strains of *V. fischeri* that have lost the ability to produce light fail to persist in

this association (12, 13). Because the symbionts provide only bioluminescence, and not any known nutrient, this binary model is ideal for studying the role of the host in driving the association's underlying metabolism (14).

Chitin, a polymeric glycan of *N*-acetylglucosamine, and its derivatives, are common host-derived nutrients and signal factors in diverse plant and animal symbioses (15-18). Chitin-like oligosaccharides are also the most abundant source of nitrogen in marine surface waters (19). As the major structural component of many invertebrates, chitin is also a potential nutrient for microbial symbionts. Moreover, the ability to degrade and metabolize chitin is widespread within the *Vibrionaceae* (20), and other marine bacteria. The principle chitin breakdown products are the disaccharide chitobiose $(GlcNAc)_2$, and the monosaccharide *N*-acetylglucosamine (GlcNAc). In *Vibrio cholerae* and *Vibrio furnisii*, the chitobiose is assimilated by ABC-type transporter, while the monosaccharide GlcNAc is transported by the phosphoenolpyruvate-pyruvate phosphotransferase system (PTS) (21, 22). The PTS transport of GlcNAc contributes to catabolite repression of natural transformation in *V. cholerae* (23). PTS transport also regulates biofilm formation, and colonization of the germfree mouse intestine by *V. cholerae* (24). Thus, PTS sugars represent an important class of regulating host-derived nutrient in the context of Vibrio physiology.

In the mutualism between *E. scolopes* and *V. fischeri*, chitin-derived sugars play several roles. First, a concentration gradient of host-derived chitobiose facilitates the establishment of symbiosis by guiding motile *V. fischeri* cells into the juvenile's nascent light organ (15, 25). Second, the symbionts initially colonize crypts free of chitin sugars: inducing chitin catabolism-dependent transcription destabilizes the population (26). Finally, after the

host matures, chitin sugars are provided as a nutrient for the symbionts, but only at night (27). The catabolism of these sugars by *V. fischeri* supports the bacteria's nocturnal bioluminescence by acidifying the crypts and liberating oxygen: a substrate of bacterial luciferase (27, 28).

The physiology of *V. fischeri* during growth on chitin sugars lead to predictions regarding the potential nodes at which host-derived chitin sugars might regulate symbiont catabolism. Chitin sugar catabolism is highly acidogenic, and yields acetate (27). The excretion of acetate is reversed under certain physiological conditions, such as occur in the in the immature light organ (29). This alternation between excretion and uptake is called the 'acetate switch', and results from the activity of acetyl-CoA synthase (encoded by the *acs* gene) (30), whose transcription is regulated by the AinSR quorum signaling circuit (29). Thus, provision of chitin sugars by the host might represent a counterbalance to the AinSR-regulated acetate switch. In addition, the correlation between chitin sugar acidification and oxygen suggests that, in the context of symbiosis, this host-derived nutrient might participate in defining a balance between the oxygen-consuming activities of luciferase and cytochrome oxidases. In this present work, I show how chitin sugar catabolism shifts the symbiont's metabolic state during the immature association by: (i) defining the pathways of chitin sugar transport in *V. fischeri*, (ii) describing the physiological consequences of chitin sugar catabolism on acetate switch and respiratory oxygen consumption, and (iii) examining the contribution of chitin sugar-driven acetate homeostasis to the colonization of the immature light organ.

MATERIALS AND METHODS:

Bacterial strains and growth conditions. Strains and plasmids used in this work are listed in **Table 5-1**. *V. fischeri* strains are derived from MJM1100 (31, 32). Unless otherwise noted, cultures were grown at 28° C, with shaking at 225 rpm, in 17 x 100-mm test tubes containing 3 mL of either a seawater-tryptone medium (SWT) (31), a high-osmolarity SWT (SWTO) (33), or Luria-Bertani salt medium (LBS) (34), as noted. *Escherichia coli* strains were grown in Luria-Bertani (LB) medium (35), containing 1.5% agar for solid media. When appropriate, antibiotics were added to LB and LBS media at the following concentrations: chloramphenicol (Cam), 5 μg/ml for *V. fischeri* and 25 μg/ml for *E. coli*; erythromycin (Erm), 5 μg/ml for *V. fischeri*; kanamycin (Kan) 100 μg/ml for *V. fischeri*. Medium reagents were purchased from ThermoFisher Scientific (Waltham, MA, USA) and Sigma Aldrich (St. Louis, MO, USA).

Molecular techniques. Plasmids were constructed using standard restriction digest and ligation methods (35). Restriction enzymes were obtained from New England BioLabs (Ipswich, MA, USA). Constructs were introduced *V. fischeri* with conjugative helper strain CC18 λ-pir (36). To construct unmarked deletion mutants in *V. fischeri*, a chimera of ~1kb DNA segments flanking a gene of interest and conjoined by a single restriction site was cloned the pKV363 vector, and homologous recombination was selected for as previously described (36-38). The region around the chromosomal lesion was sequenced to ensure that no secondary mutations had been introduced at the locus. To construct complementation plasmids, the region of DNA spanning 400 bp upstream and 200 bp downstream of the

annotated translational start codon was cloned into multiple cloning site of pEVS107 (39), or pVSV105 (40). The complementation vector was then introduced into *V. fischeri* by conjugation. The presence of the complementation construct was confirmed by PCR. LacZ transcriptional reporter constructs were constructed by cloning a region 500 bp upstream and 100 bp downstream of the annotated translational start codon into plasmid pAKD701. To test the activity of the reporter constructs, β-galactosidase activity was assessed relative to strains carrying the blank vector in 1 mL of a 3 mL LBS overnight culture.

Growth-yield measurement. To assess growth on a sole source of carbon, strains were cultivated in Minimal Salts Medium (MSM) (41), modified as described previously (26), for 24 h. The medium was buffered at pH 7.5 with 50 mM PIPES disodium salt, and contained 20 mM additions of di-N-acetyl chitobiose (Cayman Chemicals), *N*-acetyl *D*-glucosamine, glucosamine, *N*-acetyl neuraminic acid, fructose, glucose, and glycerol. Strains were first grown as LBS cultures, and then sub-cultured 1:100 into 0.2% Casamino Acids MSM, and grown to an optical density (OD_{600} nm, 1 cm path length), of 0.40 ± 0.05 absorbance units. These cultures were used to inoculate MSM supplemented with a single carbon source 1:100. Optical density was obtained after 36 h of growth.

Glycerol uptake assay. To monitor the uptake of glycerol from culture media, cells were grown in medium with a defined amount of glycerol, and the amount of glycerol was monitored over time using the Glycerol Colorimetric Assay Kit, according to the manufacturer's specifications (Cayman Chemical #10010755). To collect samples for

glycerol detection, 3 mL LBS overnight cultures were sub-cultured 1:100 into SWTO medium (which contains 3.8 g/L glycerol), and grown to an OD_{600} nm of 0.5 +/- 0.1. Duplicate 1 mL aliquots of culture were washed twice in SWTO medium without glycerol. One set of samples was resuspended in 2 mL of SWTO made with 19 mg/L glycerol (SWTO low glycerol), and the other set was resuspended in 2 mL of 20 mM GlcNAc SWTO low glycerol medium. 0.5 mL samples of culture were collected 0,1, and 2 h post-inoculation, and pelleted 15 min at 1300 rpm and 4 °C in a refrigerated tabletop microcentrifuge.

Acetate-detection assay. Cell-free culture supernatant was collected by centrifuging 1 ml samples for 15 min at 13,000 rpm and 4 ºC, and removing the top 800 µl. These samples were stored at -20 prior to assay. Acetate concentration was determined by a coupled enzyme assay (Sigma, MAK086), using the protocol recommended by the manufacturer. Briefly, the assay measures the accumulation of a colorimetric product (450nm optimal absorbance), that is proportional to the acetate present. I read the absorbance at 420 nm A_{420} using a GENiosPro 96-well plate reader (TECAN, Research Triangle Park, NC), and calculated the amount of acetate present in each sample relative to a calibration curve generated from a standard of known acetate concentration.

β-galactosidase assay. The β-galactosidase activity assays were preformed as described previously (29). Briefly, cells were grown overnight in LBS medium with antibiotic, and then sub-cultured (1:200) in duplicate tubes of SWTO medium. To collect samples, 1 mL of culture was pelleted for 15 min at 1300 rpm and 4 °C in a refrigerated tabletop

microcentrifuge. Supernatant was decanted, and cell pellets stored at -20 °C. β-galactosidase activity was determined using a microtiter-dish method modified from Slauch and Silhavy (42). Briefly, the SDS/chloroform step was omitted, and the A_{420} values of the microtiter wells were read every 30 s for 1 h using a GENiosPro 96-well plate reader (TECAN, Research Triangle Park, NC). Three replicates of two dilutions were tested for each cell pellet. The relative units of β-galactosidase activity were calculated using the formula: rate [V_{max}] / ([OD] x volume (43)). Blank vector controls revealed no non-specific β-galactosidase activity in any condition tested.

Contribution of glycerol to target promoter activity. Strains carrying either the P_{glpFK} *lacZ* transcriptional reporter plasmid pJAS223, or the empty parent vector (pADK701), were cultured in SWTO to an optical density at 600 nm (OD) of 0.5 +/- 0.1 (equivalent to 10^7 colony-forming units per mL), then sub-cultured once more after dilution (1:100) into fresh SWTO made either with no glycerol, or with 3.8 g/L glycerol. Cultures were incubated for 2 h under these experimental conditions prior to sample collection.

Contribution of COS to target promoter activity. Duplicate cultures of the *lacZ* transcriptional reporters pJAS223 (P_{glpFK}), pJAS224 (P_{acs}), or a blank parent vector (pAKD701), were grown to an OD of 0.5 +/- 0.1. At this time, 30 mM GlcNAc was added to one of the two sets of cultures. Cells were then incubated 1 h prior to sample collection.

Contribution of COS and C8-HSL quorum sensing to target promoter activity. Cultures of either the P_{acs} LacZ transcriptional reporter plasmid, pJAS224, or a blank parent vector (pAKD701), were grown to an OD of 0.5 +/- 0.1. Each culture was then diluted (1:100) into four tubes of SWTO medium, each containing separate additions: (i) 40 mM GlcNAc, (ii) 100 nM C8 homoserine lactone (C8 HSL), diluted from a stock in DMSO, (iii) GlcNAc and C8 HSL, or (iv) no addition. The cultures were incubated for 2 h prior to sample collection.

Growth curve assays. Cells were grown in LBS medium to an OD of 0.5 +/- 0.1, and then diluted to an OD of 0.02 in fresh experimental medium. Depending on the experimental condition, cells were diluted into 0.1X LBS (1/10 the concentration of yeast and tryptone, and the normal concentration of salts and buffer), or MSM buffered at pH 7.5 with PIPES. Where indicated, cultures were supplemented with 20 mM of either glucose, GlcNAc or NANA. To monitor growth in test tubes or flasks, either 3 mL cultures were placed in a 17 x 100 mm test tube, or 10 mL cultures were added to a 125 mL flask, which were incubated at 28° C, with agitation at 225 rpm in an Innova 4080 shaker (New Brunswick, CT, USA), and the OD was measured using a Biophotometer (WPA CO 8000 Cell Density Meter, biochrom, UK), at 600 nm. Where indicated, samples of the cultures were plated for enumeration of colony forming units by serial dilution in 70% Instant Ocean (United Pet Group, Blacksburg, VA), and plated onto LBS agar. To monitor growth in 1 mL of medium in 24-well plates, absorbance at 600 nm was monitored using a GENiosPro 24-well plate reader (TECAN, Research Triangle Park, NC). The plates were shaken continuously, and absorbance readings were corrected for a non-standard path length by a linear transformation. Each test was done in triplicates.

Cell-size determination. Wild-type and Δ*cco V. fischerI was* cultured in 3 mL LBS overnight, then sub-cultured by a 1:100 dilution into fresh LBS medium, and grown to an OD of 0.5 +/- 0.1, to obtain a homogenous population of cells growing in steady state. The cells were sub-cultured again into LBS, containing either 20 mM GlcNAc, 20 mM glucose, or no addition. As the cultures grew, 5-µL aliquots were spotted onto a glass slide, and visualized with an Axio Imager.M2 epifluorescence scope (Zeiss Intnl., Germany). The cell length was measured at 100X magnification using Axio Vision 4.8 software (Zeiss). Three replicates, each consisting of 40 cell-length measurements, were collected for the strains under each growth condition.

Respirometry. Cultures growing in LBS in steady state (OD = 0.5 +/- 0.1), were sub-cultured (1:100) into 3 mL of either LBS or 40 mM GlcNAc MSM buffered at pH 7.5 with 50 mM PIPES, in an 18-mm test tube. Two milliliters of this culture were transferred to a respirometry vial, and the oxygen concentration and OD were measured over time, using an oxygen probe (Oxygen Microsensor, Unisense, Denmark), and a Biophotometer (WPA CO 8000 Cell Density Meter, biochrom, UK), respectively. Three biological replicates were tested for each condition. The rate of oxygen consumption was calculated by the following formula: $\Delta O_2(t_0\text{-}t_n)/\Delta OD(t_n\text{-}t_0)$.

Squid colonization assays. *V. fischeri* strains were cultivated as overnight cultures in 3 mL LBS, containing antibiotic selection as appropriate. Strains were sub-cultured (1:100) into

SWT medium, and grown to an OD of 0.5 +/- 0.1 (equivalent to 10^7 colony-forming units per mL), for use as seawater inocula. To colonize squid, newly hatched animals were exposed for 16 h to 3000 CFU/mL of *V. fischeri* in filter-sterilized Instant Ocean (FSW). The relative ability of *V. fischeri* strains to colonize was determined by creating mixed inocula of wild-type *V. fischeri* (carrying GFP and Erm-resistance genes at the Tn*7* site; TIM302), and the appropriate mutant strain carrying only the Erm resistance at the Tn*7* site. A separate co-colonization of TIM302 and wild-type *V. fischeri* carrying only Erm^R (TIM313) was included to control for carriage of GFP. To control for the possibility of a secondary-site mutation, TIM302 was also competed against a complemented strain carrying the gene and its native promoter region *in cis* at the Tn*7* site of the mutant strain. All animals were transferred to fresh, uninoculated FSW at 16 h, and again at approximately 40 h, after inoculation. To compete strains in the presence of COS, the FSW was supplemented with 20 mM GlcNAc following the 16 h initial inoculation, and the water was subsequently exchanged for fresh 20 mM GlcNAc/FSW at least every 12 h. At 48 h post-inoculation, individual animal bioluminescence was determined using a TD 20/20 luminometer (Turner Design, Sunnyvale, CA, USA), and the animals were frozen to surface sterilize. Animals were homogenized and the homogenate was plated to determine the CFU/light organ. Uninoculated animals had no detectible bioluminescence or CFUs in all experiments.

Growth competition in culture. Wild-type *V. fischeri*, containing a chromosomal copy of GFP in the Tn*7* site (39, 44), was co-inoculated with one of several mutant strains, or a wild-type marker control carrying only the Erm resistance at the Tn*7* site. For each pairing of

strains, growth competition was determined in 0.1X SWTO (1/10 the concentration of yeast, tryptone and glycerol with the normal concentration of salts and buffer, containing 50 mM Tris-HCl, pH 7.5) either with or without the addition of 10 mM GlcNAc. The resulting cultures were incubated in a 24-well polystyrene plate at 28 ºC, with continuous shaking in a GENioPro plate reader (TECAN, Research Triangle Park, NC). A 0 and 3 h of incubation, 50 μL of cultures were removed from the test plate, serially diluted, and plated to determine the CFU of both the strains in the culture. The relative competitive index of the two strains was calculated by dividing the ratio of the two strains at 3 h by the ratio at 0 h.

Statistics. Statistical analyses were performed with the GraphPad Prism software package (Version 5.0, 2010). Data sets were assessed for normal distribution using the D'Agostino and Pearson omnibus test (45). Normally distributed β-galactosidase and growth yield data were tested for significant variation among experimental groups by two-factor analysis of variance (ANOVA) and post-hoc Bonferroni T-testing. As noted, data that failed to fit a normal distribution were assessed by the Kruskal-Wallis test with Post-Hoc Dunn's multiple comparisons to identify groups of statistically equivalent means. Competitive indexes (C.I.) for squid co-colonization assays were calculated by dividing the ratio of mutant to wild-type colonies enumerated from squid with the initial ratio of the two competing strains present in the seawater during inoculation, and log-transforming this corrected ratio. The C.I., was assessed for normal distribution, and then compared by one-sample T-test to an expected mean distribution of 1, or by two-factor ANOVA to assess the contribution of strain and the addition of chitin sugars.

Table 5-1. Strains and plasmids used in this study.

Strain or plasmid	Description	Source
V. fischeri		
ES114	Wild-type *E. scolopes* light-organ isolate	(31)
MB21124	*acs::*Tn*erm*	(29)
TIM302	*Tn7::gfp* Em^r in ES114	(44)
TIM313	ES114 Tn*7*::pEVS107 Em^r in ES114	(44)
AKD787	Δ*cco* in ES114	(46)
Δ*aceA*	Δ*aceA* (VF_1972)	E. Stabb
JAS200	Δ*nagE1* in ES114	This work
JAS201	Δ*nagE2* in ES114	This work
JAS202	Δ*crr* in ES114	This work
JAS212	Δ*crr* Tn*7*::pJAS212 Em^r in ES114	This work
JAS213	Δ*crr* Tn*7*::pEVS107 Em^r in ES114	This work
JAS215	Δ*nagE1*Δ*nagE2* in ES114	This work
E. coli		
DH5a-λpir	F^- φ80*lacZ*Δ*M15* Δ(*lacZYFargF*)U169 *supE44 deoR hsdR17 recA1 endA1 gyrA96 thi-1 relA1*, lysogenized with λ*pir*	(47)
β-3914	F^- RP4-2-Tc::Mu Δ*dapA*::(*erm-pir*) (Kmr Emr)*gyrA462 zei-298*::Tn*10* (Km^r Em^r Tc^r)	(37)
Plasmids		
pVSV105	Vector for *in trans* complementation. R6K ori Cm^r, *lacZ*α-(SphI, SalI/HincII, XbaI, SmaI/XmaI, KpnI, SacI)	(40)
pEVS104	Vector for *in cis* complementation. R6Kori RP4 *oriT trb tra* Kn^r	(36)
pKV363	Mobilizable suicide vector; Cm^r; pSW7848 + multiple cloning site sequences	(38)
pUX-BF13	R6Kori *tns bla* Amp^r	(48)
pEVS107	R6Kori *oriT mini*-Tn*7 mob* Em^r Kn^r	(39)
pAKD701	Vector containing promoterless *lacZ* gene for construction of ß-galactosidase transcriptional reporters Kan^r	(49)
pJAS200	Δ*nagE1::*pKV363	This work
pJAS201	Δ*nagE2::*pKV363	This work
pJAS202	Δ*crr::*pKV363	This work
pJAS224	*acs'-lacZ*$^+$ in pADK701,	This work
pJAS223	*glpFK'-lacZ*$^+$ in pADK701	This work
pJAS212	*crr*::pVSV105	This work
pJAS230	*acs:*:pVSV105	This work
pJAS231	*nagE1*::pVSV105	This work

RESULTS

The EIIA^{crr}–dependent PTS system prioritizes transport of monomeric and dimeric chitin sugars. During PTS transport, the enzyme II complex complete the phosphotransfer chain that pulls phosphoryl groups from glycolytic intermediate phosphoenolpyruvate to support sugar uptake (50). Enzyme II contains transmembrane B and C domains, and a kinase domain. A subset of PTS enzyme II complexes lack an A domain, and instead rely on the cytoplasmic phosphotransferase Crr (referred to subsequently as EIIA^{crr}). Glucose, sucrose, trehalose, and *N*-acetylglucosamine have been identified as EIIA^{crr}-dependent PTS sugars in *V. cholerae* (24). I identified two homologs of the putative GlcNAc EIIBC transporter NagE (*nagE1,* VF_0808; and *nagE2,* VF_A0438), and one homolog of EIIA^{crr} (*crr*, VF_1897). I constructed strains carrying individual deletions of *crr, nagE1* and *nagE2*, and a double mutant (*nagE1/2)*. I evaluated the ability of these mutants to grow on a minimal medium containing a selection of single carbon sources (**Fig. 5-1*A***). Like *V. cholerae*, growth of the *V. fischeri* Δ*crr* mutant was impaired on glucose and *N*-acetylglucosamine. Surprisingly, I also observed that the mutant was unable to grow on chitobiose or glucosamine (GlcN) as a sole carbon source. The Δ*crr* mutant grew comparably to wild type on *N*-acetylneuraminic acid (NANA), an amino sugar not derived from chitin. Collectively, these observations indicate that, unlike *V. cholerae* and *V. furnisii* (22, 24), the catabolism of all breakdown products of chitin, including the dimer chitobiose, and the monomers GlcNAc and GlcN, rely upon transport by the Crr-dependent PTS. Thus, I used GlcNAc as a representative chitin sugar in subsequent experiments.

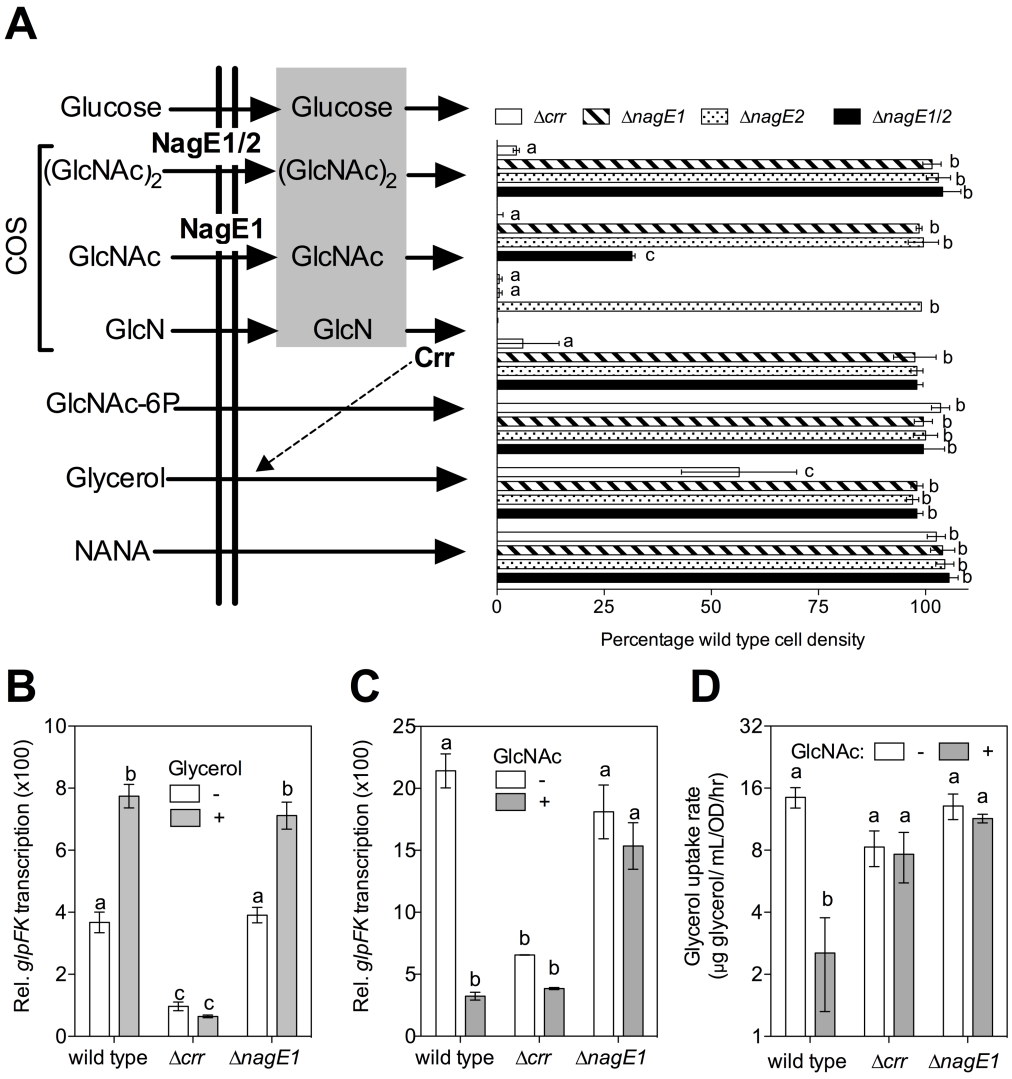
A
Glucose
Glucose
NagE1/2
(GlcNAc)2
(GlcNAc)2
COS
NagE1
GlcNAc
GlcNAc
GlcN
GlcN
Crr
GlcNAc-6P
Glycerol
NANA
Δcrr
ΔnagE1
ΔnagE2
ΔnagE1/2
0
25
50
75
100
Percentage wild type cell density
B
Rel. glpFK transcription (x100)
Glycerol
-
+
wild type
Δcrr
ΔnagE1
C
Rel. glpFK transcription (x100)
GlcNAc
-
+
wild type
Δcrr
ΔnagE1
D
Glycerol uptake rate
(μg glycerol/ mL/OD/hr)
GlcNAc:
-
+
wild type
Δcrr
ΔnagE1

Figure 5-1. Prioritization of carbohydrate catabolism in *V. fischeri*. (*A*) The effect of deletions of genes encoding PTS proteins (NagE1, NagE2, Crr) on growth yield with chitin sugars, amino sugars, or non-PTS carbohydrates as substrates. Percent cell yield (culture optical density, OD_{600nm}), relative to wild type, calculated following 24-h growth in a minimal medium containing 30 mM of one of seven sole-carbon sources (n=2): $(GlcNAc)_2$, chitobiose; GlcNAc, *N*-acetylglucosamine; GlcN, glucosamine; NANA, *N*-acetylneuraminic acid. (*B*-*C*) Relative promoter activity for the *glpF-K* locus during growth in a tryptone-based medium in the absence and presence of: (*B*) glycerol, or (C) GlcNAc (n=2, representative of two independent experiments). (*D*) Effect of GlcNAc addition on the rate of glycerol consumption by *V. fischeri* wild-type and mutant strains (n=3). 'a', 'b' and 'c' indicate statistically different mean values, determined by Two-Way ANOVA with Post-Hoc Bonferroni T-tests. Error bars indicate standard error.

Notably, the function of the two annotated GlcNAc-specific EIIBC transporters, *nagE1* and *nagE2,* was more complex. First, growth on GlcNAc required *nagE1*, but not *nagE2*. Second, while individual mutation of either of these two genes did not impact growth on chitobiose, deletion of both putative transporters reduced the growth yield by 50%. Third, neither *nagE* paralog was required for growth on GlcN (**Fig. 5-1*A***). Collectively, these data reveal both specificity and promiscuity among the chitin-sugar-associated EIIBC transporters: GlcNAc is specifically associated with the NagE1 transporter, while chitobiose may be transported by both NagE1 and NagE2.

I also observed that the growth of the *crr* mutant was impaired on glycerol: a 3-carbon carbohydrate not predicted to require PTS transport for catabolism (**Fig. 5-1*A***). The *Escherichia coli* $EIIA^{crr}$ homolog activates the transport of glycerol, and other non-PTS carbohydrates, through a mechanism called inducer exclusion (50). During inducer exclusion, the $EIIA^{crr}$-dependent transport of a PTS sugar blocks the transport of a subset of non-PTS carbohydrates, such as glycerol. These carbon sources all require their phosphorylated, intracellular form to induce transcription factors that regulate catabolism. In *E. coli,* glycerol catabolism genes *glpF* and *glpK* are targets of inducer exclusion (50). Because *glpK* is required for catabolism of glycerol by *V. fischeri* (51), I reasoned that the *V. fischeri* $EIIA^{crr}$ homolog, encoded by *crr*, might regulate the transcriptional activity of the promoter associated with the *V. fischeri glpFK* operon (VF_0235-6), in a manner similar to inducer exclusion in *E. coli*. To determine whether this operon is indeed induced by the presence of glycerol, I measured the activity of the *V. fischeri glpFK* promoter in peptide medium, with and without added glycerol. The resulting *glpFK* promoter activity was significantly increased

by the presence of glycerol in the peptide-based medium, in a *crr*-dependent manner (**Fig. 5-1*B***). Notably, in the absence of glycerol, *glpFK* promoter activity was also significantly lower in Δ*crr* than in either wild-type or Δ*nagE1 V. fischeri* cells, consistent with activation of *glpFK* promoter activity by a Crr-dependent mechanism such as inducer exclusion. When the chitin monomer, GlcNAc, was added to glycerol-containing medium, *glpFK* promoter activity decreased 7-fold (**Fig. 5-1*C***). This effect was lost in a Δ*nagE1* mutant, suggesting that transport of GlcNAc is a necessary step in the observed decrease in *glpFK* promoter activity (**Fig. 5-1*B,C***).

I also monitored glycerol uptake in the presence and absence of GlcNAc (**Fig. 5-1*D***), and found that this substrate significantly decreased the *nagE1*-dependent transport of glycerol. Glycerol uptake was slightly, but not significantly decreased in the *crr* mutant, consistent with the partial growth defect of this mutant during growth on glycerol minimal medium (**Fig. 5-1*A***). Thus, chitin sugars such as GlcNAc inhibit transcription of glycerol catabolism-associated genes by a *crr*-dependent mechanism that is indistinguishable from inducer exclusion, suggesting that the *V. fischeri* Crr-dependent PTS prioritizes chitin sugar catabolism ahead of non-PTS carbohydrates such as glycerol.

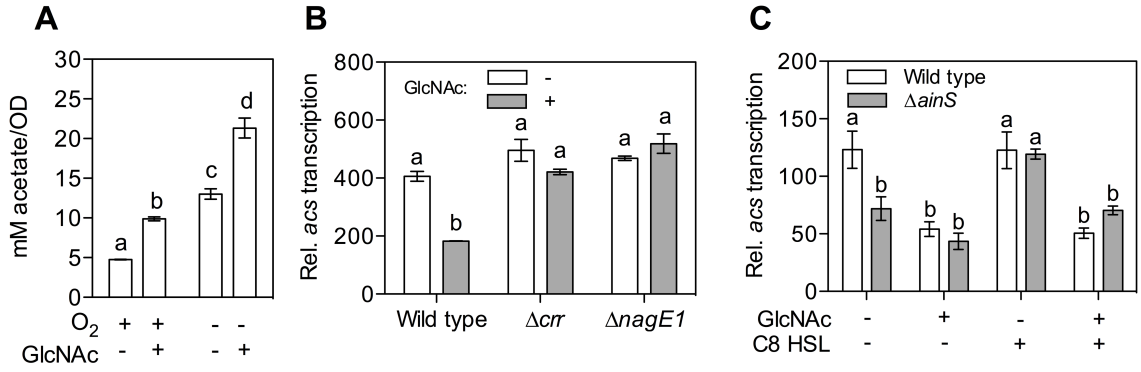

Figure 5-2. Repression of the *acs*-dependent acetate switch by chitin sugars. (A) Detection of acetate in the culture supernatant after growth in LBS under anoxic and oxic growth conditions, either with or without 20mM GlcNAc (n=2, representative of two independent experiments). Activity of the *acs* promoter region, during growth in a tryptone-based medium, either with or without 20 mM GlcNAc added, either (B) in PTS mutants (n=2, representative of two independent experiments), or (C) in the presence or absence of 20 mM GlcNAc and/or 100 nM octanoyl homoserine lactone (C8 HSL) (n=3). 'a'-'b' indicate groups of statistically similar means, determined by Two-Way ANOVA with Post-Hoc Bonferroni T-tests. Error bars indicate standard error.

The *acs*-dependent acetate switch is repressed by COS. Acetate is a major excretion product of COS catabolism by *V. fischeri* (27). To better understand the physiological conditions associated with this excretion, I measured the accumulation of acetate in culture supernatants during oxic and anoxic growth, either with or without GlcNAc, on a complex medium containing glycerol and peptides. Not surprisingly, I observed a >2-fold higher accumulation of acetate in anoxic cultures than in oxic cultures (**Fig. 5-2*A***). Further, cultures containing GlcNAc also accumulated ~2-fold more acetate, indicating that chitin sugar catabolism promotes extracellular acetate build-up, even during aerobic growth.

I reasoned that chitin sugar catabolism could promote accumulation and excretion of acetate through two metabolic mechanisms: (i) a classic Crabtree-effect, which favors the flow of acetate through glycolysis, rather than into the tricarboxylic acid (TCA) pathway, or (ii) the repression of the acetate switch (30). To address the latter possibility, I measured the transcription of *acs*, which encodes the key acetate-switch enzyme, acetyl-CoA synthase. I observed that *acs* promoter activity was significantly decreased by the presence of the chitin monomer, GlcNAc, and that this repression was dependent on a functional PTS system; specifically, *acs* promoter activity was insensitive to GlcNAc in both the Δ*crr* and Δ*nagE1* mutants (**Fig. 5-2*B***). Transcription of *acs* is also activated by the presence of octanoyl homoserine lactone (C8 HSL); the quorum signal synthesized by AinS (29). I next determined the relative strengths of GlcNAc and C8 HSL as negative and positive transcriptional effectors, respectively, by comparing *acs* promoter activity in the presence of none, either or both of these signals. Maximum *acs* activation is achieved with the addition of 100 nM C8 HSL by wild type, and 20 mM GlcNAc was sufficient to overcome this activation (**Fig. 5-**

2*C*). Interestingly, GlcNAc addition was unable to further decrease *acs* promoter activity below the baseline level of an *ainS* knock-out mutant, suggesting that the mechanism of regulation by GlcNAc (and perhaps other chitin sugars) is more of a de-activation than a repression. Thus, while the regulatory element targeted by chitin sugar catabolism remains unknown, the results indicate that catabolism of this class of host-derived sugar prevents activation of the acetate switch by AinSR-dependent quorum sensing (29).

Regulation of cytochrome oxidase activity by COS catabolism. Acetate catabolism typically generates chemical energy through respiration; therefore, I predicted that, in *V. fischeri*, chitin sugar-driven suppression of the acetate switch, and thus acetate utilization, would decrease cytochrome-based oxygen consumption. *V. fischeri* expresses two cytochrome-based terminal oxidases: a *cbb*-3-type cytochrome oxidase encoded by *ccoNOQP* (VF1299-1302), and a *bd*-type quinol oxidase encoded by *cydAB* (VF_0953-4). Both enzyme complexes are produced in culture and during at least the first few days of light-organ colonization, and their relative oxygen affinities have been estimated to be in the nanomolar range (14). However, mutation of *cydAB* severely impairs growth under aerobic culture conditions, and genetic suppressor mutations arise rapidly in such strains (46). Thus, I focused the efforts on characterizing the regulation and activity of the Δ*ccoNOQP* (designated Δ*cco*) mutant. The Δ*cco* strain had a small but reproducible decrease in growth rate relative to wild type (**Fig. 5-3*A***) when grown under micro-oxic conditions on a peptide-based medium predicted to support aerobic respiration. The divergence in rate became

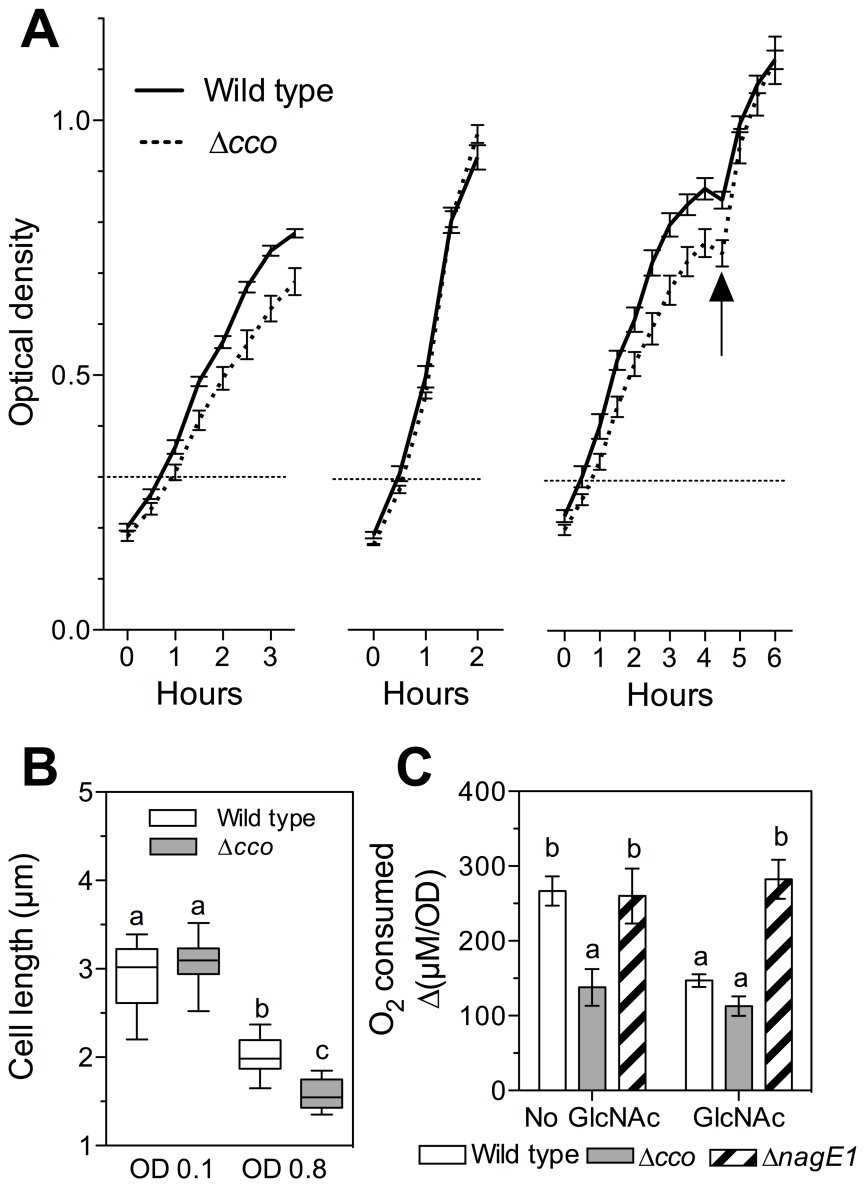
A
Wild type
Δcco
Optical density
1.0
0.5
0.0
0 1 2 3
Hours
0 1 2
Hours
0 1 2 3 4 5 6
Hours
B
Wild type
Δcco
Cell length (μm)
5
4
3
2
1
a
a
b
c
OD 0.1
OD 0.8
C
O2 consumed Δ(μM/OD)
400
300
200
100
0
b
a
b
a
a
b
No GlcNAc
GlcNAc
Wild type
Δcco
ΔnagE1

Figure 5-3. Repression of aerobic respiration by chitin sugars. (A) Growth of wild-type *V. fischeri* (solid lines), and a cytochrome oxidase mutant (Δ*cco*, dashed lines) under moderate aeration in LBS medium (left panel), or LBS containing 20 mM GlcNAc (center panel), or LBS with 20 mM GlcNAc added at the arrow (right panel); n=3. (B) Average cell length of wild-type (gray) and Δ*cco* (open) cells during growth in LBS medium at two stages of growth: early (0.1) and mid-log (0.8) phase (OD_{600nm}). (C) Oxygen consumption of wild-type (open), Δ*cco* (gray) and Δ*nagE1* (hatched), expressed as a rate per OD_{600nm} change, that takes place between 0.3-0.8 OD during growth in a peptide-based medium, either with or without 20 mM GlcNAc added. Error bars indicate standard error, n=3.

detectable within 2 h of growth under moderate aeration. However, the mutant's decreased rate was not apparent during growth with a PTS carbohydrate such as GlcNAc (**Fig. 5-3*A***), or glucose (**Fig. 5-4*A***), as the sole carbon source. Moreover, the addition of GlcNAc or glucose to growing cultures of Δ*cco* rapidly restored the mutant to a growth rate comparable to wild type (**Fig. 5-3*A***). In contrast, the addition of *N*-acetylneuraminic acid, a non-Crr-dependent amino sugar catabolized by *V. fischeri* (**Fig. 5-1*A***), failed to resolve the difference in optical density (OD) between mutant and wild-type strains (**Fig. 5-4*B***). The difference in growth rate between the Δ*cco* and wild-type *V. fischeri* was accompanied by a smaller average cell size of the Δ*cco* strain during mid-log phase growth (**Fig. 5-3*B***). I reasoned that the decrease in cell size might be correlated with a decrease in respiration at this growth stage, due to the lack of the CcoNOQP cytochrome oxidase. To address this hypothesis, I determined the respiratory rate for the cytochrome oxidase mutant and its wild-type parent during oxic growth on peptide-based medium. Wild-type *V. fischeri* and the Δ*cco* derivative consumed comparable amounts of oxygen between 0.05-0.3 OD (Fig. S1C&D), but between 0.3-0.8 OD, the Δ*cco* mutant developed a pronounced decrease in the relative rate of oxygen consumption (**Fig. 5-3*C***). Moreover, the presence of GlcNAc reduced the level of consumption by wild type to that of the Δ*cco* strain. Interestingly, the timing of this transition was coincident with the appearance of the growth-rate and cell-size phenotypes observed in this mutant (**Fig. 5-3*A,B***).

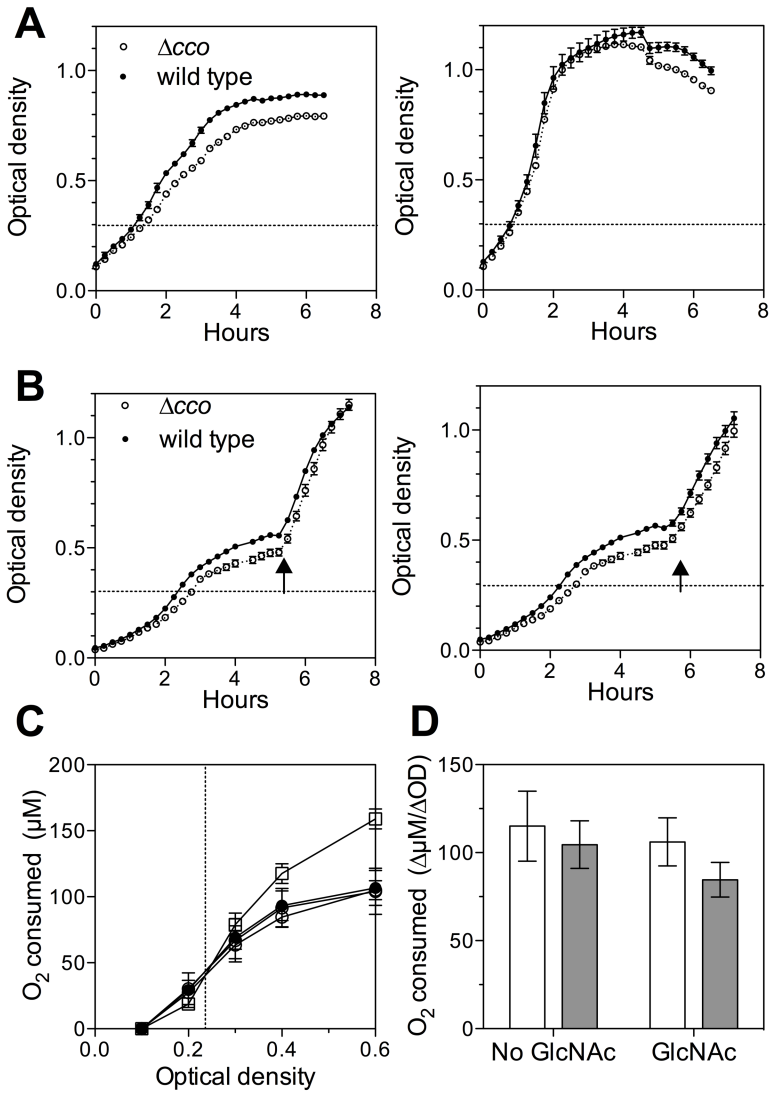
A
Δcco
wild type
Optical density
Hours
B
C
O2 consumed (μM)
Optical density
D
O2 consumed (ΔμM/ΔOD)
No GlcNAc
GlcNAc

Figure 5-4. Characterization of cytochrome oxidase-deficient *V. fischeri,* and the contribution of GlcNAc to oxygen consumption. (*A-B*) Growth of Δ*cco* (open) and wild-type (solid) *V. fischeri* in the presence of (*A*) either a peptide MSM (left), or glucose MSM (right) medium, and (*B*) SWT medium with 10 mM GlcNAc (left), or 10 mM NANA (right) added at the arrow. * indicates a significant difference in mean optical density between Δ*cco* and wild-type *V. fischeri*, determined by repeated measures two-way ANOVA with post-hoc Bonferroni multiple comparison tests, P>0.05. Error bars indicate SEM, n=3. (*C*) Oxygen consumption of wild-type *V. fischeri* (boxes), and the Δ*cco* mutant (circles), during growth on SWT medium in the presence (filled symbols) or absence (open symbols) of GlcNAc. Bars show standard error, n=3. (*D*) Oxygen consumption of wild-type (open) and the Δ*cco* mutant (gray), expressed as a rate per optical density change, that takes place between 0.05-0.3 OD units during growth in LBS medium, either in the presence or absence of 20 mM GlcNAc. Error bars indicate standard error, n=3.

COS catabolism destabilizes colonization of the immature light organ by *V. fischeri.*

Acetyl-CoA synthase, encoded by *acs,* has been shown to help *V. fischeri* maintain a normal colonization of the light organ during the first 48 h of symbiosis (29), indicating that acetate uptake is a determinant of symbiotic stability. I also observed that a mutant deficient in the glyoxylate shunt, the metabolic pathway through which acetate is converted into biomass to support anaplerosis, was as fit as wild-type *V. fischeri* during co-colonization of the light organ (**Fig. 5-5*A***). This result suggested that the benefit of acetate uptake to symbiosis is not as a carbon source, but for its contribution to respiratory energy-generation. The light organ is oxic during the first 48 h of colonization, and cytochrome oxidase genes are expressed, so I reasoned symbiont metabolism might rely on aerobic respiration of ambient acetate. Adding chitin sugars to such an environment should repress *acs* transcription and, thus, reverse the advantage in acetate utilization that wild-type cells normally have during competition with an *acs* mutant. To test this idea, I co-colonized squid with wild-type and mutant strains of *V. fischeri* defective in either acetate uptake (*acs* Tn:erm), or the GlcNAc-specific PTS (Δ*nagE1* or Δ*crr*), and compared how well they competed when GlcNAc was present or absent. As predicted, the disadvantage of the *acs* mutant at 48 h was eliminated by the addition of GlcNAc (**Fig. 5-6*A***). In addition to this 'chemical complementation', genetic complementation of the *acs* mutation also restored competitive fitness to the strain (**Fig. 5-5*B***). I next assessed the competitive fitness of the Δ*nagE1* mutant, a strain unable to metabolize GlcNAc, under the same conditions. Both this transporter mutant and wild-type *V. fischerI was* equally competitive after 48 h of colonization in the absence of GlcNAc (**Fig. 5-6*A***). However, the fitness of the Δ*nagE1* strain increased significantly relative to wild type

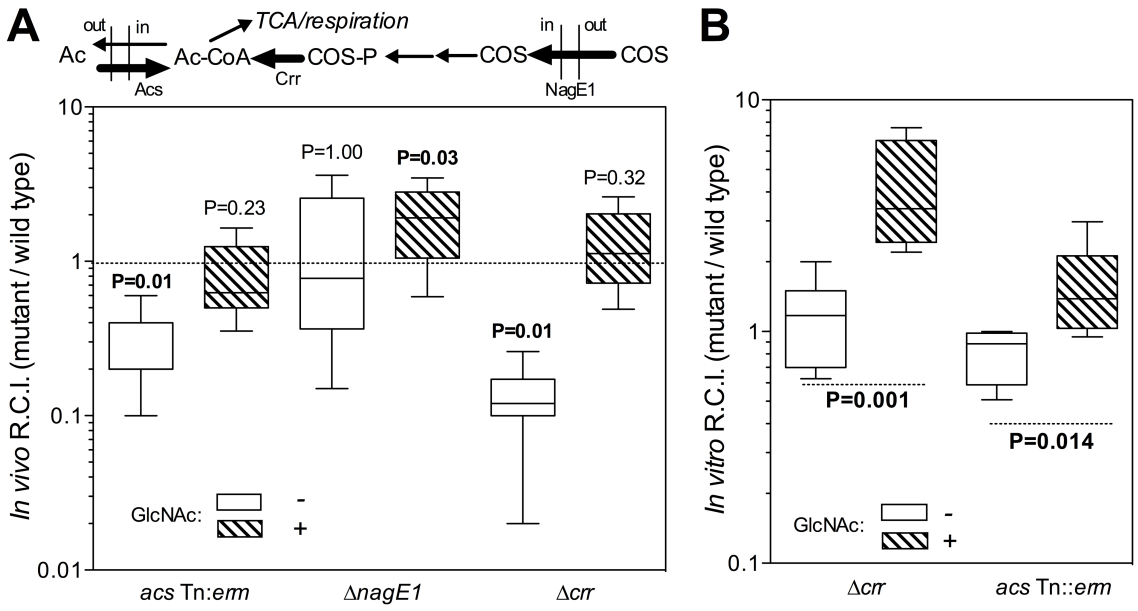

Figure 5-5. Chemical complementation of COS-modulated metabolic processes. (A) Co-colonization of squid for 48 h with wild-type *V. fischeri* and one of three isogenic strains carrying a mutation in either a PTS or an acetate-switch protein (pathway noted above plot). Co-colonizations were performed for 48 h in the absence (open), or presence (hatched) of 20 mM GlcNAc. (B) Competition in co-cultures of wild-type *V. fischeri* and the indicated mutants growing in SWT medium either without (open), or with (hatched) 10 mM GlcNAc. C.I.= competitive index. P-value above box-and-whisker plot represents statistical similarity to a theoretical mean of 1.0, as calculated by a one-sample T-test (n=20 squid per condition). Inner fences were determined by Tukey's method. Comparisons in which either the wild type or the mutant performed significantly (>95%) better have P-values given in bold. Error bars indicate standard error.

when GlcNAc was present, consistent with the inability of this PTS sugar to repress *acs* in this mutant (**Fig. 5-2*B***).

To learn more about what carbon sources are available to symbionts in the juvenile light organ, I performed the same type of co-colonization experiments, this time with the Δ*crr* strain. It has been observed previously that a Δ*crr* mutant is less competitive than wild type during the first 48 h of light-organ colonization (52). There are two alternative hypotheses to explain this phenotype: either (i) a Crr-dependent PTS sugar, or (ii) a carbohydrate that is subject to inducer exclusion, is an important nutrient present in the light organ environment, and it cannot be catabolized by the mutant. In the first case, the addition of chitin sugars to the seawater would be predicted to aggravate the competitive disadvantage of Δ*crr*, because even more of a Crr-dependent PTS substrate would be available to the wild-type, but not the Δ*crr*, strain. In the second case, the addition of chitin sugars would be expected to ameliorate the competitive disadvantage of Δ*crr*, because the presence of these sugars would lead to inducer exclusion by both wild type and Δ*crr*. I observed the latter; i.e., the addition of GlcNAc to the seawater of squid ameliorated the competitive disadvantage of Δ*crr* (**Fig. 5-6*A***), consistent with the presence in the symbiont's environment of a non-PTS carbohydrate substrate that is subject to inducer exclusion.

To further predict the nutrient conditions in the juvenile light organ that lead to the initial, GlcNAc-independent decrease of fitness in *acs* and Δ*crr* strains, and thereby test the interpretations of the symbiotic effect of chitin sugars, I performed co-culture experiments in nutrient media. During semi-aerated growth on a modified SWTO medium containing 1/10

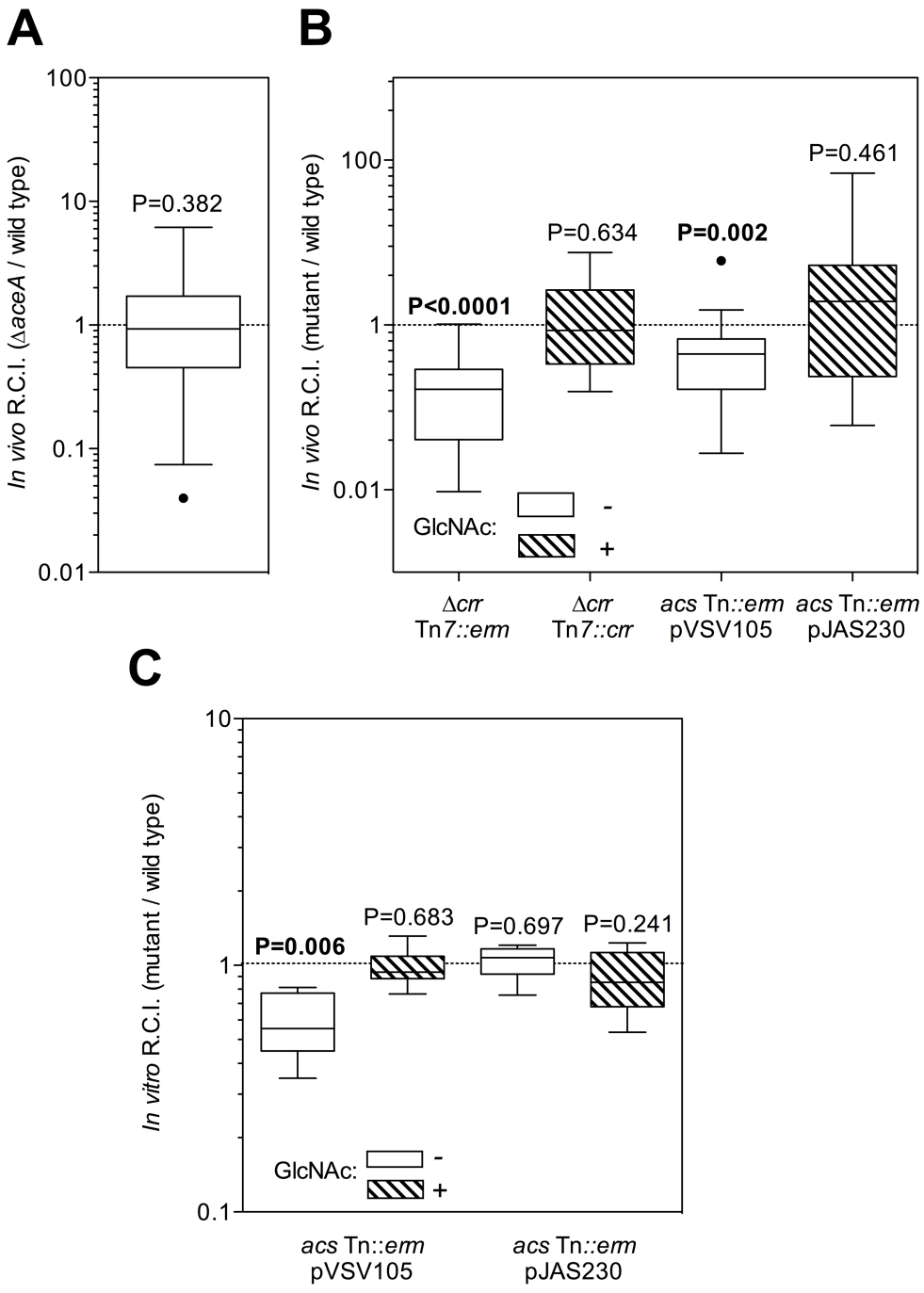
A
B
C
In vivo R.C.I. (ΔaceA / wild type)
P=0.382
In vivo R.C.I. (mutant / wild type)
P<0.0001
P=0.634
P=0.002
P=0.461
GlcNAc:
-
+
Δcrr Tn7::erm
Δcrr Tn7::crr
acs Tn::erm pVSV105
acs Tn::erm pJAS230
In vitro R.C.I. (mutant / wild type)
P=0.006
P=0.683
P=0.697
P=0.241
GlcNAc:
-
+
acs Tn::erm pVSV105
acs Tn::erm pJAS230

Figure 5-6. Competition of during 48 h co-colonization of squid light organ. (*A*) The Δ*aceA V. fischeri* mutant competes indistinguishably well with its wild-type parent. This mutant cannot use acetate *via* the glyoxylate shunt, due to a loss of isocitrate lyase activity. (*B*) Genetic complementation of Δ*crr* and *acs*-insertion mutants in the squid. The competitive fitness of the indicated mutant (open), or the genetically complimented mutant (hatched), compared to wild-type *V. fischeri* was determined. (*C*) Competition of wild-type *V. fischeri* and the indicated mutants during growth in SWTO medium either without (open), or with (hatched) 10 mM GlcNAc added. The competitive fitness of mutant strains carrying either the empty vector (open) or an *in trans* complementation vector (hatched) was determined relative to wild-type *V. fischeri*. R.C.I., relative competitive index. P-value above box-and-whisker plot represents statistical similarity to a theoretical mean of 1.0, as calculated by a one-sample T-test (n=20 squid per condition, or n=6 per culture condition). Inner fences determined by Tukey's method, outliers shown with black dots. P-values given in bold indicate comparisons in which the wild type was significantly better. Error bars show standard error.

of the normal levels of glycerol and peptides, I observed a GlcNAc-dependent shift in competitive fitness (**Fig. 5-6*B***) comparable to that seen with these mutants in the light-organ co-colonization assays (**Fig. 5-6*A***). In contrast, in the absence of chitin sugars, there was no difference in competitive fitness between either of the two mutants and wild type. I reasoned that, unlike in the light-organ environment, the batch culture conditions might not favor induction of the acetate switch. When I repeated the co-culturing experiment with the *acs* mutant and wild-type *V. fischeri* in full-strength SWTO, I observed a decrease in competitive fitness comparable to that observed in the squid (**Fig. 5-5*C***). As in the squid, this loss of competitive fitness could be reversed by the presence of GlcNAc in the culture medium. Together, these results suggest that the immature light-organ environment has a balance of carbon and oxygen availability not unlike that of aerated, full-strength SWTO; in addition, the carbon substrates in this environment (*e.g.*, glycerol) support an active acetate switch, and may be targets of inducer exclusion. The metabolic and regulatory strategies available to *V. fischeri* in such an environment, compared to those in an environment containing COS, are quite distinct.

DISCUSSION

In this study, I have shown that chitin sugars, provided by the host squid *E. scolopes,* serve as regulatory molecules whose catabolism by symbiotic *V. fischeri* leads to a shift from respiratory to fermentative metabolism in the bacteria. Notably, this shift is dependent on the developmental stage of the host; *i.e.*, while chitin sugars apparently serve only a non-nutritional, signaling role in the juvenile symbiosis (15, 25), in the mature association it is

provided each night in higher concentrations as a nutrient (27). Thus, while losing the ability to catabolize chitin sugars actually promotes a bacterium's initial colonization of the light organ (26), fermentation of these host-derived sugars is critical for the symbiont to maintain its association in the mature light organ (27). Oxygen limitation is also likely to accompany the transition from the immature to mature symbiotic state (14); therefore, during this transition, it is possible that the provision of chitin sugars may function to change the relative levels of symbiont growth, oxygen consumption and bioluminescence. In the present study, I highlight three areas of *V. fischeri* physiology that are both subject to regulation by the representative chitin sugar GlcNAc, and contribute to light-organ colonization: (i) prioritization of chitin sugar transport, (ii) modulation of metabolic functions regulated by quorum sensing, and (iii) repression of aerobic respiration (**Fig. 5-7**).

The integration of chitin sugar transport with the Crr-dependent PTS ensures that catabolism of these chitin-derived sugars is favored in *V. fischeri*. I demonstrate that one of the outcomes of transport *via* Crr is a decrease in the uptake of non-PTS carbohydrates, such as glycerol (**Fig. 5-1*A***). This phenotype is consistent with the inducer-exclusion mechanism described in other Gram-negative organisms (50). Notably, homologs of the *V. fischeri* Crr in *E. coli* and *S. typhimurium* post-translationally regulate adenylate cyclase activity, which contributes to cyclic-AMP mediated transcriptional regulation by Crp (50). However, due to a highly active cyclic-AMP phosphodiesterase in *V. fischeri*, evidence for conservation of such a function in this species' Crr remains elusive (E. Stabb, personal communication). The transport of GlcNAc and other chitin sugars by the Crr-dependent PTS is a shared trait of the

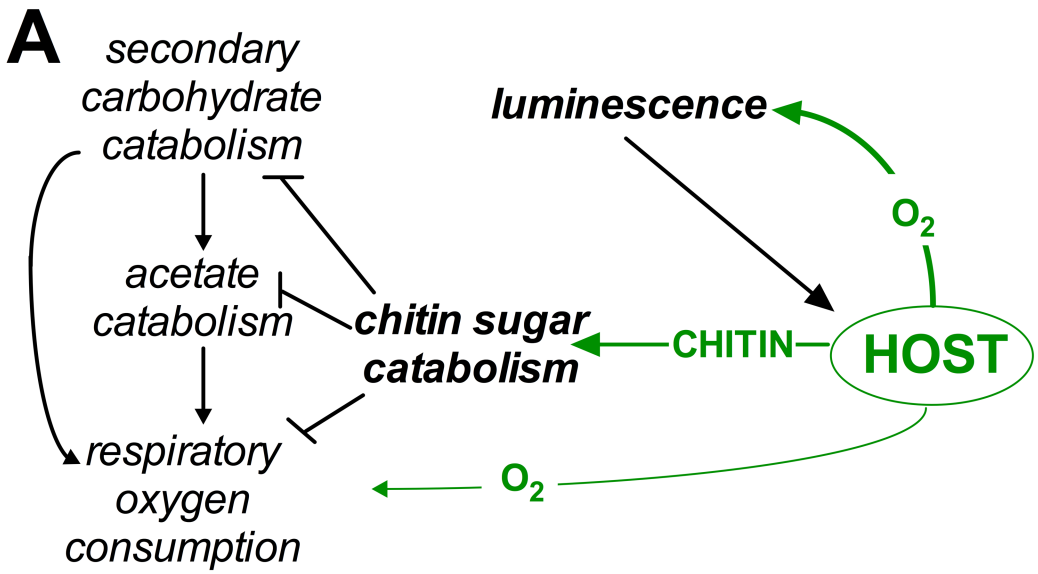

Figure 5-7. Impact of chitin sugar catabolism on symbiont physiology. Host-derived chitin is hydrolyzed to form chitin oligosaccharides (53). Chitin sugar catabolism by *V. fischeri* inhibits secondary (*i.e.*, non-PTS) carbohydrate catabolism, acetate uptake, and respiratory oxygen consumption. The result of this physiological shift is an increased availability of host-provided oxygen to the symbiont's luminescence-producing enzyme, luciferase. Luminescence, which is used in the squid's behavior, is required to support a sustained colonization of the light organ by *V. fischeri.*

Vibrionaceae (23), although the studies suggest that this branch of transport is more comprehensive in *V. fischeri* than in *V. furnisii* and *V. cholerae.* In the context of the squid-vibrio symbiosis, the expanded repertoire of PTS-dependent chitin sugars presents a flexible strategy for a single type of host glycan, chitin, to regulate symbiont physiology: if chitin sugars are present in the environment, inducer exclusion will ensure that they will be preferentially used by symbionts before other carbohydrate nutrients such as glycerol.

A second example of how chitin sugars exert metabolic control over the bacterial partner is the catabolism-dependent override of quorum-signaling-induced symbiont group behaviors. Specifically, activation of transcription of the *V. fischeri acs* gene by AinSR integrates the acetate switch into the quorum-signaling network (29), and indicates the important link between acetate homeostasis and the symbiont's activities in the light organ. Indeed, deletion of *acs*, which encodes the cell's key acetate-uptake enzyme, results in a decreased representation of this mutant during co-colonization with wild-type *V. fischeri* (29). Here, I demonstrate that, even at high cell density, the repression of *acs* transcription by chitin sugar catabolism can fully counteract the activation of *acs* by quorum signaling (**Fig. 5-2**). Previous studies have demonstrated that the *ainSR* locus is, itself, regulated by the transcription factor Crp (54), which is responsive to Crr-dependent PTS transport in Gram-negative bacteria (50). Thus, the *V. fischeri* Crp may directly regulate *acs* promoter activity, or do so by modulating *ainSR* transcription. In the latter case, while AinSR quorum signaling may have a dominant effect on the symbiont population in a juvenile organ (55), the host may override the contribution of group behaviors to acetate homeostasis at night, when chitin

sugars are provided to the symbiont (27).

Finally, host-derived chitin sugar utilization by *V. fischeri* results in a metabolic strategy that reduces respiratory activity by cytochrome oxidase (**Fig. 5-3C**). I predict that this reduction increases the availability of key substrates for bacterial luciferase, such as oxygen and reducing power (**Fig. 5-5**). Like its respiratory oxidases, the luciferase of *V. fischeri* has an affinity for oxygen in the nanomolar range (14), suggesting that these oxidases directly compete for this reactant. Because symbionts must produce bioluminescence to maintain their colonization of the light organ (12, 56), within this environment their physiology must favor light emission, at least at night. I predict that host provision of chitin sugars to symbionts will both decrease respiratory activity and promote bioluminescence (**Fig. 5-5**), thereby supporting the functional basis of the squid-vibrio mutualism (10).

Taken as a whole, this work highlights the contribution that the presence of specific glycans in the host environment can make to the physiology of a co-evolved symbiont. Glycans are emerging as a class of key regulatory nutrients in diverse host-microbe interactions. For example, the uptake and metabolism of PTS carbohydrates is a central component of the microbial ecology within the human small intestine (57); similarly, the prioritization of host-derived polysaccharide and glycan catabolism by the *Bacteroides thetaiotaomicron* starch-utilization system is a crucial regulatory point in the primary colonization of the mammalian gut (58). The fatty acids (e.g., butyrate and acetate) produced by *Bacteroides* spp. during starch fermentation are potent immunomodulators of host macrophage function (59). PTS transport also contributes to the regulation of virulence traits in several enteric pathogens (60), including *Vibrio cholerae* (23, 61). Notably, in both the

mouse gut (62), and the squid light organ (27), cells of the innate immune system contribute to the regulation of host glycan delivery to symbionts. Thus, host-derived chitin sugars, like other nutrients, may be key to elucidating the mechanisms governing stability and dysbiosis of symbiotic microbiota in general.

ACKNOWLEDGEMENTS

I thank E. Stabb, and D. Colton for contributive discussions. I also thank H. Blackwell and her research group for the gift of synthetic octanoyl homoserine lactone (C8 HSL). This work was funded by NIH grants RR12294/OD11024 to EGR and M. McFall-Ngai, and AI050661 to M. McFall-Ngai and EGR, as well as NSF grant MCB1050687 to AKD. MP was funded by a China Scholarship Council's State Scholarship Fund Award. JAS was funded by a NSF Graduate Research Fellowship, the Chemical Biology Training Program (UW-Madison, NIH-NIGMS T32 GM008505), and the Microbes in Health and Disease Training Program (UW-Madison NIH-NIAID T32 AI055397).

REFERENCES:

1. McFall-Ngai MJ (2014) The Importance of microbes in animal development: lessons from the squid-vibrio symbiosis. *Annu Rev Microbiol* 68(1).

2. Maynard CL, Elson CO, Hatton RD, & Weaver CT (2012) Reciprocal interactions of the intestinal microbiota and immune system. *Nature* 489(7415):231-241.

3. Gilbert SF (2014) A holobiont birth narrative: the epigenetic transmission of the human microbiome. *Front Genetics* 5:282.

4. Douglas AE (2014) Molecular dissection of nutrient exchange at the insect-microbial interface. *Curr Opin Insect Sci* 4:23-28.

5. Pacheco AR, Barile D, Underwood MA, & Mills DA (2014) The impact of the milk glycobiome on the neonate gut microbiota. *Ann Rev Animal Biosci* (0).

6. Comstock LE (2009) Importance of glycans to the host-*Bacteroides* mutualism in the mammalian intestine. *Cell Host Microbe* 5(6):522-526.

7. Engel P & Moran NA (2013) Functional and evolutionary insights into the simple yet specific gut microbiota of the honey bee from metagenomic analysis. *Gut microbes* 4(1):60-65.

8. Nelson MC & Graf J (2012) Bacterial symbioses of the medicinal leech *Hirudo verbana*. *Gut microbes* 3(4):322-331.

9. McFall-Ngai M (2014) Divining the essence of symbiosis: insights from the squid-vibrio model. *PLoS Biol* 12(2):e1001783.

10. Stabb EV & Visick KL (2013) *Vibrio fisheri*: squid symbiosis. *The prokaryotes*, (Springer, Berlin Heidelberg), pp 497-532.

11. Verma SC & Miyashiro TI (2013) Quorum sensing in the squid-vibrio symbiosis. *Int J Mol Sci* 14(8):16386-16401.

12. Koch EJ, Miyashiro TI, McFall-Ngai MJ, & Ruby EG (2013) Features governing symbiont persistence in the squid-vibrio association. *Mol Ecol* (doi:10.1111/mec.12474).

13. Visick KL, Foster J, Doino J, McFall-Ngai M, & Ruby EG (2000) *Vibrio fischeri lux* genes play an important role in colonization and development of the host light organ. *J Bacteriol* 182(16):4578-4586.

14. Dunn AK (2012) *Vibrio fischeri* metabolism: symbiosis and beyond. *Adv Microb Physiol* 61:37.

15. Mandel MJ*, et al.* (2012) Squid-derived chitin oligosaccharides are a chemotactic signal during colonization by *Vibrio fischeri*. *Appl Environ Microbiol* 78(13):4620-4626.

16. Oldroyd GE (2013) Speak, friend, and enter: signalling systems that promote beneficial symbiotic associations in plants. *Nat Rev Microbiol* 11(4):252-263.

17. Killiny N, Prado SS, & Almeida RP (2010) Chitin utilization by the insect-transmitted bacterium *Xylella fastidiosa*. *Appl Environ Microbiol* 76(18):6134-6140.

18. Chaston J & Goodrich‐Blair H (2010) Common trends in mutualism revealed by model associations between invertebrates and bacteria. *FEMS Microbiol Rev* 34(1):41-58.

19. Aluwihare LI, Repeta DJ, Pantoja S, & Johnson CG (2005) Two chemically distinct pools of organic nitrogen accumulate in the ocean. *Science* 308(5724):1007-1010.

20. Hunt DE, Gevers D, Vahora NM, & Polz MF (2008) Conservation of the chitin utilization pathway in the Vibrionaceae. *Appl Environ Microbiol* 74(1):44-51.

21. Meibom KL*, et al.* (2004) The *Vibrio cholerae* chitin utilization program. *Proc Natl Acad Sci U S A* 101(8):2524-2529.

22. Bassler B, Yu C, Lee Y, & Roseman S (1991) Chitin utilization by marine bacteria. degradation and catabolism of chitin oligosaccharides by *Vibrio furnissii*. *J Biol Chem* 266(36):24276-24286.

23. Blokesch M (2012) Chitin colonization, chitin degradation and chitin-induced natural competence of *Vibrio cholerae* are subject to catabolite repression. *Environ Microbiol* 14(8):1898-1912.

24. Houot L, Chang S, Absalon C, & Watnick PI (2010) *Vibrio cholerae* phosphoenolpyruvate phosphotransferase system control of carbohydrate transport, biofilm formation, and colonization of the germfree mouse intestine. *Infect Immun*78(4):1482-1494.

25. Kremer N*, et al.* (2013) Initial symbiont contact orchestrates host-organ-wide transcriptional changes that prime tissue colonization. *Cell Host Microbe* 14(2):183-194.

26. Miyashiro T*, et al.* (2011) The *N*-acetyl-d-glucosamine repressor NagC of *Vibrio fischeri* facilitates colonization of *Euprymna scolopes*. *Mol Microbiol* 82(4):894-903.

27. Schwartzman JA*, et al.* (2015) The chemistry of negotiation: rhythmic, glycan-driven acidification in a symbiotic conversation. *Proc Natl Acad Sci U S A* 112(2):566-571.

28. Kremer N*, et al.* (2014) The dual nature of haemocyanin in the establishment and persistence of the squid–Vibrio symbiosis. *Proc. R. Soc. B* 281(1785).

29. Studer SV, Mandel MJ, & Ruby EG (2008) AinS quorum sensing regulates the *Vibrio fischeri* acetate switch. *J Bacteriol* 190(17):5915-5923.

30. Wolfe AJ (2005) The acetate switch. *Microbiol Mol Biol Rev* 69(1):12-50.

31. Boettcher KJ & Ruby EG (1990) Depressed light emission by symbiotic *Vibrio fischeri* of the sepiolid squid *Euprymna scolopes*. *J Bacteriol* 172(7):3701-3706.

32. Mandel MJ, Stabb EV, & Ruby EG (2008) Comparative genomics-based investigation of resequencing targets in *Vibrio fischeri*: focus on point miscalls and artefactual expansions. *BMC Genomics* 9:138.

33. Stabb EV, Butler MS, & Adin DM (2004) Correlation between osmolarity and luminescence of symbiotic *Vibrio fischeri* strain ES114. *J Bacteriol* 186(9):2906-2908.

34. Graf J, Dunlap PV, & Ruby EG (1994) Effect of transposon-induced motility mutations on colonization of the host light organ by *Vibrio fischeri*. *J Bacteriol* 176(22):6986-6991.

35. Sambrook J, Fritsch EF, & Maniatis T (1989) *Molecular Cloning* (Cold Spring Harbor Laboratory Press New York).

36. Stabb EV & Ruby EG (2002) RP4-based plasmids for conjugation between *Escherichia coli* and members of the vibrionaceae. *Methods Enzymol* 358:413-426.

37. Le Roux F, Binesse J, Saulnier D, & Mazel D (2007) Construction of a *Vibrio splendidus* mutant lacking the metalloprotease gene *vsm* by use of a novel counterselectable suicide vector. *Appl Environ Microbiol* 73(3):777-784.

38. Shibata S & Visick KL (2012) Sensor kinase RscS induces the production of antigenically distinct outer membrane vesicles that depend on the symbiosis polysaccharide locus in *Vibrio fischeri*. *J Bacteriol* 194(1):185-194.

39. McCann J, Stabb EV, Millikan DS, & Ruby EG (2003) Population dynamics of *Vibrio fischeri* during infection of *Euprymna scolopes*. *Appl Environ Microbiol* 69(10):5928-5934.

40. Dunn AK, Millikan DS, Adin DM, Bose JL, & Stabb EV (2006) New rfp- and pES213-derived tools for analyzing symbiotic *Vibrio fischeri* reveal patterns of infection and *lux* expression in situ. *Appl Environ Microbiol* 72(1):802-810.

41. Adin DM, Visick KL, & Stabb EV (2008) Identification of a cellobiose utilization gene cluster with cryptic *B*-galactosidase activity in *Vibrio fischeri*. *Appl Environ Microbiol* 74(13):4059-4069.

42. Slauch JM, and T. J. Silhavy (1991) *cis*-acting *ompF* mutations that result in OmpR-dependent constitutive expression. *J Bacteriol* 173:4039-4048.

43. Ebert L*, et al.* (2014) Use of a learning collaborative to support implementation of integrated care for smoking cessation for veterans with posttraumatic stress disorder. *Am J Pub Health* 104(10):1935-1942.

44. Miyashiro T, Wollenberg MS, Cao X, Oehlert D, & Ruby EG (2010) A single *qrr* gene is necessary and sufficient for LuxO-mediated regulation in *Vibrio fischeri*. *Mol Microbiol* 77(6):1556-1567.

45. D'agostino RB, Belanger A, & D'Agostino Jr RB (1990) A suggestion for using powerful and informative tests of normality. *Am Stat* 44(4):316-321.

46. Dunn AK*, et al.* (2010) The alternative oxidase (AOX) gene in *Vibrio fischeri* is controlled by NsrR and upregulated in response to nitric oxide. *Mol Microbiol* 77(1):44-55.

47. Hanahan D (1983) Studies on transformation of *E. coli* with plasmids. *J Mol Biol* 166(4):557-580.

48. Bao Y, Lies DP, Fu H, & Roberts GP (1991) An improved Tn*7*-based system for the single-copy insertion of cloned genes into chromosomes of gram-negative bacteria. *Gene* 109(1):167-168.

49. Dunn AK & Stabb EV (2008) The twin arginine translocation system contributes to symbiotic colonization of *Euprymna scolopes* by *Vibrio fischeri*. *FEMS Microbiol Lett* 279(2):251-258.

50. Deutscher J, Francke C, & Postma PW (2006) How phosphotransferase system-related protein phosphorylation regulates carbohydrate metabolism in bacteria. *Microbiol Mol Biol Rev* 70(4):939-1031.

51. Brooks JF, Gyllborg MC, Kocher AA, Markey LE, & Mandel MJ (2015) TfoX-based genetic mapping identifies *Vibrio fischeri* strain-level differences and reveals a common lineage of laboratory strains. *J Bacteriol*:JB. 02347-02314.

52. Visick KL, O'Shea TM, Klein AH, Geszvain K, & Wolfe AJ (2007) The sugar phosphotransferase system of *Vibrio fischeri* inhibits both motility and bioluminescence. *J Bacteriol* 189(6):2571-2574.

53. Hentzer M*, et al.* (2003) Attenuation of *Pseudomonas aeruginosa* virulence by quorum sensing inhibitors. *Embo J* 22(15):3803-3815.

54. Lyell NL*, et al.* (2013) Cyclic AMP Receptor Protein regulates pheromone-mediated bioluminescence at multiple levels in *Vibrio fischeri* ES114. *J Bacteriol* 195(22):5051-5063.

55. Lupp C & Ruby EG (2005) *Vibrio fischeri* uses two quorum-sensing systems for the regulation of early and late colonization factors. *J Bacteriol* 187(11):3620-3629.

56. Studer SV*, et al.* (2013) Non-native acylated homoserine lactones reveal that LuxIR quorum sensing promotes symbiont stability. *Environ Microbiol* (doi:10.1111/1462-2920.12322).

57. Zoetendal EG*, et al.* (2012) The human small intestinal microbiota is driven by rapid uptake and conversion of simple carbohydrates. *ISME* 6(7):1415-1426.

58. Sonnenburg JL*, et al.* (2005) Glycan foraging in vivo by an intestine-adapted bacterial symbiont. *Science* 307(5717):1955-1959.

59. Chang PV, Hao L, Offermanns S, & Medzhitov R (2013) The microbial metabolite butyrate regulates intestinal macrophage function via histone deacetylase inhibition. *Proc Natl Acad Sci U S A* 111(6):2247-2252.

60. Görke B & Stülke J (2008) Carbon catabolite repression in bacteria: many ways to make the most out of nutrients. *Nat Rev Microbiol* 6(8):613-624.

61. Hang S*, et al.* (2014) The acetate switch of an intestinal pathogen disrupts host insulin signaling and lipid metabolism. *Cell Host Microbe* 16(5):592-604.

62. Goto Y*, et al.* (2014) Innate lymphoid cells regulate intestinal epithelial cell glycosylation. *Science* 345(6202):1254009.

Chapter 6

Synthesis and Future Directions

PREFACE

JAS wrote the chapter.

SYNTHESIS

The theme of this dissertation is the elucidation of context-dependent chemical cues from host and symbiont that shape the squid-vibrio symbiosis. The four research chapters of this dissertation (**Chapters 2-5**), provide examples of the chemical 'negotiation' that takes place between host and symbiont at each stage of the life-long association.

Acidic mucus is the first host environment encountered by *V. fischeri* (1). **Chapter 2** presents an ongoing project to test the hypothesis that the acidic pH of the mucus coordinates physiological responses of the symbiont to promote the colonization of the light organ. One of the most interesting observations from this chapter is that acid pH-induced stress responses are not a common attribute of marine microbes. This chapter presents evidence of acid-induced resistance of *V. fischeri* to the cationic antimicrobial peptide polymyxin B. This response is not conserved in *V. parahaemolyticus*, a member of the seawater bacterioplankton that can survive in the mucus in the absence of *V. fischeri* (2). Notably, antimicrobial peptides structure the beneficial microbiota of the hydra epithelium and the mammalian gut (3, 4). Thus, the characterization of the *V. fischeri* acid-induced stress response establishes a set of genetic tools with which to discover the contribution of pH and symbiont stress responses to the selectivity and specificity of the squid-vibrio model. Additionally, acid-induced stress responses are poorly studied in the context of beneficial host-microbe associations. Thus, future studies of acid-induced stress in *V. fischeri* that build off of this chapter could provide insight into the strategies by which beneficial microbes employ this signaling cascade to promote homeostasis among the microbial community, and with the host.

In **Chapter 3**, the contribution of LuxIR quorum signaling to the stability of the symbiosis is interrogated using synthetic analogs of the LuxR-specific acyl homoserine lactone signaling molecules. The analogs are used to temporally modulate the level of quorum signaling that takes place during the first days of symbiosis. The continual production of bioluminescence is revealed to be critical between 18 and 48 h of colonization. Many signaling events that structure the initiation of symbiosis occur prior to 12 post-colonization, when the symbiont delivers an irreversible morphogenic cue to the light-organ tissues (5). Thus, the data presented in **Chapter 3** help separate the contribution of bioluminescence from irreversible morphogenesis, and contribute to the existing literature characterizing bioluminescence as a microbial product that contributes to both persistence and circadian regulation of light-organ tissues (6-8).

The chemical dialog through which a host promotes persistence and development with particular microbial partners remains largely unexplored, especially within complex consortia like the human microbiota. Natural, monospecific associations, including that between bobtail squid and *V. fischeri*, have proven useful for discovering shared strategies, such as rhythmic microbial signaling and microbial-product induced development, subsequently found in mammalian associations. In **Chapter 4** of this dissertation, the diel provision of a squid-derived glycan is found to drive symbiont metabolism, resulting in tissue acidification. This event alters bacterial physiology, favoring the cyclic production of bioluminescence: the functional basis of the symbiosis. More generally, studies of the metabolic exchange between squid and vibrio can help reveal mechanisms by which other hosts modulate tissue chemistry to regulate microbial community function.

Host-derived glycans have recently emerged as a link between symbiont nutrition and innate immune function. Unfortunately, the locations at which microbes typically access these glycans are generally inaccessible to experimentation and imaging, and take place in the context of diverse microbe-microbe interactions, creating a complex symbiotic ecology. In **Chapter 5** of this dissertation, the metabolic state of a single microbial symbiont in a natural association with its co-evolved animal host is described. This approach helps to infer key points at which a host-controlled tissue environment might regulate the physiological state of its symbionts. The data presented in this chapter demonstrate that the presence of a regulatory glycan is sufficient to shift symbiont carbohydrate catabolism, acetate homeostasis, and oxygen consumption.

In summary, this dissertation contributes to the establishment of the squid-vibrio system as a model to the study of chemical exchange between host and symbiont, and as an emerging system to interrogate the mechanisms by which an initial colonization by a symbiont develops into homeostatic, yet rhythmic, state.

QUESTIONS TO DIRECT FUTURE RESEARCH

1. **How does the chemistry of the mucus contribute to the dominance of *V. fischeri* over *V. parahaemolyticus* during initiation of symbiosis, and does *V. fischeri*-specific signaling shape the chemistry of the mucus?**

   In **Chapter 2** of this thesis, the acid-induced stress responses of *V. fischeri* and *V. parahaemolyticus* are compared. A key observation is that the *V. parahaemolyticus* strain KNH1, isolated from an environment where *Euprymna scolopes* and *V. fischeri* are endemic (9), do not share an acid-induced resistance to cationic antimicrobial peptide polymyxin B. However, when grown as adjacent colonies on SWT agar plates, *V. parahaemolyticus* inhibits the growth of *V. fischeri.* Perhaps this model can be manipulated to discover physiological conditions under which *V. fischeri* is able to survive the chemical inhibition of *V. parahaemolyticus*, thereby enabling further characterization of the mechanism by which *V. fischeri* establishes dominance over *V. parahaemolyticus* in the mucus environment.

2. **Is the pH of the immature symbiotic crypts acidic, and is there evidence of diel fluctuations in pH?**

   The stages of light-organ crypt development are just beginning to be characterized beyond the first days of symbiosis. A remaining question regarding this development is whether the initial environment of the light-organ crypts is characterized by diel chemical and physiological rhythms. If the pH is indeed part of the diel symbiotic

rhythm early on, then this rhythm might modulate the activity of secreted host enzymes such as alkaline phosphatase (10), peptidoglycan recognition protein 2 (11), hemocyanin (12), and chitinase (1), in the context of the immature crypts. Elucidation of the transcriptional regulation of *eptA*, and other pH-responsive genes identified in **Chapter 2** will help define robust transcriptional biomarkers to detect subtle diel variations in light-organ crypt chemistry. Specifically, the transcription of pH-responsive genes *eptA* (VF_A0210), *ompU* (VF_0475), VF_1795 and VF_1010 may be compared at points over the diel cycle, or perhaps in different genetic backgrounds, to detect acidification. The recent adaption of hybridization chain reaction (HCR) for use in the squid-vibrio model (13), will enable the use of these biomarkers to detect heterogeneous acidification of the light-organ crypts, as well as diel variations in crypt pH.

3. **What is the mechanism by which non-bioluminescent *V. fischeri* is detected and eliminated by the host?**

In **Chapter 3** of this dissertation, a model is proposed linking the continuous production of bioluminescence by *V. fischeri* to persistence in the light-organ crypts. A prediction of the requirement for bioluminescence is that a subset of symbiont cells might 'cheat' their neighbors, by directing the metabolic resources toward growth rather than bioluminescence. Remarkably, the host prevents the survival of even a few non-bioluminescent cells, suggesting that the strategy of host surveillance operates at the cellular level (7). The current model ties host selection to a substrate or product of

luciferase. Apart from bioluminescence, the consumption of oxygen, and the production of aliphatic acid present potential mechanisms of host surveillance. Insufficient oxygen consumption fuels the catalysis of the toxic melanin precursor dopaquinone from tyrosine derivatives by the host enzyme phenoloxidase (12). Aliphatic acid limitation leads to the accumulation of hydrogen peroxide, rather than bioluminescence and water, from the incomplete reduction of oxygen by luciferase (14), fueling production of hypochlorous acid by the host enzyme halide peroxidase (15). Phenoloxidase and halide peroxidase are abundant enzymes in the crypt matrix (12, 16). Moreover, the hydrogen-peroxide consuming enzyme catalase is required for *V. fischeri* to maintain a stable colonization of the light organ (17), and selective pressures in the light organ optimize aldehyde production in the symbiotic environment (18, 19). The genetic manipulation of *V. fischeri* to modulate oxygen consumption and aldehyde production, as well as the chemical inhibition of host halide peroxidase and phenoloxidase will provide opportunities to test these models of host surveillance.

4. **What aspects of symbiosis entrain the migratory rhythm of hemocytes to the light organ?** The description of a diel rhythm of hemocyte migration presented in **Chapter 4** of this dissertation raises several questions regarding the mechanisms underlying this rhythmic behavior. First, the cue required for symbiont-dependent hemocyte migration into the light-organ body is unidentified. **Appendix B** of this dissertation presents evidence that the migratory rhythm of hemocytes is not dependent on the production

of bioluminescence by the symbiont. Other migratory behaviors of hemocytes are attributed to MAMP signaling (20), thus, assessment of hemocyte migration in squid colonized by mutants that produce chemically altered MAMPS, such as the O-antigen-deficient *V. fischeri waaL* mutant (21), or aposymbiotic squid incubated with lipopolysaccharide (LPS) or peptidoglycan may be informative. Notably, the migration of hemocytes into the body of the light organ precedes dusk (**Chapter 4**). This is a period when the abundance of the host enzyme alkaline phosphatase decreases in the crypts (10). Alkaline phosphatase dephosphorylates LPS, reducing the reactivity of this MAMP. Thus, future studies of hemocyte migration should give priority to the testing of LPS-dependent signaling.

The migration of hemocytes is not only rhythmic, but is also symbiont-dependent. This observation leads to the question of how the symbionts contribute to the behavioral differences of hemocytes in immature and mature light organs. The presence of the symbiont apparently 'educates' host hemocytes to avoid phagocytosis (22), and hemocytes isolated from the circulation of the squid reveal proteomic differences that are symbiont-dependent (23). Moreover, the release of COS by hemocytes is a characteristic of the mature light-organ symbiosis (**Chapter 4**), suggesting that an aspect of hemocyte behavior (migration or the release of COS), is linked to development. In mammals, the circadian release of mature immune cells from bone marrow into circulation occurs at the beginning of the resting phase, and levels of pro-inflammatory cytokines peak at the beginning of the active phase (24). Thus, profiling the numbers of hemocytes present in the squid's circulation, as well as

the diel transcriptional and proteomic profiles of these cells in aposymbiotic and symbiotic adult squid, may help reveal the signaling responsible for diel migration. In addition, transcriptional and proteomic analysis of hemocytes and white body tissue (the hematopoietic organ), in which the environmental light cue is manipulated, will help to reveal whether the migration of hemocytes is a circadian behavior and, if so, where the rhythm is entrained.

5. **Does oxygen availability and host tissue redox balance cycle as part of the daily chemical rhythm of symbiosis?**

   A prediction of **Chapters 4 and 5** of this dissertation, as well as of transcriptional profiling of the symbiont during the mature diel cycle (25), is that catabolism of COS by *V. fischeri* might modulate the availability and consumption of oxygen in the crypts. In **Appendix B** of this dissertation, approaches to characterize host and symbiont oxygen consumption are developed. A preliminary observation from this work is that the epithelial tissue lining the crypts of the mature light-organ apparently experience hypoxia at night: the stage of the mature diel cycle where the crypts acidify, and consumption of oxygen by symbiont bioluminescence is predicted to pull oxygen out of the circulation, much like a sink (12). The hypoxic state of the crypt epithelium at night suggests that these tissues may be subject to rhythmic, redox-responsive regulation by proteins such as peroxiredoxin (26, 27). Future characterization of symbiont oxygen consumption, as well as host-tissue redox balance, will help reveal additional rhythmic attributes of host tissue chemistry, and

perhaps shed light on the remarkable stability with which *V. fischeri* is maintained in the light organ throughout the lifetime of the squid.

REFERENCES

1. Kremer N*, et al.* (2013) Initial symbiont contact orchestrates host-organ-wide transcriptional changes that prime tissue colonization. *Cell Host Microbe* 14(2):183-194.

2. Nyholm SV & McFall-Ngai MJ (2003) Dominance of *Vibrio fischeri* in secreted mucus outside the light organ of *Euprymna scolopes*: the first site of symbiont specificity. *Appl Environ Microbiol* 69(7):3932-3937.

3. Cullen T*, et al.* (2015) Antimicrobial peptide resistance mediates resilience of prominent gut commensals during inflammation. *Science* 347(6218):170-175.

4. Fraune S & Bosch TC (2007) Long-term maintenance of species-specific bacterial microbiota in the basal metazoan Hydra. *Proc Natl Acad Sci U S A* 104(32):13146-13151.

5. Koropatnick TA*, et al.* (2004) Microbial factor-mediated development in a host-bacterial mutualism. *Science* 306(5699):1186-1188.

6. Visick KL, Foster J, Doino J, McFall-Ngai M, & Ruby EG (2000) *Vibrio fischeri lux* genes play an important role in colonization and development of the host light organ. *J Bacteriol* 182(16):4578-4586.

7. Koch EJ, Miyashiro TI, McFall-Ngai MJ, & Ruby EG (2013) Features governing symbiont persistence in the squid-vibrio association. *Mol Ecol* (doi:10.1111/mec.12474).

8. Heath-Heckman EA*, et al.* (2013) Bacterial bioluminescence regulates expression of a host cryptochrome gene in the squid-vibrio symbiosis. *mBio* 4(2).

9. Nyholm SV, Stabb EV, Ruby EG, & McFall-Ngai MJ (2000) Establishment of an animal–bacterial association: recruiting symbiotic vibrios from the environment. *Proc Natl Acad Sci U S A* 97(18):10231-10235.

10. Rader BA, Kremer N, Apicella MA, Goldman WE, & McFall-Ngai MJ (2012) Modulation of symbiont lipid A signaling by host alkaline phosphatases in the squid-vibrio symbiosis. *mBio* 3(3).

11. Troll JV*, et al.* (2010) Taming the symbiont for coexistence: a host PGRP neutralizes a bacterial symbiont toxin. *Environ Microbiol* 12(8):2190-2203.

12. Kremer N*, et al.* (2014) The dual nature of haemocyanin in the establishment and persistence of the squid–vibrio symbiosis. *Proc. R. Soc. B* 281(1785).

13. Nikolakakis K, Lehnert E, McFall-Ngai M, & Ruby E (2015) Using hybridization chain-reaction fluorescent in situ hybridization (HCR-FISH) to track gene expression by both partners during initiation of symbiosis. *Appl Environ Microbiol*:AEM. 00890-00815.

14. Hastings J & Balny C (1975) The oxygenated bacterial luciferase-flavin intermediate. reaction products via the light and dark pathways. *J Biol Chem* 250(18):7288-7293.

15. Small AL & McFall-Ngai MJ (1999) Halide peroxidase in tissues that interact with bacteria in the host squid *Euprymna scolopes*. *J Cell Biochem* 72(4):445-457.

16. Weis VM, Small AL, & McFall-Ngai MJ (1996) A peroxidase related to the mammalian antimicrobial protein myeloperoxidase in the euprymna-vibrio mutualism. *Proc Natl Acad Sci U S A* 93(24):13683-13688.

17. Visick KL & Ruby EG (1998) The periplasmic, group III catalase of *Vibrio fischeri* is required for normal symbiotic competence and is induced both by oxidative stress and by approach to stationary phase. *J Bacteriol* 180(8):2087-2092.

18. Boettcher KJ & Ruby EG (1990) Depressed light emission by symbiotic *Vibrio fischeri* of the sepiolid squid *Euprymna scolopes*. *J Bacteriol* 172(7):3701-3706.

19. Schuster BM, Perry LA, Cooper VS, & Whistler CA (2010) Breaking the language barrier: experimental evolution of non-native *Vibrio fischeri* in squid tailors luminescence to the host. *Symbiosis* 51(1):85-96.

20. Koropatnick TA, Kimbell JR, & McFall-Ngai MJ (2007) Responses of host hemocytes during the initiation of the squid-vibrio symbiosis. *Biol Bull* 212(1):29-39.

21. Post DM*, et al.* (2012) O-antigen and core carbohydrate of *Vibrio fischeri* lipopolysaccharide composition and analysis of their role in *Euprymna scolopes* light organ colonization. *J Biol Chem* 287(11):8515-8530.

22. Nyholm SV, Stewart JJ, Ruby EG, & McFall-Ngai MJ (2009) Recognition between symbiotic *Vibrio fischeri* and the haemocytes of *Euprymna scolopes*. *Environ Microbiol* 11(2):483-493.

23. Schleicher TR, VerBerkmoes NC, Shah M, & Nyholm SV (2014) Colonization state influences the hemocyte proteome in a beneficial squid–vibrio symbiosis. *Mol Cell Proteom* 13(10):2673-2686.

24. Scheiermann C, Kunisaki Y, & Frenette PS (2013) Circadian control of the immune system. *Nat Rev Immunol* 13:190-198.

25. Wier AM*, et al.* (2010) Transcriptional patterns in both host and bacterium underlie a daily rhythm of anatomical and metabolic change in a beneficial symbiosis. *Proc Natl Acad Sci U S A* 107(5):2259-2264.

26. Edgar RS*, et al.* (2012) Peroxiredoxins are conserved markers of circadian rhythms. *Nature* 485(7399):459-464.

27. Hoyle NP & O'Neill JS (2014) Oxidation-reduction cycles of peroxiredoxin proteins and non-transcriptional aspects of timekeeping. *Biochemistry*. 54(2):184-93.

Appendix A

Additional Scientific Contributions

In addition to the work described within this thesis, I performed research that was incorporated into the following four publications:

1. Miyashiro T, Klein W, Oehlert D, Cao X, Schwartzman J, Ruby EG. The *N*-acetyl-d-glucosamine repressor NagC of *Vibrio fischeri* facilitates colonization of *Euprymna scolopes*. Mol Microbiol. 2011;82(4):894-903.

I constructed and characterized a Δ*nagB* mutant, and characterized the growth of other mutants described in the paper on chitin oligosaccharides as a sole source of carbon.

2. Kremer N, Philipp EE, Carpentier M-C, Brennan CA, Kraemer L, Altura MA, et al. Initial symbiont contact orchestrates host-organ-wide transcriptional changes that prime tissue colonization. Cell Host Microbe. 2013;14(2):183-94.

I developed a method to measure the pH of the mucus outside of the light organ, assisted in sample collection for a transcriptional profiling experiment, and assessed the induction of an early symbiont-dependent host phenotype (hemocyte trafficking).

3. Kremer N, Schwartzman J, Augustin R, Zhou L, Ruby EG, Hourdez S, et al. The dual nature of haemocyanin in the establishment and persistence of the squid–Vibrio symbiosis. Proc R Soc B. 2014;281(1785).

I developed a method to measure the pH of the light-organ crypts and hemolymph of adult squid. I applied this method to assess the pH of crypts and hemolymph just before dawn.

4. JA Schwartzman and EG Ruby. Stress as a cue for microbial symbionts (Tentative title). Invited Review, *Trends in Microbiology.* To be submitted August 2015.

Appendix B

Assessment of diel hemocyte trafficking in light organs colonized by Δ*lux* and wild-type *V. fischeri*

JAS designed the experiment, performed the experiment and wrote the appendix.

A remaining question from Chapter 5 of this dissertation is: what is the cue for diel trafficking of hemocytes? Rhythmic attributes of light-organ physiology include the growth of the symbiont population (1), the bioluminescent rhythm (2), transcription of alkaline phosphatase (3), and bioluminescence-entrained transcriptional oscillation of the peripheral circadian cryptochrome gene *escry1* (4). In this section, I test the hypothesis that the migration of hemocytes is related to production of bioluminescence by the symbiont.

I compared hemocyte trafficking in light-organs colonized by wild-type *V. fischeri* strain ES114, the bioluminescence-deficient Δ*luxCDABEG* mutant EVS102 (5), or no symbiont (**Fig. B-1**). If colonized, animals were exposed to ~5,000 CFU/mL overnight. The collection of samples, labeling of hemocytes, and enumeration of hemocytes was performed as described previously (Chapter 5, (6)). Briefly, permeabilized light organs were stained with 1mg/mL FITC-DNAseI (globular-actin specific) for 3 days at 4 °C, and 0.025µg/mL rhodamine phalloidin (filamentous actin) overnight at 4 °C in marine phosphate buffered saline (50 mM Phosphate Buffer, pH 7.4, 0.45 M NaCl), containing 1% triton-X. Hemocytes were detected by confocal microscopy as cells enriched in globular actin.

The number of hemocytes present in both wild-type and Δ*lux* colonized light-organ tissues was greatest just prior to dusk (**Fig. B-1**). I noted only a small decrease in the number of hemocytes infiltrating Δ*lux* light organs before dusk, relative to wild-type colonized light organs. As previously observed in Chapter 5, the number of hemocytes per light organ was lower prior to dawn, and counts were comparable among animals colonized wild-type, Δ*lux* and uncolonized animals. I noted no differences in the distribution of hemocytes in wild-type and Δ*lux*-colonized light organs, *i.e.* there was no evidence that

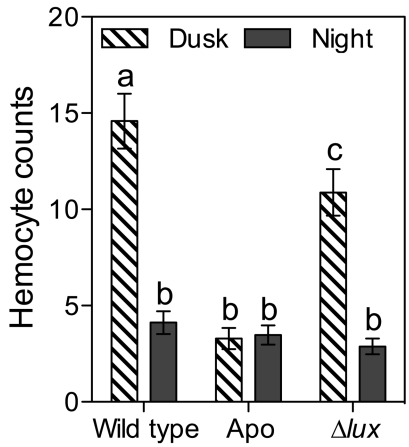

Figure B-1. Migration of hemocytes into post-24 h old light organ tissues. Samples were collected at dusk (10 h post dawn), at night (22 h post dawn). 'a', 'b' and 'c' indicate different mean hemocyte counts, determined by two-factor ANOVA with post-hoc Bonferroni multiple comparisons tests, n=16 light organs per sample.

hemocytes trafficked to Δ*lux*-colonized crypts in greater numbers than wild-type colonized crypts. Collectively, these observations suggest that the daily infiltration of hemocytes into light-organ tissues just prior to dusk is a phenotype largely independent of symbiont bioluminescence.

Bioluminescence also makes a small contribution to the trafficking of hemocytes into accessory appendage of the light organ during the first stages of colonization (7), although the predominant signals are lipopolysaccharide (LPS) and peptidoglycan (8). Notably, the *E. scolopes* gene encoding the homolog of alkaline phosphatase decreases just before dusk, leading to a decrease in enzyme levels secreted into the crypts (3). This cycle mirrors the influx of hemocytes into the light organ tissues. Alkaline phosphatase dephosphorylates LPS, making this microbe-associated molecular pattern less able to elicit host responses (3). Thus, a logical hypothesis to direct future research would be to determine whether the rhythm of hemocyte migration is linked to a transient increase in LPS just before dusk.

Mutants with decreased, or increased shedding of LPS may be effectively used to test this hypothesis. The lysine auxotroph *lysA*, which is impaired in colonization of the crypts (9), could also be a useful control to assess cell-density dependence of hemocyte trafficking. Alternately, the chemotaxis of isolated hemocytes towards chemical compounds such as LPS might be used to further characterize the basis of the daily migratory rhythm. In summary, both genetic and chemical approaches may be readily used to characterize this emerging immune rhythm.

REFERENCES

1. Ruby EG & Asato LM (1993) Growth and flagellation of Vibrio fischeri during initiation of the sepiolid squid light organ symbiosis. *Arch Microbiol* 159(2):160-167.

2. Boettcher K, Ruby E, & McFall-Ngai M (1996) Bioluminescence in the symbiotic squid *Euprymna scolopes* is controlled by a daily biological rhythm. *J Comp Physiol* 179(1):65-73.

3. Rader BA, Kremer N, Apicella MA, Goldman WE, & McFall-Ngai MJ (2012) Modulation of symbiont lipid A signaling by host alkaline phosphatases in the squid-vibrio symbiosis. *mBio* 3(3).

4. Heath-Heckman EA*, et al.* (2013) Bacterial Bioluminescence Regulates Expression of a Host Cryptochrome Gene in the Squid-Vibrio Symbiosis. *mBio* 4(2).

5. Bose JL, Rosenberg CS, & Stabb EV (2008) Effects of *luxCDABEG* induction in *Vibrio fischeri*: enhancement of symbiotic colonization and conditional attenuation of growth in culture. *Arch Microbiol* 190(2):169-183.

6. Schwartzman JA*, et al.* (2015) The chemistry of negotiation: Rhythmic, glycan-driven acidification in a symbiotic conversation. *Proceedings of the National Academy of Sciences* 112(2):566-571.

7. Koropatnick TA, Kimbell JR, & McFall-Ngai MJ (2007) Responses of host hemocytes during the initiation of the squid-Vibrio symbiosis. *Biol Bull* 212(1):29-39.

8. Koropatnick TA*, et al.* (2004) Microbial factor-mediated development in a host-bacterial mutualism. *Science* 306(5699):1186-1188.

9. Graf J & Ruby EG (1998) Host-derived amino acids support the proliferation of symbiotic bacteria. *Proc Natl Acad Sci U S A* 95(4):1818-1822.

Appendix C

Tools to characterize oxygen availability in symbiosis.

JAS designed and performed the experiments, and wrote the chapter.

SUMMARY

The temporal and developmental regulation of oxygen availability is a central prediction of the models presented in this thesis. Moving forward, it will be necessary to measure oxygen availability in the light-organ crypts in order to test and expand upon these models. This appendix describes several methods developed to approach the detection of oxygen in the light-organ crypts.

Measurement of hypoxia in host tissues.

Acidification in the light-organ crypts decreases the affinity of the carrier protein hemocyanin for oxygen (1). A prediction from this observation is that the delivery of oxygen to the host tissues will be disrupted, leading to hypoxia. To characterize oxygenation of the crypt epithelium, we performed an *in vivo* labeling experiment, using the oxygen-sensitive chemical marker pimonidazole hydrochloride (PIM) (2). PIM is a 2-nitroimidazole that requires the partial reduction of the nitro group on the azide moiety to react with protein thiol groups and form an adduct (3). PIM adducts are a non-native epitope that may be recognized by a monoclonal antibody, enabling the detection of PIM *via* immunocytochemistry (4). The reduction of the nitro group requires cytoplasmic NAD(P)H. In most eukaryotic cells, the amount of PIM activation is proportional to the competition between NAD(P)H and oxygen (**Fig. C1-*A***), and PIM labeling occurs if intracellular oxygen tensions are below 10 mmHg (5). Thus, PIM has been broadly used as a marker of tissue hypoxia, particularly in field of cancer biology.

To deliver the PIM to the light organ of live squid, we injected the compound into the cephalic vessel (1). We collected PIM-labeled samples of symbiont-associated light-organ tissue during the day, and at night. Tissue samples were collected from the gills to ensure that any PIM

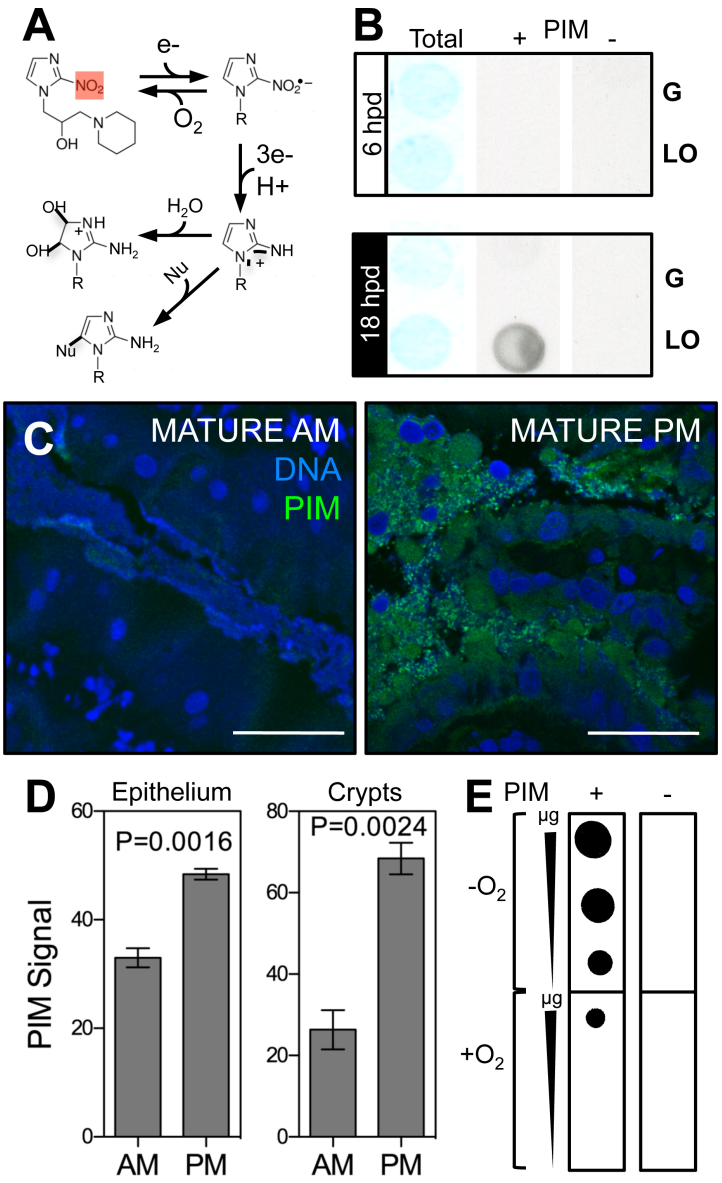
A
e-
O_2
3e-
H+
H_2O
Nu
B
Total
+ PIM -
6 hpd
18 hpd
G
LO
C
MATURE AM
DNA
PIM
MATURE PM
D
Epithelium
Crypts
P=0.0016
P=0.0024
PIM Signal
AM
PM
E
PIM
+
-
µg
$-O_2$
$+O_2$

Figure C-1. PIM labeling of host and symbiont proteins *A*) Mechanism of PIM adduct formation (modified from reference (2). To activate PIM, the nitro group (highlighted in red), must undergo a 4-electron reduction. Oxygen competes with the addition of the first electron to block reduction of the nitro group. Activated PIM reacts with nucleophilic biomolecules, such as the sulfhydryl groups of proteins, or water. The anti-PIM mouse monoclonal antibody recognizes the epitope created by modification of protein sulfhydryl groups by PIM. ***B***) Immunoblot of 5µg total protein isolated from mature squid during the day (6 h post dawn, hpd), or at night (18 hpd). Total protein (Total) was spotted onto Whatman paper, and stained to qualitatively control for the spotting of equal amounts of protein among conditison. PIM labeling was compared between gill (G), and symbiont-associated light-organ tissue (LO). To control for non-specific binding of the anti-PIM antibody, signal was compared between tissues isolated from squid injected with PIM (+) or a buffer-only vehicle control (-). Data are representative of independent experiments using tissue from three squid. ***C-D***) Fluorescence immunocytochemistry of sectioned light-organ tissues. DNA was stained with TOTO-3 iodide, which labels visualize host nuclei and symbiont cells. Time points compared are the same as in (*B*). Scale bar represents 20 µm. Signal from light-organ epithelium and crypts is quantified in (*D*), error bars are SEM, n=4. T-tests were used to compare mean signal intensity. ***E***) Detection of PIM modification by cultured *V. fischeri.* Total protein isolated from cells grown with ($+O_2$) and without ($-O_2$) oxygen, and with (+) and without (-) the same concentration of PIM used to inject squid. 5, 2.5 and 1.25 µg of total protein from each condition was spotted onto membranes. Blots are representative of results from 3 biological replicates.

labeling detected in the light organ did not result from systemic oxygen deprivation. Immunoblots were used to detect of adducts in total protein (**Fig. C1-*B***). A control tissue sample, not injected with PIM, lacked detectable signal, indicating that the antibody does not cross-react with squid or symbiont proteins. In addition, we detected only a small amount of PIM labeling of gill tissue, and this signal was consistent between day and night (**Fig. C-1*B***), suggesting that PIM does not label highly oxygenated squid tissues. Samples of light-organ tissue collected at night, but not during the day, revealed robust PIM labeling, in comparison to gill tissue samples (**Fig. C-1*B***). Thus, PIM labeling is sensitive to day/night differences in the chemistry of symbiont-associated tissues.

To visualize the location of PIM labeling in light-organ tissues, we performed immunocytochemistry of paraffin-embedded 5µm tissue sections, and analyzed the sections by confocal microscopy. These studies revealed that the PIM labeling localized to epithelial cells in direct contact with the symbiont (**Fig. C-1*C***). This staining excluded the nucleus, which is consistent with the NAD(P)H-dependent mechanism of PIM adduct formation. The increased signal from the crypt epithelial cells at night is suggestive of hypoxia. Consistent with the immunoblot results, PIM labeling in the crypt epithelial tissues was significantly greater at night than during the day (**Fig. C1-*D***). Surprisingly, PIM labeling was also observed in the crypt lumen (a matrix containing symbionts, secreted host enzymes, intact host cells and cellular debris) (**Fig. C1-*C***). The signal observed in the crypt lumen was also significantly greater at night than during the day (**Fig. C1-*D***). Collectively, the imaging studies suggest that PIM labeling of crypt epithelium, and the crypt lumen, are sensitive to diel changes in tissue chemistry.

To determine the origin of PIM labeling in the crypts, we isolated total protein from *V. fischeri,* grown under oxic and anoxic conditions. Upon immunoblot, we noted a robust PIM signal from anoxic cells (**Fig. C1-*E***). This signal was not present in well-aerated cultures (225 rpm shaking, 5 mL medium in a 125-mL flask), suggesting that modification of PIM by *V. fischeri* occurs under anoxic conditions. It is tempting to conclude that PIM labeling of *V. fischeri* reflects hypoxia, however, there is precedent for imidazole activation by oxygen-independent eukaryotic and prokaryotic nitroreductases (2, 6). For example, the oxygen-insensitive NADPH nitroreductase of *Helicobacter pylori* activates the 2-imidazole metronidazole (6). *V. fischeri* encodes two putative oxygen-insensitive nitroreductases: *nsfA* (VF_A0965), and *nsfB* (VF_A0691). Thus, the modification of PIM by *V. fischeri* under anoxic, but not oxic conditions, only indicates that anoxia is one possible explanation of PIM labeling.

There are at least two hypotheses to explore that could lead to oxygen-independent PIM labeling of *V. fischeri*. First, NAD(P)H is predicted to accumulate as during aerobic fermentation of amino sugars by *V. fischeri* (Chapter 4), indicating that the catabolism of amino sugars, even in the presence of oxygen, may yield sufficient reducing power to support PIM labeling in the presence of oxygen. Second, *V. fischeri* anaerobically respires nitrate, fumarate, and TMAO (7), suggesting that some anoxic environments may not correlate with elevated NAD(P)H. Moreover, nitric oxide inhibits aerobic respiration in *V. fischeri (8),* and could confound correlation of *V. fischeri* PIM labeling with intracellular hypoxia. The ability to attribute PIM labeling to any set of these physiological states would inform the understanding of crypt chemistry.

If PIM labeling of the symbiont in the nocturnal crypts is linked to intracellular oxygen tensions, then this presents a paradox: why do symbionts in the crypt modify PIM at night, but not during the day? The symbiont is highly bioluminescent at night (9), and the enzymatic

process that produces bioluminescence consumes oxygen. Proteomic analysis of the crypt contents has revealed abundant enzymes associated with oxidative stress, and the nocturnal acidification of the crypts is predicted to increase oxygen delivery to the symbiont (1). In contrast, the *V. fischeri* is predicted to experience oxygen limitation during the day. Transcriptional studies suggest that the symbiont responds to oxygen limitation during this period, and may rely on anaerobic respiration to remain metabolically active (10). In summary, detailed characterization of PIM as a marker for *V. fischeri* metabolic activity, paired with alternative approaches such as the use of HCR-FISH to detect oxygen-sensitive transcripts (Chapter 3), will provide further insight into the biology underlying the diel pattern of PIM labeling in host and symbiotic tissues.

Defining transcriptional biomarkers of symbiont oxygen limitation.

A common strategy to describe the environment of a host-associated microbe is by monitoring the transcriptional response of reporter genes (11, 12). However, the quality of such biomarkers is dependent on the robust characterization of the environmental cues and transcription factors that coordinate gene expression. In this section, we describe work that has been done to define transcriptional reporters of oxygen availability in the light-organ crypts.

V. fischeri encodes several cytochrome oxidases (13), including two cytochrome c-type oxidases: *ccoNOQPS* (VF1299-1302, VF1306), and *ccmIHGEA* (VF1816-18, VF1820, VF1824), and a cytochrome d-type oxidase *cydAB* (VF0953-4). The expression of cytochrome oxidase *cydAB* may contribute to the stability of *V. fischeri* in the immature crypts (8), although it is also essential for aerobic respiration and survival in seawater, complicating colonization studies in the animal. To determine whether *cydAB* is expressed in symbiosis, we constructed a fluorescent transcriptional reporter construct, and characterized the activity of the construct in

culture. This construct uses the *tetA* promoter to constitutively express the red fluorescent protein mCherry, and a promoter of interest to express green fluorescent protein (GFP)(14). Thus, the ratio of the two fluorescent signals can be used to detect a change in activity of the promoter of interest. Upon exposure to oxic conditions in seawater-tryptone (SWT) medium, we found that the *cydAB* promoter was activated approximately 4-fold (**Fig. C-2*A***). The activity of this promoter was partially repressed by the transcription factor ArcAB: a histidine-kinase response-regulator pair that responds to the cellular redox status (15). Notably, overflow metabolism, resulting from a surplus of carbon, can lead to aerobic fermentation: potentially impacting the cellular redox status and regulation by ArcAB (16). Thus, more detailed studies of *cydAB* promoter activity in response to growth rate, nutrient status, and oxygen-independent contributions to cellular redox status will be needed to disambiguate oxygen-related and unrelated regulation of *cydAB* promoter activity. A conservative interpretation is that *cydAB* promoter activity is positively correlated with an oxidative environment, which can be caused by the presence of oxygen.

To determine whether the symbiotic environment changes over the first days of light-organ development in a manner that affects *cydAB* promoter activity, we colonized squid with wild-type *V. fischeri* carrying the fluorescent reporter construct, and measured signal from the crypts using epifluorescent microscopy between 24 and 48 h post-colonization (**Fig. C-2*B***). To control for potential effects of oxygen availability on the fluorescence of the green-fluorescent protein label (17), the light-organs were preserved by fixation in paraformaldehyde prior to analysis. We observed a moderate, and gradual (>2-fold) decrease in *cydA* promoter activity between 24 and 48 h. A longer time-course in the squid will be necessary to determine if the

Table C-1 Oxygen-responsive transcripts

VFID	Gene name	Chit +- O2	Gly +- O2
VF0032	Thiamine biosynthesis protein ThiC	6.9	5.5
VF0033	Thiamin-phosphate pyrophosphorylase (EC 2.5.1.3)	79.3	41.9
VF0034	Molybdopterin biosynthesis protein MoeB	63.1	23.2
VF0035	Thiazole biosynthesis protein ThiG	83.6	53.3
VF0036	ThiH protein	49.0	37.1
VF0267	Thiamine-binding protein	23.9	16.2
VF0281	Conserved hypothetical protein	31.1	11.7
VF0317	Acetyltransferase (EC 2.3.1.-)	-3.8	-3.4
VF0339	Serine--pyruvate aminotransferase (EC 2.6.1.51)	3.7	6.2
VF0451	Hypothetical protein	-3.0	-3.9
VF0492	Putative protease yhbV precursor (EC 3.4.-.-)	-4.4	-5.6
VF0495	Sterol binding protein	4.3	3.6
VF0616	Rrf2 family protein	-3.4	-18.6
VF0617	Selenocysteine lyase (EC 4.4.1.16)	-9.5	-3.5
VF0619	HesB protein family	-3.4	-5.1
VF0621	Chaperone protein HscA	4.8	3.8
VF0776	Nitrite reductase [NAD(P)H] large subunit (EC 1.7.1.4)	4.2	5.5
VF0780	CopG protein	4.2	5.9
VF0878	Multidrug resistance protein A	-19.4	-7.2
VF0920	SSU ribosomal protein S4P	-3.6	-4.4
VF0927	Hypothetical protein	3.5	10.5
VF0942	Molybdopterin converting factor, small subunit	-3.4	-3.4
VF1052	Transporter, Divalent Anion:Sodium Symporter family	37.5	13.2
VF1053	Sensory transduction protein kinase (EC 2.7.3.-)	3.1	6.0
VF1060	Peptidase T (EC 3.4.11.-)	-5.1	-12.3
VF1061	Anaerobic C4-dicarboxylate transporter	-13.9	-22.7
VF1089	Immunogenic protein	-4.8	-4.9
VF1090	Transporter	-42.8	-91.2
VF1151	Hypothetical protein	-11.4	-13.4
VF1155	Proton glutamate symport protein	8.9	4.1
VF1188	Alcohol dehydrogenase II (EC 1.1.1.1)	5.5	5.2
VF1190	Hypothetical protein	103.3	33.8
VF1191	Hypothetical protein	3.7	3.2
VF1192	Hypothetical protein	-34.2	-20.1
VF1193	Hypothetical protein	254.0	53.3
VF1220	Hemin transport system ATP-binding protein HmuV	31.5	22.5
VF1221	Hemin transport system permease protein HmuU	18.4	12.2
VF1222	Hemin-binding periplasmic protein HmuT precursor HmuT	31.8	17.1
VF1223	TolR protein	25.3	26.7
VF1224	TolQ protein	73.8	89.1
VF1225	TonB protein	62.3	51.6
VF1226	Coproporphyrinogen oxidase, anaerobic (EC 1.-.-.-)	143.6	63.3

VFID	Gene name	Chit +- O2	Gly +- O2
VF1227	Hypothetical protein	113.8	65.1
VF1228	Hypothetical protein	180.0	154.4
VF1234	Hemin receptor	114.4	67.8
VF1262	Glutaredoxin	150.0	66.2
VF1375	Kinase autophosphorylation inhibitor KipI	30.7	16.9
VF1376	Lactam utilization protein LAMB	74.3	30.3
VF1377	Hypothetical cytosolic protein	3.2	3.5
VF1451	NUCLEASE	-25.6	-7.5
VF1472	Zinc finger protein	-33.8	-10.2
VF1494	Transporter	-3.7	-24.5
VF1510	Transcriptional regulator	3.4	3.0
VF1529	Hypothetical protein	7.9	4.1
VF1551	NrfD protein	-5.1	-7.7
VF1552	Thiosulfate reductase electron transport subunit (EC 1.8.99.-)	-3.3	-6.3
VF1553	Cytochrome c-type protein NrfB	-10.1	-22.1
VF1554	Cytochrome c552 (EC 1.7.2.2)	-3.8	-22.1
VF1615	Hypothetical protein	-4.6	-23.2
VF1630	Na(+) H(+) antiporter	-4.0	-24.2
VF1724	Anaerobic C4-dicarboxylate transporter	-8.9	-40.9
VF1730	Sodium proline symporter	3.4	6.4
VF1798	Chloride channel protein	-6.3	-5.1
VF1863	Flagellin, FlaD	5.8	4.3
VF1866	Flagellin, FlaA	-19.1	-11.6
VF1889	Outer membrane porin protein precursor	-3.6	-6.2
VF1972	Isocitrate lyase (EC 4.1.3.1)	-20.9	-3.9
VF2055	Cytochrome c peroxidase (EC 1.11.1.5)	4.8	3.9
VF2064	Anaerobic C4-dicarboxylate transporter	13.1	5.5
VF2115	Formate acetyltransferase (EC 2.3.1.54)	-4.2	-5.4
VF2123	Fe-S OXIDOREDUCTASE (1.8.-.-)	-6.7	-3.8
VF2141	Chitooligosaccharide transport system permease protein	-4.6	-5.5
VF2150	Iron(III)-transport system permease protein SfuB	-4.3	-3.4
VF2151	Iron(III)-binding protein	-9.5	-7.6
VF2335	Fumarate reductase iron-sulfur protein (EC 1.3.99.1)	-6.9	-26.5
VF2336	Fumarate reductase (EC 1.3.99.1)	-5.9	-7.5
VF2337	Fumarate reductase, 13 kDa hydrophobic protein	-5.5	-8.4
VF2376	Hypothetical protein	-3.5	-5.0
VF2377	Hypothetical protein	-4.5	-5.3
VF2378	Sodium:solute symporter family protein	-4.1	-5.1
VF2381	Cyclic nucleotide binding protein 2 CBS domains	55.5	17.8
VF2382	DNA polymerase III, epsilon chain	8.6	3.6
VF2383	Acetyl-coenzyme A synthetase (EC 6.2.1.1)	23.2	10.5
VF2384	Acetyl-coenzyme A synthetase	69.5	11.3
VF2441	Hypothetical protein	23.2	5.6
VFA0004	Peptidase T (EC 3.4.11.-)	20.0	11.6

VFID	Gene name	Chit +- O2	Gly +- O2
VFA0013	Chitin-binding protein	21.6	8.8
VFA0073	Di- tripeptide transporter	-3.5	-4.8
VFA0080	Anaerobic DMSO reductase chain C (EC 1.8.99.-)	3.5	4.6
VFA0081	Anaerobic DMSO reductase chain B (EC 1.8.99.-)	-16.0	-20.1
VFA0082	Anaerobic DMSO reductase chain A (EC 1.8.99.-)	-8.5	-6.8
VFA0083	Anaerobic DMSO reductase chain ynfI (EC 1.8.99.-)	-57.2	-18.7
VFA0084	Ferredoxin-type protein NapF	-53.5	-13.2
VFA0122	Hypothetical protein	-89.7	-42.9
VFA0123	Di- tripeptide transporter	-29.8	-75.6
VFA0124	Di- tripeptide transporter	-9.3	-13.0
VFA0131	CAAX amino terminal protease family	-10.5	-19.0
VFA0156	Hypothetical conserved protein	-19.0	-13.6
VFA0157	Permease	-12.6	-8.8
VFA0158	Ferrichrome transport ATP-binding protein FhuC	8.3	5.9
VFA0159	Ferrichrome-binding protein	5.6	4.6
VFA0160	Ferrichrome transport system permease protein FhuB	26.8	16.8
VFA0161	Aerobactin siderophore biosynthesis protein IucA (EC 6.-.-.-)	32.8	29.5
VFA0162	N(6)-hydroxylysine O-acetyltransferase (EC 2.3.1.102)	14.4	15.7
VFA0163	Siderophore biosynthesis IucC protein (EC 6.-.-.-)	13.4	10.4
VFA0164	L-lysine 6-monooxygenase (EC 1.14.13.59)	276.6	703.0
VFA0165	Ferric aerobactin receptor precursor	95.7	179.3
VFA0188	Trimethylamine-N-oxide reductase (EC 1.7.2.3)	93.4	179.0
VFA0189	Cytochrome c-type protein TorC	165.9	339.5
VFA0190	Hypothetical protein	119.6	136.9
VFA0191	FhuE receptor precursor	-18.2	-7.4
VFA0192	Hypothetical protein	-16.9	-8.1
VFA0193	TolQ protein TolR protein	13.4	26.6
VFA0194	TolQ protein	17.7	25.4
VFA0195	TolR protein	15.0	17.6
VFA0196	TonB protein	10.7	13.7
VFA0197	TPR domain protein	10.3	12.2
VFA0198	Transcriptional repressor	4.9	6.9
VFA0199	Oligosaccharide transport ATP-binding protein	5.2	7.1
VFA0200	Oligosaccharide transport ATP-binding protein	4.7	6.0
VFA0204	Hypothetical protein	6.8	4.8
VFA0205	Hypothetical membrane spanning protein	48.3	45.2
VFA0251	NADP-dependent formate dehydrogenase (EC 1.2.1.43)	121.5	189.0
VFA0259	Hypothetical transcriptional regulatory protein	-17.9	-20.4
VFA0274	Acyl-CoA desaturase (EC 1.14.19.1)	-4.0	-3.7
VFA0281	Anaerobic ribonucleoside-triphosphate reductase (EC 1.17.4.2)	-6.6	-3.1
VFA0287	Hypothetical protein	-3.1	-6.7
VFA0316	Hydroxymethylpyrimidine kinase (EC 2.7.1.49)	4.6	7.0
VFA0317	Hydroxymethylpyrimidine transport ATP-binding protein	-3.4	-6.8
VFA0318	Hydroxymethylpyrimidine transport system permease protein	-7.4	-3.1

VFID	Gene name	Chit +- O2	Gly +- O2
VFA0319	Hydroxymethylpyrimidine-binding protein	26.9	14.8
VFA0320	Transcriptional activator TenA	10.2	9.2
VFA0321	Hydroxyethylthiazole kinase (EC 2.7.1.50)	10.5	8.7
VFA0322	Thiamin-phosphate pyrophosphorylase (EC 2.5.1.3)	6.9	9.5
VFA0333	Protease II (EC 3.4.21.83)	8.8	10.2
VFA0363	Sodium proton-dependent alanine carrier protein	5.1	6.6
VFA0364	Transporter	3.5	5.6
VFA0371	Hypothetical protein	3.6	3.9
VFA0386	Formate transporter	4.8	4.2
VFA0502	Outer membrane protein	7.0	8.3
VFA0553	ATP-dependent RNA helicase	-4.7	-6.0
VFA0616	Hypothetical protein	-203	-178
VFA0642	Hypothetical protein	-9.2	-3.2
VFA0669	Hypothetical protein	-3.4	-4.9
VFA0756	Putative Lipoprotein	-15.3	-3.0
VFA0758	Hypothetical membrane protein	7.7	11.0
VFA0784	Ferrichrome-iron receptor	-9.9	-4.5
VFA0794	Acetate kinase (EC 2.7.2.1)	14.1	14.7
VFA0823	Vulnibactin utilization protein VIUB	6.3	5.0
VFA0824	Ferric anguibactin transport ATP-binding protein	5.1	4.1
VFA0827	Ferric anguibactin-binding protein	-23.7	-5.2
VFA0829	Sodium proline symporter	3.0	3.3
VFA0848	Hypothetical protein	13.8	7.6
VFA0876	Hypothetical protein	-7.6	-4.5
VFA0928	Hypothetical protein	14.2	31.0
VFA0929	Hypothetical protein	-3.4	-6.1
VFA0930	Carboxypeptidase G2 precursor (EC 3.4.17.11)	-23.5	-20.0
VFA0961	Hypothetical protein	-11.0	-14.6
VFA0962	Pyruvate formate-lyase activating enzyme (EC 1.97.1.4)	-5.3	-7.3
VFA0979	Conserved hypothetical protein	-4.0	-5.1
VFA0982	Hypothetical protein	-3.2	-7.1
VFA0983	Hypothetical protein	-3.4	-7.4
VFA1094	Cold shock protein	-28.0	-30.3
VFA1106	Hypothetical protein	5.8	4.1
VFA1108	Hypothetical protein	24.1	4.8
VFB22	Hypothetical protein	3.2	4.4
VFB23	Hypothetical protein	-3.4	-4.6
VFB47	Outer membrane protein	-3.3	-5.7
VFB48	Hypothetical protein	-3.2	-45.3
VFB49	Hypothetical protein	-3.2	-44.5
VFB51	Hypothetical protein	-4.2	-13.2
VFB52	Hypothetical protein	-3.2	-12.3
VFB53	Hypothetical protein	-3.3	-17.6

N=3 samples per condition. Chit, chitobiose; Gly, glycerol; $+O_2$, oxic; $-O_2$ anoxic. Gly $–O_2$ contains nitrate.

decrease in *cydAB* promoter activity is meaningful in the timeframe of light-organ morphogenesis, and whether this decrease reflects a change in the redox state of the crypts.

To define other candidate reporter genes to detect oxygen, we performed a global transcriptional analysis. Previous work demonstrated that growth on PTS-transported sugars, such as *N*-acetylglucosamine (GlcNAc) and glucose changes the consumption of oxygen by the *V. fischeri* (Chapter 3), leading us to suspect that carbon source might be a confounding factor in the selection of transcriptional biomarkers to detect extracellular oxygen. To control for the effect of carbon source, we assessed the transcriptional response of *V. fischeri* to oxygen during growth on chitobiose (PTS-transported), and glycerol (not PTS-transported) (**Table C-1**). The set of 192 genes that was differentially expressed more than 3-fold in response to oxygen under both conditions represent good candidates to be developed as transcriptional biomarkers of extracellular oxygen. The expression of 101 of these genes was greater in oxic conditions, while 91 genes showed greater expression under anoxic conditions. Thus, a robust reporter strategy could be developed to indicate both the presence and absence of oxygen. Particularly in a complex host environment, such a dual-reporter gene strategy could prove useful to characterize oxygen gradients in the crypts.

In summary, we have developed methods to testing the activity of reporter genes in response to oxygen, and other physiological inputs that can influence the cellular redox status. A method of monitoring promoter activity in immature squid has also been developed. In addition to the characterization of *cydA*, we present a list of candidate reporter genes that respond to both oxic and anoxic conditions, which can be used as a starting point to develop a more robust strategy to characterize extracellular oxygen availability in the light-organ crypts. Characterization of several reporter constructs will likely be a key to interpreting changes in

crypt oxygen availability. An important consideration is that low oxygen tensions are common in host environments (18). The current microarray analysis compares the presence and absence of oxygen; the oxic cultures were well aerated, but measurements of oxygen availability in these cultures were not made. A more detailed transcriptional study, using an oxygen electrode to quantify, and control for PO_2 during growth on a range of PTS and non-PTS carbon sources could help define more precise transcriptional biomarkers to characterize the oxygenation of the light-organ crypts. Such studies may also be useful to develop probes to assess the presence of heterogeneity of crypt oxygenation, such in a mixed colonization of wild-type and Δ*lux V. fischeri.*

Assessing aerobic respiration in symbiosis.

A complementary method to determine the physiological state of a symbiotic microbe is to assess the resistance of the microbe to a stress. This approach has been effectively used in the squid-vibrio symbiosis to detect acidification of the crypts *via* induction of the *V. fischeri* acid tolerance response (19). We applied the same approach to develop a method to test for aerobic respiration by the symbiont, taking inspiration from recent studies published by the Imlay and Lewis groups (20, 21). Briefly, the two groups demonstrated that the sensitivity of *E. coli* to the aminoglycoside antibiotic kanamycin is proportional to flux through aerobic respiration. Following the method developed by the Imlay group, we validated this observation in *V. fischeri* (**Fig. C-3**). The percent of viable cells detected in cultures of *V. fischeri* decreased over time in response to kanamycin exposure, in a manner dependent on the presence of a respiratory terminal electron acceptor, such as oxygen or nitrate (**Fig. C-3*A***). Thus, the respiration of *V. fischeri* strains during light organ colonization may be interrogated by measuring the kanamycin sensitivity of the microbes, although complementary approaches, such as the use of reporter

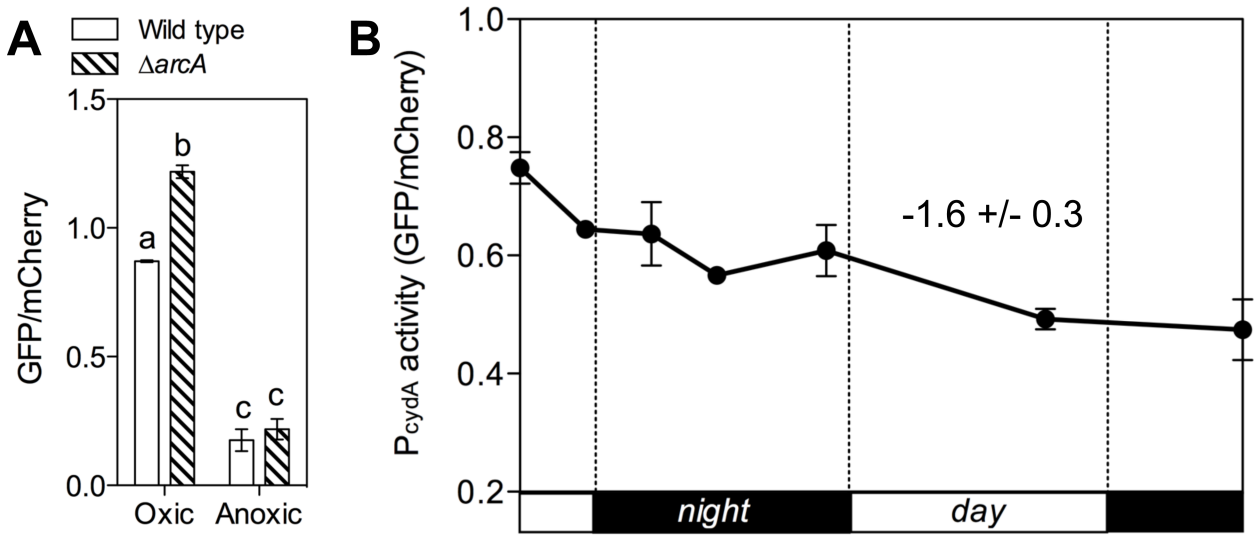

Figure C-2. Characterization of *cydAB* promoter activity in culture and squid. ***A)*** Activity of the fluorescent transcriptional reporter pJAS610 was monitored in wild-type (strain ES114), and Δ*arcA* (strain AMJ2) *V. fischeri.* The ratio of GFP to mCherry fluorescence was calculated for strains grown under oxic and anoxic conditions. 'a', 'b', and 'c' represent groups of statistically similar means, determined by Two-Way ANOVA with Bonferroni multiple comparison tests. Bars indicate SEM, n=3. ***B)*** Promoter activity of pJAS610 in post-24 h old light organs colonized by wild-type *V. fischeri.* Each point represents measurements from 4 individual light organs. Bars represent SEM. Fold change in reporter activity from start to finish is noted +/- standard deviation.

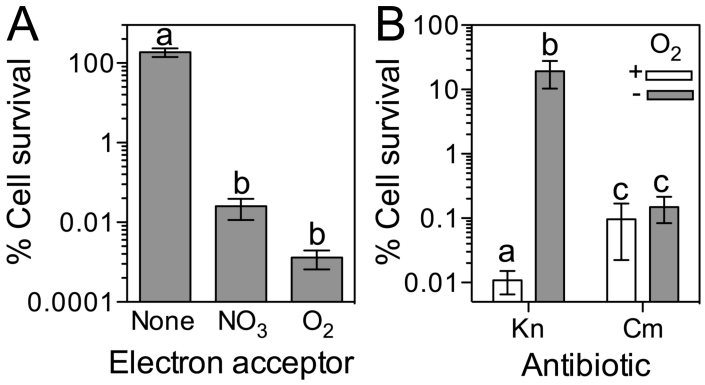

Figure C-3. Oxygen-dependence of *V. fischeri* antibiotic sensitivity Antibiotic resistance in groups 'a' and 'b' and 'c' are statistically significant means, determined by Two-Way ANOVA with Bonferroni multiple comparison tests, standard error calculated from n=3 biological replicates. ***A)*** Survival of *V. fischeri* after kanamycin exposure (50 mg/mL) in the presence of no terminal electron acceptor (None), 30 mM sodium nitrate, or oxygen. *B*) Comparison of *V fischeri* survival upon exposure to kanamycin or chloramphenicol under oxic ($+O_2$), and anoxic ($-O_2$), conditions.

genes, will be necessary to differentiate between the several substrates respired by *V. fischeri* (such as trimethylamine *N*-oxide, dimethylsulfoxide, fumarate, and oxygen (13)).

A straightforward approach to modifying this assay to detect symbiont respiration in the squid system would be to assess the ability of kanamycin to cure live squid of their symbiont. To control for changes in the efficiency of antibiotic delivery to the crypts caused by light-organ morphogenesis, and host development, it will be necessary to include a delivery control in the experimental design, such as a non-respiration dependent antibiotic. Chloramphenicol and gentamicin have both been used previously to cure the squid (22, 23). To define an appropriate 'delivery' control, we assessed the oxygen-dependence of *V. fischeri* chloramphenicol toxicity. The decrease in culture viability upon exposure to chloramphenicol was comparable in oxic and anoxic conditions (**Fig. C3-B**), suggesting that chloramphenicol could be used as a respiration-independent delivery control.

MATERIALS AND METHODS

Detection of tissue hypoxia

Sample collection

All squid experiments conform to guidelines developed for invertebrate animal models at the University of Wisconsin, Madison. Wild-caught mature (>18 mm mantle length) squid were maintained in ambient light conditions in circulating seawater tables at the Kewalo Marine facility, University of Hawaii, Manoa. At 12 pm, (~6 hours post dawn), and 12 am (~18 h post dawn), squid were anaesthetized in seawater containing 2% ethanol. Squid were injected through the cephalic vessel with 0.5 mg of pimonidazole hydrochloride (PIM, Hypoxyprobe, Inc, Burlington, MA) in pH 7.4 squid ringer's buffer (50 mM $MgCl_2$, 10 mM $CaCl_2$, 10 mM KCl,

530 mM NaCl, 10 mM HEPES), or a squid-ringer's only vehicle control. This dose delivers approximately 1 mg/g body mass, which is within the range cited by the manufacturer for use in mice. The total volume of injection was 7.5 µl. A non-toxic dye previously used to inject the squid (carboxy-SNARF-4F, Invitrogen, Carlsbad, CA), was used to visualize the patency of the injection. Following injection, the squid were removed from the ethanol solution, and placed in seawater. All squid assayed regained normal behaviors within 10 minutes of anesthesia cessation. The squid were maintained for an additional 2 h to allow for circulation of the probe, and the metabolism or excretion of free PIM. After 2 h, the squid were again anaesthetized, and the light organ was exposed by ventral dissection. The symbiont-containing light-organ tissue was removed, and tissue sample from the gills was also collected. Samples were either frozen at -80 °C for immunoblot, or placed in 4% paraformaldehyde marine phosphate-buffered saline (mPBS: pH 7.4, 50 mM Phosphate Buffer, pH 7.4, 0.45 M NaCl) for 30 minutes at room temperature. Fixed samples were washed 3 times for 5 minutes in mPBS to remove excess paraformaldehyde, and stored in the dark at 4 °C prior to embedding and sectioning.

Immunoblot

Because PIM labeling targets all proteins with sulfydril groups, a dot blot was used to compare labeling of tissues between day and night time-points. To isolate total protein, tissues were homogenized with glass pestles in pH 7.4 phophate-buffered saline (137 mM NaCl, 2.7 mM KCl, 10 mM Na_2HPO_4, 1 mM KH_2PO_4), containing 2% SDS and 1% protease inhibitor cocktail (Sigma, #P8340). One gill was homogenized in 200 µl of this buffer, and symbiont-containing epithelial tissues from one light organ were homogenized in 50 µl. Homogenates were centrifuged at 10,000 x g for 20 min to separate protein from other cell material. The supernatant

was removed, and protein concentration was quantified by Qbit (Life Technologies). Typical yields from isolation were 3.5 µg/µl for gill tissue, and 2 µg/µl for symbiont-associated tissue. 5 µg of protein from each sample was spotted onto 0.25 µm nitrocellulose membrane. The dry membrane was submersed in TBS-T 4% skim milk (TBS-T; 20 mM Tris with 0.5 M NaCl and 0.1% Tween-20; pH 7.4) for 1 h at room temperature to block non-specific antibody binding. The membrane was incubated in 1% milk TBS-T containing 1:250 mouse monoclonal anti-PIM antibody (clone 4.3.11.3, MAb1, Hypoxiaprobe, Burlinton, MA) for 30 min, and washed three times for 5 min in TBS-T. To detect the antibody, the membrane was incubated for 30 min in 1:150 goat-anti-mouse conjugated to horserasish peroxidase (Bio-Rad, #171-1011). The membrane was rinsed twice for 10 min in TBS-T, and once for 10 min in TBS (no Tween). The membrane was exposed using Pierce ECL reagent and CL-X film (Life Technologies), following the manufacturer's instructions.

Localization studies

Fixed tissue samples were embedded in paraffin, and sectioned into 5µm slices at the UW Surgery Department Histology facility. Parraffin sections were processed as described elsewhere (1), with minor modifications. Briefly, following deparaffinization, ethanol rehydration, and antigen retrieval, slides were blocked overnight at 4 °C in mPBS containing 0.5% BSA and 1% goat serum. Slides were incubated in α-PIM primary antibody 1:250 in the blocking solution overnight at 4°C. After washing, slides were incubated for 1 h at room temperature with a 19 µg/mL goat-anti-mouse FITC-conjugated secondary antibody (Jackson Labs, #115-095-003) in blocking solution. Rinsed slides were counterstained with a 1:1000

dilution of TOTO-3 for 10 min at RT, and mounted in Vectashield (Vector Laboratories, Burlingame, CA), and samples were visualized by confocal microscopy.

Affymetrix Microarray Gene Expression Analysis

Growth of cells

Overnight cultures of *V. fischeri* ES114 were cultivated in 3 mL LBS. In the morning, cultures were diluted 1:100 into fresh LBS, and grown to an optical density (600 nm) of 0.2 units. This culture was diluted 1:100 into 15 mL of minimal salts medium (0.340 mM $NaPO_4$ [pH 7.5], 0.05 M Tris [pH 7.5], 0.3 M NaCl, 0.05 M $MgSO_4$-$7H_2O$, 0.01 M $CaCl_2$-$2H_2O$, 0.01 M NH_4Cl, 0.01 M KCl, 0.01 mM $FeSO_4$-$7H_2O$)(24), containing either 5 mM chitobiose, or 40 mM glycerol and 4 mM sodium nitrate, in an anoxic culture tube. Anoxic conditions were established by degassing the cultures for 3 rounds of 15 minutes under a vacuum manifold. The gas in the cultures was replaced by argon. Cultures were grown at 28 °C, until the OD of the cultures reached 0.2 units. Triplicate samples were collected. The average amount of cells collected for each samples was $1.1x10^8$ colony forming units (CFU) per mL for chitobiose samples, and $1.4x10^8$ CFU/mL for glycerol samples (standard deviation for the three replicates was less than 10%).

Isolation of RNA, synthesis, fragmentation and labeling of cDNA, hybrization, and reading of Affymetrix GeneChips

The entire 15 mL of culture was added to 30 mL of RNAProtect reagent (Qiagen), and incubated for 5 min at room temperature. The cultures were split into 22 mL aliquots in RNAse-free glass centrifuge tubes, and spun at 6722 rpm for 30 min at 4 °C. Supernatant was decanted from the tubes, and the pellet was resuspended in 190 µl RNAse-free TE buffer. Cell pellets from the

same condition were combined, and 20 µl of 40 mg/mL lysozyme was added. Samples were incubated at room temperature for 10 min with intermittent vortexing. RNA was isolated using an RNeasy kit (Qiagen), following the manufacturer's instructions. One column was used per sample, and the elution step was repeated to maximize sample recovery. To remove any contaminating DNA, 50 µg of each RNA sample was treated with 5 µg of RQ DNase (Promega), according to the manufacturer's instructions, followed by an on-column DNAse digestion (Qiagen). Samples with a 260:280 ratio greater than 1.9 were submitted to the UW Gene Expression Center, where samples were tested for quality with an Agilent 2100 Bioanalyzer, using the Prokaryote Total RNA Nano Series II algorithm. RNA was processed using a protocol developed for the *Escherichia coli* genome project at UW Madison (25). Briefly, 10 µg samples of RNA were used to synthesize and fragment the cDNA. 2 µg of fragmented cDNA was end-terminus labeled, and hybridized to a rhofispaa520260F GeneChip (Affymetrix).

Analysis of Affymetrix GeneChip Data

The samples were post processed on an AFX Fluidics450 Station, following protocol ProkGE_WS2v3_450, and data were extracted from GC3000 7G scanned images using Affymetrix Expression Console version 1.1 software. To assess oxygen-dependent gene expressionThe resulting data were combined with a set of data from Affymetrix arrays previously performed using RNA isolated during growth on GlcNAc or glycerol under oxic conditions by Amy Schaeffer. The data were analyzed using two methods: the CyberT algorithm (http://cybert.microarray.isc.uci.edu/) (26, 27), and ArrayStar software (DNAStar, Madison WI). For CyberT analysis, an unpaired, two-factor analysis was performed using Bayes-regularized analysis parameters, using default analysis options, except where noted: 3 non-zero replicates, 3-

beta iterations, and a posterior probability of differential expression greater than 0.995. For ArrayStar analysis, the group of genes analyzed was defined as the set differentially expressed more than three fold in each of the 4 possible comparisons among the 4 datasets (oxic glycerol, anoxic glycerol, oxic GlcNAc, anoxic GlcNAc), as defined by T-tests (FDR=0.05). Venn diagrams were used to elucidate groups of genes that responded to the presence of oxygen in carbon-source dependent and independent patterns.

Construction and assay of P_{cydAB} transcriptional reporter construct.

Cloning

The P*cydAB* promoter reporter construct was cloned using a strategy very similar to that described in Chapter 3 of this thesis. Briefly, the promoter was amplified with primers TAGGATCCCGGGGAAGATGTTATTGAAC (5' XmaI site Tm 57 °C) and TAGGATTCTAGACCTAGTGCAAGTTAAT (5' XbaI site Tm 58 °C), and cloned in front of the *GFP* gene on the pTM267 plasmid (14). The construct, named pJAS610 was maintained in DH5-alpha lambda pir *Escherichia coli* in the presence of 2.5 µg/mL chloramphenicol. pJAS610 was transferred to *V. fischeri* strains ES114 and *arcA*-deficient AMJ2 (15), by conjugative transfer (28), and selection with chloramphenicol. pTM267-derived vectors are carried in ~10 copies in *V. fischeri,* and at *tetA* promoter is used to expresses the red fluorescent protein mCherry (14). The expression of mCherry provides a reference for quantification of GFP signal.

Culture characterization

Cultures of ES114 and Δ*arcA V. fischeri* carrying pJAS610 were started in SWT (5 g/L Bacto-Tryptone, 3 g/L yeast extract, 3 mL/L glycerol, 24.5 ppt instant ocean) (9), from single colonies.

Cultures were grown to an OD of 0.2, then sub-cultured 1:100 into SWT under oxic (10 mL in a 125 mL flask, 225 rpm), or anoxic (established under a vacuum manifold, gas-exchanged with argon) growth conditions. Cultures were grown to an OD of 0.6. 1 mL aliquots of each culture were centrifuged to collect cell pellets. The pellets were resuspended in 0.5 mL of PIPES MIC buffer (50 mM $MgSO_4$, 10 mM $CaCl_2$, 300 mM NaCl, 10 mM KCl, 10 mM PIPES, pH 6.3) (1). 200 µl aliquots of each resuspension were distributed between two wells of a 96-well plate. The fluorescent signal of GFP (excitation 485/emission 535 filter set) and mCherry (excitation 535/emission 612 filter set) were detected using a Tecan Genios Pro plate reader (Tecan Group Ltd. Männedorf, Switzerland). Autofluorescence was corrected by subtraction of GFP and mCherry signal of *V. fischeri* with no reporter from isogenic reporter-containing strains.

Squid characterization

To monitor the activity of *V. fischeri* transcriptional reporter constructs in the light organ, squid were colonized overnight with ~5,000 CFU/mL of *V. fischeri*. To prepare *V. fischeri* strains for inoculation, cultures were grown overnight in LBS chloramphenicol, and sub-cultured 1:100 in SWT. After 24 h of colonization, 10 animals were euthanized every 6 hours by placing them in 4% paraformaldehyde mPBS. Squid were incubated at 4 °C overnight, then rinsed 3 times for 10 minutes in mPBS. Light organs were dissected from the fixed animals, and placed in Vectashield mounting medium. To quantify reporter signal, the light organs were visualized on a Ziess Axio Imager M2 epifluorescence microscope, equipped with TexasRed (mCherry), and GFP filters. The mean intensity of GFP and mCherry signal was collected from a 50 µm sector across the crypt space. The signal from the crypts of squid colonized by non-fluorescent *V. fischeri* was subtracted from each of these readings to control for autofluorescence. Experimental and control

samples were matched by time-point to control for changes in autofluorescence due to morphogenesis or symbiont growth.

Kanamycin sensitivity assays

The susceptibility of *V. fischeri* to killing by kanamycin was measured using a protocol modified from studies of *E. coli* (20). Briefly, *V. fischeri* was cultivated in oxic and anoxic culture conditions to an optical density (600 nm) of 0.2, after which 50 mg/mL kanamycin was added, and anoxia re-established where necessary. Aliquots of the cultures were serially diluted and plated to determine colony-forming units per mL at 0, 3 and 6 h post kanamycin addition. Oxygenated growth conditions were established by shaking 10 mL of LBS at 225 rpm in a 125 mL flask, and anoxic growth was established using 3 mL of LBS in a 5-mL anaerobic tube with a rubber stopper. Anoxic conditions were established as described for RNA isolation above. Where indicated, 30 mM sodium nitrate was added to the LBS to support anaerobic nitrate respiration.

REFERENCES

1. Kremer N*, et al.* (2014) The dual nature of haemocyanin in the establishment and persistence of the squid–Vibrio symbiosis. *Proc. R. Soc. B* 281(1785).

2. Kizaka-Kondoh S & Konse-Nagasawa H (2009) Significance of nitroimidazole compounds and hypoxia-inducible factor-1 for imaging tumor hypoxia. *Cancer Sci* 100(8):1366-1373.

3. Varghese AJ, Gulyas S, & Mohindra JK (1976) Hypoxia-dependent reduction of 1-(2-nitro-1-imidazolyl)-3-methoxy-2-propanol by Chinese hamster ovary cells and KHT tumor cells in vitro and in vivo. *Cancer Res* 36(10):3761-3765.

4. Arteel G, Thurman R, Yates J, & Raleigh J (1995) Evidence that hypoxia markers detect oxygen gradients in liver: pimonidazole and retrograde perfusion of rat liver. *Br J Cancer* 72(4):889.

5. Gross MW, Karbach U, Groebe K, Franko AJ, & Mueller-Klieser W (1995) Calibration of misonidazole labeling by simultaneous measurement of oxygen tension and labeling density in multicellular spheroids. *Int J Cancer* 61(4):567-573.

6. Goodwin A*, et al.* (1998) Metronidazole resistance in *Helicobacter pylori* is due to null mutations in a gene (*rdxA*) that encodes an oxygen-insensitive NADPH nitroreductase. *Mol Microbiol* 28(2):383-393.

7. Proctor LM & Gunsalus RP (2000) Anaerobic respiratory growth of *Vibrio harveyi*, *Vibrio fischeri* and *Photobacterium leiognathi* with trimethylamine *N*-oxide, nitrate and fumarate: ecological implications. *Environ Microbiol* 2(4):399-406.

8. Dunn AK*, et al.* (2010) The alternative oxidase (AOX) gene in *Vibrio fischeri* is controlled by NsrR and upregulated in response to nitric oxide. *Mol Microbiol* 77(1):44-55.

9. Boettcher KJ & Ruby EG (1990) Depressed light emission by symbiotic *Vibrio fischeri* of the sepiolid squid *Euprymna scolopes*. *J Bacteriol* 172(7):3701-3706.

10. Wier AM*, et al.* (2010) Transcriptional patterns in both host and bacterium underlie a daily rhythm of anatomical and metabolic change in a beneficial symbiosis. *Proc Natl Acad Sci U S A* 107(5):2259-2264.

11. Chang D-E*, et al.* (2004) Carbon nutrition of *Escherichia coli* in the mouse intestine. *Proc Natl Acad Sci U S A* 101(19):7427-7432.

12. Wang Y*, et al.* (2010) H-NOX–mediated nitric oxide sensing modulates symbiotic colonization by *Vibrio fischeri*. *Proc Natl Acad Sci U S A* 107(18):8375-8380.

13. Dunn AK (2012) *Vibrio fischeri* metabolism: symbiosis and beyond. *Adv Microb Physiol* 61:37.

14. Miyashiro T, Wollenberg MS, Cao X, Oehlert D, & Ruby EG (2010) A single *qrr* gene is necessary and sufficient for LuxO-mediated regulation in *Vibrio fischeri*. *Mol Microbiol* 77(6):1556-1567.

15. Bose JL*, et al.* (2007) Bioluminescence in *Vibrio fischeri* is controlled by the redox-responsive regulator ArcA. *Mol Microbiol* 65(2):538-553.

16. Vemuri G, Altman E, Sangurdekar D, Khodursky A, & Eiteman M (2006) Overflow metabolism in *Escherichia coli* during steady-state growth: transcriptional regulation and effect of the redox ratio. *Appl Environ Microbiol* 72(5):3653-3661.

17. Inouye S & Tsuji FI (1994) Evidence for redox forms of the *Aequorea* green fluorescent protein. *Febs Letters* 351(2):211-214.

18. Morris RL & Schmidt TM (2013) Shallow breathing: bacterial life at low O_2. *Nat Rev Microbiol*11(3):205-212.

19. Schwartzman JA*, et al.* (2015) The chemistry of negotiation: rhythmic, glycan-driven acidification in a symbiotic conversation. *Proc Natl Acad Sci U S A* 112(2):566-571.

20. Liu Y & Imlay JA (2013) Cell death from antibiotics without the involvement of reactive oxygen species. *Science* 339(6124):1210-1213.

21. Keren I, Wu Y, Inocencio J, Mulcahy LR, & Lewis K (2013) Killing by bactericidal antibiotics does not depend on reactive oxygen species. *Science* 339(6124):1213-1216.

22. Claes MF & Dunlap PV (2000) Aposymbiotic culture of the sepiolid squid *Euprymna scolopes*: role of the symbiotic bacterium *Vibrio fischeri* in host animal growth, development, and light organ morphogenesis. *J Exp Zool* 286(3):280-296.

23. Koch EJ, Miyashiro TI, McFall-Ngai MJ, & Ruby EG (2013) Features governing symbiont persistence in the squid-vibrio association. *Mol Ecol* (doi:10.1111/mec.12474).

24. Adin DM, Visick KL, & Stabb EV (2008) Identification of a cellobiose utilization gene cluster with cryptic B-galactosidase activity in *Vibrio fischeri*. *Appl Environ Microbiol* 74(13):4059-4069.

25. Perna NT*, et al.* (2001) Genome sequence of enterohaemorrhagic *Escherichia coli* O157: H7. *Nature* 409(6819):529-533.

26. Kayala MA & Baldi P (2012) Cyber-T web server: differential analysis of high-throughput data. *Nucl Acid Res* 40(W1):W553-W559.

27. Baldi P & Long AD (2001) A Bayesian framework for the analysis of microarray expression data: regularized t-test and statistical inferences of gene changes. *Bioinformatics* 17(6):509-519.

28. Stabb EV & Ruby EG (2002) RP4-based plasmids for conjugation between *Escherichia coli* and members of the vibrionaceae. *Methods Enzymol* 358:413-426.